Understanding the Mechanisms Affecting Gridded Ion Engine Operation in Ground Test Facilities

by

Tyler J. Topham

A dissertation submitted in partial fulfillment
of the requirements for the degree of
Doctor of Philosophy
(Nuclear Engineering and Radiological Sciences)
in the University of Michigan
2025

Doctoral Committee:

Professor John E. Foster, Chair
Professor Deborah Levin
Professor Ryan McBride
Michael Patterson, Desert Works Propulsion
Professor Alexander Thomas

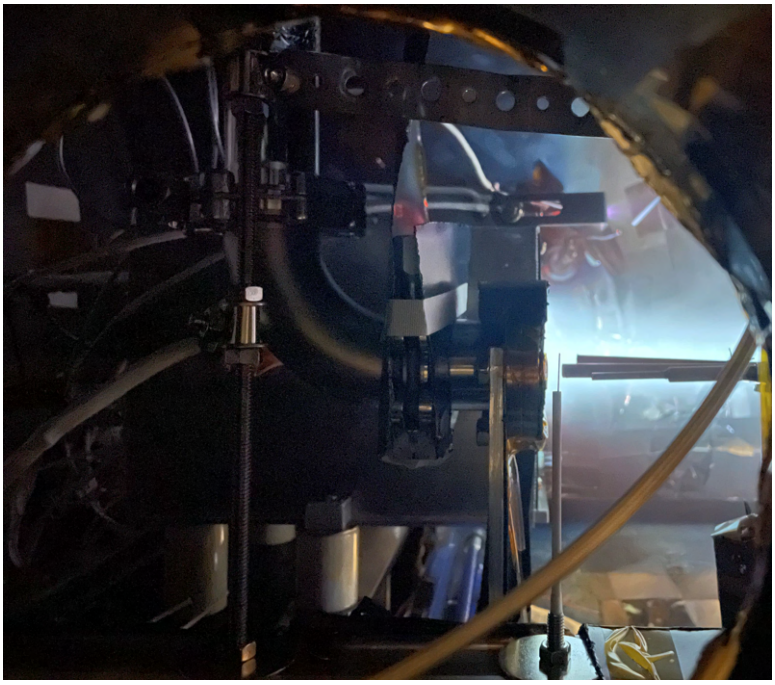

“It’s Working!”

Tyler J. Topham
tytopham@umich.edu
ORCID iD: 0009-0001-1880-4993

© Tyler J. Topham 2025

DEDICATION

To my wife, family, and all the teachers & coaches who have gotten me here.

ACKNOWLEDGMENTS

My time at the University of Michigan has been extremely rewarding. I am extraordinarily grateful for all those now and in the past who have helped me along the way. First and foremost, I would like to thank my wife, Kiersten, for being there for me through all of it over the last five years. Her support and sacrifice is the only way any of this is possible.

A special thanks to my committee members, Ryan McBride, Alec Thomas, Debbie Levin, and Mike Patterson for taking the time to read, encourage, and guide this work. Sincere appreciation to my advisor and committee chair, John Foster, who took the risk and brought me into his lab. Thank you for the countless hours of guidance in the lab and for the numerous discussions pertaining to alien life!

I would also like to thank the funding agencies throughout my graduate studies: The Department of Defense (DoD) through the National Defense Science & Engineering Graduate (NDSEG) Fellowship Program and NASA through the **J**oint **A**dva**N**ced Prop**U**lsion In**S**titute (JANUS), a NASA Space Technology Research Institute, grant number 80NSSC21K1118. Also, the Penn State 2018 Toshiba-Westinghouse fellows program for jump starting my interest in research and nuclear engineering as an undergraduate student. Special thanks to professors Peter Miraldi and William Walters of Penn State for their mentorship and guidance.

None of this could be done with out the great support from those in the Nuclear Engineering and Radiological Sciences (NERS) department. Special shout-outs to the following for their time and support throughout the years: Garnette Roberts, Rob Blackburn, Tommy Tunks, Rebecca Duguay, Sarah Galea, Jennifer Melms, Besnik Topulli, and Michelle Sonderman.

To the Plasmacrew of the Plasma Science & Technology Laboratory (PSTL), you all have made my time here unforgettable. Thank you to Chris Durot, Joe Greole, Zimu Yang, Nate Wirgau, and Roxanne Walker for showing me the ways and creating such a great working environment to join into. To Anil Bansal, Chelsea Tischler, Sophia Bergmann, Elijah Wilson, Jesus Diaz Alcala, and Ana Clecia Alves Almeida, thank you for all your help in the lab and continuing to foster a great working lab group. And to all of my PSTL labmates, thank you for the countless hours of laughter and distractions! I would be remiss if I did not acknowledge all of the work by the undergraduate and master students that have also contributed to this work. Thank you to Emeline Hanna, James "Jimmy" Baker, James Judge, Gaines Morrison, and Rochan Yakkundi for your

labor and time, hopefully you learned as much from me as I learned from you all. To my brothers in the qualifier exam trenches, Ryan Revolinsky and Joe Chen, the pain and suffering is worthwhile and I appreciate all those hours of study together.

A special thanks to my colleagues at the Plasmadynamics & Electric Propulsion Laboratory for their support of our NSTAR test in their facility. Thank you specifically to Ben Jorns, Eric Viges, Leanne Su, Tate Gill, Parker Roberts, Will Hurley, Madison Allen, Grace Zoppi, and Konrad Shire for assistance during testing. Thank you to all those as well who made and are apart of the JANUS institute. I have learned a lot from all of you and have made great friendships along the way as well. Thank you to the High-Power Electric Propulsion Laboratory (HPEPL) for hosting the first JANUS FIT test. Special thanks to Janice Cabrera and Nia Butler-Craig (Georgia Tech), Austen Thomas (Western Michigan), Jon Stienike and Emily Ku (Colorado State), and Sean Clark (UIUC) during that testing. Additionally, the modeler collaborations with professor Levin's group from UIUC with Keita Nishii, Sashank Srinivasan, Tanapat Bhakyapaibul, and Gyuha Lim & professor Wirz's group from UCLA/Oregon State with Chris Cretel and Rich Obenchain.

There is a special list of people I would like to acknowledge that are often overlooked but who are the ones that have shaped me into the person I am today. To my fifth grade teacher Mrs. Ortega, thank you for inspiring me to be a scientist from an early age. Dr. Pleese, my high school chemistry teacher, thank you for your sacrifice to teach high school students and being the best science teacher. To my high school math teachers, Mr. Ridgely, Mrs. Beam, Mr. Artmann, and Mr. Mele, thank you for instilling an appreciation of mathematics and stretching my abilities. To Coach Domingo Lucero, thank you for teaching me I can do hard things. To Coach Ed Smith, thank you for being an example of the kind-of charitable and patient person we should all strive to be. To all my teachers and coaches, thank you for your sacrifices and services to me. You all have helped me grow tremendously over the years by the values and skills you have taught me.

To the Chronister, Faught, Warren, and Lucero families, thank you for being great family friends that my family could always rely on growing up. Kevin Lucero, thank you for your friendship and all the years of sports together and against each other. Brandon Simpkins, Nick Rudolph, Tyler Smith, and Moises Butios, thank you for befriending me and getting me through middle and high school. Jeff Chronister, Oni Elvenia, Weston Robinson, Koby Okuda, and Sean Wadsworth, thank you for your friendship in hard-times with your support, laughter, and Tacobell runs. And my cousin Kyler Mikami for being a great example and friend to me, along with all the midnight runs to In-n-Out with the cousins.

Lastly, I would like to thank my parents, April and Joseph, for their sacrifices and support over the countless athletic competitions and practices, school events, and extracurricular activities. To my sister, Kaelamae, thank you for forcing me to graduate now so I can claim I became a doctor before you. But also for your support and laughter through the years. Thank you to all my

grandparents, aunts, uncles, and cousins who have done so much and taught me so much. I have been so blessed over the years and am so grateful for the opportunity to study at the University of Michigan and would like to thank God for His hand and guidance throughout my life.

Tyler J. Topham
March 2025

TABLE OF CONTENTS

DEDICATION ii

ACKNOWLEDGMENTS iii

LIST OF FIGURES ix

LIST OF TABLES xx

LIST OF APPENDICES xxiii

LIST OF ACRONYMS xxiv

LIST OF SYMBOLS xxviii

ABSTRACT xxxiii

CHAPTER

1 Introduction 1

1.1 Overview 1
1.2 Background 2
1.3 Introduction to Electric Propulsion 4
1.3.1 General Thruster Principles 4
1.3.2 Gridded Ion Engine 8
1.3.3 Hall Effect Thruster 12
1.4 Intro to GIE Facility Effects 13
1.4.1 Abstract 13
1.4.2 Introduction 13
1.4.3 Review of Facility Effects 22
1.4.4 Flight and Ground Test Comparisons 42
1.4.5 Mitigation and Correction Strategies 54
1.4.6 Concluding Remarks 57

2 Objectives & Methods 59

2.1 Testing Objectives 59
2.2 Methods 62

3 Experimental Considerations 63

3.1 Test Facilities . . . 65
3.1.1 PEPL Alec D. Gallimore LVTF . . . 66
3.1.2 HPEPL VTF-2 . . . 67
3.1.3 PSTL RC . . . 70
3.2 Test Articles . . . 75
3.2.1 H9 . . . 75
3.2.2 NSTAR . . . 77
3.2.3 NASA 8 cm . . . 79
3.3 Diagnostics . . . 87
3.3.1 Langmuir Probe . . . 87
3.3.2 Faraday Probe . . . 89
3.3.3 Emissive Probe . . . 90
3.3.4 Retarding Potential Analyzer . . . 92
3.3.5 ExB . . . 92
3.3.6 Ion Gauge . . . 93
3.3.7 Residual Gas Analyzer . . . 94
3.3.8 Plasma Spectroscopy . . . 94

4 Low Power-Density Facility Effects . . . 97

4.1 Motivation & Objectives . . . 97
4.2 Experimental campaign & thruster operating conditions . . . 97
4.3 Plasma-Facility Interactions . . . 99
4.3.1 Facility Boundary Conditions . . . 99
4.3.2 Electrical Coupling & Beam Neutralization . . . 113
4.3.3 Neutralizer Characterization & Margin . . . 118
4.3.4 Ion Energies . . . 132
4.4 Thruster-Facility Interactions & Performance . . . 133
4.4.1 Plasma Screen Shielding . . . 134
4.4.2 Doubles-to-Singles Production . . . 135
4.5 Conclusions . . . 137

5 High-Power Facility Effects . . . 140

5.1 Motivation & Objectives . . . 140
5.2 Experimental campaign & thruster operating conditions . . . 140
5.2.1 2024-05 NASA 8 cm experimental campaign . . . 140
5.2.2 2024-11 NASA 8 cm experimental campaign . . . 144
5.2.3 2025-01 NASA 8 cm experimental campaign . . . 145
5.3 Plasma-Facility Interactions . . . 147
5.3.1 Facility Boundary Conditions . . . 148
5.3.2 Electrical Coupling & Beam Neutralization . . . 177
5.4 Thruster-Facility Interactions & Performance . . . 191
5.4.1 Neutral Ingestion . . . 191
5.5 Conclusions . . . 200

6 Low & High-Power Density Ground Testing . . . 206

6.1 Motivation & Objectives . . . 206
6.2 Low & High-Power Density Comparison . . . 206
6.3 Guidelines & Recommendations . . . 211
6.4 Future Work . . . 212

7 Target Plasma & Impurities . . . 214

7.1 Motivations & Objectives . . . 214
7.2 Investigation of Target Glow . . . 214
7.3 Plasma Impurities . . . 219
7.4 Conclusions . . . 224

8 Conclusion . . . 225

8.1 Summary . . . 232
8.1.1 Low-Power Density . . . 233
8.1.2 High-Power Density . . . 235
8.1.3 Target Glow & Impurities . . . 238
8.2 Recommendations & Future Work . . . 239

APPENDICES . . . 241

BIBLIOGRAPHY . . . 279

LIST OF FIGURES

FIGURE

1.1 Gridded ion engine circuit diagram. The potential of the neutralizer cathode (NC) serves as the reference potential for the thruster. The high energy ion beam is formed by acceleration of the ions from the high potential difference between the grids. This high potential is created by elevating the potential at which the ions are created at in the discharge chamber with respect to NC via the beam power supply. An Accel power supply on the downstream grid is then biased negative to NC to repeal electrons from streaming into the discharge chamber. 10

1.2 Gridded ion engine potentials in operation. The screen voltage is the potential at the first (screen) grid created by the elevation in potential of the discharge chamber by the beam power supply. The accelerator voltage is the potential of the second (accelerator) grid using the accelerator power supply. Downstream of the grids, the exhausted positive ions create a high potential but as they reach the neutralization plane, the beam becomes well neutralized decreasing in potential. However, in a non-well neutralized beam this potential will propagate downstream lessening the effective beam voltage lessening the effective beam current that can be extracted and lowering the produced thrust. 11

1.3 Center-mounted cathode Hall effect thruster circuit diagram where a plasma is sustained between the cathode and anode via a discharge power supply. Acceleration of ions created in the channel occurs due to the axial electric field. A radial magnetic field is produced by electromagnets, retarding immediate electron collection to the anode. An ExB drift in the angular direction arises resulting in the acceleration of electrons that enhances electron-impact ionization. Extra electrons from the cathode neutralize the produced ion beam. 14

1.4 Hall effect thruster potentials are in reference to the potential of the cathode. The Discharge power supply elevates the anode with respect to cathode potential. As ions are accelerated out and electrons are dragged along, the plasma plume will saturate to a potential. The difference between this potential and the anode potential dictates the effective beam voltage which this in turn dictates the amount of ions that can be extracted and resulting thrust. 15

1.5 1.5 m mercury ion thruster at NASA VF 6—Engine operated at 200 kW 16

1.6 Gridded ion performance envelope 17

1.7 Schematic depiction of gridded ion thruster subsystems 18

1.8 Potential distribution between grids up to the hypothetical neutralization plane 19

1.9 Comparison between space (a) and ground test (b) engine operation. The darker purple color represents the increased neutral gas and plasma densities. Alternative neutralization pathways through the facility walls are in green. Backsputtered material from the walls are depicted by the blue arrows. 23
1.10 Electrical circuit depiction of DC electrical pathways associated with beam neutralization with coupling represented by resistors. 24
1.11 Apparatus used to study effect of grounded surfaces near neutralizer 26
1.12 Difference in neutralizer coupling voltage for floating and grounded structures 26
1.13 Beam neutralization processes in space as inferred from SERT II experiments 28
1.14 In-house observation of curved cathode jet from a high current cathode with conical anode 29
1.15 Comparison between accelerator grid before and after long duration test 32
1.16 Comparison and agreement between simulation and LDT camera imaging data on accelerator grid erosion 32
1.17 Burn lines associated with electron collection at magnetic cusps. 34
1.18 Test facility derived deposition and normal engine wear/deposition processes. Deposition processes derived external to discharge chamber shown on left with discharge chamber deposition processes derived from engine wear is shown on the right 37
1.19 Carbon deposition on discharge chamber just upstream of ion optics at high resolution 38
1.20 The 30,000-h Extended-Life Test of the Deep Space 1 Flight Spare Ion (NSTAR) Thruster outer perimeter accelerator grid downstream face heavily coated with backsputtered material 38
1.21 NEXT ELT accelerator grid surface deposition transition from net erosion near center to net deposition on-axis 39
1.22 Spatial profile of doubles to singles ratio for NEXT ion engine taken —82 cm downstream as a function of engine throttle level 41
1.23 Molybdenum grid erosion rate variation with background pressure 42
1.24 Artist conception of SERT II spacecraft 44
1.25 Variation in spacecraft potential with neutralizer bias voltage. Nominal operation at neutralizer bias of 0 V 45
1.26 Ground and flight thrust comparison with calculated thrust 47
1.27 Accelerator grid current variations in space and on ground 48
1.28 Neutralizer keeper voltage variations in space and in ground test vs throttle level . . . 49
1.29 Neutralizer potential relative to ground comparison with flight 49
1.30 Plasma conditions near engine at different throttle conditions 51
1.31 The facility effect—background pressure of VF 6 vs flow and the response, the local plasma density at the multi-thruster array 55
1.32 Secondary electron emission yield for beam relevant energies on dirty and clean metal surfaces 57

3.1 University of Michigan Alec D. Gallimore Large Vacuum Test Facility (LVTF) the best simulation of a spacelike pressures for EP testing in at the university level 67

3.2 University of Michigan LVTF diagnostic layout used over a variety of background pressures. Pressure measurements are made to the side of the thruster with an ion gauge. The beam of the thruster terminates on a beam target downstream. Langmuir probes line the wall for measurements of ambient plasma properties far from the beam plasma. A lateral Faraday probe sweep characterized the beam plasma. 68
3.3 Layout of locations of the cryopumps in the LVTF used to control background pressure in the facility. The left image is a 2D map of pump locations with the two different types of cryopumps emphasized based on color and shape. The right side image is a 3D model of the facility. 68
3.4 Various pumping configurations used during testing at LVTF to control background pressure. The red "X" indicates a pump is turned off. 69
3.5 Georgia Tech Vacuum Test Facility-2 is another premier academic EP test facility that was used for facility effect impacts on the H9 Hall thruster. 70
3.6 University of Michigan Rocket Chamber is a smaller test bed for smaller thrusters testing. This facility underwent major upgrades for facility effect testing on EP devices. 71
3.7 University of Michigan Rocket Chamber fully-upgraded layout. Includes pressure measurements, throttleable pumping speeds, and a plethora of plasma diagnostics throughout the chamber for characterizing thruster operation and the impacts of facility effects on thruster operation. This setup was used for the 2024-11 and 2025-01 test campaigns using the NASA 8 cm gridded ion engine. 73
3.8 University of Michigan Rocket Chamber previous layout mid-way during chamber upgrades. Testing layout used for the 2024-05 test campaign before all upgrades were completed. 74
3.9 H9 Hall effect thruster used at Georgia Tech VTF-2 for investigating facility effects on Hall thruster operation. 76
3.10 H9 Hall thruster performance and firing envelop capabilities. The H9 can be operated up to 9 kW. 76
3.11 NSTAR gridded ion engine operation in a ground test environment with proven flight history used in Deep Space 1 and Dawn missions 78
3.12 NSTAR Long-Duration Test discharge losses variation over time during ground testing. The degraded overtime highlights the need to understand if facility effects such as backsputtered wall material are obscuring results or because of thruster operation over time is the main contributing factor. 80
3.13 NSTAR Long-Duration Test beam ion production cost for varies power levels to indicate thruster performance will vary based on operating conditions 80
3.14 Top view of the NASA 8 cm gridded ion engine 80
3.15 Schematic showing the meaning of the NASA 8 cm converging-diverging beam. The cross-over point d is the distance at which the converging and diverging intersect. . . . 81
3.16 NASA 8 cm discharge losses obtained by Patterson during initial characterization of this thruster. 83
3.17 NASA 8 cm discharge losses with the impact of floating ring cusps during testing at NASA Glenn. 83
3.18 NASA 8 cm discharge hollow cathode impedance characterization for various main flows. 83

3.19 NASA 8 cm discharge hollow cathode simulated beam extraction used to characterize the thruster performance and compare to previous obtained results from NASA Glenn. 84
3.20 NASA 8 cm discharge hollow cathode simulated beam extraction with no main flow to show importance of the additional flow added in the discharge chamber to produce the beam. 84
3.21 NASA 8 cm discharge scandate cathode operation circuit the cup electrode either being tied to a power supply, floating, or tied to cathode potential. 85
3.22 NASA 8 cm discharge scandate cathode simulated beam extraction for comparison to nominal hollow cathode operation. 86
3.23 NASA 8 cm discharge scandate cathode simulated beam extraction with no main flow to show the difference in thruster performance due to the propellant flow around the planar scandate cathode diffusing into the discharge chamber. Less propellant flow is needed in the discharge chamber. 86
3.24 NASA 8 cm "super" neutralizer hollow cathode impedance characterization to compare to the nominal neutralizer cathode. 87
3.25 Sample solved Langmuir IV trace. The left is an IV trace obtained directly from the probe. The right is the IV trace for electron current contributions after ion current has been removed from the overall probe current. Blue region is the ion saturation, green is the electron retarding region, and pink is the electron saturation region. 88
3.26 Spherical Langmuir probe example (used during the LM-NSTAR testing at LVTF to increase collected current due to low ambient background plasma densities) 89
3.27 Various types of Faraday probes used in this dissertation. Decisions of the type of Faraday probe used varied on easy of implementation and testing environment considerations based on recommended practices for Faraday probe use in EP testing. . . . 90
3.28 Heat 'n float emissive probe circuit to describe how plasma potentials were obtained with an emissive probe. A rheostat is used to control the electron emission current and the potential of the plasma is measured by the voltage difference of the filament to facility ground. 91
3.29 An example of a six-grid RPA like installed in the Rocket Chamber to obtain most prominent ion energy measurements. 93
3.30 An ExB probe used to obtained doubles-to-singles ratios for thruster discharge chamber performance corrections and characterization. This probe is being designed at the University of Michigan Plasma Science and Technology laboratory to investigated doubles-to-singles ratios for the NASA 8 cm gridded ion engine. 94
3.31 Ion gauge in the Rocket chamber to make pressure measurements. 95
3.32 Residual gas analyzer used in the Rocket Chamber to identify potential gas species in the plasma using mass spectroscopy. 96

4.1 Plasma properties of the spherical Langmuir probes at the walls of the facility that are located in the ambient background plasma using the LM-NSTAR GIE operating at the TH01 throttle condition. 102
4.2 Plasma properties of the spherical Langmuir probes at the walls of the facility that are located in the ambient background plasma using the LM-NSTAR GIE operating at the TH05 throttle condition. 104

4.3 Plasma properties of the spherical Langmuir probes at the walls of the facility that are located in the ambient background plasma using the LM-NSTAR GIE operating at the TH10 throttle condition. . . . 105
4.4 Plasma potential variations measured using Langmuir probes at various locations throughout the facility as background pressure was controlled by limiting pumping speed. . . . 108
4.5 Electron plasma density variations measured using Langmuir probes at various locations throughout the facility as background pressure was controlled by limiting pumping speed. . . . 109
4.6 Electron temperature variations measured using Langmuir probes at various locations throughout the facility as background pressure was controlled by limiting pumping speed. . . . 110
4.7 Electron Debye lengths variations measured using Langmuir probes at various locations throughout the facility as background pressure was controlled by limiting pumping speed. . . . 112
4.8 Observed plume broadening in the wings of the sweep due to elevated ambient background plasma using a lateral plume sweep via a guarded Faraday probe. . . . 113
4.9 The relative percent change in neutralizer-facility coupling voltage for the LM-NSTAR GIE in LVTF between the grounded (nominal) and the floating plasma screen electrical configuration as background pressure is varied. A more negative neutralizer-facility coupling voltage (increase of coupling of the thruster with the facility) is observed with the change from a grounded to a floating plasma screen. . . . 116
4.10 H9 Hall thruster heat'n float emissive probe results on a 1 m radially arm sweep of the thruster plume. Asymmetry in potential measurements. . . . 117
4.11 H9 Hall thruster radial arm probes at the Georgia Institute of Technology VTF-2 test facility. . . . 118
4.12 LM-NSTAR gridded ion engine and diagnostics near neutralizer (in red) used to measure plasma properties. There was a cylindrical Langmuir probe for plasma potential, electron density, and electron temperature measurements. Additionally, a retarding potential analyzer (RPA) was used to obtain the ion energy distribution function with the corresponding most prominent ion energy obtained by taking the first-derivative of the ion energy distribution function. . . . 119
4.13 Important thruster operating conditions during the neutralizer margin characterization of the LM-GIE in LVTF at the TH10 throttle condition for various background pressure. An indicator of the onset of an unstable high voltage mode of the neutralizer cathode is an increase in the peak-to-peak oscillations of the neutralizer cathode potential with respect to facility ground in sub-figure (d). . . . 122
4.14 Plasma properties near the neutralizer using a cylindrical Langmuir probe during the neutralizer margin characterization of the LM-NSTAR GIE in LVTF at the TH10 throttle condition for various background pressures. . . . 124
4.15 Most prominent ion energy near the neutralizer perpendicular to the direction of beam propagation using a retarding potential analyzer during the neutralizer margin characterization of the LM-NSTAR GIE in LVTF at the TH10 throttle condition for various background pressure. . . . 125

4.16 Plasma screen electrical configuration circuit diagram with an electrical switch to change between the grounded and floating plasma screen configuration. 126
4.17 Comparison of the plasma properties obtained with a spherical Langmuir probe near the plasma screen between the grounded and floating plasma screen configurations at the P1 pumping speeds and corresponding background pressures for three throttle conditions: TH01, TH05, and TH10. 128
4.18 Comparison of the plasma properties obtained with a cylindrical Langmuir probe near the neutralizer between the grounded and floating plasma screen configurations at the P1 pumping speeds and corresponding background pressures for three throttle conditions: TH01, TH05, and TH10. 129
4.19 Abbreviated thruster telemetry results for the characterization of the neutralizer with floating plasma screen at the TH05 throttle condition at the P2 pumping speed configuration. 130
4.20 Near the neutralizer plasma properties from a cylindrical Langmuir probe during the characterization of the neutralizer with floating plasma screen at the TH05 throttle condition at the P2 pumping speed configuration. 131
4.21 Most prominent ion energies elastically scatted from thruster beam at thruster flats measured with a retarding potential analyzer during the characterization of the neutralizer with floating plasma screen at the TH05 throttle condition at the P2 pumping speed configuration. 132
4.22 Measurement of the most prominent ion energies of the elastically scattered beam ions perpendicular to thruster flats for various pumping configurations and corresponding background pressures. Observed was a decrease in the most prominent ion energies with an increase of the background pressure. 133
4.23 Impact of the plasma screen configuration on measured beam current from the telemetry system for the LM-NSTAR at LVTF for two background pressure (P1 and P2) and the three throttle conditions (TH01, TH05, and TH10). 134
4.24 Relative percent change on measured beam current between a grounded and a floating plasma screen configuration for the LM-NSTAR at LVTF for two background pressure (P1 and P2) and the three throttle conditions (TH01, TH05, and TH10) 135
4.25 LM-NSTAR at LVTF ExB doubles-to-singles ratios measured 2.08 m downstream on beam center-line and additionally corrected for CEX attenuation to recapture the ratio at the thruster exit plane for TH01, TH05, and TH10 throttle conditions for four background pressures. Doubles-to-singles ratio increased in value with the increase of pressure even after corrections. 136

5.1 2024-05 NASA 8 cm test campaign at the 100 W power level with the “super” neutralizer cathode, grounded plasma screen, and grounded beam target measured plasma properties in the ambient plasma near the facility walls obtained from the cylindrical Langmuir probes. Background pressure was controlled by throttling pumping speed of the downstream turbomolecular pump. 150
5.2 2024-05 NASA 8 cm test campaign plasma potentials obtained from Langmuir probes in various locations in the PSTL RC using the “super” neutralizer cathode over a variety of background pressures. 152

5.3 2024-05 NASA 8 cm test campaign floating potentials obtained from Langmuir probes in various locations in the PSTL RC using the "super" neutralizer cathode over a variety of background pressures. 153
5.4 2024-05 NASA 8 cm test campaign electron densities obtained from Langmuir probes in various locations in the PSTL RC using the "super" neutralizer cathode over a variety of background pressures. 154
5.5 2024-05 NASA 8 cm test campaign electron temperatures obtained from Langmuir probes in various locations in the PSTL RC using the "super" neutralizer cathode over a variety of background pressures. 155
5.6 2024-05 NASA 8 cm test campaign electron Debye lengths obtained from Langmuir probes in various locations in the PSTL RC using the "super" neutralizer cathode over a variety of background pressures. 156
5.7 2024-11 NASA 8 cm test campaign at the 200 W power level with the nominal hollow neutralizer cathode, grounded plasma screen, and grounded or floating beam target measured plasma properties in the ambient plasma near the facility walls obtained from the cylindrical Langmuir probes. Background pressure was controlled by throttling pumping speed of both turbomolecular pumps. 158
5.8 2024-11 & 2025-01 NASA 8 cm test campaigns at the 100 W power level. 2024-11 campaign used a nominal hollow cathode for the neutralizer whereas the 2025-01 test campaign used the "super" neutralizer cathode. A combination of grounded or floating plasma screen, and grounded beam target electrical configurations were used. Plasma properties in the ambient plasma near the facility walls shown here were obtained from cylindrical Langmuir probes. Background pressure was controlled by throttling pumping speed of both turbomolecular pumps. 159
5.9 2024-11 & 2025-01 NASA 8 cm test campaigns plasma potentials obtained from Langmuir probes in various locations in the PSTL RC. A nominal hollow cathode was used during the 2024-11 test campaign where as the "super" neutralizer cathode was used in the 2025-01 test campaign. Variations in the background pressure was done by throttling both turbomolecular pumps. 162
5.10 2024-11 & 2025-01 NASA 8 cm test campaigns floating potentials obtained from Langmuir probes in various locations in the PSTL RC. A nominal hollow cathode was used during the 2024-11 test campaign where as the "super" neutralizer cathode was used in the 2025-01 test campaign. Variations in the background pressure was done by throttling both turbomolecular pumps. 163
5.11 2024-11 & 2025-01 NASA 8 cm test campaigns electron densities obtained from Langmuir probes in various locations in the PSTL RC. A nominal hollow cathode was used during the 2024-11 test campaign where as the "super" neutralizer cathode was used in the 2025-01 test campaign. Variations in the background pressure was done by throttling both turbomolecular pumps. 164
5.12 2024-11 & 2025-01 NASA 8 cm test campaigns electron temperatures obtained from Langmuir probes in various locations in the PSTL RC. A nominal hollow cathode was used during the 2024-11 test campaign where as the "super" neutralizer cathode was used in the 2025-01 test campaign. Variations in the background pressure was done by throttling both turbomolecular pumps. 166

5.13 2024-11 NASA 8 cm test campaign at the 100 W power level of the Langmuir probe geometry and orientation effects on measured plasma properties with a varying background pressure at 80 cm downstream of the thruster along the wall of the RC facility. 168
5.14 2024-11 NASA 8 cm test campaign at the 200 W power level of the Langmuir probe geometry and orientation effects on measured plasma properties with a varying background pressure at 80 cm downstream of the thruster along the wall of the RC facility. 169
5.15 2025-01 NASA 8 cm test campaign at the 100 W power level lateral Faraday probe sweep at downstream distances of 0.5 cm and 16.0 cm highlighting examples of plume broadening and high ambient background plasma densities just outside the beam plasma. 171
5.16 2024-11 NASA 8 cm test campaign beam converging and diverging half-angels and cross-over distance varying with background pressure. 173
5.17 2024-11 & 2025-01 NASA 8 cm test campaigns at the 100 W and 200 W power levels total integrated current from lateral Faraday probe sweeps up to 95% beam diameter with variations in downstream position. 174
5.18 2024-11 NASA 8 cm test campaign at the 100 W power level comparison of the wall Langmuir probe plasma potentials to the beam heat'n float emissive probe plasma potentials. Comparisons were made at 0.5 cm, 16.0 cm, and 32.0 cm downstream of the thruster. The electrical configuration during testing included the plasma screen and the beam target being grounded. Horn-like structure at 0.5 cm downstream position show incomplete neutralization of the beam. 176
5.19 2024-11 NASA 8 cm test campaign at the 200 W power level comparison of the wall Langmuir probe plasma potentials to the beam heat'n float emissive probe plasma potentials. Comparisons were made at 0.5 cm, 16.0 cm, and 32.0 cm downstream of the thruster. The electrical configuration during testing included the plasma screen and the beam target being grounded (left column) whereas the plasma screen was grounded but comparison between a grounded and floating beam target is also made (right column). The floating beam target cases show the plasma potential in the chamber raises everywhere in comparison to the corresponding grounded beam target case. 178
5.20 2025-01 NASA 8 cm test campaign at the 100 W power level comparison of the wall Langmuir probe plasma potentials to the beam heat'n float emissive probe plasma potentials. Comparisons were made at 0.5 cm, 16.0 cm, and 32.0 cm downstream of the thruster. The electrical configuration during testing included the comparison of the plasma screen being grounded or floating and the beam target being grounded. Floating the plasma screen increased the plasma potential in the very near field but higher background pressures dampens this effect. 179
5.21 Neutralizer-facility coupling voltages for the all test campaigns in the PSTL Rocket Chamber and for all of the different electrical configurations of the plasma screen and beam targe. Additionally, all the different power levels and their variations with background pressure are plotted here. Grouping by test campaigns reveals there is a decrease in the value (increases in the negative magnitude) of the neutralizer-facility coupling voltages with background pressure resulting in more coupling with the facility at higher background pressures. 182

5.22 2024-11 NASA 8 cm test campaigns at the 100 W and 200 W power levels comparison of the maximums of the true-coupling voltages as a function of downstream position from the thruster. The electrical configuration during the testing were all with a grounded plasma screen and grounded beam target. The true-coupling voltage increased with background pressure for all cases indicating poor direct neutralization of the beam by the neutralizer. 183
5.23 2014-11 NASA 8 cm test campaign at the 100 W power level comparison of the plasma properties near the plasma screen and neutralizer. The electrical configuration included a ground plasma screen and grounded beam target. 183
5.24 2024-11 NASA 8 cm test campaign at the 200 W power level comparison of the plasma properties near the plasma screen and neutralizer. The electrical configuration included a ground plasma screen and both a grounded and floating beam target. 184
5.25 2024-11 NASA 8 cm test campaign at the 200 W power level comparison of the maximum true-coupling voltages as a function of downstream position from the thruster. The electrical configuration during the testing were all with a with ground plasma screen and of both a grounded and floating beam target. The true-coupling voltages for the floating beam target cases match regardless of background pressure indicating that coupling in the floating beam target case between the neutralizer and the beam is less affected by background pressure. 185
5.26 2025-01 NASA 8 cm test campaign at the 100 W power level comparison of the maximum true-coupling voltages as a function of downstream position from the thruster. The electrical configuration during the testing were all with both a grounded and floating plasma screen while the beam target was grounded. The high plasma potential in the very near field increases the true-coupling voltage there significantly. 187
5.27 2025-01 NASA 8 cm 100 W plasma properties comparison of grounded and floating plasma screen with a grounded beam target. 188
5.28 2024-05 NASA 8 cm test campaign at the 100 W power level and 70% pumping speed measured values of V_p, V_{cg}, and V_{cp} for grounded plasma screen and beam target as neutral gas is injected into the plasma bridge. 189
5.29 2024-05 NASA 8 cm test campaign at the 100 W power level impacts of neutral flow injection in the plasma bridge on the measured neutralizer-facility coupling voltages. . 190
5.30 2024-05 NASA 8 cm test campaign at the 100 W power level impacts of neutral flow injection in the plasma bridge on the measured plasma potentials using a cylindrical Langmuir probe approximately 4 cm downstream of neutralizer. 192
5.31 2024-05 NASA 8 cm test campaign at the 100 W power level impacts of neutral flow injection in the plasma bridge on the measured electron temperatures using a cylindrical Langmuir probe approximately 4 cm downstream of neutralizer. 193
5.32 2024-05 NASA 8 cm test campaign at the 100 W power level impacts of neutral flow injection in the plasma bridge on the measured plasma potentials using a planar Langmuir probe near the plasma screen on the left-side of the thruster. 194
5.33 2024-05 NASA 8 cm test campaign at the 100 W power level impacts of neutral flow injection in the plasma bridge on the measured electron temperatures using a planar Langmuir probe near the plasma screen on the left-side of the thruster. 195
5.34 Schematic of gridded ion ingestion. Ambient neutral gas leaks through the grid holes and alters the discharge performance. 196

5.35 2024-11 NASA 8 cm test campaign ingestion impacts on discharge voltage, neutralizer keeper voltage, and beam current background pressure is varied by throttling the turbomolecular pumps. . . . 198
5.36 2024-11 NASA 8 cm test campaign ingestion impacts on discharge impedance with varying background pressures normalized to lowest pressure. . . . 199
5.37 2024-11 NASA 8 cm test campaign ingestion flow ratio to total flow with varying background pressures. . . . 199
5.38 2024-11 NASA 8 cm test campaign ingestion impacts on performance with varying background pressures normalized to lowest pressure. . . . 201

6.1 Venn diagram comparison of low & high-power density ground testing facility effects. 207

7.1 Target glow during LM-NSTAR operation at PEPL LVTF. Reveals a whitish glow around the target of unknown composition that is suspected to not be the xenon propellant. A non-spacelike condition to have this material sputtered off and enter the plasma environment. . . . 215
7.2 GEC bell jar test chamber plasma spectroscopy experimental setup. . . . 216
7.3 GEC bell jar test chamber Poco carbon sputtering test sample to emulate the target glow seen in thruster testing. . . . 216
7.4 Sputtered carbon spectra with some identified peaks using the emulated thruster ion beam in the GEC bell jar chamber. . . . 217
7.5 Sputtered carbon spectra OH bands over time after exposure to the emulated thruster ion beam in the GEC bell jar chamber after 30 minutes. An observed decrease in the OH levels after the 30 minutes of outgassing. . . . 218
7.6 2024-11 NASA 8 cm test campaign mass spectroscopy using a residual gas analyzer on sputtered material in the ambient plasma in the Rocket Chamber near the beam target. . . . 218
7.7 2024-11 NASA 8 cm test campaign mass spectroscopy using a residual gas analyzer in the Rocket Chamber near the beam target for two focused ranges. Shows increases in carbon species and hydrocarbon species found in the plasma spectroscopy results as the thruster power level is increased. . . . 220
7.8 Rocket Chamber in-plane wall cylindrical Langmuir probes 1 (left-side) & 5 (right-side) IV trace changes during test campaigns that became more dirty over time. . . . 221
7.9 Rocket Chamber glass witness plate in front of one of the in-plane wall cylindrical Langmuir probes that had an increase in deposited material overtime. Shows location and resulting deposited material on the glass witness plate after only two days of testing. 222
7.10 2025-01 NASA 8 cm test campaign at the 100 W power level ExB spectra with unusual peak before the main singly ionized beam ions. Suspected to be attributed to CEX ions. . . . 223

B.1 NSTAR probes floating potentials pressure study . . . 252
B.2 NSTAR probes ion density pressure study . . . 253

C.1 2024-05 NASA 8 cm 100 W with “super” neutralizer, grounded plasma screen, and grounded beam target wall probes pressure study . . . 255

C.2 2024-05 NASA 8 cm 100 W with “super” neutralizer, grounded plasma screen, and floating beam target wall probes pressure study . . . 256
C.3 2024-05 NASA 8 cm 100 W with “super” neutralizer, floating plasma screen, and grounded beam target wall probes pressure study . . . 257
C.4 2024-05 NASA 8 cm 100 W with “super” neutralizer, floating plasma screen, and floating beam target wall probes pressure study . . . 258
C.5 2024-05 NASA 8 cm with “super” neutralizer ion density pressure study . . . 259
C.6 2024-11 NASA 8 cm 100 W with normal neutralizer, grounded plasma screen, and grounded beam target wall probes pressure study . . . 260
C.7 2024-11 & 2025-01 Debye length pressure study . . . 261
C.8 2024-11 & 2025-01 ion density pressure study . . . 262
C.9 2024-11 NASA 8 cm 300 W wall probe to beam emissive probe potentials comparison 263
C.10 2024-05 NASA 8 cm 100 W neutralizer-facility coupling voltage with ground plasma screen and compression of grounded floating beam target and injected neutral flow versus pressure . . . 264
C.11 2024-05 NASA 8 cm 100 W neutral flow injection floating potentials 4 cm downstream of neutralizer . . . 265
C.12 2024-05 NASA 8 cm 100 W neutral flow injection electron density 4 cm downstream of neutralizer . . . 266
C.13 2024-05 NASA 8 cm 100 W neutral flow injection ion density 4 cm downstream of neutralizer . . . 267
C.14 2024-05 NASA 8 cm 100 W neutral flow injection Debye length 4 cm downstream of neutralizer . . . 268
C.15 2024-05 NASA 8 cm 100 W neutral flow injection floating potentials to the left-side of the plasma screen . . . 269
C.16 2024-05 NASA 8 cm 100 W neutral flow injection electron density to the left-side of the plasma screen . . . 270
C.17 2024-05 NASA 8 cm 100 W neutral flow injection ion density to the left-side of the plasma screen . . . 271
C.18 2024-05 NASA 8 cm 100 W neutral flow injection Debye length to the left-side of the plasma screen . . . 272

LIST OF TABLES

TABLE

1.1 Comparison between space and ground test engine operation conditions. 22

3.1 Summary of the objectives and methods of the gridded ion engin test campaigns. . . . 64
3.2 Available diagnostic data from the gridded ion engine test campaigns. 65
3.3 List of active and in-active cryopumps for each pumping configuration in ascending pressures order. 67
3.4 Summarized H9 telemetry performance in SN03 at JPL on Xenon. 77
3.5 High-current density operation of the H9 on xenon at 300 V discharge. 77
3.6 High-current density operation of the H9 on krypton at 300 V discharge. 78
3.7 Abbreviated DS1 NSTAR throttle table performance numbers highlighting the range of the NSTAR gridded ion engine performance envelope. 79
3.8 Abbreviated DS1 NSTAR throttle table telemetry highlighting the range of the NSTAR gridded ion engine performance envelope. 79
3.9 NASA 8 cm performance targets used for setting flows and operating conditions for the 100 W, 200 W, and 300 W power levels. 81
3.10 NASA 8 cm performance Patterson results. 82

4.1 In-plane background pressures corrected for xenon approximately 1-1.5 beam diameters to the side of the thruster flats. 98
4.2 NSTAR telemetry results in PEPL LVTF at the TH01 throttle condition. 98
4.3 NSTAR telemetry results in PEPL LVTF at the TH05 throttle condition. 98
4.4 NSTAR telemetry results in PEPL LVTF at the TH10 throttle condition. 99
4.5 LM-NSTAR neutralizer-facility coupling voltages in LVTF for TH01, TH05, and TH10 throttle conditions and various background pressures controlled by limiting the pumping speed. The impacts of a floating plasma screen on neutralizer-facility coupling voltages are also presented with the "F" after the pumping configuration indicating a floating plasma screen was used instead of the nominal grounded plasma screen configuration used in all other cases. 114
4.6 The impacts of the plasma screen electrical configuration on currents through the plasma screen (grounded) and floating potentials of the plasma screen (floating) as the background pressure is varied for different throttle conditions. 126
4.7 Sputtering threshold from ions for common EP materials. 133
4.8 LM-NSTAR at LVTF plasma screen configuration impact on beam current for two background pressure (P1 and P2) and the three throttle conditions (TH01, TH05, and TH10). 134

5.1 2024-05 NASA 8 cm test campaign background pressures corrected for xenon in the Rocket Chamber while thruster is in operation at the 100 W power level with the "super" neutralizer cathode. The plasma screen configuration is defined first as either "G" for grounded or "F" for floating. The beam target configuration follows this same convention. Thus, "GF" means grounded plasma screen with a floating beam target. . 141
5.2 2024-05 NASA 8 cm test campaign telemetry results in the PSTL RC at 100 W with "super" neutralizer, grounded plasma screen and grounded beam target. 142
5.3 2024-05 NASA 8 cm test campaign telemetry results in the PSTL RC at 100 W with "super" neutralizer, floating plasma screen and grounded beam target. 142
5.4 2024-05 NASA 8 cm test campaign telemetry results in the PSTL RC at 100 W with "super" neutralizer, grounded plasma screen and floating beam target. 143
5.5 2024-05 NASA 8 cm test campaign telemetry results in the PSTL RC at 100 W with "super" neutralizer, floating plasma screen and floating beam target. 143
5.6 2024-11 NASA 8 cm test campaign background pressures corrected for xenon in the Rocket Chamber while thruster is in operation at the 100 W, 200 W, and 300 W power levels with the nominal hollow cathode neutralizer. The plasma screen configuration is defined first as either "G" for grounded or "F" for floating. The beam target configuration follows this same convention. Thus, "GF" means grounded plasma screen with a floating beam target. 144
5.7 2024-11 NASA 8 cm test campaign telemetry results in the PSTL RC at 100 W with nominal neutralizer and heater on, grounded plasma screen and grounded beam target. 145
5.8 2024-11 NASA 8 cm test campaign telemetry results in the PSTL RC at 200 W with nominal neutralizer and heater on, grounded plasma screen and grounded and floating beam target. 146
5.9 2025-01 NASA 8 cm test campaign background pressures corrected for xenon in the Rocket Chamber while thruster is in operation at the 100 W power level with the "super" neutralizer cathode. The plasma screen configuration is defined first as either "G" for grounded or "F" for floating. The beam target configuration follows this same convention. Thus, "GF" means grounded plasma screen with a floating beam target. . 146
5.10 2025-01 NASA 8 cm test campaign telemetry results in the PSTL RC at 100 W with "super" neutralizer, grounded and floating plasma screen and grounded beam target. . 147
5.11 Summary and explanations of the different couplings refereed to during testing. 180

8.1 2023-02 low-power density LM-NSTAR gridded ion engine testing summary at LVTF. 226
8.2 2024-05 high-power density NASA 8 cm gridded ion engine testing summary in the Rocket Chamber. 228
8.3 2024-11 high-power density NASA 8 cm gridded ion engine testing summary in the Rocket Chamber. 229
8.4 2025-01 high-power density NASA 8 cm gridded ion engine testing summary in the Rocket Chamber. 231

C.1 2024-11 NASA 8 cm at PSTL RC at 300 W with nominal neutralizer and heater on, grounded plasma screen and grounded beam target 263

D.1 Plasma spectroscopy common line spectra of interest for argon 274

D.2 Plasma spectroscopy common line spectra of interest for hydrogen, carbon & water species 275

E.1 Hydrocarbon & cracking patterns RGA mass spectra 1-30 AMU 277
E.2 Hydrocarbon & cracking patterns RGA mass spectra 41-132 AMU 278

LIST OF APPENDICES

A Review of Beam Neutralization of Gridded Ion Thrusters 241

B Additional NSTAR Data 251

C Additional NASA 8 cm Data 254

D Plasma Spectroscopy 273

E Mass Spectroscopy 276

LIST OF ACRONYMS

ACCL or ACCEL accelerator

AFRL Air Force Research Laboratory

AMU atomic mass unit

Ar argon

BD beam dump

BEAM beam

BT beam target

C carbon

C cathode flow rate

CCD charge-coupled device

CEX change-exchange

CLP cylinderical Langmuir probe

DART Double Asteroid Redirection Test

DC direct-current

DISC discharge

DS1 Deep Space 1

DSMC Direct Simulation Monte Carlo

EM electromagnetic

EM1 engineering model 1

EMI electromagnetic-interference

EMT Engineering Model Thruster

ELT extended-life test

EP electric propulsion

ES electrostatic

ESW electrostatic solitary waves

F floating

FGRND facility ground

FMT Functional Model Thruster

FP Faraday probe

FWHM full width at half maximum

G grounded

GEC Gaseous Electronics Conference

GIE gridded ion engine

GIT gridded ion thruster

HET Hall effect thruster

HiPEP High Power Electric Propulsion

HPEPL High Power Electric Propulsion Laboratories

IDS Ion Propulsion Diagnostic Subsystem

IG ion gauge

IIEE ion-induced electron emission

Isp specfic impulse

IV current-voltage trace

JANUS Joint AdvaNced PropUlsion InStitute

JAXA Japan Aerospace Exploration Agency

Kr krypton

LCIF laser collisional induced fluorescence

LDT long-duration test

LEO low-Earth orbit

LP Langmuir probe

LTE local thermal equilibrium

LVTF Large Vacuum Test Facility

M main flow rate

MCC Monte Carlo Collision

MEX momentum exchange

MHD magnetohydrodynamic

ML mission throttle level

N neutralizer flow rate

N6 neutralizer "super" cathode serial #006

NDSEG National Defense Science and Engineering Graduate

NEP nuclear electric propulsion

NEXT NASA's Evolutionary Xenon Thruster

NEXT-C NASA's Evolutionary Xenon Thruster–Commercial

NKPR neutralizer keeper

NSTAR NASA Solar Technology Application Readiness

ODE ordinary differential equation

PEPE plasma experiment for planetary exploration

PEPL Plasmadynamics & Electric Propulsion Laboratory

PIC particle-in-cell

PLP planar Langmuir probe

PS plasma screen

PSTL Plasma Science and Technology Laboratory

RC Rocket Chamber

RF radio-frequency

RGA residual gas analyzer

RPA retarding potential analyzer

Se effective pumping speed

SEE secondary electron emission

SEM scanning electron microscope

SERT Space Electric Rocket Test

SDA space domain awareness

SLP spheciral Langmuir probe

SMU source measurement unit

SNAP Systems Nuclear Auxiliary Power

SOA state-of-the-art

TG Trivelpiece–Gould

TH throttle level

VF Vacuum Facility

VTF-2 Vacuum Test Facility-2

Xe xenon

LIST OF SYMBOLS

Variables

A	Area	m^2
α	Doubles correction factor	-
α_m	Multiple species correction factor	-
B	Magnetic field	T
$\vec{B}$	Magnetic field vector	T
$\bar{c}$	Mean thermal speed	m/s
β_n	Sticking coefficient of the neutrals	-
d	Distance	m
d_{grid}	Grid gap distance	m
E	Electric Field	V/m
$\vec{E}$	Electric Field vector	V/m
E_{ion}	Ion Energy	eV
f	Frequency	Hz
$\vec{F}$	Force vector	N
F_t or β	Divergence correction factor	-
I	Current	A
Isp	Specific impulse	s
j or J	Current density	A/m^2
k	Rate coefficient	cm^3/s
k_BT or KT	Temperature	eV
L	Length	L
λ_D	Debye length	m

λ_{mfp}	Mean free path	m
M	Neutral mass	kg
$\mathbf{M}$	Total mass	kg
m	mass	kg
$\dot{m}$	mass flow rate	sccm
n	Particle density	m^{-3}
$\dot{n}_i$	Arrival rate of ions	particles/s
$\dot{n}_n$	Arrival rate of neutrals	particles/s
N	Neutral gas density	m^{-3}
N_0	Surface density of substrate adsorption sites	m^{-2}
$\dot{N}$	Escaping neutral flux	particles/s
η	Efficiency	-
$\eta_{Clausing}$	Clausing factor	-
η_n	Neutral surface converge	-
p	Pressure	Torr
P	Power	W
Φ	Potential	V
ϕ	Potential	V
Q	Flow rate	particles/s
q	Charge state	Coulombs
r	Radial distance	m
R	Beam radius	m
σ	Collision cross-section	m^2
$\sigma_{cond.}$	Conductivity	S/m
$\mathbf{T}$	Thrust	N
t	time	s
θ	Angle	radians
θ_c	Total fractional surface converge	-
U_∞	Drift velocity	m/s

V	Voltage	V
$\mathbf{v}$ or $\vec{v}$	Velocity (vector)	m/s
v	Velocity	m/s
$\Delta\mathbf{v}$	Delta-v	m/s
ν	Collision frequency	1/s
Y_n	Energy dependent sputter yield	-
$Y_{C-Mo\theta_c}$	Sputter yield for single carbon adsorbate adlayer Mo substrate	-
Γ	Particle flux	particles
γ_C	Carbon back-sputter flux	1/m^{2}s
z	Distance downstream	m
z	Charge state	-
Z	Impedance	Ω

Constants

e	Electron charge	1.60217663×10^{-19} coulombs
g	Gravitational constant	9.81 m/s^2
π	Pi constant	3.14 radians

Subscripts

0	At thruster exit-plane
a or $ACCL$	Accelerator
b or B or $BEAM$	Beam
c	Cutoff
cg	Facility coupling
ck	Cathode keeper
$cond.$	Conductivity
cp or $cath.$	Beam coupling or True-coupling
CEX	Charge exchange
d or $disc$ or $DISC$	Discharge

D	Debye length
e	Electron
$e - impact$	Electron-impact
$elec.$	Electrical
ex	Exhaust
eV	Electron volt
$final$	Final state
$full$	Full integration
$FLOAT$	Floating
g or gas	Gas
$GRND$	Ground
i	Ion
$initial$	Initial state
in	Input
jet	Jet
L	Lorentz
$left$	Left-half integration
m	Mass-utilization
$mom.$	Momentum transfer
n	Neutrals
nk	Neutralizer keeper
NC	Neutralizer common
p	plasma
$p0$	Within the plume
$p1$	At plume edge
pp	Peak-to-peak
ps	Plasma screen
Q	Electrostatic
$right$	Right-half integration
s	Screen power supply

SC	Spacecraft
T	Total
W	Wein

Superscripts

$+$	Singly ionized ions
$++$	Doubly ionized ions

ABSTRACT

Gridded ion engines are an option for high-power nuclear electric propulsion missions supporting science, cargo, and human missions to the moon, Mars, and beyond. Current state-of-the-art systems operate in the sub-10 kW range. High-power missions will require systems to operate at 100s of kW, with the power processed by multiple thrusters. Being able to test such high-power engines in a spacelike environment requires pumping speeds in the 10s of ML/s which is well beyond the capabilities of ground-based test facilities presently. Chamber size is important to minimize plasma wall interactions both from sputtering and electromagnetic coupling. In lieu of a facility with ideal attributes that circumvent these problems, a ground testing approach that utilizes current facilities must be used. To develop such high-power engines that will operate predictably in space, a combination of extensive measurements of engines operating at high-powers relative to chamber volume densities is needed in addition to computational models correcting for performance differences such that spacelike operation can be recovered.

In response to the need to understand electric propulsion ground testing and the impact of these facility effects on engine performance, the **J**oint **A**dva**N**ced Prop**U**lsion In**S**titute (JANUS) was formed. As a part of the JANUS project, this work specifically focuses on understanding facility related mechanisms affecting gridded ion engine operation under high-power conditions, whether simulated or actual, in marginal and submarginal facilities, and using models to correct deviations from spacelike operation.

The approach here is to first measure the impact of facility effects in a chamber that is of modest size and pumping speed achieving the low-power densities akin to spacelike conditions. The next step would be to operate an engine at high-power densities to simulate 100 kW class engines to assess deviations, preferably in the same facility. Unfortunately, 100 kW class engines do not currently exist. To emulate the high-power density facility effects of a 100 kW system, a smaller, 8 cm NASA gridded ion engine was used in a small facility to simulate the effect of operating the larger engines. A comparison between the impacts of facility effects on thruster operation for low and high-power densities is then made with comments on recommended gridded ion engine ground testing best practices. Here these processes are identified that deviate from spacelike conditions, providing a test database for model validation such that these models can be later used to correct for facility effects and recover spacelike operation.

Overall, the goal of this thesis is to quantify these facility effects, provide a database for model validation, and to identify power density considerations. Along with this it was found that the ambient background plasma can have a large impact on gridded ion engine operations such as neutralization and facility coupling. Furthermore, it was identified that there is a problematic nature of graphite surfaces beyond simple sputter deposition that involves water embedded in the carbon lattices such that impacting high energy ions from the beam can cause plasma chemical effects that can lead to dirty probes which affects interpreted plasma properties or gives rise to changes in the operation or lifetime of the thruster. This effect suggests the need for chamber conditioning akin to what is done in the fusion community.

CHAPTER 1

Introduction

1.1 Overview

Current electric propulsion systems are in the sub-10 kW range with interest to develop 100 kW systems. Unfortunately, there are not presently available facilities that can reasonably ground test such high-power systems and still be able to accurately meet the ideal "test like you fly" requirements such that accurate spaceflight performance can be predicted. As a result, if one desires to ground test these high-power systems, one must test in present facilities that would provide a non-ideal testing environments for these high-power systems. This would result in causing deviations in the performance of the test article from actual spaceflight performance due to facility related effects. Corrections for these facility effects would then need to be made to recover spaceflight performance. These corrections can come from validated models. The validation of these models will need experimental data from current ground testing in different test facilities with different test articles. Some experimental attempts have been made to correct for facility effects by running a thruster in suboptimal facilities but often it is difficult to identify potential issues over a small range of power densities (thruster power level-to-chamber volume). This dissertation work tackles two aspects of this problem. First, facility effects at these high-power densities are investigated and compared to low-power density testing to provide a wider range of facility effects under different power densities. This allows for facility effects to potential be magnified at one of the two extremes. Additionally the large power density testing ranges aides in the second part–provide a database of experimental data to be used for model validation. To progress high-power electric propulsion an understanding of the mechanisms affecting thruster operation in ground tests is the required in being able to accurately predict the spaceflight performance of these devices by correcting for facility effects in the absences of proper ground test facilities for these high-power levels.

1.2 Background

Electric propulsion (EP) systems are capable of high exhaust velocities which reduces the amount of propellant needed for a given mission. Such a feature is desirable for high delta-v missions where the exhaust velocity exceeds the mission delta-v. Here delta-v is the impulse per unit of spacecraft mass or in other words the change in velocity with current fuel supply. The high performance delta-v of EP systems not only reduces propellant mass required but also reduces launch and mission costs due to lower payload masses. The concept of electric propulsion devices dates back to the early 1900s by work in U.S. and Russia (outlined history of EP in Ref. [1]). The current most mature EP technologies today include the arc jet, the gridded ion engine and Hall effect thruster.

Gridded ion engines (GIE) are unrivaled in their specific impulse and dynamic range of their performance envelope, among current mature EP technologies. Because of their ability for long-life and high-specific impulse, gridded ion technology has cemented its place as the propulsion unit of choice in deep-space scientific missions. Additionally, gridded ion engines have relevance in today's space domain for orbit raising and station keeping in Earth orbits. With space domain awareness (SDA) becoming more relevant to both military and commercial interest, high-specific impulse is desired to maintain these systems in operation for long periods of time while performing many maneuvers. Pushing debris into junkyard orbits is another application for gridded ion engines because of their high-specific impulse. This allows for more maneuvers to be made consuming the same amount of propellant than lower specific impulse engine types. The highly-collimated beam of the gridded ion engine is also advantageous in that it minimizes plume impacts on spacecraft structures.

The current state-of-the-art (SOA) power level of EP devices range between 100 W to around 10 kW. However, because of the scalability of gridded ion technology, these devices are one option for high-power operation on nuclear electric propulsion missions supporting science, cargo, and human missions to the Moon, Mars, and beyond. This will require systems in excess of 100s of kW, with the power processed via an array of engines. Exploring such high-power operating conditions on the ground while maintaining the conditions necessary to replicate operations in space is beyond the capabilities of current vacuum facilities. The pumping speed of even the best test facility available is at least an order of magnitude too low [2]. Before flight, such engine systems must be qualified via performance testing in a relevant environment simulating space. No such facilities currently exist that can simulate spacelike conditions at such high-power levels of a 100 kW thruster system. As such, ground testing is performed under non-ideal situations. Diagnostics and models together may be able to correct the performance data such that spacelike operation can be recovered [3].

The deviations from actual space operation constitute facility effects include, but are not limited to: 1) elevated background neutral and plasma densities, 2) artificial electrical coupling with chamber structures, 3) propellant ingestion, and 4) the deposition of backsputtered material on the thruster that is derived from ions impacting on the chamber walls. Each of these effects are typically categorized separately but are often coupled. Furthermore, as future missions will only demand greater thruster power levels, decoupling of these facility effects will need to be done such that their individual impacts on thruster operation can be known and quantified. Besides the possibility of testing these systems in space, one is left to test high-power EP systems in current ground facilities that are inadequately equipped to handle such power densities. As such, ground testing must capture the deviations due to facility effects on thruster operation and provide a means to correct these deviations until future technologies can either alleviate the cost of in-space testing or improve ground testing capabilities.

The main objective of the **J**oint **A**dva**N**ced Prop**U**lsion In**S**titute (JANUS) is to investigate the impacts of these facility effects on engine performance and the corresponding predicted spaceflight performance based on data obtained from ground tests [4]. The objectives of JANUS are: 1) to advance and proliferate high-power EPs by preparing ground testing environments acceptable for the development of predictive engineering models of spaceflight, 2) to develop standards, procedures, and techniques for thruster operation and testing, 3) to create and validate computation models with experimental results, and 4) to educate the next generation of EP engineers and scientists.

This document includes a review of the aforementioned facility effects and their impacts on gridded ion engine operation. The focus of this work is to understand and prepare for high-power density ground testing of high-power GIE in facilities lacking the ability to accurately represent a spacelike environment. Additionally, this document is to serve as a guidebook of current best practices for GIE ground testing to minimize, or at least identify, the associated facility effects impacting the performance and characterization of the thruster. These guidelines are based on the complete characterization of the environment in which the thruster operates in. An accompanying task is to thereby provide parametric experimental data for model validation to fill gaps in the community database.

This chapter contains the relevant background information for understanding the problems facing high-power density gridded ion engine operation. This includes a brief introduction into operations of gridded ion engines and Hall effect thrusters (HET) and their relevant characterization techniques. Following this introduction to GIEs and HETs, an overview of flight history and facility effects on GIEs is presented, adopted from a previous journal publication in Foster and Topham, "A review of the impact of ground test-related facility effects on gridded ion thruster operation and performance," Phys. Plasmas **31**,030501 (2024).

1.3 Introduction to Electric Propulsion

Over the years, two EP systems have matured to regular implementation and use. The two systems are gridded ion engines and Hall effect thrusters. Both are electrostatic devices that ionize neutral propellant and then accelerate particles using electrostatic fields to produce thrust. There are three parameters often used to quantify the performance of these thrusters: 1) thrust-to-power ratio, 2) specific impulse, and 3) efficiency. The general governing equations for EP thrusters are described in the following subsection. Here the relevant equations are presented, but more in-depth derivations can be found in reference [5]. Following the general thruster principles section are two sections focused on relevant specific thruster principles to this work.

1.3.1 General Thruster Principles

1.3.1.1 Thrust

The rocket thrust equation is given as

$$\mathbf{T} = \frac{\partial}{\partial t}(\mathbf{M}_{sc}\mathbf{v}), \tag{1.1}$$

where $\mathbf{M}_{sc}$ is the rate of change of the mass of the spacecraft, and $\mathbf{v}$ is the spacecraft velocity. Changing the momentum of the propellant of the spacecraft results in a force equal and opposite on the spacecraft resulting in

$$\mathbf{T} = -v_{ex}\frac{dm_{propellant}}{dt}. \tag{1.2}$$

Here $m_{propellant}$ is the propellant mass and v_{ex} is the exhaust velocity.

The total mass of the spacecraft at any given moment in time is defined as

$$\mathbf{M}_{sc}(t) = m_{delivered} + m_{propellant}. \tag{1.3}$$

Here $m_{delivered}$ is the delivered mass or in other words the portion of the spacecraft that is constant during flight. Taking the time rate of change of equation (1.3) and substituting into equation (1.2) and equating the results to equation (1.1), a simplified ordinary differential equation (ODE) arises as

$$dv = -v_{ex}\frac{\mathbf{M}(t)}{dt}. \tag{1.4}$$

Solving the ODE with spacecraft velocity with $v_{initial}$ and v_{final} for initial and final velocities, and $m_{initial} = m_{delivered} + m_{propellant}$ and with $m_{final} = m_{delivered}$ for the initial and final spacecraft

mass. This results in the required delta-v written as

$$\Delta \mathbf{v} = v_{initial} - v_{final} = v_{ex} \ln \left(\frac{m_{delivered}}{m_{delievered} + m_{propellant}} \right). \tag{1.5}$$

The thrust on the spacecraft from the exhausted propellant of the engine is equal to and opposite of equation (1.2) resulting in

$$\mathbf{T} = v_{ex} \frac{dm_{propellant}}{dt} = v_{ex} \dot{m}_{propellant}. \tag{1.6}$$

Here $\dot{m}_{propellant}$ is the mass flow rate of the propellant defined as

$$\dot{m}_{propellant} = Qm, \tag{1.7}$$

where Q is the propellant particle flow rate in particles per second and m is the mass of the particles. In EP devices such as GIE and HET, thrust comes from ions due to their mass being far greater than the electrons. Neutrals do not contribute much to thrust either due to their low velocities. Kinetic energy to the ions is transferred via the electrostatic fields. Thus, equation (1.6) can be written as

$$\mathbf{T} \approx \dot{m}_i v_i = \sqrt{\frac{2m_i}{e}} I_b \sqrt{V_b}. \tag{1.8}$$

Here, $\dot{m}_i$ is the ion mass flow rate given as

$$\dot{m}_i = \frac{I_b m_i}{q}, \tag{1.9}$$

where I_b is the beam current, m_i is the ion mass, and q is the charge state. Additionally, v_i is the ion velocity defined as

$$v_i = \sqrt{\frac{2qV_b}{m_i}}. \tag{1.10}$$

Here, V_b represents the beam voltage, and e is the Coulomb charge and comes from $q = e$ for singly charged ions.

There are correction factors that must be applied to the thrust equation of (1.8) for both beam divergence and for multiply charge ion species. The resulting corrected thrust equation with correction factor for beam divergence is

$$\mathbf{T} \approx \dot{m}_i v_i = \alpha F_t \sqrt{\frac{2m_i}{e}} I_b \sqrt{V_b}. \tag{1.11}$$

The correction for beam divergence is given as

$$F_t = \frac{\int_0^r 2\pi r J(r) cos\theta(r) dr}{I_b}, \tag{1.12}$$

with r being the radius from the center axis of the thruster, θ being the divergence half-angle, and J being the ion current density. Correction for multiply charged states is given as

$$\alpha = \frac{\sum_{n=1}^{n=\infty} T_n}{T} = \frac{\sum_{n=1}^{n=\infty} \sqrt{\frac{1}{n}} I^{+n}}{\sum_{n=1}^{n=\infty} I^{+n}}, \tag{1.13}$$

where T_n is the thrust contributions of the n charged state ion species (i.e n=2 doubly charge ion) and I is the n charge state corresponding current contribution. Assuming that there are negligible beam current contributions from charge species greater than doubly charged, equation (1.13) simplifies to

$$\alpha = \frac{1 + \frac{1}{\sqrt{2}} \frac{I^{++}}{I^{+}}}{1 + \frac{I^{++}}{I^{+}}}. \tag{1.14}$$

1.3.1.2 Specific Impulse

Missions are defined by their required delta-v. The efficiency of the propulsion system affects how well a propulsion system can meet these delta-v requirements. Specific impulse (Isp) is defined as a measurement of thrust efficiency as a ratio of the thrust produced per the rate of propellant consumed and is given as

$$\text{Isp} = \frac{T}{\dot{m}_{propellant} g}, \tag{1.15}$$

where the constant g is equal to acceleration of gravity. The specific impulse of a GIE or HET is given as

$$\text{Isp} = \frac{v_{ex}}{g}, \tag{1.16}$$

by combing equations (1.6) and (1.15). Due to the mass differences between ions and electrons, thrust is produced by the ions. As a result equation (1.16) can be written in terms of v_i and $\dot{m}_i$. The result is written as

$$\text{Isp} = \frac{v_i}{g} \frac{\dot{m}_i}{\dot{m}_{propellant}}. \tag{1.17}$$

Equation (1.16) can also be substituted into equation (1.5) such that the delta-v equation can be written in terms of Isp as

$$\Delta \mathbf{v} = v_i - v_f = (\text{Isp} \cdot g) \ln \left(\frac{m_{delivered}}{m_{delivered} + m_{propellant}} \right). \tag{1.18}$$

The efficient of the use of the propellant is quantified as the ratio of ion mass flow rate over the total propellant flow rate and is called mass utilization efficiency and is written as

$$\eta_m = \frac{\dot{m}_i}{\dot{m}_{propellant}} = \frac{I_b}{e} \frac{m_i}{\dot{m}_{propellant}}. \tag{1.19}$$

The mass utilization corrected for multiply charged ion species is given as

$$\eta_m = \alpha_m \frac{I_b}{e} \frac{m_i}{\dot{m}_{propellant}}, \tag{1.20}$$

where α_m is the correction factor for mass utilization due to multiply charged species. The general equation is

$$\alpha_m = \frac{\sum_{n=1}^{n=\infty} \eta_n}{\eta} = \frac{\sum_{n=1}^{n=\infty} \frac{1}{n} I^{+n}}{\sum_{n=1}^{n=\infty} I^{+n}}, \tag{1.21}$$

and the correction factor for doubly charge ions only is defined as

$$\alpha_m = \frac{1 + \frac{1}{2} \frac{I^{++}}{I^{+}}}{1 + \frac{I^{++}}{I^{+}}}. \tag{1.22}$$

Combing equations (1.11) and (1.19), Isp can be written as

$$\text{Isp} = \frac{\alpha F_t \eta_m}{g} \sqrt{\frac{2eV_b}{m_i}}, \tag{1.23}$$

where the uncorrected mass utilization equation is used since the corrected thrust equation defines the singly ionized ions as the beam current.

1.3.1.3 Efficiency

The electrical efficiency of the thrust is defined as

$$\eta_{elec.} = \frac{P_b}{P_T}, \tag{1.24}$$

where P_b is the beam power and P_T is the total electrical power inputs.

The cost of producing ions or ion cost production has unit of W/A or eV/ion and is

$$\eta_d = \frac{P_d}{I_b}. \tag{1.25}$$

Here, P_d is the ratio of power to produce the discharge plasma and I_b is the extracted ion current of the beam current.

The total efficiency of the thruster is defined as

$$\eta_T = \frac{P_{jet}}{P_{in}} = \frac{T^2}{2\dot{m}_{propellant} P_{in}}, \tag{1.26}$$

where P_{jet} is the kinetic thrust power of the beam or jet power and P_{in} is the total electrical input power. Jet power is defined in terms of thrust using equation (1.6) as

$$P_{jet} = \frac{1}{2}\dot{m}_{propellant} v_{ex}^2 = \frac{T^2}{2\dot{m}_{propellant}}. \tag{1.27}$$

The total corrected efficiency combing equations (1.11), (1.26), and (1.19) is

$$\eta_T = (\alpha F_t)^2 \eta_{elec.} \eta_m. \tag{1.28}$$

The ratio of thrust-to-input power is another key metric used to quantify engine performance– how much thrust per power input and is given as

$$\frac{T}{P_T} = \frac{T\eta_{elec.}}{P_b}, \tag{1.29}$$

where $\eta_{elec.}$ is the electrical efficiency and P_b is the beam power. High ion acceleration and high mass utilization results in high specific impulse. Lower the ion mass would increase specific impulse but would lower thrust and the thrust-to-power ratio.

Thrust-to-power can also be written in terms of total truster efficiency and specific impulse as

$$\frac{T}{P_T} = \frac{2}{g}\frac{2\eta_T}{\text{Isp}}. \tag{1.30}$$

1.3.2 Gridded Ion Engine

Gridded ion engines have the most dynamic performance envelope of any current EP device. There are a number of GIEs legacy deep space flight operations, including Deep Space I (DSI) and Dawn [6, 7]. A gridded ion engine has a discharge cathode where electrons are created. These electrons are supplied to the discharge chamber. In the discharge chamber the effective mean free path of the electrons is increased by the superposition of a magnetic field. This increases the probability that an electron will undergo an inelastic collision with a neutral propellant atom before it arrives at the anode surface. There are a plethora of different magnetic field designs that have been explored in the past to confine electrons for improved performance [5]. Two configurations have emerged over the years as the most dominate types and they are the divergent-field and ring-cusp. As a

plasma is made in the discharge chamber, the ions drift towards the grid electrodes. The first grid, known as the screen grid, is either allowed to float to the discharge plasma potential or tied to cathode potential. A second grid, the accelerator (accel) grid, is held at a sufficiently large negative potential to prevent back-streaming external electrons from entering the discharge anode. The gap between the two is often less than a few millimeters to limit space-charge effects. The large negative potential on the accel grid creates a negative sheath potential that extends past the screen grid into the discharge chamber plasma. This pulls the ions towards the screen grid and additionally the extended accel sheath helps with the ion optics and prevents direct ion impringment on the screen and accel grids. As the ions enter the gap between the grids, the ions are accelerated and focused through the holes of the accel grid. Sometimes a decelerate grid is added as a third grid and is at a low magnitude negative value that keeps energetic backflowing ion impringment on the accel grid. As the ions exit the grids, a very well collimated ion beam is formed and needs to be neutralized to prevent beam blowup and to maintain current neutrality of the spacecraft. An external neutralizer cathode is used to produce electrons that are injected into the beam. A sample electrical circuit diagram of a NASA-style gridded ion engine is found in figure 1.1. The corresponding potentials during ground testing are displayed in figure 1.2.

1.3.2.1 Beam Neutralization

Beam neutralization is a key aspect of gridded ion engine operation. As ions are accelerated out and form the beam, the spacecraft would charge up negatively. This would lead to beam turnaround or space-charge drag. An external neutralizer cathode expels the electrons to the ion beam sourced from the electrons collected by the discharge anode. This keeps the spacecraft and the beam neutral.

The coupling of the neutralizer to the beam is described by the true-coupling voltage. In Figure 1.2, this is V_{cp} which is obtained by the potential difference between the beam and neutralizer cathode. In ground testing V_{cg}, the potential of neutralizer cathode with respect to facility ground, is often used as metric of coupling of the neutralizer to the beam. This is because it is assumed the potential in the beam approaches the potential of the facility. However, this V_{cg} is an indicator of the neutralizer coupling to the facility and assumes a fully neutralized beam. This can be argued to be true during ground testing as the beam is almost always neutralized by some point in the facility because the beam will eventually terminate on the walls.

Ensuring beam neutralization in space was a necessity. This was a heavy area of focus in GIE technology development and was the primary mission of SERT I of 1964 [8]. Heavy emphasis has been made on the modeling of beam neutralization. A brief summary of modeling efforts over the years can be found in the appendix that was previously submitted for an internal class assignment. However, ensuring the beam is properly neutralized during ground testing via the neutralizer can

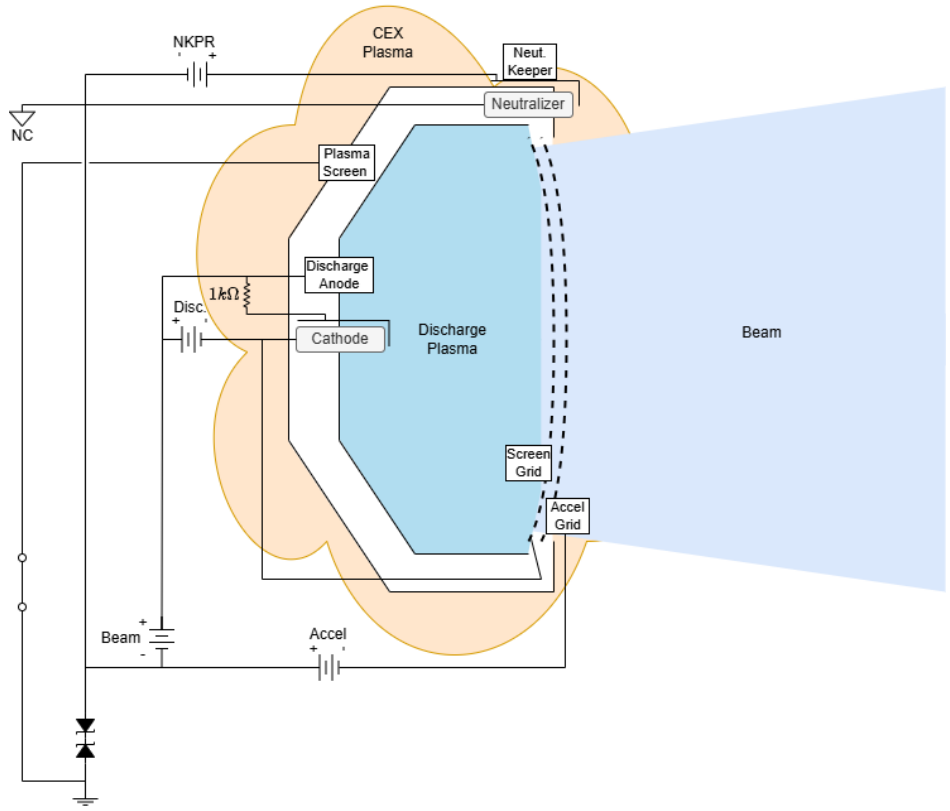

Figure 1.1: Gridded ion engine circuit diagram. The potential of the neutralizer cathode (NC) serves as the reference potential for the thruster. The high energy ion beam is formed by acceleration of the ions from the high potential difference between the grids. This high potential is created by elevating the potential at which the ions are created at in the discharge chamber with respect to NC via the beam power supply. An Accel power supply on the downstream grid is then biased negative to NC to repeal electrons from streaming into the discharge chamber.

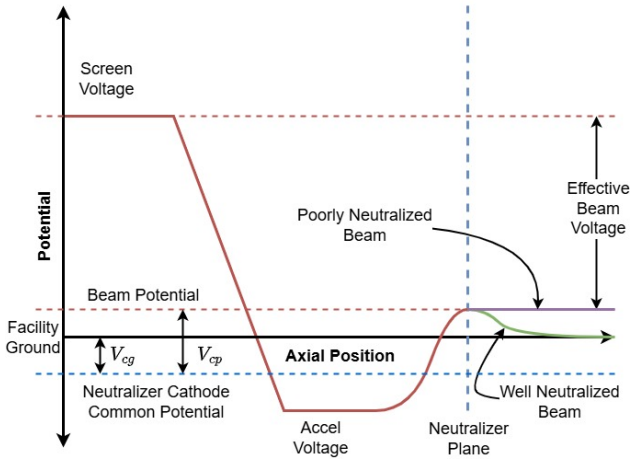

Figure 1.2: Gridded ion engine potentials in operation. The screen voltage is the potential at the first (screen) grid created by the elevation in potential of the discharge chamber by the beam power supply. The accelerator voltage is the potential of the second (accelerator) grid using the accelerator power supply. Downstream of the grids, the exhausted positive ions create a high potential but as they reach the neutralization plane, the beam becomes well neutralized decreasing in potential. However, in a non-well neutralized beam this potential will propagate downstream lessening the effective beam voltage lessening the effective beam current that can be extracted and lowering the produced thrust.

at times prove to be difficult. If not done properly, parameters like neutralizer margin (discussed in the next section) can be calibrated wrong during ground testing and cause havoc during spaceflight such as leading to thruster and system propulsion failure. This is further discussed in follow section on facility effects as well with ground testing of Hayabusa 2.

1.3.2.2 Neutralizer Characterization and Margin

The neutralizer characterization and margin are used to define the minimum power operating conditions and minimum flow rates the neutralizer can operate at without transiting to plume mode. Plume mode occurs when there is insufficient ion production to support the required electron emission in a plasma-bridge device—such as in a hollow cathode neutralizer [9]. In this condition an unstable sheath forms to facilitate extraction of the electrons to counter the space-charge caused by demanding an electron current which exceeds the Bohm criterion. Characterizing the neutralizer operating limits defines the flow rate margin and defines the region of flow below which high voltage operation of the neutralizer cathode occurs which can limit cathode lifetime. Neutralizer margin is import characteristic because the neutralizer propellant flow does not contribute to thrust production, decreasing the mass utilization efficiency.

Characterizing the neutralizer and determining the margin is done by adjusting the flow rate,

then recording the corresponding keeper voltage and coupling voltage. This is repeated at various throttle conditions (i.e. beam currents). The minimum flow that can be used before transition from spot to plume mode is the neutralizer margin. In spot mode, the neutralizer plasma at the orifice hole is quiescent and stable. In plume mode, there is a demand for a higher electron emission current than can be supported by the Bohm velocity for a stable sheath. This is due to an insufficient number of low-energy ions resulting in a space-charge flow of electrons. Plume mode is a dangerous mode to operate in as it is destructive to the cathode and will shorten the overall lifetime. This is due to the space-charge that causes the ions to be accelerated back to the neutralizer surfaces that are at cathode potential and this leads to sputtering of the substrates. As a result, determining the minimum power levels for a given flow rate before the plume mode transition is critical.

1.3.2.3 Spacecraft-plume Interactions

Even in spaceflight there is ambient plasma that surrounds the spacecraft due to the beam and discharge plasmas. The interaction of the thruster with the ambient and plume plasmas in space needs to be understood to prevent any mishaps or unexpected results. Some models have shown that there are large amounts of high-energy elastically scattered ions, even at 90° from the thruster plane [10, 11]. Theses may or may not be observed during ground testing due to elevated background pressures by decreasing the observed energies of theses ions. As a result, spaceflight planning may place components too close to the exit plane of the thruster and be inadvertently sputtered away by high-energy ions.

Additionally, understanding how the plume of the thruster interacts with the ambient environment is also important, but even more so for future plans of running an array of engines. Some work has been done in modeling and running multi-array engines but with many unanswered questions about performance in space to still be answered as multi-array system running synonymously has yet to be performed [12, 13, 14, 15, 16, 17]. The coupling of the spacecraft and thruster to its surroundings must be characterized and the impacts of the facility on its performance need to be identified to get accurate spaceflight performance by adjusting for these facility effect contributions.

1.3.3 Hall Effect Thruster

Hall thrusters have also be used in a number of missions, with Psyche being one of the most recent. With the trade-off of lower Isp and lifetimes, Hall thrusters have been used in a lot of satellite-keeping and orbit transfers due to their higher thrust yields. An electromagnet is created with an iron core that has a channel etched into it. At the base of the channel there is an anode electrode. A cathode to supply electrons is placed either at the center of the thruster or mounted externally. A

discharge power supply provides the axial electric field between the anode and cathode on which the electrons travel to the anode. Their progress is impeded by a strong radial magnetic field applied by the electromagnet. An ExB drift occurs resulting in an azimuthal current that energizes the electrons to ionizing potentials. As neutral gas is injected into the channel, the energetic electrons ionize the gas and the ions are accelerated out due to the electrostatic axial field. The corresponding beam is neutralized by other electrons sourced from the cathode. Although these systems are proven, there are complex phenomenon in Hall effect thrusters that are currently unexplained. The rate of electron diffusion across the magnetic fields lines, anomalous diffusion, is much greater than theocratically predicated. In addition, the discharge voltage and current experience a "breathing mode" low-frequency oscillation. It has been suggested that these breathing modes are due to predator-prey behaviors between electrons and neutrals [18, 19]. There is a significant amount of active research into the many instabilities that occur during HET operation. Figure 1.3 has an example of a HET with a center mounted cathode and Figure 1.4 has the corresponding potentials.

1.4 Intro to GIE Facility Effects

The following has been adopted from a previous journal publication in Foster and Topham "A review of the impact of ground test-related facility effects on gridded ion thruster operation and performance", Phys. Plasmas **31**,030501 (2024).

1.4.1 Abstract

A key consideration in the interpretation of ground test data of electric propulsion devices purposed for spaceflight is understanding how facility-effects influence thruster operation. This understanding is critical to the prediction of actual thruster performance in space. The necessity of science-based predictions gleaned from ground tests are particularly critical at higher thruster power levels. Operation of engines at higher power levels in vacuum chambers leads to considerable elevation in background pressure, background plasma density, and backsputter rates. This review examines the influence of ground test facility effects on gridded ion thruster operation. Ground test operation is compared with flight data, where available, to obtain a clear picture of operational differences. Mitigation strategies to alleviate facility effects are also commented upon.

1.4.2 Introduction

Gridded ion thruster technology has been used on missions ranging from commercial communication satellite station-keeping to deep space exploration. This technology has been demonstrated over a broad range of power levels extending from 2.3 kW on the Deep Space 1 mission to the

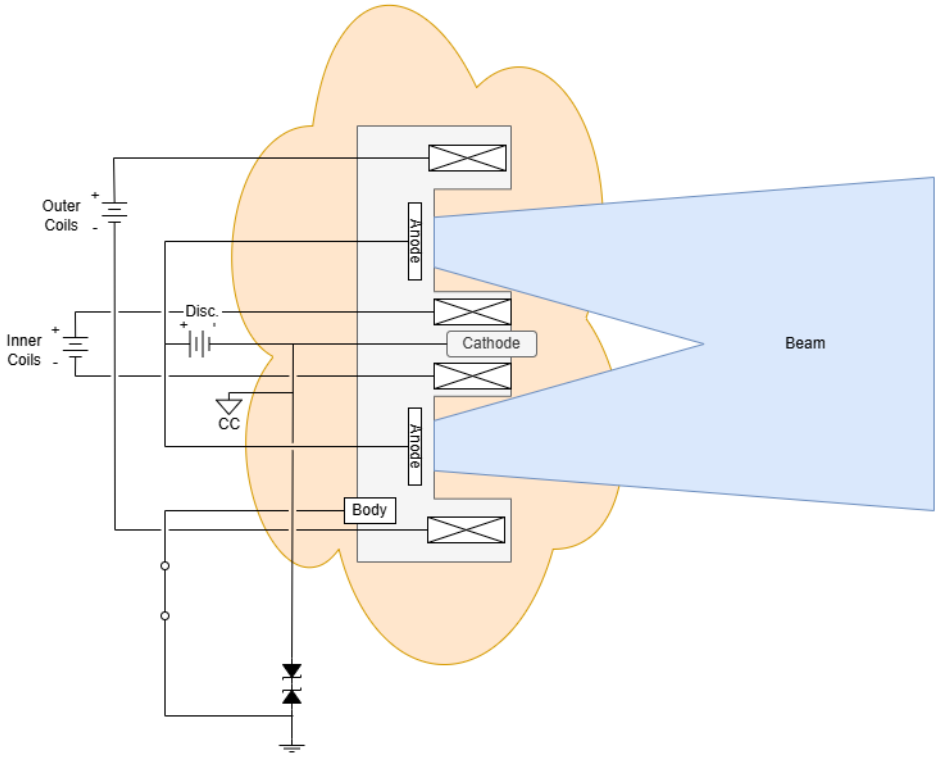

Figure 1.3: Center-mounted cathode Hall effect thruster circuit diagram where a plasma is sustained between the cathode and anode via a discharge power supply. Acceleration of ions created in the channel occurs due to the axial electric field. A radial magnetic field is produced by electromagnets, retarding immediate electron collection to the anode. An ExB drift in the angular direction arises resulting in the acceleration of electrons that enhances electron-impact ionization. Extra electrons from the cathode neutralize the produced ion beam.

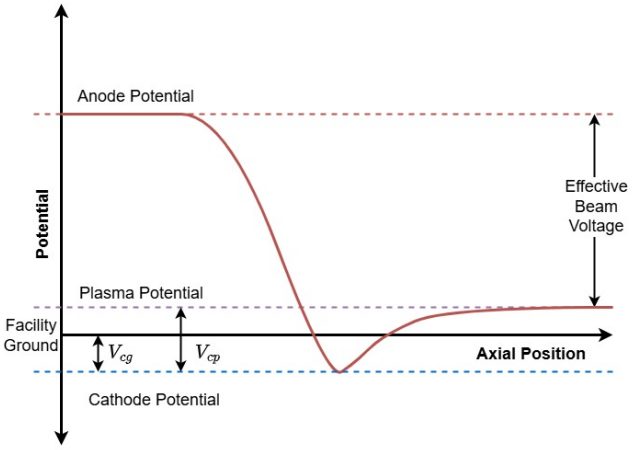

Figure 1.4: Hall effect thruster potentials are in reference to the potential of the cathode. The Discharge power supply elevates the anode with respect to cathode potential. As ions are accelerated out and electrons are dragged along, the plasma plume will saturate to a potential. The difference between this potential and the anode potential dictates the effective beam voltage which this in turn dictates the amount of ions that can be extracted and resulting thrust.

200-kW testbed engine (Fig. 1.5) operated at NASA Glenn back in the 1960s [20, 21]. As plans are formulated for human missions to the moon and Mars, gridded ion thruster technology is an attractive, scalable propulsion option, but high-power operation at 100 kW and above, with associated long operating times, will be required [22]. In this section, an overview of gridded ion thruster operation and its subsystems are discussed. This will then be followed by a synopsis of ground testing procedures along with an overview of facility effects considerations for higher power operation and testing. Following the introduction, a detailed review of a range of effects brought on by the interaction of the thruster during operation with the facility and the associated impacts on assessing engine performance. Space flight data are also presented and compared, where possible, with ground test data to provide insight into the magnitude of the facility effects. Potential mitigation and correction strategies are then commented on with identifications of needed areas of research, followed by a summary with concluding remarks. It should be noted that while most of the discussion described herein focuses on direct-current (DC) ion thrusters primarily derived from NASA test and flight data, and to a limited extent Japan Aerospace Exploration Agency (JAXA) microwave engine, the discussion in general, is broad and thus applies to most gridded ion thruster systems.

1.4.2.1 Gridded ion operation

Gridded ion engines are among the most efficient electrostatic engine systems built and flown to date and as such, are an attractive system for high-power electric propulsion. As can be seen in

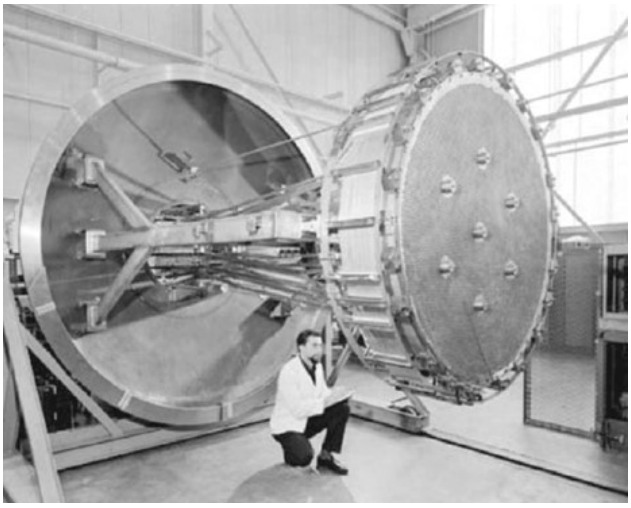

Figure 1.5: 1.5 m mercury ion thruster at NASA VF 6—Engine operated at 200 kW [21]. Reproduced with permission from Patterson and Sovey, J. Aerosp. Eng. 26, 300–316 (2013). Copyright 2013 American Society of Civil Engineers.

Fig. 1.6, technology also has the largest performance envelop of any electric propulsion system under investigation with applications extending to nuclear electric propulsion missions. The large performance envelop enables varied throttling for deep space missions. In fact, the first nuclear electric propulsion system ever flown employed a gridded ion thruster on the SNAP 10 A mission [23].

The ion thruster consists of essentially three subsystems: (1) the discharge chamber, where the beam plasma is formed, (2) ion acceleration grids, where high voltage beam extraction and acceleration takes place, and (3) the neutralizer which injects neutralizing electrons into the extracted ion beam. Figure 1.7 depicts a two-grid ion engine with its power supply configuration [6]. Inside the gridded ion engine's discharge chamber, a plasma is generated. The discharge chamber typically features a magnetic field, either a divergent or consisting of alternating polarity rings forming magnetic cusps that serve to increase ionization efficiency of primary electrons and to reduce the electron loss rate. The function of the discharge chamber is to provide ions that are subsequently extracted to produce the ion beam. The discharge plasma can be produced electrodelessly via radio frequency (RF) [25] or microwave excitation—via electron cyclotron resonance [26] or via the application of a direct-current (DC) voltage applied between a thermionic emitter, such as a hollow cathode, and the anode, where the anode collects emitted charge. The ions drift toward the exit plane containing closely spaced ion extraction grids. Ions that enter the grid gap are accelerated across the potential difference between closely spaced multi-aperture grids to form the beam. As the beam is exhausted from the thruster, a neutralizer emits electrons that couple to beam, neutralizing it. The potential distribution downstream of the engine is shown in Fig. 1.8. The effective

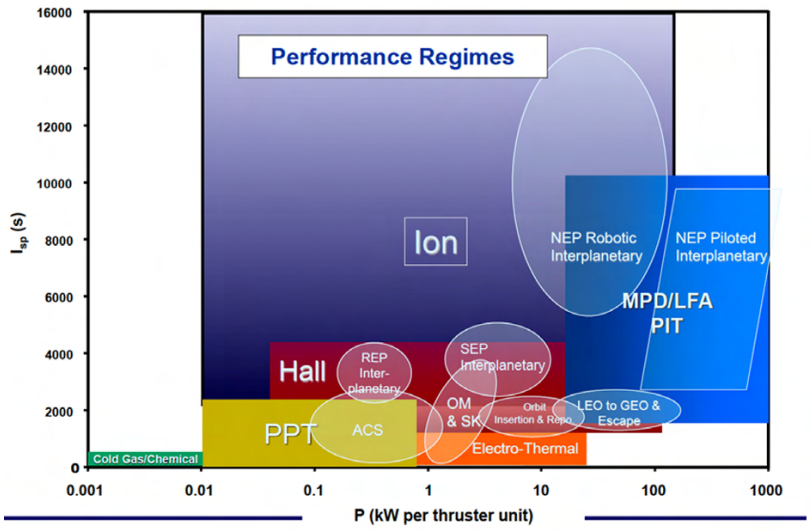

Figure 1.6: Gridded ion performance envelope. Reproduced with permission from M. Patterson, private communication (2022) [24].

beam voltage (the ion acceleration voltage) is defined as the voltage between the screen voltage and the beam potential. Thus, a poorly functioning neutralizer results in a reduced beam voltage which leads to reduced thrust. Each of these three subsystems may be affected to varying degrees by the physical presence of the facility (wall effects) and physical processes therein (gas phase).

The neutralizer assures both current and charge neutralization. Current neutralization (current balancing) refers to the emission of equal amounts of electron and ion currents from the thruster such that the thruster does not charge up. Otherwise, thruster charge build-up would lead to beam turn-around—which occurs when the beam partially or fully bends back to the thruster due to potential differences between the thruster and the beam. Charge neutralization refers to equal amounts of electrons and ions in the beam itself such that it remains nearly quasineutral, which facilitates beam transport and prevents beam blow up. In most cases the neutralizer is externally mounted, with the notable exception of variants that emit both alternating negative and positive ions to achieve current neutralization[27]. There is typically a coupling plasma present, formed at the neutralizer, that forms a low impedance path or "bridge" to the ion beam [28, 29, 30, 31, 32]. The externally injected neutralizing electrons enter the beam with greater thermal speeds than that of ion beam ions owing to the mass difference. The actual underlying mechanisms in the beam that give rise to neutralization are complex and remain poorly understood [33]. It is hypothesized that the positive potential on axis of the beam traps low energy electrons to enable neutralization. Instabilities are assumed to play some role in the turbulent mixing of electrons and ions to give rise to neutralization [34]. Recent studies show evidence that electrostatic solitary waves (ESWs) [35, 36] excite Trivelpiece–Gould (TG) surface waves, in the beam during the neutralization process

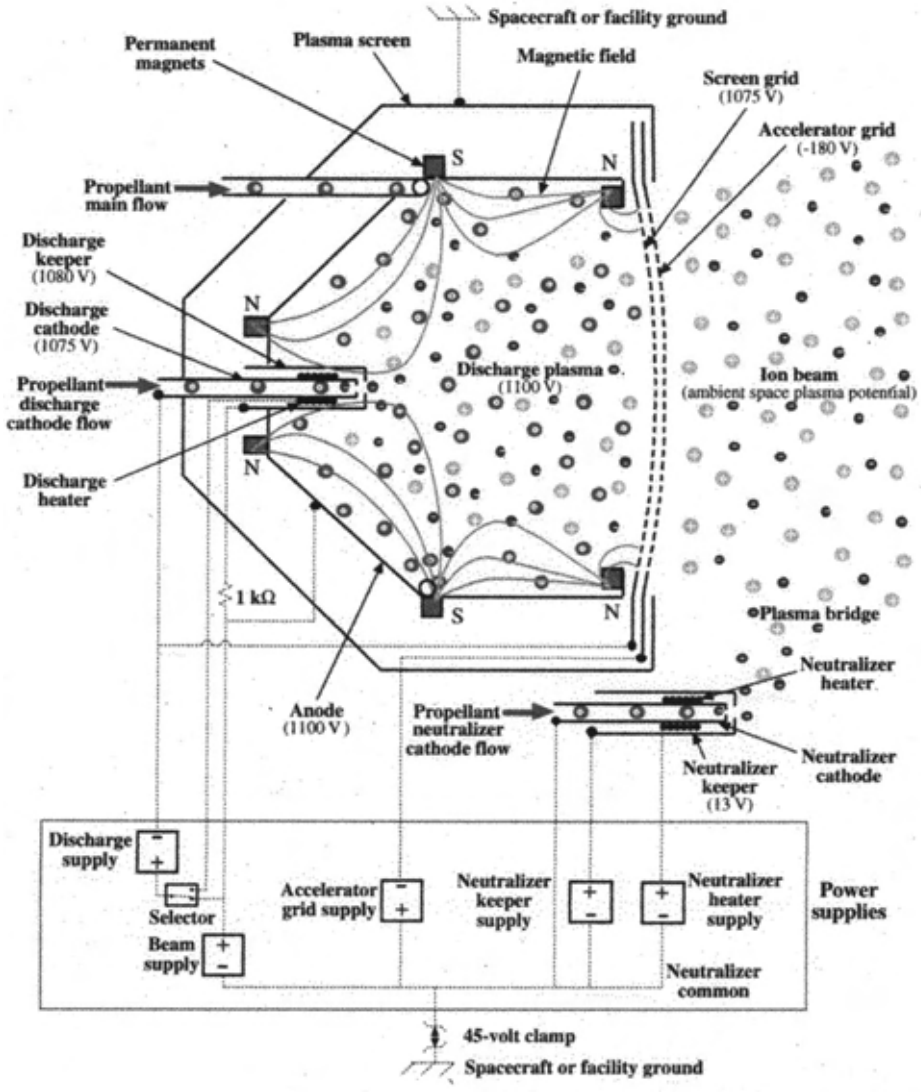

Figure 1.7: Schematic depiction of gridded ion thruster subsystems [6]. Reproduced with permission from J. R. Brophy, "NASA's Deep Space 1 ion engine (plenary)," Rev. Sci. Instrum. 73(2), 1071–1078 (2002). Copyright of AIP Publishing.

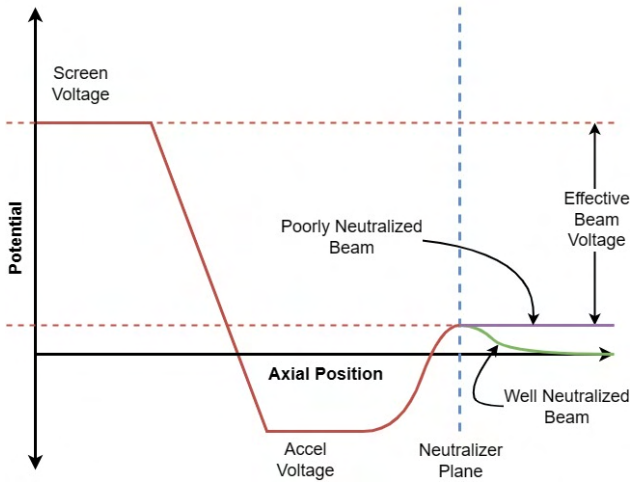

Figure 1.8: Potential distribution between grids up to the hypothetical neutralization plane.

[37, 38].

1.4.2.2 Test preparation for space flight

To qualify a thruster for space, ground testing in a relevant environment is required. The ground test must be carried out in a manner such that both performance and lifetime are accurately assessed before flight. Ground testing is particularly challenging for engine systems proposed to support human missions to Mars. These systems are expected to include arrays of 100 kW-class engines in arrays totaling over a MW in total thruster power [39]. This is to be contrasted with the highest power system under development at this time, the 12.5 kW advanced electric propulsion system (Hall thruster) and the 8 kW NEXT engine (gridded ion). Associated with high power operation, is increased propellant throughput, and thus the accompanying need for increased facility pumping speed to maintain appropriate background pressure. Moreover, at higher powers, there is the need to manage the increased backsputter rate from beam- chamber wall interactions—which invariably leads to higher deposition rates on the engine. Past studies recommend that to minimize facility effects such as enhanced background plasma density associated with charge exchange production which scale with the elevated background pressure the engine needs to operate at pressures of less than 1.5×10^{-5} Torr [40]. Under such conditions, accelerated wear on grids due to charge exchange ions approaches the charge exchange current levels observed in space. Considering pumping speed limitations of existing facilities, it will be necessary to characterize high power engines at pressures near the upper limit of desired background or perhaps even higher. For example, at high specific impulse operation and power levels up to 2.5 MW, pumping speeds approaching 50 ML/s would be required for such systems, which is currently first order of magnitude higher than the state of the art [41, 42, 2]. In this respect, to credibly develop flight, high-power gridded ion engines, one

must be able to identify and separate facility-related effects present during ground tests from actual thruster related processes which would otherwise skew interpretation of engine performance and lifetime in space. The general design of gridded ion engines has an ion acceleration zone defined between grids takes place over distances that are much smaller (d_{grid}) than scattering mean free paths of interest ($\lambda_{mfp} = \frac{1}{\sigma n_n}$) such as that of charge exchange (i.e., $\lambda_{mfp} \gg d_{grid}$), resulting in ions being assumed to be collisionless between the grids. Correction for background gas ingestion into the discharge chamber is also straightforward. Nevertheless, there are local and downstream processes such as charge-exchange (CEX) plasma formation that can impact overall operation in facilities and thus can have a major impact on engine performance and lifetime. Additionally, beam contact with chamber walls can augment neutralization processes which would not appear in space as well as give rise to significant backsputtering that can augment apparent engine life by obscuring grid erosion by facility-carbon deposition, giving rise to uncertainty to actual in-space lifetime estimates.

As an example of the reaches and commingling of facility effects during experimental design and operation of ground test, a brief overview of facility effects on beam neutralization is highlighted here. Being the neutralization process occurs outside the enclosed thruster, the neutralization process is largely affected by facility effects. The sensitivity to the neutralization process to background gas density is not well understood or characterized as one may suspect the electron temperatures to decrease as a function of increased background gas density. It has also been shown that the beam potential profile is affected by the presence of the chamber walls via limitations in beam potential expansion [43]. As a result, the potential difference from the beam to the coupling neutralizer-bridge plasma may also alter electron temperatures entering the beam. Premature termination of the beam less than 10 beam diameters downstream is also shown to affect beam expansion [44] but has yet to be well characterized experimentally to the knowledge of the authors. Adding to the complexity of facility effects on neutralization is electrical configuration of the thruster relative to the test facility. The thruster system in ground tests is typically isolated from earth-ground using an isolation transformer. The neutralizer cathode serves as the common tie point reference and is also isolated from ground using a Zener diode clamp, allowing the thruster to be floated from earth-ground potential but still maintaining a tethered reference point such that thruster potential does not runaway. However, limited studies have been done to validate this method creates a spacelike test condition, meaning, does the tethered floating condition settle at a spacelike operating condition with reference to the ground potential of the facility such that beam expansion is spacelike? Or should the thruster system be floated at a specified biased during ground tests? Are there additional effects of this engine potential relative to the facility on the neutralization processes and pathways in conjunction with the effects on beam potential expansion? In addition, how do the effects of the engine electrical potential with respect facility ground scale with

increased background pressure? The electrical configuration of the thruster adds to the complexity presented by facility effects on neutralization. Understanding and quantifying the processes and mechanisms linked to facility effects on systems, such as on beam neutralization, during ground tests is critical to mimicking a spacelike environment.

Philosophically, ground testing is a vital element of space qualification. The challenge is in understanding the test and how it translates to operation in space. On orbit, gas pressures are less than 10^{-9} Torr (at 1000 km) and decrease with increasing orbital radius [45]. This pressure is some three orders of magnitude lower than typical operating pressures of ion engines on the ground. At elevated background pressure, discharge properties can be altered via ingestion of background gas. Additionally, ion grid lifetime in test facilities is not simply driven by charge exchange erosion derived from neutrals escaping from the engine but rather the balance between increased chamber-derived charge exchange flux associated with elevated background pressure and deposition due to thruster sputtering of facility walls. Ion beam neutralization is also drastically different from the process prevailing in space. In general, charge and current neutralization are dependent on the neutralizer-to-ion beam plasma bridge properties, which are affected by the presence of nearby wall surfaces, background plasma conductivity, and collisions with background gas. The ion engine also consists of high voltage insulators whose tendency to flashover depends on background pressure. It should also be pointed out that the local Earth magnetic field may even influence beam symmetry and the introduction of anisotropy of charge transport in the discharge itself and in the beam, as compared with space, where beyond low Earth orbit (LEO) these are negligible. Test chamber plasma density is much higher than that in space by two–three orders of magnitude. In general, test chambers cannot practically simulate the large length scales over which the beam interacts with the local plasma as occurs in space [46]. Indeed, Wang has shown that the potential of the beam and its profile cannot be simulated in finite sized vacuum chambers because the location of the bounding walls impose a limit on plasma expansion of the plume in contrast to space [47]. In this respect there are a number of potential areas of concerns regarding interpreting engine operation in Earth-based test facilities. Fortunately, a wealth of knowledge regarding facility effects can be gleaned from in-flight test data. Six flights in particular,—SERT 1, SERT II, Deep Space 1, Hayabusa 2, Dawn, and DART—provide a range of insight into how well operation in ground facilities faithfully replicates actual space operation.

In this paper, we review reported facility related effects on ion engines operation dating back to the 1960s. We also survey experiments and modeling efforts aimed at understanding these effects and pose a range of experiments aimed at clarifying facility-related effects on this technology. We review in-flight engine studies where engine performance in space—the gold standard for reference performance—is compared with its respective ground test operation. The goal of this cursory review that aims to compile credible facility effects associated with gridded ion operation

and weigh the relative impact on the interpretation of engine operation in space.

1.4.3 Review of Facility Effects

The operating conditions during space flight and ground tests differ drastically. Figure 1.9 schematically illustrates key thruster plasma-chamber wall interactions that are not present in space. Table 1.1 contrasts the differences between space and ground testing environments. In space, background pressure and ambient plasma densities are low, dropping significantly with increasing altitude above LEO, represented by the lighter background purple of Fig. 1.9. The earth's magnetic field drops nearly an order of magnitude from its value at LEO (roughly half that of the surface magnetic field) at a 7000 km altitude. The neutralizer which establishes the common reference for the engine system is typically tied to spacecraft ground via Zener clamping diodes. In this respect, for the system to faithfully represent space conditions, it must essentially be completely floating. Currents from space plasma can contribute to a limited degree to charge and current balance if the spacecraft chassis surfaces are exposed to the space plasma and are conducting. Yet/However owing to low current densities in LEO (ion current density $\sim \mu$A/cm^2) [48] and at higher orbital distances, this effect is small. However, off nominal operation of the neutralizer, for example, such as conditions where there is finite conductivity between neutralizer common and the spacecraft chassis can lead to the double probe effects where chassis can be driven negative leading to potentially damaging spacecraft sputtering from back flowing CEX ions. In general, the issues that affect or obfuscate interpretation of ground test data can be categorized into three problem areas: (1) the electrical and magnetic interactions of the thruster plume and neutralizer plasmas with the facility, (2) gas phase collisions with background and thruster derived neutrals, and ionized gas, and (3) physical plasma–material interactions that give rise to processes such as sputtering and subsequent deposition. Often these problem areas are interconnected as well.

Table 1.1: Comparison between space and ground test engine operation conditions.

Condition (units)	**Space (LEO)**	**Ground Testing**
Background pressure (Torr)	$< 10^{-9}$	$> 10^{-7}$
Background plasma density (1/cc)	$< 10^{6}$	$< 10^{9}$
Earth's magnetic field strength (G)	< 0.35	~ 0.5

1.4.3.1 Electrical and magnetic effects—Thruster plume and plasma environment interactions

Ion beam neutralization processes are difficult to access in a vacuum chamber. The system of circulating currents that can develop during ground testing of a gridded ion engine, as illustrated in

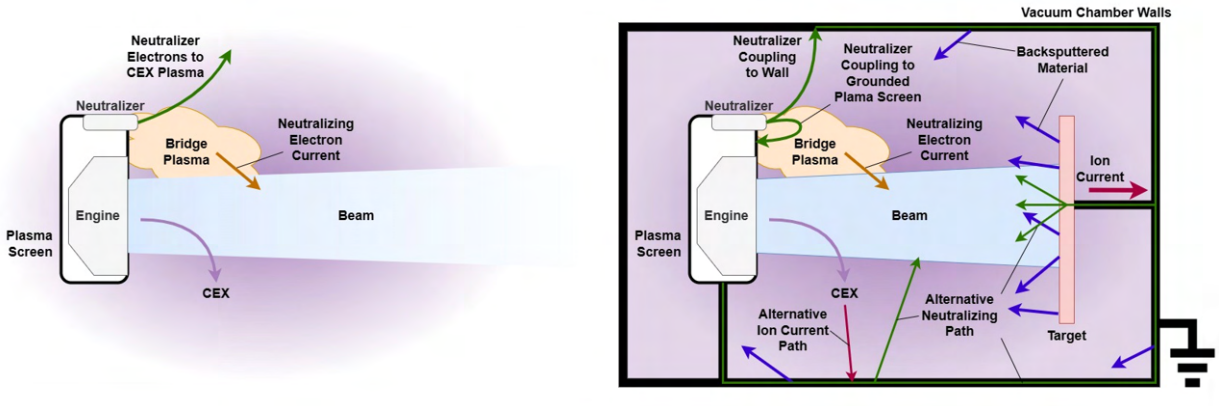

Figure 1.9: Comparison between space (a) and ground test (b) engine operation. The darker purple color represents the increased neutral gas and plasma densities. Alternative neutralization pathways through the facility walls are in green. Backsputtered material from the walls are depicted by the blue arrows.

Figs. 1.9 and 1.10, complicates the interpretation of neutralizer operation. The circulating current systems are dramatically different in the case of ground tests. Perhaps the biggest problem is related to the function of the neutralizer itself. The neutralizer's function is to rid the discharge chamber of excess electrons to prevent engine and spacecraft charging. However principle, it does not matter where these electrons are rejected to. In ground test facilities the neutralizer electrons are collected on grounded structures of the engine housing or on the grounded walls of the facility in addition to the beam, resulting in not all neutralizer electrons traveling directly to the beam as intended. As such, proper experimental design of the electrical configuration of the thruster housing and relative position of the thruster to grounded chamber components must be made to limit these alternate neutralization pathways[49], but careful design will not eliminate these alternate neutralization pathways completely. In principle an ion engine can operate with a poorly neutralized beam in a ground test facility with the beam current neutralized via the grounded target. Ambient charge exchange plasma also supplies electrons along the path of the beam. A key question is, therefore, how does one subtract out these effects to recover or predict how the engine would function in space?

In general, a measure of the ease with which neutralizer emitted electrons are transported to the beam is coupling voltage—essentially the potential difference between the neutralizer cathode and the beam. In space, a low coupling voltage corresponds to a well coupled beam. In a vacuum facility, low coupling voltages can arise if neutralizer electrons can flow to nearby grounded surfaces. One issue is that the neutralizer-to-beam coupling voltage can impact the operating mode of the neutralizer. The higher coupling voltage operating mode, which is associated with a condition known as the plume mode, can lead to reduced neutralizer lifetime [50, 51]. In the plume mode,

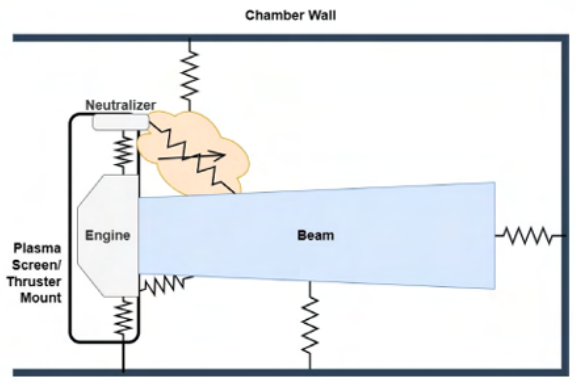

Figure 1.10: Electrical circuit depiction of DC electrical pathways associated with beam neutralization with coupling represented by resistors.

the neutralizer discharge voltage between the keeper electrode is higher, electrically noisy, and is associated with a luminous plume extending from the cathode, generated largely by energetic electrons ionizing and exciting escaping gas locally. It is therefore desired to have the coupling voltage as low as possible but under conditions where electrons flow exclusively into the ion beam. In this case, the neutralizer tends to operate in the "spot" mode, which is associated with low keeper voltages and low peak-to-peak voltage oscillations. Getting this operating mode correct is a key aspect of engine-neutralizer operation. In general, one increases gas flow to the neutralizer cathode to drive it from plume to spot mode. This flow characterizes the neutralizer's flow margin. A neutralizer operating in spot mode on the ground may give the false impression of greater flow margin than that which would be required for space ultimately leading to a shorter lifetime in space. Ideally, it would be desirable to track where all neutralizer derived electrons go. If this were possible then one could assess true neutralizer flow margin by either eliminating the alternative pathways or computationally predicting neutralizer operation without such pathways.

Perhaps the most obvious difference between operating in space and in a ground test facility is the fate of the thrust producing beam. As discussed previously in Figs. 1.9 and 1.10, the beam terminates on a surface or target typically at ground potential. In this regard, the ion beam can be neutralized on grounded surfaces—with ground providing the inflow of neutralizing electrons as well as the emission of secondary electrons and backsputtered material. This assures current neutralization if the target is grounded. The secondary electrons can propagate upstream and contribute to beam charge neutralization. The contribution, however, from secondaries is relatively small since the yield, at least for xenon, for beam energies of state-of-the-art medium power thrusters such as the NEXT ion engine ($<$2 kV) is less than 0.1, but it increases for high powered, higher beam voltage engines. For example, the beam energy for the HiPEP ion engine designed for a nuclear electric propulsion system was approximately 5500 V which translates to a considerably

higher secondary electron emission yield [52]. For example, at 5500 V, the yield of argon ions on tungsten is 0.3 and increases linearly with incident ion energy. In general, there is a lack of data on noble gas ion-derived secondary electron emission at relevant energies, which indeed will be a necessary area of research to understand high power engine operation in facilities [53].

In conventional ion engine ground tests, a Zener diode is incorporated to isolate neutralizer common from ground. If the potential difference between neutralizer common and ground exceeds 45 V, the Zener will clamp and current can be passed under these conditions allowing for charge neutralization to occur at the grounded beam dump. The neutralizer coupling voltage for a properly isolated engine is typically around 10 V below ground. For an engine that is not well isolated from ground, current and charge neutralization occur via charge flow to and from ground—the coupling voltage is reduced in this case. Having a well-isolated engine is therefore a key ground test requirement.

The sensitivity of coupling voltage to isolation of engine structures was explored by Patterson [54]. In that work, using a switch, he was able to float the plasma screen—the mesh-like outer housing structure which protects engine high potential surfaces from the ambient plasma—of the engine as well as the external enclosure of the neutralizer—both of which otherwise would be grounded. A diagram of electrical conduction paths associated with beam neutralization and coupling in the presence of a chamber for this experiment with external engine surfaces floating or grounded is schematically illustrated in Fig. 1.11. With the structures grounded, it was found that the neutralizer coupling voltage was insensitive to flow rate changes indicating that the neutralizer was not well coupled to the beam and that other processes were carrying out current and charge neutralization, as shown schematically in the Fig. 1.11. It was observed that actual beam current neutralization was achieved via the grounded target and partial neutralizer coupling to the beam. In this case, the neutralizer was dumping most of its emitted electrons to nearby ground potential surfaces such as the engine housing and chamber walls. It was energetically easier for the electrons to neutralize the beam through alternative pathways by collecting on nearby grounded surfaces, such as the plasma screen, and be reemitted on the grounded target than to be directly travel to the beam via the plasma bridge. When the exterior neutralizer housing and thruster plasma screen were allowed to float, the coupling voltage was highly sensitive to neutralizer flow rate—which determines the operating mode of the neutralizer (spot or plume) and the plasma conditions—and, thus, impedance of the coupling bridge. The stark difference in coupling voltage sensitivity to floating and grounded screen and neutralizer enclosures conditions is illustrated in Fig. 1.12. Here, the neutralizer flow rate is given in milliamperes, where 1 sccm is equal to 72 mA for xenon [5]. In the floating case, the neutralizer's coupling voltage magnitude decreases with increasing flow as the neutralizer transitions from plume mode to spot mode with increasing flow rate.

It is difficult to assess this neutralizer performance in practice if the engine is only partially

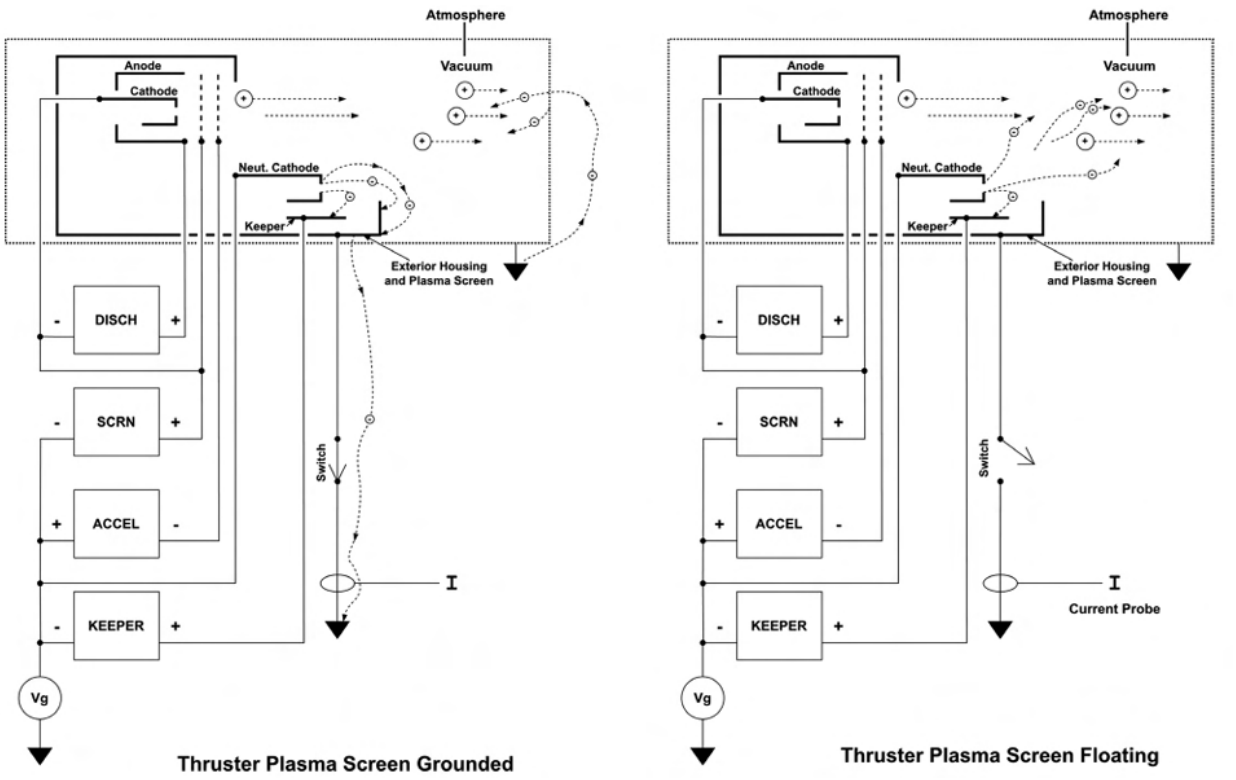

Figure 1.11: Apparatus used to study effect of grounded surfaces near neutralizer [54] Adapted with permission from Patterson and Mohajeri, Report No. NASA-TM-105578, 1991. Copyright 1991 Work of the US Gov. Public use permitted.

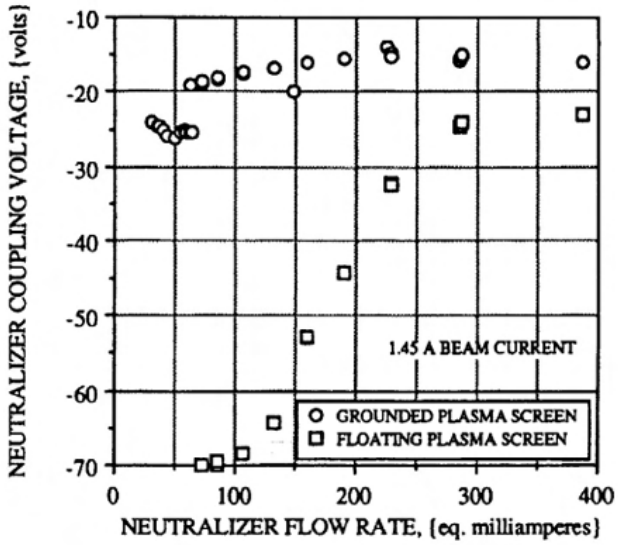

Figure 1.12: Difference in neutralizer coupling voltage for floating and grounded structures as related to configures in Fig. 1.10 [54]. Patterson and Mohajeri, Report No. NASA-TM-105578, 1991. Copyright 1991 Work of the US Gov. Public use permitted.

isolated (nonzero impedance to ground) since part of the neutralizer emission can go to ground and part to the beam, depending on the relative impedance of the plasma bridge to the beam. The indicator of how well the beam is in fact directly neutralized is the plasma potential of the beam itself relative to ground—which should be small in a well neutralized beam. Wall collection area proximity to the neutralizer plasma can therefore have a significant effect on beam plasma potential. Incomplete neutralization (charge) can lead to beam blow up which is an issue for assessing spacecraft plume interactions as well as impacting backsputter rate spatial distribution owing to increased divergence. Thrust can also be impacted since the beam voltage to plasma potential difference is reduced owing to a more positive space potential. Note, as mentioned earlier, and as pointed out by Wang and colleagues, the potential distribution across the beam is markedly different in a chamber of finite size since walls limit the beam expansion process.

Another consideration is the local plasma environment, which varies depending on whether the spacecraft is in low Earth orbit or in interplanetary space. In LEO, ionospheric plasma can also participate in beam neutralization. Figure 1.13 illustrates these physical processes schematically displaying the local plasma environment and its interaction with the thruster for the SERT II test which featured 2 ion engines T/S-1 and T/S-2. Here the diagram depicts conditions with only one engine operating with beam extraction. The local plasma environment has five contributors: the beam, the charge exchange plasma, the neutralizer plasmas, the space plasma, and the ion engine main discharge plasma associated with one of the engines being operated in discharge-only mode. Discharge-only mode refers to the operation of the thruster without high-voltage beam extraction. In this case, the neutralizer electron emission shortfall could be made up through the collection of ions emitted from the discharge to spacecraft grounded surfaces or the net emission of electrons the discharge. It was shown in the SERT 2 experiment that the presence of spacecraft-produced plasma reduced the coupling voltage of the neutralizer varying from roughly a potential difference of -25 V with one beam on and the second engine's discharge off, to -15 V with one beam on and the other with discharge-only. Additionally, it was shown that the engine could run for nearly an hour without any neutralizers operating at all with a beam current operating at 85 mA, but it did not operate long enough to make spin-rate thrust measurements [55]. This was enabled by both CEX ions and returning beam ions to spacecraft ground potential surfaces [32].

The neutralization is also affected by stray magnetic field lines which can affect the coupling voltage. Yu-Cai and Wilbur explored the effect of stray magnetic field on neutralizer coupling [56]. It was shown that beam plasma potential could be driven to values as high as 40 V, (near Zener clamping voltage) in the presence of 10 G stray field located outside the thruster (for reference, typical magnetic field strength within the discharge volume is less than 60 G) [5]. As mentioned earlier, neutralizing electrons do not need to couple to the beam directly but could take a lower impedance path via chamber ground potential surfaces. In this regard, ground test structures that

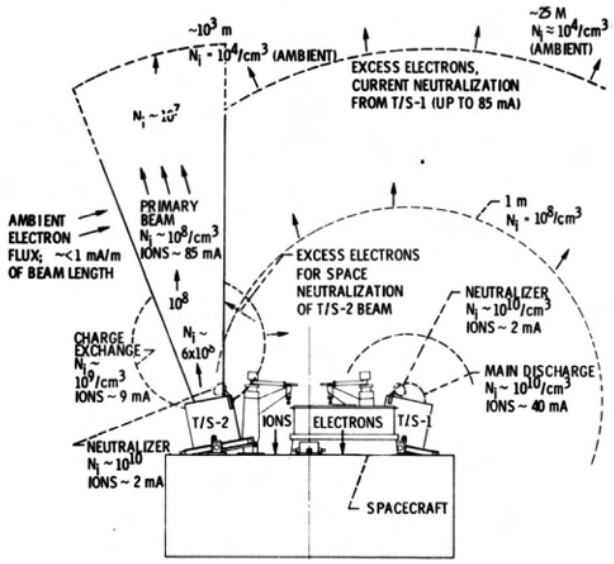

Figure 1.13: Beam neutralization processes in space as inferred from SERT II experiments [32]. Reproduced with permission from Kerslake and Domitz, Report No. NASA TM-79271, 1979. Copyright 1979 Work of the US Gov. Public use permitted.

augment, weaken, or obstruct the stray magnetic field give rise to uncertainty in the actual coupling voltage that the engine will operate at in space. Additionally, the magnetic field could potentially guide electrons into ground structures or the chamber walls as well favoring these in contrast to deposition into the beam. Such guided flows would not be present in space thus they have the effect of introducing uncertainty into the actual coupling voltage. Additionally, Yu-Cai and Wilbur also found that Earth field strength can impact neutralizer-beam coupling as well, even at large separation distances. For example, they found that the coupling voltage increased by 1 V for a neutralizer and beam distance on the order of 1 meter when in the presence of a magnetic field of 0.5 G. Remotely located neutralizers on high power systems could potentially be impacted by Earth's field in this case during ground tests and thus, this potential problem should be examined if large neutralizer-beam coupling distances are involved. The importance of this configuration is highlighted by high power thruster variants that feature arrays of engines with a centralized neutralizer or multiple neutralizers.

The SERT II mission explored beam neutralization using a remote neutralizer. Here the neutralizer of one engine is used to neutralize the beam of the second thruster which was located $\sim$1 m away. In those experiments, it was found that the coupling voltage was actually lower for the case with the distant neutralizer (see Fig. 1.12). The effect of the residual, thruster-derived magnetic field over the large neutralizer-to-beam separation distance was postulated to be the explanation for low coupling voltages observed on SERT II. It was concluded that the coupling voltage required to neutralize its respective beam was higher because electrons had to crossover field lines to reach



Figure 1.14: In-house observation of curved cathode jet from a high current cathode with conical anode (no magnets present).

the beam whereas the remotely located neutralizer's emitted electrons could travel along field lines into the adjacent beam [57]. Stray fields are indeed important to consider when their magnitudes and direction will lead to non-spaceflight like charge particle transport due to reduced impedance pathways.

Finally, the earth's magnetic field can also affect internal discharge uniformity through deflection. It has been shown by Bell and colleagues that stray fields can have significant effect via deflection in mass spectrometer ionizers, impacting overall instrument sensitivity [58]. In these instruments, low energy electron beams ($<$50 eV) were used for ionization. Energies above this are too stiff to be appreciably affected by the Earth's field over the instrument characteristic length scales of interest. In general, as with centrally mounted cathodes inside gridded ion thrusters, a cathode jet is typically apparent. This jet is associated with primary electrons interacting with the background but confined by the modest axial magnetic field. The primary electrons emitted ($\sim$10 eV) would have a Larmor radius of order just over 10 cm, which is of the order or smaller than the dimensions of the discharge chamber (and certainly smaller in larger, high-power engines). In this respect, Earth's field could introduce asymmetry in the discharge profile, especially if the on-axis field is weak, as would be expected far from wall surfaces in large engines, giving rise to nonuniformity. Such nonuniformity can not only perturb the thrust vector which causes the spacecraft to spin (also known as roll torque) but also causes nonuniform erosion of the grids due to charge exchange ions. In this regard, especially for higher power engines with larger characteristic beam diameters, this effect will be more pronounced and thus requires some level of investigation. Figure 1.14 depicts the operation of a high current cathode operating with a conical discharge chamber without any magnets, only Earth's magnetic field is present. Clearly, a deflection is apparent. Hence, local magnetic field affects must be acknowledged during ground testing and accounted for.

1.4.3.2 Background pressure effects—Neutral and background plasma collisional processes

Another difference between in-space thruster operation and ground test facilities is elevated background gas pressure. While space conditions define the ideal pressure to operate an engine, the de facto test pressure standard for non-lifetime impacting operation is in the 2.4-4$\times 10^{-6}$ Torr range as inferred from NASA's Evolutionary Xenon Thruster (NEXT) and NASA Solar Technology Applications Readiness program thruster (NSTAR) life tests, respectively. It is observed anecdotally that at pressures in 10^{-5} Torr range can impact engine life not only due to an increased CEX production rate but also due to an increased recycle frequency [40]. Standardization is needed regarding acceptable background pressure to provide a more science-based metric for engine operation. Gas phase collisional processes are dependent on mean free paths normalized to the characteristic length-scale of the facility. In this regard, any pressure standard may need to take into consideration facility physical size as well.

In this subsection, we focus on gas phase processes associated with the CEX plasma. The CEX ion production rate is given as

$$\frac{dn_{CEX}}{dt} = n_b n_n v_b \sigma_{CEX}, \tag{1.31}$$

where n_b is the ion density of the beam, n_n is the background neutral density, v_b is the velocity of the beam ions, and σ_{CEX} is the cross section for charge exchange collisions. Furthermore, the background neutral density profile as a function of distance R from a point source r_{SC} behind the thruster exit plane (where background neutral density at the exit plane is n_{n0}) and θ is the angle from thruster axis to R, where r_{SC} is the radius of grids, has been used in previous simulation models for deep space 1 thruster [59],

$$n_n(R,\theta) = a n_{n0} \left\{ 1 - \left[1 + \left(\frac{r_{SC}}{R} \right)^2 \right]^{-\frac{1}{2}} \right\} cos\theta \tag{1.32}$$

Here, a is a correction factor and r_{SC} is the location of the point source one thruster radius upstream of the exit plane of the engine. The ne density at the thruster exit plane as

$$n_{n0} = \frac{\dot{N}}{A_n \bar{c}}, \tag{1.33}$$

where $\dot{N}$ is the escaping neutral flux, A_n is the ion optics flow-through area, and $\bar{c}$ is the mean thermal speed using the thermal wall temperature of neutral (typically approximately 500 K or 0.04 eV).

Even in large facilities, such as NASA Glenn's VF 6 with pumping speed of 400 kl/s on xenon, the background pressure when operating a $\sim$ 10 kW ion engine is of order 10^{-6} Torr—some

three orders of magnitude higher than low Earth orbit. The fast ions charge exchange with the background gas give rise to slow ions and fast neutrals. Altogether, these species along with neutralizer plasma, scattered ions, and secondary electrons emitted from the wall, are designated as the background charge exchange plasma. The density of this plasma increases with engine power level. These ions in the vicinity of the engine drive the erosion of the accelerator grid. The combination of Eqs. (1.31) and (1.32) can be used to estimate the charge exchange production rate and distribution near the engine.

A key life limiter of ion engines is the charge exchange plasma erosion of the accelerator grid. CEX ion bombardment of the downstream face of the accelerator grid can give rise to the so-called pit and groove erosion as can be seen in Fig. 1.15 [60]. Such erosion can lead to the weakening of the webbing which in turn can lead to the cantilevering of portions of the accelerator grid into the screen grid, resulting in a short between the grids. The erosion can lead to rogue holes which can lead to increased backstreaming as well as the accumulation of material which has the potential to bridge the inter-electrode grid gap. While all this is going on, accelerator grid holes are also enlarged by erosion as well, which when sufficiently enlarged, can lead to engine failure via electron backstreaming. It should also be pointed out that charge exchange erosion occurring in facilities with elevated pressure is reasonably well understood and that higher pumping speed and associated reduced background pressure can decrease the accelerator grid current. The primary complicating factor in predicting grid life is the effects of backsputtered material, which can be protective. In this case, one must contend with competition between enhanced erosion due to charge exchange and the sputter yield reducing effect of deposited target material such as carbon on the grids. These facility effects need to be subtracted out to assess true lifetime in space.

To a limited extent, modeling can predict these deposition and erosion effects, as shown in Fig. 1.16 [61, 62]. The figure illustrates the predictive ability of the model to track accelerator grid hole wear as a function of time for the NEXT engine long duration test (LDT). Here experimental wear data are obtained optically during the test. The fidelity of the predictive capability of models is heavily dependent on engine and test facility specific parameters such as the neutral distribution near the engine. Even at high utilization, the accelerator grid current does not go to zero as the other physical processes that create background plasma persist (e.g., neutralizer, ion neutral scattering and Coulombic scattering). If these are not accounted for, which are invariably tied to facility conditions, then one can erroneously under-predict erosion rate; even if the engine operates at high utilization [61, 63].

The local plasma and neutral background can impact the engine performance in many ways and, thus, must be accounted for when projecting engine performance in space. Elevated background pressure can also affect neutralizer coupling to the beam particularly in the presence of stray magnetic fields, as was discussed earlier. At elevated background pressure, the coupling of electrons

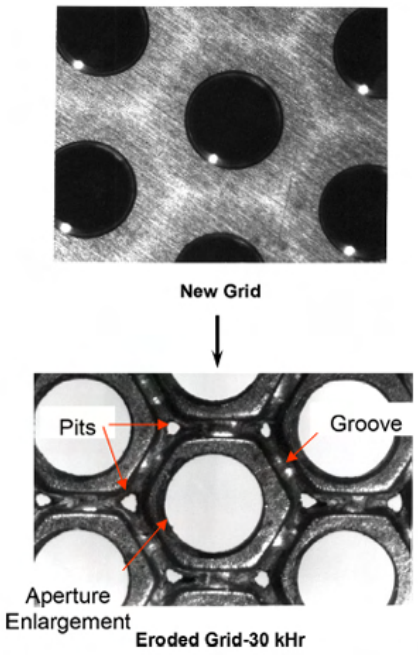

Figure 1.15: Comparison between accelerator grid before and after long duration test [60]. Reproduced with permission from Soulas, Report No. NASA TM-2001-211275, 2001. Copyright 2001 Work of the US Gov. Public use permitted.

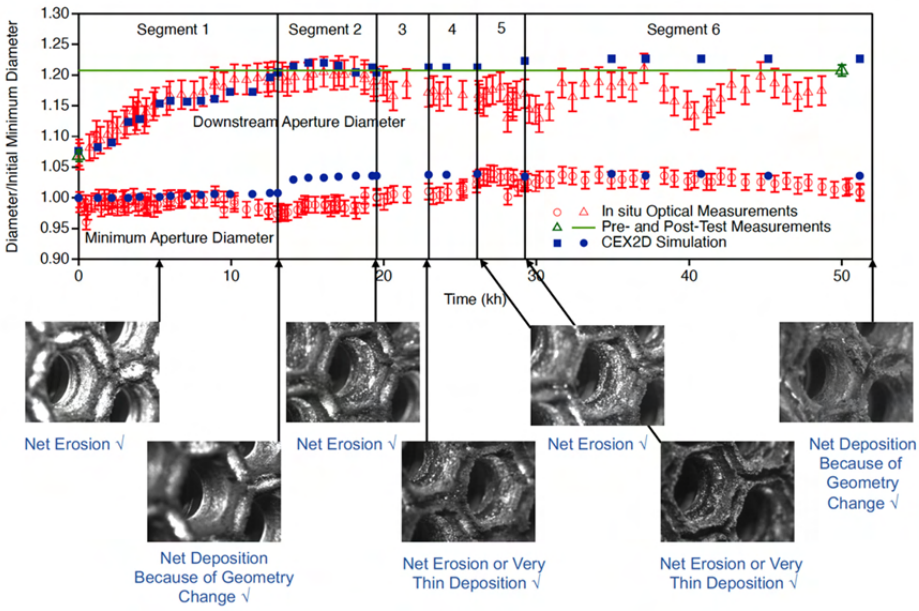

Figure 1.16: Comparison and agreement between simulation and LDT camera imaging data on accelerator grid erosion [62]. Reproduced with permission from Polk et al., J. Electr. Propul. 2(1), 14 (2023).Copyright 2023 Springer Nature.

into the beam is modified by collisional transport and thus care must be taken to make sure that fields are quantified along with local pressure so that this enhanced transport can be accounted for example in computational models and thus subtracted out to recover actual space operation. The background CEX plasma can also impact engine performance in other ways as well. The CEX plasma densities in the near field of the engine has been measured as high as 10^8/cc as observed during the NEXT-3 engine multi-thruster array (>20 kW) test, which is considerably higher than that which is expected in space. For example, ionospheric plasma densities in LEO do not exceed 10^6/cc and in interplanetary space those densities drop to few particles per cc. Despite the low ambient space plasma density, during engine operation in space it has been found that local densities due to CEX flows from the plume are elevated above background space levels ($\sim 10^6$/cc on Deep Space 1 at $\sim$1.82 kW) though still lower than what one would expect extrapolating from ground tests. The elevated neutral and CEX plasma densities are due to the discharge chamber and neutralizer efflux.

The backflow of CEX ions rejected from the plume can be guided upstream to spacecraft surfaces and their flow is thus a key spacecraft plume interaction concern. Such ion flows can lead to sputtering or shorting of low potential surfaces and thus can impact the overall functionality of the spacecraft. The requirement for backflow of CEX ions from the plume to the spacecraft surfaces is determined by the ratio of the potential difference between the potential of the plume and spacecraft to the potential difference between the plume and beam edge. The potential difference between the plume and spacecraft must be greater for backflow to occur. Wang and colleagues show that for this backflow condition to prevail [64], the following must be satisfied:

$$\sqrt{\frac{\Phi_{p0} - \Phi_{SC}}{\Phi_{p0} - \Phi_{p1}}} \geq 1 + \frac{L}{r_{SC}}, \tag{1.34}$$

where subscript 0 refers the potential within the plume, the subscript 1 refers to the plume edge location at the same downstream distance of subscript 0, L refers to the distance from the thruster exit plane that subscripts 0 and 1 are located, subscript SC refers to spacecraft and subscript p refers to the plasma potential. In addition, Φ is the potential at the locations given by the subscripts and r_{SC} refers to the upstream distance behind the thruster exit plane at a distance equal to the radius of the thruster beam. The equation provides a basis for comparing flight and ground test charge exchange flows provided plume potentials are known.

Electrons derived from facility augmented CEX plasma can also be problematic. For example, the diffusion of plasma electrons through the plasma screen are accelerated and terminate on the anode, thus loading the engine. These electrons contribute to heat load and can give rise to uncertainty in beam current since the neutralizer has to pump these additional electrons away. This effect is exacerbated as the CEX density increases and the associated Debye screening is reduced.

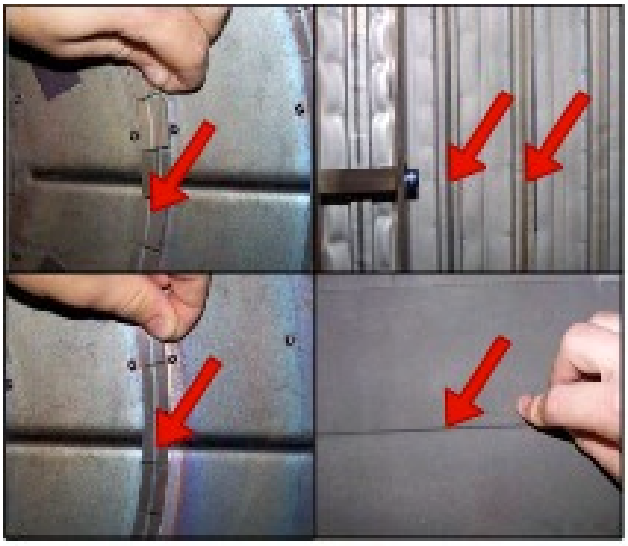

Figure 1.17: Burn lines associated with electron collection at magnetic cusps.

The tell-tale evidence of electron collection on the external surface of the anode due to electron diffusion through the plasma screen is the presence of burn lines located on anode's plasma screen facing surface at the location of magnetic rings—implying that the external field, which is also cusp like, controls this external flow. These burn lines are routinely observed on the external surface of the anode. Such energetic (beam voltage) electron flux has the potential to burn-through obstacles in line-of-sight, such as a wiring harness. Figure 1.17 illustrates burn lines typically observed on internal discharge chamber surfaces associated with center of the magnetic cusp generated by considerably lower energy electrons. Discoloration is associated with electron surface texturing, localized annealing effects, and the cracking of residual oil contaminants. The interaction of beam ions with the background plasma, particularly the electrons, also introduces streaming instabilities that modify neutralization and leads to anomalous divergence [65]. Because the background plasma conditions in space and in test facilities are so different, plume characteristics cannot be assumed to be the same.

The ingestion of facility background gas associated with operation at elevated pressure increases ion engine ionization efficiency, an effect that would not be apparent in space. The ingestion driven flow rate increases due to background gas uptake is directly proportional to the chamber pressure and so is a first order facility effect correction [66]. The additional flow increases the apparent propellant utilization efficiency. Ingestion can be corrected for in a relatively straightforward manner through the calculation of input flow based on grid geometry and background neutral density and temperature. This additional flow would not be present in space and thus it is necessary to lean out the flow to account for the additional flow if one is forced to operate at elevated pressures. This correction is like akin to that used to simulate ion engine operation without beam extraction,

as described by Brophy, which in this case accounts for ion recombination on the grid surfaces, which leads to additional effective gas flow into the engine [67].

Ingestion can also lead to changes in production of doubly and triply charged ions. In the presence of increased background pressure, the apparent double to singly charged xenon ion ratio changes—essentially increasing. This increase is largely due to the fact the CEX cross section for singly charged xenon with background neutrals is larger than the corresponding exchange between doubly charged xenon ions and neutrals. This facility effect diminishes the contribution of the singly charged xenon, giving the impression that the engine is producing a higher fraction of doubly charged ions. This doubles to single ratio, if not corrected, can contribute to significant error in modeling internal erosion as well as grid erosion. Typically, the true doubles to singles ratio is determined by measuring the ratio as a function of distance downstream of the engine starting in the near field. The true ratio is found by then extrapolating back to the location of the plane of the optics (z=0 m). At the plane of the engine's ion optics, it is assumed that the ratio represents that of the plasma in the discharge chamber and it is thus faithful to the true ratio one would expect in space [68]. As discussed earlier, the neutral density at the exit plane and downstream varies spatially both radially and axially. This results in the doubles to singles ratio having a spatial dependence as well. More advanced methods can be applied to determine the correct doubles to singles ratio provided one has a realistic model (or measurements) for the true neutral density profile in the plume [68].

1.4.3.3 Surface material effects—Accelerator grid erosion and facility sputtering

Beam ions sputter vacuum chamber surfaces. Elastically scattered beam ions, whose flux on the ion optics increases with background pressure, also participate in sputtering of upstream surfaces as well. The sputtered efflux in turn deposits on engine surfaces, thereby altering physical surface characteristics as well as contributing to shorting of subcomponents including the potential for the formation of a grid-to-grid conducting bridge. Deposition of carbon or exposed accelerator grid surfaces lead to an apparent, reduced wear rate [69, 70]. If carbon coatings form on the accelerator grid for example, then the wear rate reflects the degree to which the deposits affect the surface sputter yield. This facility effect therefore depends on not only the geometry of the beam target, but also the background pressure which determines the charge exchange rate, the elastic scattering rate and gas phase scattering of the sputtered material derived from chamber walls and the beam target. Additionally, regarding the sputtering of grid and engine surfaces by charge exchange ions or those elastically scattered ions, the actual sputter yield is also sensitive to background pressure. In a ground test facility, background gas can absorb into surfaces. This adsorbed layer has a shielding effect, reducing the sputter yield of that surface. The fraction of surface covered by gases can be calculated. As a rule of thumb, it has been shown that if this coverage ratio is less than 0.1

then one can neglect the impact of this effect. Here, the arrival rate of the neutral gas is one-tenth or less than that of the beam ions,

$$\eta_n = \frac{\beta_n \dot{n}_n}{Y_n \dot{n}_i} \leq 0.1, \tag{1.35}$$

where η_n is the neutral surface coverage, Y_n is the energy dependent sputter yield of the surface, β_n is the sticking coefficient of the neutrals, $\dot{n}_n$ is the arrival rate of the neutrals, and $\dot{n}_i$ is the arrival rate of beam ions. Monolayer formation time is a function of background pressure and at 10^{-6} Torr, it is about 10^{15} atoms per cm^2 per second. In this regard, monolayer formation in ground tests at elevated background pressure can also impact erosion rates. It should be noted around 10^{-6} Torr, the coverage is 0.05 [71]. High power systems are expected to operate in existing facilities with pressures at least an order of magnitude greater than this, thus highlighting the need for higher pumping speed.

Thruster components erode due to normal processes such as accelerator grid ion impingement and ion-driven cathode erosion. In the case of the NSTAR thruster, the keeper was constructed of tantalum, whereas the keeper is made of graphite in the NEXT engine, which is more resistant to sputter erosion. Obviously, the engine service life assessment of an ion engine developed for an actual flight requires the separation of facility-related deposition effects and their implications from normal engine wear of engine subcomponents. Such an assessment is required to validate the engine for a particular mission and thus it is at the heart of the facility effects problem—how do we assess life for high power systems in that are being tested in environments far different from space? Deposition processes derived from direct engine erosion, the redeposition of grid material, and the deposition of backsputtered material due to beam impact on chamber surfaces are shown schematically by Groh and colleagues, as shown in Fig. 1.18 [72]. Such processes can lead to flake formation inside the engine and on the surface of the grids.

A great deal of insight can be gained from the examination of the NSTAR and the NEXT extended wear tests of 30 and 51 kHrs, respectively, regarding the effect of backsputtered material deposition. In both cases, deposition on the discharge chamber wall and free flakes inside the discharge chamber were observed. Figure 1.19 illustrates deposition on the NEXT discharge chamber wall. The coating consisted of grid material due to ion bombardment, which occurs in space as well. These deposited nodules, as can be seen in Fig. 1.19, also contained carbon [73]. The composition of flakes observed, as determined from scanning electron microscope (SEM) analysis, revealed contributions primarily from the chamber carbon panels and molybdenum derived from accelerator grid erosion. It was found that some flakes were in fact layered suggesting spalled carbon is sputter coated with molybdenum in the discharge chamber. In this case, the flakes were possibly derived external to the discharge chamber and electrostatically attracted into the engine.

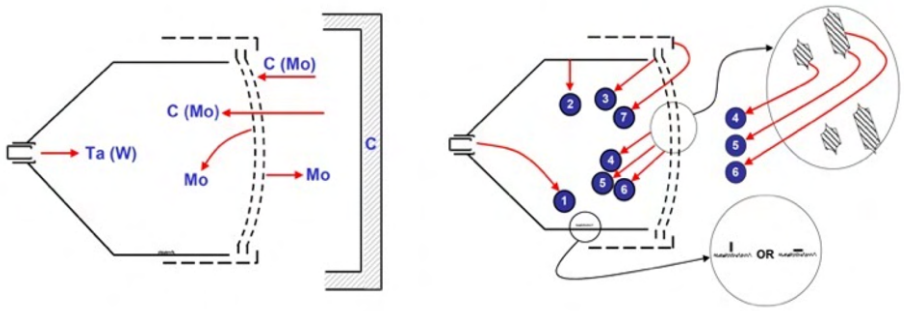

Figure 1.18: Test facility derived deposition and normal engine wear/deposition processes. Deposition processes derived external to discharge chamber shown on left with discharge chamber deposition processes derived from engine wear is shown on the right [72]. Reproduced with permission from de Groh et al., Report No. NASA/TM-2005-213195, 2005. Copyright 2005 Work of the US Gov. Public use permitted.

The very nature of flake formation is therefore convoluted in facility effects. Indeed, admixtures of carbon and molybdenum have different physical properties than adherent molybdenum flakes. Thus, spalling leading to flake formation of such mixtures is peculiar to facility testing. Such processes would not happen in space but nonetheless they confound interpretation in ground test facilities. In the NEXT extended-life test (ELT), deposition reduced impedance between anode and screen grid. The reduction in impedance was attributed to the deposition of molybdenum and carbon, which gave rise to the formation of a bridge between the screen connector and the anode insulating grommet. It is not clear that such an effect would occur in space due to normal grid wear derived deposition alone—such a question may be addressable via computational modeling.

The presence of deposition on the grids is particularly problematic in that it (1) can lead to grid-to-grid shorting and (2) depending on composition can affect overall grid lifetime. In both NSTAR and NEXT ELTs, the screen grid and accelerator grid mass loss were masked by deposition from backsputtered carbon from the facility. Mass from accelerator grid erosion also deposits on the screen grid. In both engine tests, the accelerator grid downstream surface displayed significant deposition derived from the vacuum facility. Figure 1.20 depicts heavy carbon flake buildup on the outer perimeter of the accelerator grid [72]. Again, it is postulated that the source of some internal discharge flakes derived from the external coatings on the accelerator grid. Such flakes can also deposit into screen apertures and can lead to ion beamlet deflection which in turn may result in rogue hole formation on the accelerator grid.

In space, accelerator grid erosion is primarily due to charge exchange ion bombardment or direct impingement if the beam is poorly focused. In this regard, one would, therefore, expect net erosion to take place on this surface over time monotonically and reflect the spatial distribution of the beam. However, during ground testing, deposition of backsputtered material from vacuum

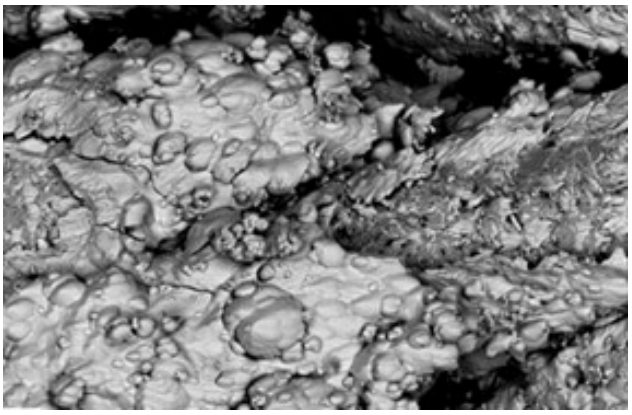

Figure 1.19: Carbon deposition on discharge chamber just upstream of ion optics at high resolution [73]. A point to carbon nodules. Adapted from with permission Shastry and Soulas, Report No. NASA TM-20210009633/AIAA 2016-4630, 2016. Copyright 2016 Work of the US Gov. Public use permitted.

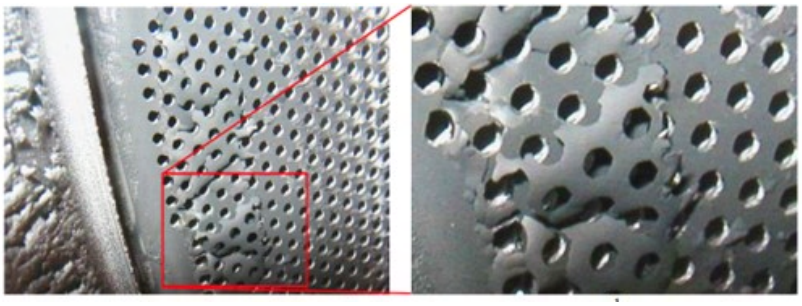

Figure 1.20: The 30,000-h Extended-Life Test of the Deep Space 1 Flight Spare Ion (NSTAR) Thruster outer perimeter accelerator grid downstream face heavily coated with backsputtered material [72]. Reproduced with permission from de Groh et al., Report No. NASA TM-2005-213195, 2005. Copyright 2005 Work of the US Gov. Public use permitted.

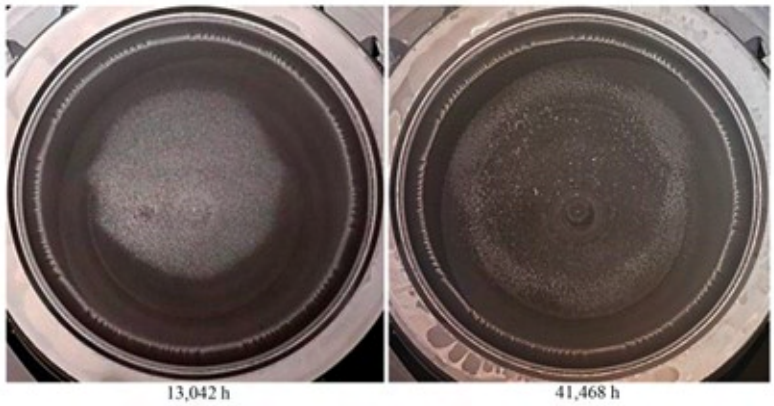

Figure 1.21: NEXT ELT accelerator grid surface deposition transition from net erosion near center to net deposition on-axis [74]. Lighter regions indicate net erosion. Reproduced with permission Soulas and Shastry, Report No. NASA TM 20210009717, 2021. Copyright 2021 Work of the US Gov. Public use permitted.

chamber walls is also present. It was found that during the NEXT ELT, a transition in the spatial distribution of charge exchange flux took place at the downstream surface of the accelerator grid after approximately 36.5 kH [74]. Beyond this time point, at inner radii where presumably ion current density is highest, net deposition was observed. Even the pits and grooves in the central region experienced net deposition. This puzzling transition can be observed in Fig. 1.21 where an early time operating point is compared with a post transition point. Here the clean central region of the grid indicates net erosion at early times in the figure on the left while at later times, clearly only an annular region at larger radii on the downstream surface experiences net erosion. This puzzling observation suggests that the external charge exchange flux spatial distribution may have changed. At the time of this publication, the underlying mechanism that gave rise to this transition is not known or fully understood. Additionally, post-test analysis of the accelerator grid erosion was 75% of the grid thickness instead of the expected 35% predicted by the model. This difference is attributed to net carbon deposition. For comparison purpose at full power operation the facility carbon backsputter rate was 3 μm/kH and the accelerator grid current density was approximately 50 μA/cm^2[75].

In general, it is difficult to predict the actual erosion pattern of the grids in the presence of backsputtered material because the backsputtered material coverage, backsputtered material flux, and CEX ion backflow to the grid profiles are usually not all known. Attempts have been made to account for the coverage. Following the NSTAR thruster analysis, the time-rate coverage can be expressed as

$$N_0 \frac{d\theta_c}{dt} = \gamma_C - \frac{j_a}{e} Y_{C-Mo} \theta_c, \tag{1.36}$$

where N_0 is the surface density of substrate adsorption sites, θ_c is the total fractional surface coverage of substrate adsorption sites by adsorbate, γ_C is the carbon back-sputter flux, Y_{C-Mo} is the sputter yield for single carbon adsorbate adlayer on a molybdenum substrate, j_a is the average accelerator current density in the pit and groove erosion pattern, and e is the electron charge. A weakness of the model is it assumes only a single carbon layer, but multiple carbon layers may be present. A more rigorous approach was developed by Soulas to give a more realistic picture of surface conditions on the grids in the presence of sputtering CEX ions [75]. This model requires extensive experimental inputs, such as spatial variation of backsputtered flux, accelerator grid current, and ion impact energy. Measured spatial backsputtered carbon rates have been made by Crofton et al [76].

Pollard and colleagues measured the spatial distribution of the NEXT engine's doubles to singles ratio which has an annular shape just downstream of the grid exit, as shown in Fig. 1.22 [77]. The charge exchange cross section for Xe^{2+} + Xe $\rightarrow$ Xe + Xe^{2+} at these tested beam energies is comparable to that of Xe^{+} charge exchange [78] and thus may play a role in the formation of this annular pattern. At 1100 V the Xe^{+} cross section with Xe is approximately 45 $Å^2$ whereas Xe^{2+} is of similar magnitude of around 20 $Å^2$. The asymmetric reaction Xe^{2+} + Xe $\rightarrow$ Xe^{+} + Xe^{+} is also possible [78]. Interestingly, in the very near field, the local plasma potential radial profile also reflects this profile as observed by Arthur and Williams [79], suggesting the need to understand how local CEX plasma spatial variations particularly in the near field is influenced by the facility. Additionally, is it possible that the target underwent some form of change that altered its relative sputter rate? Or did the neutral gas distribution near the engine somehow change? The mechanisms underlying these questions remain not well understood [78].

Near field assessment (within a few beam diameter) of neutral density field and the plasma conditions is critical for assessing the grid erosion related facility effects. The doubles-to-singles ratio is highly dependent on this spatial profile. Additionally, assessing the spatial distribution of backsputtered carbon flux in the near field is also critical to accessing true lifetime. These represent critically needed diagnostics to assess grid failure (direct short or electron backstreaming), as it is the primary failure mode of an ion engine. At high power, these effects are all exacerbated and thus are a high priority.

Another impact of backsputtering is the deposition of conductive films of carbon on insulators. This was observed during the 30,000 h. Deep Space 1 life test [51]. It was found that neutralizer keeper to ground and neutralizer common to keeper impedance degraded over time. In fact, the keeper to ground potential dropped from 10 GΩ to only 40 kΩ. While these levels were still sufficiently high to mitigate any issues with performance, the drop in impedance would interfere with the clamping function of the Zener diode that isolates the neutralizer from spacecraft ground as well as obscure total current collected by the keeper. This purely facility effect also requires that

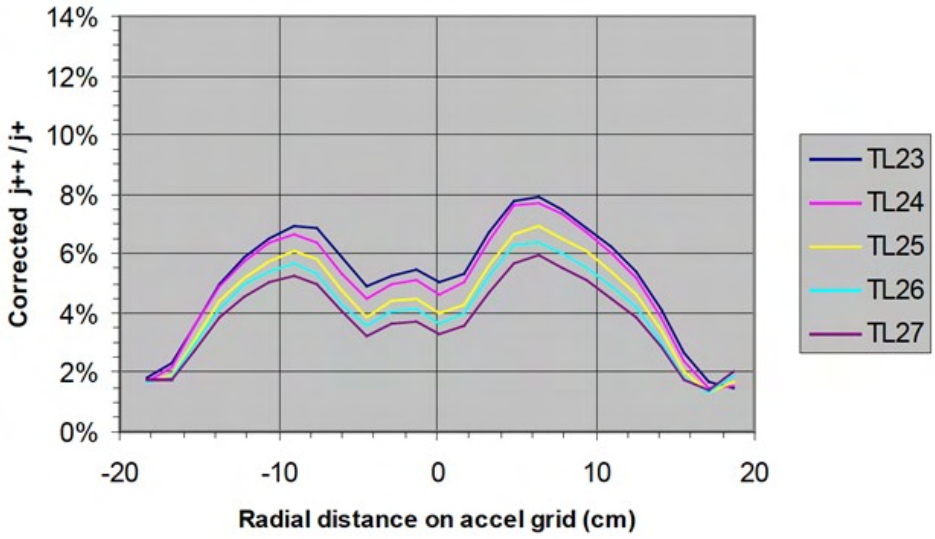

Figure 1.22: Spatial profile of doubles to singles ratio for NEXT ion engine taken —82 cm downstream as a function of engine throttle level [77]. Reproduced with permission from Pollard et al., AIAA Paper No. AIAA 2010-6779, 2010. Copyright 2010 Work of the US Gov. Public use permitted

attention is paid to adequate shadow shielding to prevent ambiguous neutralization, which in turn, affects coupling voltage and ultimately the inferred neutralizer performance and lifetime.

A lesser-known gas phase surface process that is associated with facility effects is related to the actual composition of gas in the chamber at base pressure. Base pressure represents for all practical purpose the pressure associated with the residual air. The interaction of the thruster plasma with this background gas generates nitrogen ions that can find their way to negatively biased surfaces such as the accelerator grid or to cathode potential surfaces inside the discharge chamber. The impact of the ionized nitrogen on surfaces chemically gives rise to the formation of metal nitrides. Such nitrides have a lower sputter yield and so the formation of these monolayers can lead to error in the interpretation of actual subcomponent lifetime. The magnitude of this effect is significant and should be studied computationally. Wilbur developed a chemisorption model for atomic nitrogen and nitrogen ion deposition on cathode potential surfaces in the discharge chamber [80]. One goal of the model was to determine the effect of chemisorbed nitrogen on sputter erosion processes in the discharge chamber. The effect of nitrogen on the erosion of negatively biased thruster components was also confirmed by Rawlin and Mantenieks [81]. As shown in Fig. 1.23, nitrogen was added to the background to augment background pressure during thruster operation. A clear reduction in the wear rate was observed. However, the actual dependence on base pressure has yet to be determined. It may require revisiting as thruster power is increased giving rise to higher pumping load and associated higher operating background pressure. An example of this

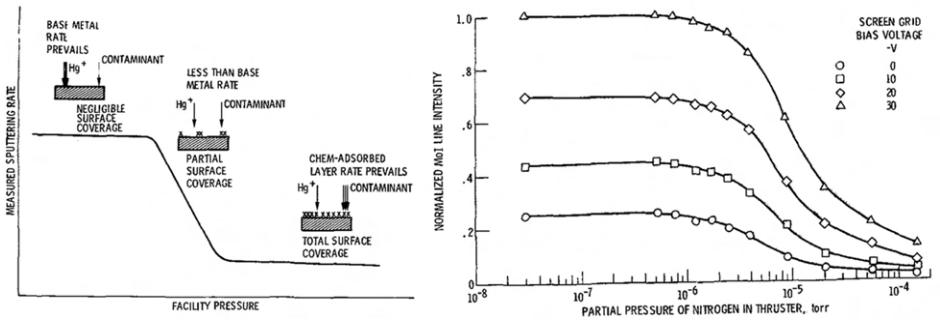

Figure 1.23: Molybdenum grid erosion rate variation with background pressure [82]. Reproduced with permission from V. Rawlin and M. Mantenieks, AIAA Paper No. AIAA 78–665, 1978. Copyright 1978 Work of the US Gov. Public use permitted.

that may need to be revisited is if the relative concentration of nitrogen increases under these conditions due to desorption from cryo-surfaces because of elevated heat load, then these chemical effects may be a factor. Additionally, if the test is long duration, then even at low levels, the nitriding effect may manifest over time. In either case, background nitrogen should always be monitored for long duration tests to account for this possibility.

Several confounding physical processes germane to engine operation in ground test facilities are possible. By subtracting out these effects, it may be possible to predict engine operation in actual flight. These require careful measurement of neutral and ion species and well as the potential distribution in the plume and in near vicinity of the engine. These experiments provide critical data for predictive model validation and performance prediction. Comparison between a flight spare engine tested on the ground with the actual flight engine operated in space allows one to put context to observations made on the ground—providing some guidance as to what the actual key considerations in are making the ground test more space-like. Flight data, though limited quantity, can give insight into processes obscured by test facility effects. We next review key flight data derived from the SERT, NSTAR, μ10, and NEXT engines.

1.4.4 Flight and Ground Test Comparisons

Understanding facility effects has been an important consideration in the research and development of ion engine technology since the inception of the technology. The Solar Electric Rocket Test I and II (SERT I-1964 and SERT II 1970) missions were aimed at verifying beam neutralization/thrust production and long life on-orbit operation, respectively. At the time, it wasn't clear from ground tests that neutralization approaches would even work in space. The flight tests provided some of the earliest data sets comparing on-orbit and ground test performance. The Deep Space 1 mission was a proof-of-concept demonstration of solar electric propulsion technology for deep space science

missions and was equipped with a suite of diagnostics that was used to characterize the particle and field environment around the ion engine. The Dawn and Hayabusa missions also provided engine flight data that can be compared with ground test performance. The findings of these missions are reviewed in this section with differences between ground testing and space-flight data highlighted.

1.4.4.1 SERT I

The SERT I mission was the first demonstration of ion beam neutralization in space. The mission involved a 31-min engine test in space as the spacecraft proceeded along a ballistic trajectory for a total of 47-min at altitudes above 400 km [8]. A caesium contact engine and an electron bombardment mercury ion thruster were tested. The flight provided insight into the interpretation of how facility effects impact actual engine operation. These included understanding the role secondary electron emission produced by the beam at the target, the role of dilute plasma produced on the ground during engine operation and its role in neutralization, and the role of coupling effects between beam and chamber walls. Thrust production was used as the indication of beam neutralization, which to first order, was in good agreement with ground tests. Engineers observed a 44% higher beam current on-orbit than during ground tests—suggesting degraded beam neutralization in ground tests. On the other hand, they found beam spreading in facility was like that on-orbit meaning that the divergence observed was mainly a function of the ion optics. Another difference between in space operation and ground testing was electron flow to discharge chamber surfaces. They also found that electron flow through thruster screens gave rise to higher indicated beam current for ground tests suggesting effect of background plasma requires robust screening. The comparative ground tests took place in a 5 m diameter, 20 m long chamber with an operating test pressure of 5×10^{-6} Torr [82]. In terms of chamber dimensions and background pressure, the ground testing parameters of SERT I meet ground testing requirements but the elevated beam currents indicate that even at acceptable ground conditions, facility effects can alter thruster performance from that of its in space performance.

1.4.4.2 SERT II

SERT II, shown via artist conception in Fig. 1.24, was a testbed for assessing ion rocket performance in space [83]. The engine test ran from 1970 to 1981. The spacecraft was placed in a 1000 km polar orbit. Two 15-cm diameter mercury ion engines (1 kW each) with a plasma potential emissive probe onboard for plume sweep were tested. One engine was a spare. In this flight test, the neutralizer potential was varied relative to spacecraft ground to demonstrate control over spacecraft potential relative to space. Figure 1.25 shows that as neutralizer bias voltage was varied, the spacecraft potential in space was approximately 10 V more negative than was observed on the



Figure 1.24: Artist conception of SERT II spacecraft [83]. Reproduced with permission from W. Kerslake and L. Ignaczak, Report No. NASA TM 105636, 1993. Copyright 1993 Work of the US Gov. Public use permitted.

ground [84]. Here a negative neutralizer bias with respect to the spacecraft potential is important as it aides in driving electrons into the beam. Therefore, if the neutralizer is biased more negatively with respect to spacecraft potential, the beam should become more neutralized and the potential of spacecraft should approach that of the local space potential. This appears to occur in space but during ground testing the spacecraft potential is driven more positive indicating that some fraction of the electrons from the neutralizer are being collected on grounded surfaces instead of the beam, requiring the neutralizer to emit more electrons than it would in space (as neutralizer electrons make their way to nearby ground potential surfaces, they complete the circuit and reduce the coupling voltage required by using the grounded surfaces as an alternative lower impedance path to the beam) [85]. Note the dependence on orbital location, which suggests a local space plasma condition effect.

Accelerator grid current observed on the ground and in space were similar in magnitude, suggesting a similar charge exchange plasma environment. The test also found that on orbit, under certain conditions, there was a shortfall in neutralizer emission current; that is, it was less than the beam current. Experiments on-orbit observed an shortfall that was made up by potentially one of three sources: (1) collection of charge exchange ions along with background plasma ions falling back to grounded spacecraft surfaces, (2) plasma from the spare engine operating in discharge-only mode (no high voltage applied), or (3) ions from the neutralizer plasma collecting on grounded surfaces. The on-orbit data suggests that background plasma conditions modify emission requirements of the neutralizer—thus highlighting the importance of accounting for facility-derived CEX plasma in neutralizer performance characterization [32].

Additionally, the SERT II experiment demonstrated that the engines generate thrust in discharge mode-only operation and that it was possible to run the engines in this plasma beam mode without a neutralizer operating suggesting return currents to the spacecraft were balancing the charge flow.

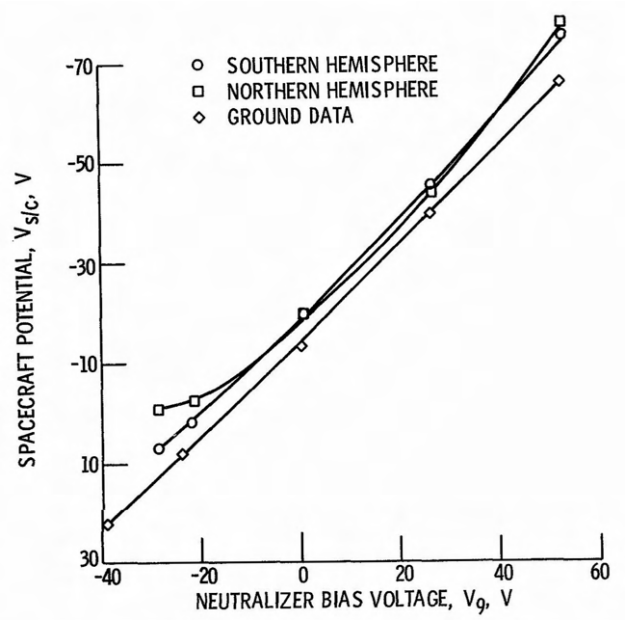

Figure 1.25: Variation in spacecraft potential with neutralizer bias voltage. Nominal operation at neutralizer bias of 0 V [84]. Reproduced with permission from S. G. Jones, J. V. Staskus, and D. C. Byers, Report No. NASA-TM-X-52856, 1970. Copyright 1970 Work of the US Gov. Public use permitted.

It was also demonstrated that with two neutralizers operating, one could vary the emission contribution from one neutralizer by varying its potential relative to spacecraft ground such that the total emission current was constant and commensurate with the beam current. It was also observed that at high negative bias, the neutralizer current was higher than the beam current, suggesting spacecraft collection of space plasma current or neutralizer current directly contacting spacecraft surfaces. Furthermore it was also observed that it was possible to run the engine without any neutralizer at all. In this case, the beam attained very high potential—an indication of a poorly neutralized beam. Neutralization was facilitated by the returning of the beam and CEX ions to spacecraft surfaces, and the spacecraft charged to very large negative voltages.

It should be pointed out that SERT II neutralizers were directly biased relative to spacecraft ground and not allowed to float as is the case in current NASA thrusters. It was also found that the current emitted by the neutralizer at a fixed bias voltage was larger in ground tests than in space, indicating the facility was playing some role. This indicates that higher bias voltages (more negative) are necessary for space coupling as opposed to that needed on ground. This would be the consequence of plasma wall interactions or the elevated background pressure local to the engine in ground tests. In summary, while the SERT tests demonstrated that for the most part, the engine's performance on the ground closely represented space, it did highlight the need to correctly assess neutralizer coupling and the charge exchange background plasma in ground tests to truly account

for and understand deviations from space behavior. Any credible qualification test must assess the underlying drivers that give rise to the measured neutralizer coupling voltage so that the in-space value can be predicted.

1.4.4.3 Deep Space 1

The Deep Space 1 mission featured onboard diagnostics that allowed for the measurement of the in-flight plasma environment associated with engine operation. In this regard, the CEX environment experienced by an engine in deep space could be compared directly to ground tests of the same engine. The DS1 spacecraft was a technology demonstration mission under the NASA Solar Technology Applications Readiness program (NSTAR) where several mission critical technologies—the ion engine among them—was demonstrated for space science missions. The single 30-cm gridded ion engine onboard was used as the primary space propulsion system for a space science fly by mission that ultimately included both an asteroid and a comet.

The objective of the DS1 thruster flight test was to verify that its total impulse capability and overall lifetime was compatible with deep space missions of interest. A secondary goal was to demonstrate control technology for the solar electric propulsion system. At full power, 2.3 kW the 30-cm engine could develop 92 mN of thrust with a 3100 s specific impulse at a total efficiency of 62% with an initial design goal of 87 kg of throughput [6]. Thrust developed by the DS1 ion engine was measured using Doppler shift method which was accurate to less than 0.5 mN. Measured thrust was compared to the thrust calculated using beam voltage and current. The difference between experimentally measured in-flight thrust and calculated thrust was compared with the ground test data (measured ground test data derived from thrust stand) over the engine's throttle range. In all cases, it was found that measured thrust was less than calculated thrust for both DS1 engine and ground test engines. There is good fidelity between ground testing and flight measurements in this instance. However, the calculated thrust deviates from the measured thrust at high throttle levels, shown in Fig. 1.26. Some insight into the deviation can be explored by revisiting the thrust equation, given as

$$T = \alpha\beta I_b \sqrt{\frac{2m_i}{e}} \sqrt{(V_s - V_{cg})}, \tag{1.37}$$

where α is the correction factor associated with the fraction of beam ions that are doubly charged, β is the correction factor for beam divergence, I_b is the beam current, V_s is the voltage of beam power supply, and V_{cg} is the coupling voltage, the potential between neutralizer common and ground (facility ground during ground test and spacecraft ground in space flight). Plume divergence is sensitive to background pressure and thus tends to increase with increasing background pressure owing to elastic scattering and charge exchange production. In general, a plume cur-

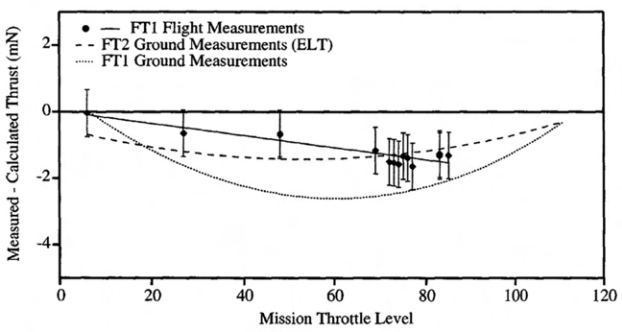

Figure 1.26: Ground and flight thrust comparison with calculated thrust [86]. Reproduced with permission from Polk et al., "In-flight performance of the NSTAR ion propulsion system on the Deep Space One mission," in IEEE Aerospace Conference Proceedings (Cat. No. 00TH8484), Big Sky, MT (IEEE, 2000), Vol. 4, pp. 123–148. Copyright 2000 IEEE.

rent density probe typically cannot distinguish between beam ions and CEX ions, thus at elevated pressures, the plume profile is artificially broadened. The doubles to singly charged ion ratio is also dependent on background pressure and in general, must be corrected for owing to the large difference in the cross section for charge exchange for each species with background neutrals. In general, a higher doubles fraction tends to reduce the overall thrust since the contribution of a double is less than that of two individual ions accelerated across the grid gap. The correction factor for double ions is given below using J^+ is the current density of singly charged ions and J^{++} is the current density of doubly charge ions, both should be evaluated at the thruster exit plane.

$$\alpha = \frac{1 + \left(\frac{\sqrt{2}}{2}\right)\left(\frac{J^{++}}{J^+}\right)}{1 + \left(\frac{J^{++}}{J^+}\right)} \tag{1.38}$$

The differences in the functional dependence of the ground test thrust deviations with increasing thruster power in comparison to the flight test data suggests a facility effect may be at play, but the direct cause is not yet known. The fact that the calculated thrust did not agree with the measured suggests a higher doubly charged ion content, a higher beam divergence at exit plane, or a difference in the ambient plasma potential locally, resulting in a change in coupling voltage. As discussed and shown previously in Fig. 1.8, the energy of accelerated ions is related to the potential difference between the screen voltage and the ambient plasma potential at approximately the neutralization plane. A poorly neutralized beam results in a reduced effective beam voltage and thus a reduced measured thrust. In space, one would expect the thruster-enhanced plasma density surrounding the spacecraft to increase linearly with thruster power. The deviation in thrust during spaceflight is relatively linear in nature, indicating CEX plasma is playing a role—resulting in increasing neutralizer coupling to spacecraft ground potential surfaces. Because the plasma screen was grounded in the facility test, the neutralizer coupling voltage may behave in a nonlinear

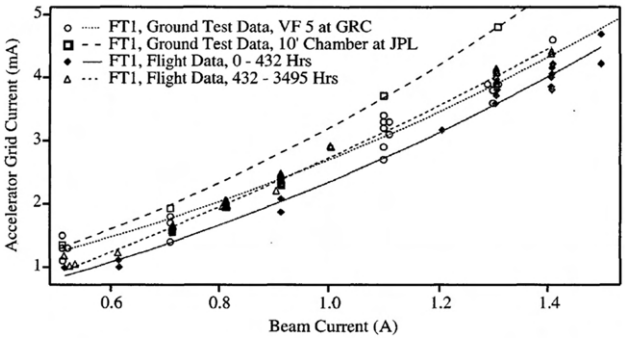

Figure 1.27: Accelerator grid current variations in space and on ground [86]. Reproduced with permission from Polk et al., "In-flight performance of the NSTAR ion propulsion system on the Deep Space One mission," in IEEE Aerospace Conference Proceedings (Cat. No. 00TH8484), Big Sky, MT (IEEE, 2000), Vol. 4, pp. 123–148. Copyright 2000 IEEE.

fashion since the neutralizer can couple to both the beam and ground potential surfaces. Charge exchange plasma density will increase with increasing beam current, increasing plasma density in the neutralizer-to-beam plasma bridge, and increasing background pressure, leading to reduced neutralizer coupling impedance to the beam. As a result, one would expect the deviations between calculated and measured thrust on the ground to decrease with power, which was observed [86]. In conclusion, limiting ambient thruster produced CEX plasma density to space-like levels in ground tests is critical to decrease the thrust deviation as seen in DS1.

In general, in ground tests, increased accelerator grid current in the presence of elevated background pressure is typically observed. The elevated accelerator grid flux is due to increased charge exchange plasma density which accompanies higher background pressure in the facility relative to the that experienced in space. Figure 1.27 illustrates a comparison between ground test accelerator grid current and that observed in space for the DS1 engine. As can be seen here, while accelerator grid current is lowest in space, as expected, when compared to ground test facilities the magnitude of the difference is relatively small. Flight data after 432 h. and ground test at GRC though are in good agreement. The accelerator grid current difference between ground test and space impacts overall service life predictions [87]. It is unknown whether the spatial distribution of neutrals, which determines in part the CEX driven spatial erosion pattern of the accelerator grid, in the ground test is like that occurring in space.

The neutralizer as discussed earlier is also sensitive to test conditions such as background pressure, CEX plasma density, and proximity to grounded surfaces. As can be seen in Fig. 1.28, neutralizer keeper voltage in space was of order 2 V lower than that on the ground. The required keeper voltage tended to decrease over time as well. This drift has been attributed to cathode conditioning and was observed on the ground test as well. As to why the keeper voltage was lower in space is not well understood. It is possible that this may be an electron temperature effect.

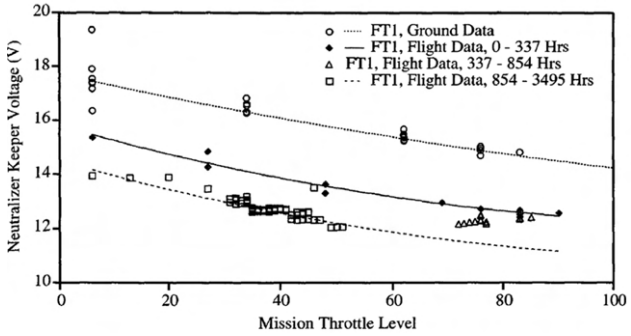

Figure 1.28: Neutralizer keeper voltage variations in space and in ground test vs throttle level [86]. Reproduced with permission from Polk et al., "In-flight performance of the NSTAR ion propulsion system on the Deep Space One mission," in IEEE Aerospace Conference Proceedings (Cat. No. 00TH8484), Big Sky, MT (IEEE, 2000), Vol. 4, pp. 123–148. Copyright 2000 IEEE.

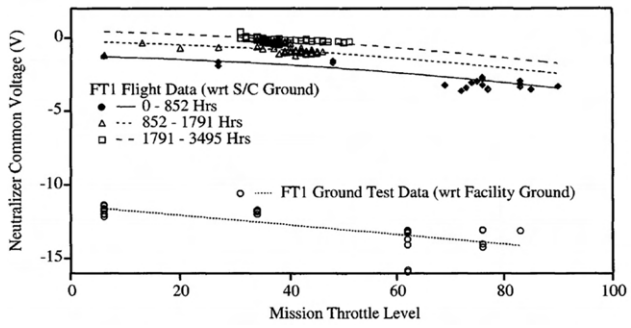

Figure 1.29: Neutralizer potential relative to ground comparison with flight [86]. Reproduced with permission from Polk et al., "In-flight performance of the NSTAR ion propulsion system on the Deep Space One mission," in IEEE Aerospace Conference Proceedings (Cat. No. 00TH8484), Big Sky, MT (IEEE, 2000), Vol. 4, pp. 123–148. Copyright 2000 IEEE.

Electrons are confined in the beam via a potential well and thus if the beam is better neutralized in space, then this potential is shallower. As a result, for neutralization of the beam, lower energy electrons are therefore required [34]. This is consistent with the reduced neutralizer potential relative to spacecraft ground as seen in DS1 data of Fig. 1.29. Here clearly the inferred coupling voltage is larger for the ground test cases, suggesting extra voltage is needed to get the electrons into the beam—likely due to competition with other facility grounded structures. Additionally, CEX plasma Debye shielding effects present in ground test facilities can reduce the actual coupling field allowing for greater competition for electrons between grounded facility surfaces and the beam. A larger coupling voltage may naturally develop under those conditions along with the need for a larger keeper voltage.

The DS1 spacecraft contained a suite of electrostatic probes to examine the local thruster-generated plasma environment. The so-called Ion Propulsion Diagnostic Subsystem (IDS) was

located radially about a meter off axis of the thruster centerline roughly in the exit plane. The subsystem included a retarding potential analyzer, a planar Langmuir probe, and a spherical Langmuir probe. The module also housed two flux gate magnetometers. This package allowed for unprecedented analysis of the plasma-plume environment generated by an ion thruster operating in interplanetary space and thus specifies the target environment for ground tests. High quality data were obtained during the so-called S-Peak operating period of the mission where the engine was throttled sequentially through three operating points up to a peak power of 1.94 kW. Both electron temperature and local plasma potential varied with thruster operating condition. The local CEX plasma density at the IDS was around $\sim 10^6$/cc. It was also observed that at the highest power throttle point, the CEX ion production rate tended to go down owing to the higher utilization. This is the opposite of what is observed during ground testing. At higher power throttle conditions, the facility struggles to keep up with throughput and results in an increasing background neutral pressure. As with any plasma in a bound volume, there are confining sheaths at the walls whose voltage drop is dependent on the electron temperature. The sheath adjusts to assure equal electron and ion loss rates to the wall. In this respect, the sheaths act to confine the lower energy electrons and thus CEX plasma density in the chamber can build up with increasing throttle power. This contrasts with space flight, where the bounding loss surface and associated confining sheaths are absent. The absence of natural expansion in ground test facilities prevents the beam from developing the potential profile that prevails in space. These processes affect not only beam neutralization but also electric fields that control CEX plasma transport.

The DS1 NSTAR engine flight data has since been studied and compared to models and the findings are discussed here. Local plasma properties as measured from the IDS are shown in Fig. 1.30 where ML represents mission throttle level and is typically increasing in throttle and power [64]. The engine essentially flies in a cloud of self-produced CEX plasma. Backflowing CEX ion energy and charge exchange plasma environmental conditions produced by the engine are also shown. Note the marked difference between plasma density in the beam in the near field (calculated at the exit plane) and the surrounding charge exchange plasma density (measured $\sim$1 m off axis). The expansion of the higher density plume into the low density CEX plasma gives rise to a drop off in plasma potential. The steepness of this potential gradient depends on the relative differences in the plasma density. This suggests that an artificially high CEX density in a ground test facility will affect the plume potential profile and thus neutralization dynamics along with CEX ion transport. It also implies that the sensitivity of plume potential profile will depend on power level due to the CEX background plasma density created. Additionally, during space flight it was found that the electron temperature increased with increasing beam current, suggesting that the heating is due to the higher electric field associated with the potential gradient. Neutralization dynamics are dependent on the ratio of electron thermal velocity to ion beam velocity so in some

Calculated Beam Properties at Exit Plane

Thrust level	$\Phi_p - \Phi_{IDS}$, V	$(\Phi_p - \Phi_{IDS})/T_e$	J_{cex}, A/cm^2	v_{cex}, km/s	n_{cex}, cm^{-3}
ML 6	9	7.7	1.1×10^{-7}	3.45	2×10^6
ML 36	9	6.8	1.2×10^{-7}	3.45	2.2×10^6
ML 83	15	7.2	0.9×10^{-7}	4.46	1.2×10^6

Measured CEX Plasma Properties (Energy)

Thrust level	I_{cex}, μA	E_{cex}, eV	T_e, eV	$\Phi_{IDS} - \Phi_{scg}$, V
ML 6	2.2	15	1.17	6
ML 36	2.4	14	1.33	5
ML 83	1.8	19	2.09	4

Measured CEX Plasma Properties (Density)

Thrust level	J_{b0}, A/m^2	v_b, km/s	n_{b0}, 1/cm^3	$\dot{N}_n$, 1/s	n_{n0}, 1/cm^3	dn_{cex0}/dt, 1/cm^{3}s
ML 6	7.36	29.8	1.54×10^9	6.2×10^{18}	1.4×10^{12}	2.3×10^{13}
ML 36	11.6	37.0	1.96×10^9	4.3×10^{18}	0.95×10^{12}	2.4×10^{13}
ML 83	19.8	38.7	3.22×10^9	1.1×10^{18}	0.23×10^{12}	1.0×10^{13}

Figure 1.30: Plasma conditions near engine at different throttle conditions [64]. Reproduced with permission from Wang et al., J. Spacecr. Rockets 37(5), 545–555 (2000). Copyright 2000 American Institute of Aeronautics and Astronautics.

respects, this is expected to be different in ground tests owing to the smaller gradient in density and the corresponding potential gradient.

The difference in dynamics of CEX ions in space flight compared to ground tests is also not well understood. Interestingly, it was found that CEX ions could make it all the way to the plasma sensor called the plasma experiment for planetary exploration (PEPE) located on the opposite side of the engine (opposite side of the beam) when running at high power during the DS1 space flight tests. It was postulated by Wang and colleagues that one can model this mechanism as follows: the sheath around the spacecraft is associated with ambient space plasma yielding a Debye length of $\sim$10 m, which is fairly large. This invariably overlaps with the layer of CEX ions repelled out of the ion beam. The CEX ions can therefore be channeled to the opposite side of the spacecraft by fields in the space plasma sheath. This effect is difficult to simulate in ground tests owing to the large length scales over which the transport takes place and the fact that the weaker space plasma halo does play a role as well. In this case, we see that a plume-spacecraft interaction process would be difficult to assess if one does not match the local plasma environment or at least be able to test sensitivity to changes in this environment (altering artificially the plasma density via quenching or

electron cooling/heating locally).

1.4.4.4 Hayabusa 2

While the engine determines in large part the charge transport from the vehicle, if the vehicle contains structures such as biased solar arrays, then collection here also becomes part of the circuit and charge balance. It is likely necessary that subscale tests such as that which was carried out by Kuninaka and colleague to understand neutralization processes, will be ultimately necessary to truly understand system level differences between facility testing and space operation [87]. The importance of addressing facility effects from a system rather than thruster-centric perspective is critically important if one is to access an electric propulsion spacecraft's performance in space. Indeed, charging effects on the Hayabusa 2 mission led to significant spacecraft sputtering owing to operational problems with the neutralizer. In this case, the potential of the spacecraft was driven sufficiently negative allowing CEX plasma to bombard the spacecraft [88]. If one is to capture or study such events, it is critical that facility effects include aspects of the system that will be affected by engine operation, which is clearly different on the ground relative to space.

Additionally, it was pointed out that on the Hayabusa 2 mission the neutralizer coupling performance degraded over time at a rate ten times that which was observed during standalone ground testing. The neutralizer on this asteroid sample return mission was configured in a manner like that of SERT II where it was biased relative to spacecraft ground. With the neutralizer supply set in constant current mode, the coupling voltage shifts to whichever value is necessary to neutralize the beam. This means that the actual emission current does not need to be equal to the beam current. Under these conditions the electrons can also couple to any surface at a higher potential, this could include any nearby spacecraft ground potential surfaces. To understand the origin of the increase in coupling voltage over time, a series of ground tests were carried out to investigate the effect of neutralizer current going to surrounding grounded surfaces. It was found that the presence of surrounding ground potential surfaces reduced the coupling voltage. The neutralizer is more efficient if there are nearby ground potential surfaces to collect some of the emitted electron current—which means that the neutralizer emission current is higher than the beam current. It was concluded that future missions should incorporate sputter resistant, conductive ground potential surfaces around the thruster to assure lower coupling voltages. It was conjectured that during Hayasbusa 2 mission, the ground potential surfaces near the engine, which consisted of a thin conductive film coating, was sputtered away over time leading to the more rapid upward drift in the absolute value of the coupling voltage, which also would tend to hasten the erosion rate [89]. This example illustrates the sensitivity of neutralizer coupling to overall ground test configuration.

1.4.4.5 DAWN

While the DS1 mission was a technology demonstration that was complete with diagnostics suite, the Dawn mission, which also featured the same gridded ion thrusters, was not outfitted with a diagnostics suite as the engine system was only integrated as an off the shelf propulsion system. In this regard, only engine telemetry data are available for the engine's operation in space. Based on these data, the engine operation very closely matched the ground tested thruster used in the NSTAR ELT. There were two exceptions: (1) observed roll torque—which truly can only be assessed in space and (2) neutralizer common error, were the neutralizer potential exceeds the clamping voltage of Zener diode between the neutralizer common and spacecraft ground.

The roll torque about the Dawn thruster axis was observed at a magnitude of $\sim$10 μN m. This roll torque was most likely due to grid clocking error or the interaction of ions with stray magnetic fields leaking out of the discharge chamber [90]. The neutralizer common fault occurred because of the interaction between the spacecraft and the CEX plasma while no beam extraction was occurring. Since the vehicle is floating, it will be driven to negative voltage when immersed in a plasma of a few eV. Neutralizer common on the other hand acts like a plasma contactor and clamps to a potential near space plasma ground. If a large solar array is attached to the spacecraft, then its collection of electrons can drive the potential of the spacecraft ground very negative, which means neutralizer common will be above spacecraft ground on the order of the voltage of the array and thus can exceed the Zener diode isolation of 40 V relative to ground. In this respect, this effect would not necessarily be observed in a ground test facility as it also involved interaction with the solar array, but it does point to the care that must be taken in isolating experiments where charging can give rise to unexpected results and mask operation in space as previously discussed [7]. This result also suggests the need for mock-ups that mimic the entire spacecraft to account for on some level other sources of charge pumps and collectors associated with nominal vehicles operation (e.g., solar arrays).

1.4.4.6 DART

NASA's Double Asteroid Redirection Test (DART) used a low-cost impactor spacecraft targeted for the asteroid Dimorphos that utilized a NEXT-C gridded ion engine, the commercial version of the NEXT engine. The NEXT-C inaugural space flight on the DART mission began operation as expected but was cut short due to an anomaly in the spacecraft's power system electronics (PSE) [91]. It was found that PSE's Interface-Controller-Low-voltage-power-supply (ICL) component clamped due to electromagnetic-interference (EMI) that was produced during a recycle during engine operation. Recycles are high voltage arcs that can occur between the grids, from the grids to spacecraft ground, or grid to anode. Recycle events are typically fast and can create line noise.

The magnitude of ground test background plasma density and neutral gas density influences recycle frequency, which will be different from space operation at higher-power operation, thus making this a facility effect in addition to a system engineering problem. As a result, out of precaution, the engine was prematurely turned-off. Later, it was determined that the issue could be replicated in ground test. Due to cost and time restraints, an integrated thruster on the spacecraft system was not properly tested and deemed an acceptable risk. From this event, it was realized that the thruster and the spacecraft system should be ground tested to mimic spaceflight as ground testing cannot be only thruster-centric but must also include the whole spacecraft system as events which occurred on the Hayabusa and DART missions have shown. Furthermore, characterization of gridded ion engine recycles in ground test compared to space flight also should be performed. Differences in magnitude, frequency, and type of recycle is important to understanding if damage to the spacecraft system may occur and how it may differ as functions of background pressure or electrical ground test configuration.

In addition to NEXT-C flight data, the NEXT array ground test, which featured a diagnostic suite, provides some insight into ground test challenges of testing high power engine systems. The magnitude of impact of the facility effect associated with background pressure on CEX plasma density as mentioned previously and can be seen here in Fig. 1.31 [16, 15]. Here the ground test of 3-NEXT engines along with a dormant thruster was tested in an array at NASA VF 6 With increasing power/throughput, there is a monotonic increase in facility pressure (Fig. 1.31, left). The denotation of "EM1" refers to engine number one, and "FP" refers to full power. The concomitant increase in CEX plasma density is observed as well. The CEX plasma density in space is also expected to increase with power but likely not with the same slope as ground tests owing to the ability of the space CEX plasma to expand, not being limited by grounded wall surfaces.

1.4.5 Mitigation and Correction Strategies

A range of processes germane to ion engine ground testing exists that can confound the interpretation of how the engine will operate space. It is clear that the key issues associated with interpreting the impact of facility effects that require attention include, but not limited to, are: (1) beam neutralization, (2) engine lifetimes due to facility backsputtered material that deposits on the engine, (3) thruster-plume interactions from gas phase and CEX plasma effects associated with elevated background pressure. Gridded ion engine performance in space appears to faithfully represent performance on the ground at least for low to medium power operation. Operation at higher powers exacerbates the aforementioned issues. For higher power engine testing, these four focus areas must be carefully examined. This can also be done in combination with simulation.

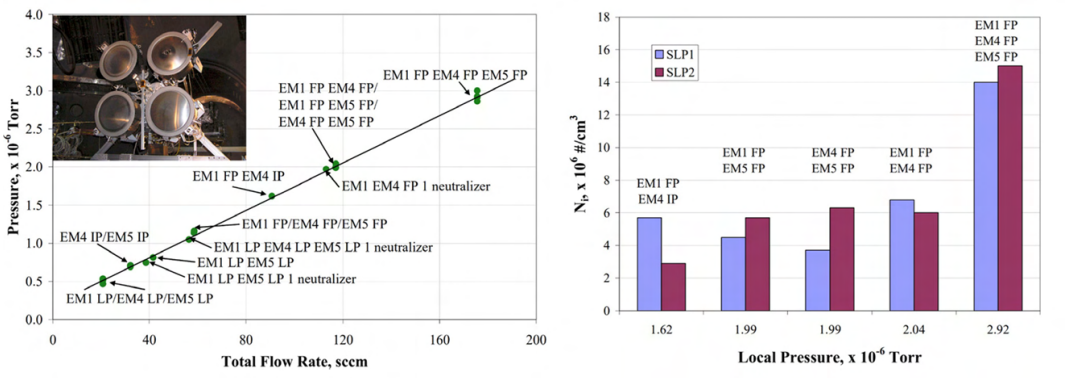

Figure 1.31: The facility effect—background pressure of VF 6 vs flow and the response, the local plasma density at the multi-thruster array (FP nominally 7 kW per thruster-NEXT) [16, 15]. Adapted with permission from McEwen et al., AIAA Paper No. AIAA 2006-5183, 2006. Copyright 2006 American Institute of Aeronautics and Astronautics and Foster et al., Report No. NASA TM-2006-214402, 2006. Copyright 2006 Work of the US Gov. Public use permitted.

1.4.5.1 Beam neutralization

Simulations can predict, for example, the multitude of neutralization and circulating current pathways in a vacuum facility. Models that account for these unique elements of ground tests are needed such that the prediction of thruster performance in space can be made in the absence of these elements. The problem is that the model required must be multiscale. This is to say, that tracking the current pathways is not enough. Current flow pathways have associated with them impedance considerations and thus ultimately must be self-consistent with the prevailing neutralizer operating conditions and the CEX environment. So, performance modification to the neutralizer must be predictable. Thus, modelers and experimentalist must collaborate to validate simulations via experimental data to understand first, the neutralization pathways, then use that knowledge to create experimental standards and procedures to create test environments that mimic space impedance conditions for neutralization. Key needed areas include, realistic modeling of neutralizer coupling bridge and electron–ion beam plasma mixing.

1.4.5.2 Engine lifetimes

Deposition of backsputtered material (which is protective) influences the wear rate of the grids. Additionally, if the wear rate is modified over time during a life test, then the neutral losses may also be modified (aperture enlargement rate). As result, the discharge performance and the spatial distribution of the neutral losses are modified, leading to changes in the CEX spatial distribution near the engine. So, none of the effects are truly isolated. It is the job of the facility test engineer to determine those key parameters that quantify the system and the key facility effects. These are

the inputs for a model. Again, working with the modelers, experimentalists can determine best practices for ground testing, and using corrections for the deposited material where needed from the models. This too is still an active area of research.

1.4.5.3 Thruster-plume interactions

The way the thruster interacts with the gas/plasma environment it operates in is of the upmost importance when preparing correction strategies for ground test facility effects. Regarding back-sputtered material, it is important to map out the spatial distribution of the flux toward the engine to assess spatial variations in arrival rates and the flux magnitude. What is the ionization fraction of the sputtered efflux? It may be possible to generate such maps using laser absorption spectroscopy. Mapping is necessary primarily in the near field. For the neutralizer it is critical that the engine is isolated from ground surfaces or at least a quantification of the distribution of ground potential surfaces to which the neutralizer can couple. As was seen with the Hayabusa 2 mission, this collection area critically determines the magnitude of the coupling voltage. In the near field, neutralizer plasma and CEX plasma electrons diffuse to the walls. How does one separate neutralizer plasmas electrons from the background CEX plasma electrons? Is it possible to map out the current loops? It may be possible to use diagnostic like collisional laser collisional induced fluorescence (LCIF) to create electron maps in the near field of the neutralizer to track charge flow [92]. Tracking the current at the beam target is also important. The ideal situation would be to tag the exiting ion beam—using a laser to place them in a long-lived excited state and then read the flux at the target. This tagging method has been used successfully in the plumes of chemical rockets [93]. One can then compare actual beam current with the combination of CEX plasma ions and the beam. This may be possible if a small engine is used with flat grids. Additionally, the role of secondary electrons has not been well explored at the beam target or chamber walls. The secondary electron emission yields from beam ions are typically ignored because the emission coefficient is small ($<$0.1), but this applies only to clean metal surfaces. It has been shown that the secondary electron coefficient for ions with typical ion thruster energies ($>$0.5 keV) on "dirty" (oxides) wall surfaces exceeds unity suggesting they may play an important role determination of CEX plasma and neutralization processes [94] These effects therefore must be accounted for realistic simulations and interpretation of ground test performance. Figure 1.32 shown here from reference [94] illustrates the large yield observed on oxidized surfaces for argon ions. Spatially mapping and modeling the charge exchange plasma in the near field is also critical as it influences not only neutralizer coupling but also the spatial distribution of ions that erode the downstream surface of the accelerator grid. As idealized test facilities are elusive, we are left with models.

The experimental isolation of key processes along with an assessment of their sensitivities is important to not only improve our understanding but also to serve as validation points for the

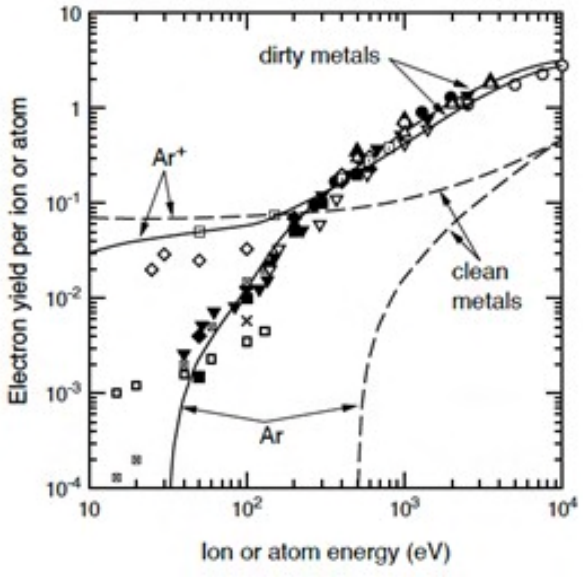

Figure 1.32: Secondary electron emission yield for beam relevant energies on dirty and clean metal surfaces [94]. Reproduced with permission from Phelps and Petrovic, Plasma Sources Sci. Technol. 8, R21 (1999). Copyright 1999 IOP.

development of advanced models to truly interpret ground test data and extrapolate operation in space. Such models, when fully developed, should prove useful in the establishment of testing standards for ground-based experiments where key measurements are taken to provide adequate inputs. Initial experimental studies that quantify and provide corrections for the effects of increased background pressure on operation have been made for doubles-to-singles ratios and simulation work has shown the effects of CEX plume broadening, limitations of plume expansions, and backflow of CEX ions and sputtered material to spacecraft and thruster. However, even these finding are just the beginning as even being armed with this knowledge, there is much factors such as off-axis doubles being greater than on-axis. As such, much collaboration between experimentalists and modelers is needed to derive models based on experimental ground and test flight data to predict future results.

1.4.6 Concluding Remarks

An idealized ion thruster test facility would be too difficult and costly to build in practice. Such an ideal test facility would include walls that absorb all particles incident-neutral and charged. In this case background CEX plasma converges to space conditions and backsputter processes disappear. This absorbing boundary is still problematic for neutralizer operation. The neutralizer's job is just to evacuate excess electron charge whether that's to the absorbing surface or to the beam, it matter little where the electrons end up after emission from the neutralizer. The neutralizer is forced to

couple to primarily the beam, provided the absorption surface (the chamber walls) is less positive than the potential of the beam. To absorb electrons at the same rate as ions, the absorbing surface would effectively be at the floating potential. This would mean that a sheath now exists at the boundary that would not exist in space. This sheath would filter out energetic electrons and reflect lower energy ones.

An absorbing boundary's primary benefit would be the control and removal of neutrals, but neutrals are only part of the problem. Stray fields-both electric and thruster derived magnetic field lines—can guide charge to the loss surface as well. In space, these fields establish charge transport in the plasma cloud generated by the engine. The complexity and difficulty of realizing an idealized absorbing surface is immediately realized with this thought experiment. During space flight, large scale plasma structures evolve that facilitate neutralization and transport of charge to the spacecraft. In ground tests, a rather large facility with walls far removed so that plasma structures can develop is needed such that a spacelike environment can be mimicked. In addition, neutral pressures of similar magnitude are required. Such an idealized facility is difficult to realize in practice, rather we are forced to make measurements to understand the magnitude of the facility effects.

With this realization of key facility effects, one can make a series of recommendations to at least quantify the nature of the facility effects, and if possible, adjust the degree to which that effect is impacting thruster operation. This also involves assessing the sensitivity of thruster operations to a facility effect at various operating conditions, with the end goal providing a means of extrapolation to space conditions. It may be possible to benchmark models by capturing engine operation under scaling conditions that more closely mimic space conditions, for example operating small engines in very large vacuum chambers. Additionally, while understanding how engine operation in a vacuum facility differs from flight operation, the engine is part of a system—the spacecraft.

Both experimental and modeling research need to be performed to first identify the effects contributing to error, then to quantify the magnitude of those effects, and finally develop strategies for mitigation and correction. The work on facility effects has just begun but will require collaboration between different agencies as well for establishing best practices and mitigation strategies such that better isolation and corrections for facility effects can be elucidated. This document reviews a fraction of what is known regarding facility-ion thruster interactions and presents along the way key takeaways from ground tests and space performance. It is not meant to be completely comprehensive but more a less a survey of present knowledge on facility impacts. Many of the processes discussed herein are not germane to gridded ion engines but aspects of this review apply to Hall engines as well. High power electric propulsion systems are mission enabling but their deployment and ultimate success will be dependent on a thorough understanding facility effects and strategies to interpret these effects for accurate prediction of performance in space.

CHAPTER 2

Objectives & Methods

2.1 Testing Objectives

This chapter outlines the objectives of each of subsequent facility effect chapters. Each of these chapters contribute to the understanding of the mechanisms affecting gridded ion engine operating during ground testing. The objective of this thesis is to give insight into the how and the extent these facility effects impact the thruster performance. As a companion to this effort there are mitigation strategies to lessen or decouple the thruster from the facility that are investigated along the way. An aim of this thesis is also to serve as a guidebook for gridded ion thruster ground testing. Lastly, this work provides database for modelers to use for model validation. In this chapter, objectives of each of the main science and experimental chapters are explained. At the end of this chapter is a brief introduction of the methods and procedures used to obtain the experimental data. Chapter 3 then gives more detail of the experiential facilities, test articles, and diagnostics used.

2.1.0.1 Low-Power Density Facility Effects

The main objective of this first experimental chapter was to characterize facility effects at low-power densities–thrust power/chamber volume. This was done by operating a laboratory model (LM) of an engine similar to 2.3 kW legacy class gridded ion engine, NSTAR, in the Alec D. Gallimore Large Vacuum Test Facility (LVTF) at the University of Michigan Plasmadynamcis and Electric Propulsion Laboratory (PEPL). Performing ground testing in such a facility with a medium sized thruster provided a very good spacelike environment for testing. In addition, NSTAR space-flight data exists for this engine and its flight demonstrations provide a basis to show how space-flight operation can be predicted to a certain degree. The LVTF testing environment represents the facility effects currently observed in today's thruster operations and spaceflight qualification. During this testing, there were facility effects that were being specifically investigated and others that were being partially explored to help identify possible future facility effects to explore during

the high-power density facility effects test campaigns. Data obtained here was also to be supplied to modelers for model validation.

Facility effects that were investigated during this low-power density testing included the characterization of wall plasma properties (quantifying interactions between the beam plasma and the facility walls), pressure effects on beam plume profiles, neutralizer characterization and margin, and doubles-to-singles production ratio, all of which as functions of background pressure. Comprehension of the changes in the plasma properties at the wall gave insight into the beam coupling to the facility as well as transport of ions back to the spacecraft. Understanding the coupling of the beam with the walls gave revelation into the needed size of the facility and distance to the walls necessary to limit facility wall interactions with the beam plasma. Additionally, increased background pressure was known to increase charge-exchange collisions (CEX) and lead to plume broadening. As beam neutralization is an essential quality of gridded ion engine operation, understanding how the neutralizer performance and margin change with background pressure was necessary. In addition, the change of doubles-to-singles production ratio gave insight to how the discharge performance of the thruster varies over a range of pressures. Quantifying the impact of these facility effects at this level, where flight engines have been operated, and later comparing to results from a high-power density ground testing gave insight into how thruster characterization may change and lead to poor spaceflight predictions.

Other areas that were partially explored during the low-power density testing for future areas of focus are how changes in the electrical configuration affect performance and facility coupling. Changing the plasma screen from its nominally grounded configuration to allowing it to float is done to see if the facility coupling voltages and beam current at a given operating condition change. These effects prompted the exploration of plasma properties near the thruster and neutralizer characterization.

Needed future work based on findings from the studies described in this section are commented on here. There is some missing data and experimental conditions from this test campaign. These gaps are then used to populate the future testing objectives in the high-power density ground testing. At high-power densities, the purpose was to exaggerate these facility effects to get a clearer understanding of expectations of what ground testing of a 100 kW thruster systems would be like.

2.1.0.2 High-Power Density Facility Effects

Lessons learned and gaps in knowledge were further explored in the high-power density testing after the previous low-power density testing at PEPL LVTF with LM-NSTAR. High-power density facility effects were explored using a low-power 8 cm gridded ion engine developed at NASA Glenn Research Center with some similar designs to the NSTAR engine. To emulate running a 100 kW system in a facility like LVTF, the 8 cm was operated in an undersized and marginal pumping

speed capable facility at Plasma Science and Technology Laboratory (PSTL) Rocket Chamber (RC). This environment had an elevated background pressures due to limited pumping speeds and reduced wall proximity. Similar studies on wall plasma properties and beam plume current profiles were obtained to compare to the low-power density facility effects with LM-NSTAR. However, additionally facility effects were explored based on the previous LM-NSTAR studies. As with the low-power density testing, this data was also obtained to be supplied for model validation.

One major objective of the high-power density facility effects tests was to determine best practices of gridded ion engine ground testing operation to ensure more spacelike performance. This includes determining the electrical configuration of the plasma screen of the thruster and the downstream potential of the beam target. A determining factor for best practices involves determining which of these setups over a variety of background pressure would limit coupling with the facility and provide the most direct neutralization by the neutralizer and not other effects associated with the facility. Furthermore, localized pressure effects on beam neutralization were explored to understand the impact of neutral density effects.

After testing, more areas of interest are identified for future work. Although facility effects are nowhere complete by the end of this work, this work provides the guidance needed to begin high-power density testing by highlighting the mechanisms that are causing these facility effects. Full understanding of facility effects will require collaborations between experimentally obtained results and extrapolations of validated models. This work provides the initial data for this collaborative effort at high-power densities.

2.1.0.3 Comparison of Low & High-Power Density Testing

The similarities and differences between the two power densities are made to determine the commonalities and potential pitfalls that could arise at high-power density ground testing. In addition, this chapter focuses on identifying facility effects that matters most in impacting the performance of the thruster. A summary of guidelines and recommendations for testing at low and high-power densities are also made in this chapter. The work still needed for a better comparison between the two regimes is commented upon as well.

2.1.0.4 Target Plasmas & Impurities

This last chapter investigates the observed target glow witnessed during the initial LM-NSTAR testing. The glow is common occurrence in that it is a physical process that is associated with beam surface interactions, but for all practical purposes, it is a plasma and thus can effect transport of target material and contaminants within the material. The goal of this section was to identify composition of this glow and relay potential impacts this may have. In addition, impurities in the

plasma in general are also seen during testing and commented on further. The combination of the target plasma and the impurities impacting ground testing are discussed in this section as well.

2.2 Methods

The approach taken throughout this work involves a suite of of diagnostic tools. Chapter 3 summarizes the arsenal of probes used and the schematics of the testing environments. Not only are there a plethora of diagnostics, but also a variety of analysis methods. As such, best practices outlined by the community are used on this data, including corrections for facility effects such as charge-exchange attenuation of beam ions. To understand the affect of facilities on gridded ion engine operations, multiple facilities were used over a range of pressures. First, a baseline was established by testing at PEPL LVTF with LM-NSTAR, then testing was moved to high-power density at PSTL RC with the 8 cm. However, testing of beam target plasma composition proved difficult to over come signal-to-noise ratios using plasma spectroscopy thus, simulated beam ions impacting on a graphite target was done using a bell jar background plasma with a DC biased electrode. The following chapter, Chapter 3, describes in further details the setups and diagnostic tools used.

CHAPTER 3

Experimental Considerations

This chapter comprises information regarding the experimental setups, test articles, and diagnostics used in this dissertation. A summary of the different test facilities/gridded ion test articles and the corresponding goals of each test campaign are outlined in Table 3.1. Key studies of each campaign along with the methods used are also provided in this table. Further explanations and details of the test are commented on later in this chapter and in the corresponding chapters containing the results of these test campaigns. Following the summary of the goals and methods is Table 3.2 of the available diagnostic data obtained in each test campaign.

For each gridded ion test campaign, a separate table summarizing the important measured values and the methods used to obtain these values is found in the concluding chapter of this dissertation (Chapter 8). Additionally, the section the dataset is located in this dissertation for easier navigation is made available. Key impacts, certain limitations, and possible application of the results from each test campaign are also commented upon as well in these tables. These tables include Table 8.1 for the 2023-02 test campaign at LVTF using LM-NSTAR for low-power density facility effects and Tables 8.2, 8.3, and 8.4 for high-power density facility effects of the NASA 8 cm GIE in the Rocket Chamber for test campaigns 2024-05, 2024-11, and 2025-01.

Table 3.1: Summary of the objectives and methods of the gridded ion engin test campaigns.

Low-Power Density	High-Power Density		
LVTF	Rocket Chamber		
LM-NSTAR	NASA 8 cm		
2023-02	2024-05	2024-11	2025-01
Characterize low-power density facility effects	Impacts of neutral flow injection in plasma bridge formation	Implications of a floating beam target & ingestion	Implications of a floating plasma screen
Operated with the beam target always grounded: • Variation in background pressure (4 pressures) • Variation in throttle level (3 throttle levels) • Differences between a grounded and a floating plasma screen	Operated at 100 W power level: • Variation in background pressures (3 pressures) • Combination of grounded and floating plasma screen and/or beam target (4 combinations) • Neutral flow injection into plasma bridge (4 flow rates at 4 plasma screen/beam target combinations and 3 pressures)	Operated with the plasma screen always grounded: • Variation in background pressures (4 pressures) • Variation in thruster power level (2 power levels) • Differences between a grounded and a floating beam target • Different Langmuir probes (5 shapes and orientations for 4 pressures and 2 power levels)	Operated at 100 W power level and with the beam target always grounded: • Variation in background pressures (2 pressures) • Differences between a grounded and a floating plasma screen

Table 3.2: Available diagnostic data from the gridded ion engine test campaigns.

	Low-Power Density	High-Power Density		
	LVTF	Rocket Chamber		
	LM-NSTAR	NASA 8 cm		
	2023-02	2024-05	2024-11	2025-01
Telemetry	✓	✓	✓	✓
Background Pressure	✓	✓	✓	✓
Wall Langmuir probes	✓	✓	✓	✓
Lateral Faraday probe	✓	✓	✓	✓
Lateral Emissive probe	**X**	**P**	✓	✓
Langmuir probe near plasma screen	✓	**P**	✓	✓
Langmuir probe near neutralizer	✓	✓	✓	✓
Langmuir probe in beam	✓	**X**	**X**	**X**
Retarding Potential Analyzer	✓	**X**	**X**	**X**
ExB probe	✓	**X**	**X**	**X**
Residual Gas Analyzer (see Chpt. 7)	**X**	**X**	✓	✓
✓=Data available, **X**=Data unavailable, **P**=Partial data available				

3.1 Test Facilities

The approach "test like you fly" in characterizing high throughput engines is often challenging to implement in practice owing to the difficulty in simulating the correct vacuum levels and boundary conditions found in space. The decision of which facility to perform ground testing can have a large impact on the apparent or implied measured performance and qualification of a test article because of the limitations of the testing facility. Although characterizing of electric propulsion devices in space would be ideal, the time, cost, and liability risks of this endeavor is currently not feasible for most organizations or companies. Ground testing time and cost can also be expensive. Qualifying a small, low-power thruster in a facility such as the Space Power Facility at NASA Glenn Research Center's Plum Brook Station would most accurately represent space but may not be time and cost efficient. As such, it is imperative to chose a test facility where facility effects are either low or predictable, but that is also within budget. A few parameters to considering in choosing a facility are discussed here followed by a size and capabilities discussion of test facilities used in this work. In addition, the experimental considerations of these facilities are further commented upon.

Two facility parameters that must be considered in regards to facility effects include the relative

chamber size and pumping speed. The former attribute following the convention the larger the test volume the better, but a huge pumping speed can be limiting factor if a specific background pressure is desired and throttleable pumping speeds or neutral injection are unavailable. The overall size and volume of a facility are important for not only the trivial issue of realistically accommodating the test article but also with minimal wall interference, reasonable sized (length and shielded) cabling, and reasonable diagnostics suite located in a manner to make meaningful measurements. Pumping surface area, wall proximity, chamber layout, chamber temperature, electrical coupling, and neutral/material backflow are all driven by the facility size.

Available pumping surface area is limited by the size of the chamber and thus size and pumping speed are in many respects coupled. At increased propellant throughput, limited pumping speeds result in elevated background neutral and plasma densities that are dissimilar to that of spaceflight. Additionally, in regards to cryopumps, too high of a throughput and elevated background pressures can overload the capturing surface and the heat flux from the plume can reduce cryopumpng performance.

Wall proximity to either the test article or beam plasma can also have significant impacts on electrical coupling. Nearby grounded surfaces can alter thruster operation and performance such as neutralizer margin. Free beam expansion is also constrained by the Dirichlet electrical boundary conditions of the walls and can impact the potentials observed in the plume and altering thruster processes like neutralization.

Chamber layouts and materials coating the chamber can have impacts additionally on testing results. Work by Sabiston and Wirz show that downstream reflection panel angles can have a dramatic effect on sputtered material returning back to the thruster [95]. This deposition can have significant impacts on determining the actual lifetime of the thruster. Placing pumps in-line of energetic ions can also have detrimental effects. Cryopumps can have particles knocked off and turbomolecular pumps and can be damaged by high energy ions or have material deposited on them. For both pump types, placement is key to reduce losses in pumping speeds.

3.1.1 PEPL Alec D. Gallimore LVTF

The Alec D. Gallimore Large Vacuum Test Facility (LVTF) at the University of Michigan Plasmadynamic Electric Propulsion Laboratory (PEPL) has the greatest pumping speed of any academic test facility [96]. With an effective pumping speed of 600 kL/s on Xenon using cryopumps, the LVTF at PEPL was upgraded for higher power EP testing. The chamber is 6 m in diameter and 9 m in length with a base pressure below 4×10^{-8} Torr. Utilizing a graphite chevron-like beam target to protect the pumps, the LVTF beam target deflects neutrals and sputtered material away from the thruster face as well. Due to its size, the facility walls and beam target are currently only



Figure 3.1: University of Michigan Alec D. Gallimore Large Vacuum Test Facility (LVTF) the best simulation of a spacelike pressures for EP testing at the university level [97].

Table 3.3: List of active and in-active cryopumps for each pumping configuration in ascending pressures order.

Configuration Name Designation	Active
Full	2,4-6, 7-19
P0	7-19
P1	7-16
P2	8,10,13-15

able to be tied to facility ground. With an open-loop liquid N_2 for the 15+ cryopumps testing in such a facility can become costly quickly, if it can even be managed to find available testing time. With its great pumping speed and volume of 254 m^3, the LVTF is ideal test facility for a few 10s of kW Hall effect and gridded ion thrusters. Testing at higher power levels needed for NEP systems for trips to Mars for example will require power levels up to 1000x than currently available.

Facility effects were characterized in this chamber using a medium power gridded ion thruster. The diagnostics layout is depicted in Figure 3.2. The locations of the pumps in relation to the thruster are found in Figure 3.3. Background pressure could be adjusted by turning pumps on/off. The configuration designations of “FULL”, “P0”, “P1”, and “P2” are in decreasing order of pumping speed with “FULL” representing the full pumping speed configuration. Table 3.3 list which pumps were active during each configuration. Figure 3.4 visually displays the locations in which the pumps were on/off.

3.1.2 HPEPL VTF-2

The Vacuum Test Facility 2 (VTF-2) at Georgia Institute of Technology (Georgia Tech) High-Power Electric Propulsion Laboratories (HPEPL) is a premier academic test facility for testing

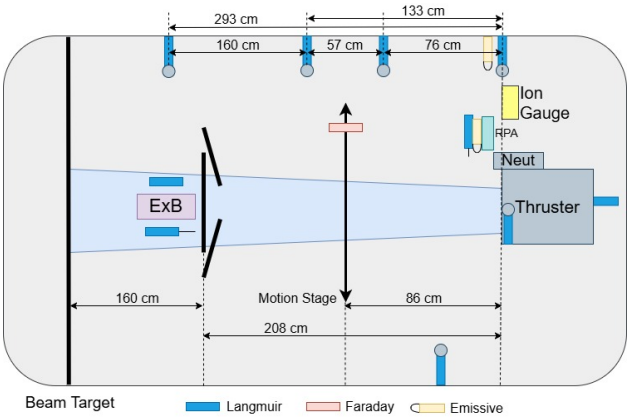

Figure 3.2: University of Michigan LVTF diagnostic layout used over a variety of background pressures. Pressure measurements are made to the side of the thruster with an ion gauge. The beam of the thruster terminates on a beam target downstream. Langmuir probes line the wall for measurements of ambient plasma properties far from the beam plasma. A lateral Faraday probe sweep characterized the beam plasma.

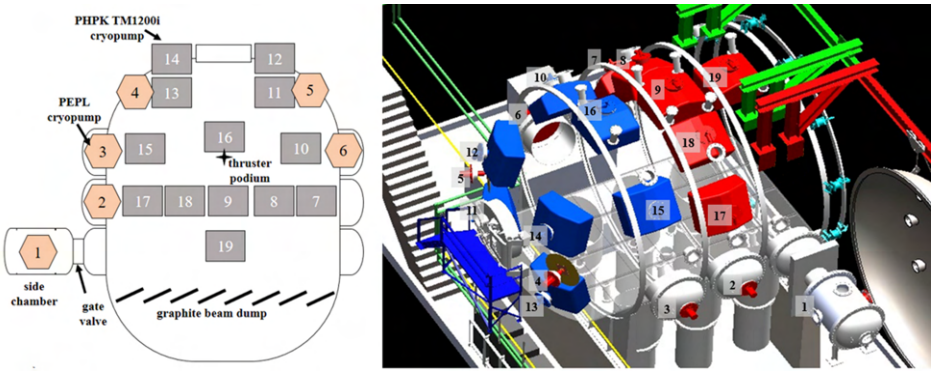

Figure 3.3: Layout of locations of the cryopumps in the LVTF used to control background pressure in the facility [97]. The left image is a 2D map of pump locations with the two different types of cryopumps emphasized based on color and shape. The right side image is a 3D model of the facility.

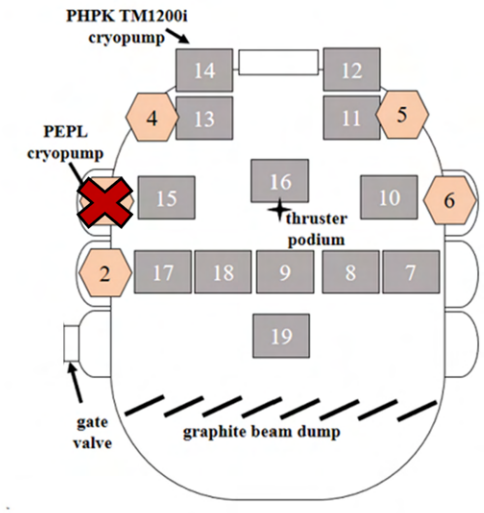

(a) LVTF "FULL" pumping configuration

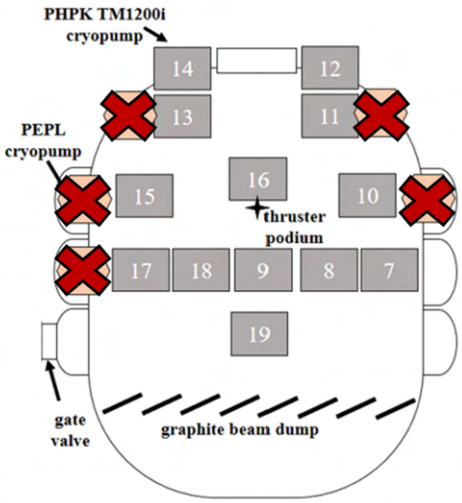

(b) LVTF "P0" pumping configuration

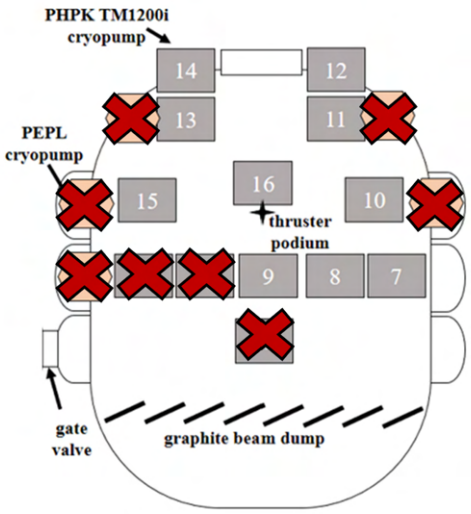

(c) LVTF "P1" pumping configuration

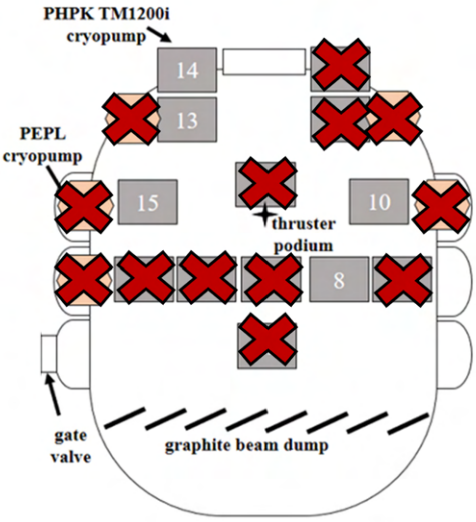

(d) LVTF "P2" pumping configuration

Figure 3.4: Various pumping configurations used during testing at LVTF to control background pressure. The red "X" indicates a pump is turned off.



Figure 3.5: Georgia Tech Vacuum Test Facility-2 is another premier academic EP test facility that was used for facility effect impacts on the H9 Hall thruster [99].

high power electric propulsion [98]. It has an effective pumping speed of 350 kL/s on Xenon using cryopumps. The chamber has a diameter of 4.9 m and is 9.2 m in length. It has achieved an ultimate base pressure of 1.9×10^{-9} Torr. Additionally, VTF-2 uses a graphite conical beam target design to mitigate reflected particles towards the thruster. This beam target can also be isolated from the grounded facility. Not as wide as LVTF, VTF-2 could have wall proximity effects for larger diameter thrusters that would potential not be observed in LVTF. Although there is a recycler for the liquid N_2 cryopumps, not all of it is captured and can be unreliable. Although VTF-2 is a great test facility, cost and time can also be a factor.

3.1.3 PSTL RC

The Rocket Chamber (RC) at the University of Michigan Plasma, Science, and Technology Laboratory (PSTL) is a smaller test bed configured for low-power electric propulsion testing in efforts to emulate higher power operation of a large thruster in larger, but still inadequately sized facilities such as LVTF and VTF-2. The chamber has a diameter 2 ft (0.61m) of is 6 ft (1.83 m) in length. The main cylindrical body has a volume of approximately 0.53 m^3. This chamber is the main testbed for this dissertation work and the following capabilities listed here have been added or upgraded during this project as a part of this dissertation work:

1. Upgraded feedsytem from one propellant line to three with an additional optional line that all meet NASA specifications
2. Increased pumping speed from 520 L/s to 4,200 L/s on N_2
3. Reduced sputter by installing grafoil on facility surfaces

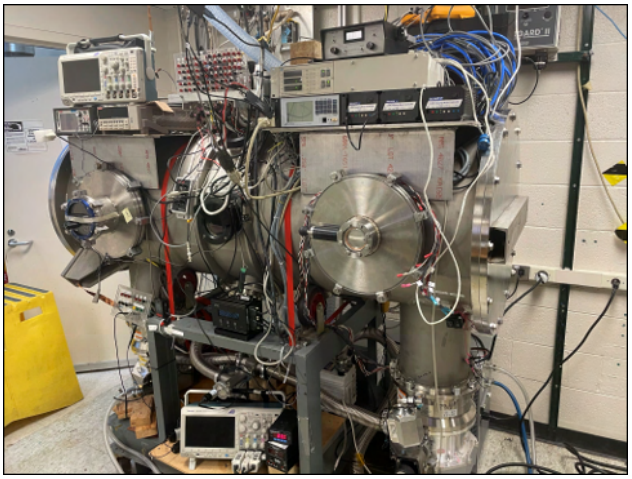

Figure 3.6: University of Michigan Rocket Chamber is a smaller test bed for smaller thrusters testing. This facility underwent major upgrades for facility effect testing on EP devices.

4. Added numerous diagnostics such as Langmuir probes, emissive probes, Faraday probes, retarding potential analyzer, ExB probe, ion gauges, residual gas analyzer, oscilloscopes for recycle capture and potential fluctuations, and quartz crystal microbalances for sputter rates

5. Developed a LabVIEW code for automated data collection for Langmuir probes, emissive probes, Faraday probes, retarding potential analyzer, and ExB probes that could have customized settings for each probe based on a configuration settings text file

6. Designed and coded a python graphical user interface package for automated analysis of Langmuir probe traces that also accounts for sheath shape and type that gives the user the ability to adjust the algorithm as necessary

7. Improvements to the power consol for thruster operation included a telemetry system and better isolated measurements of thruster operation parameters such as current and voltage– recorded chamber background pressure synchronously as well

8. Setup a pressure and pumping monitoring system and alert system was designed to constantly view the chamber and send an automated notification via app, text message and/or email if an issue occurred

9. Established a control room for the pumping monitoring and alert system, diagnostic control and automation, and the telemetry system

10. Created a safety cart for the end-cap flange for safer and easier install/removal

3.1.3.1 Pumping Capabilities

The chamber was supported by two turbomolecular pumps, one located below the thruster stand centered about 29.32 cm, and the other located at the corresponding mirrored position on the opposite end. The two turbopumps are Shimadzu TMP-V2304LM (PB21) with a pumping speed of each of 2,100 L/s (N_2) and each could be throttled from 100% down to 25% to vary background pressures and neutral density gradients. The total theoretical pumping speed for the facility is 4,200 L/s (N_2). Ultimate base pressure of the chamber was 3-4$\times 10^{-7}$ Torr-N_2 depending on the measurement location in the chamber.

3.1.3.2 Facility Configuration

Due to the smaller size, lower cost of operation, and availability, the breath of configurations and adaptability of the PSTL RC allows for rapid changes and variable testing configurations. The downstream beam target was made of a thin aluminum plate that was isolated from the facility walls via ceramic isolators. This allowed for the beam target to be electrically grounded, floating, or biased with respect to facility ground. In addition, the interior of the chamber and the beam target was lined with grafoil to reduce sputtering. Installation of graphite material did require conditioning pumping of the facility after extended exposure at atmospheric pressures due to absorption and out-gassing of water vapor.

The thruster was placed such that its exit plane is 38.74 cm from the chamber back wall and the beam dump is located 124 cm downstream of the thruster plane. Four ion gauges were used to measure local pressure at various locations within the chamber. A 370194 Stabil Ion Gauge (IG0) was placed in-plane with the thruster about 2 beam-diameters (16 cm) to the side of the thruster. A Inficon BPG402 (IG1) was placed approximately 2.3 beam-diameters (18.3 cm) behind the thruster plane. Additionally, an Inficon BCG450 was placed at 6.59 beam-diameters (52.72 cm) and 13.7 beam-diameters (109.6 cm) downstream (IG2 and IG3). A residual gas analyzer (RGA) was also installed next to IG3 for gas composition and accurate pressure measurements.

Various motion stages were placed throughout the chamber. A two-axis motion stage with inductive encoders for position were utilized to perform radial lateral sweeps across the thruster face at various downstream positions. The radial sweep is $\pm$14.7 cm with a total downstream movement distance of 74.9 cm. There were three additional motion stages with approximately 11 cm of lateral movement that can be placed in the chamber. Two of these stages were used. One was placed on the side of the chamber with motion in downstream direction and was used to move a planar Langmuir probe from the beam target to 11 cm upstream from the beam target. A second motion stage was used behind a modified beam target that had a 5 cm diameter hole through the center. The motion stage was used to move mini-beam target grafoil-covered plate in-and-out of

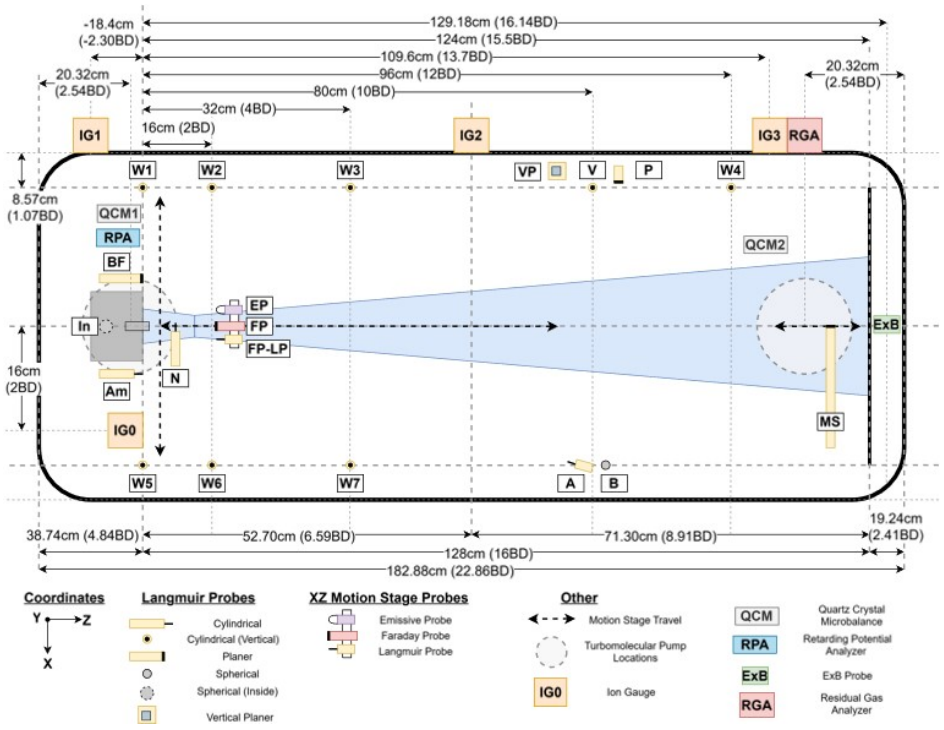

Figure 3.7: University of Michigan Rocket Chamber fully-upgraded layout. Includes pressure measurements, throttleable pumping speeds, and a plethora of plasma diagnostics throughout the chamber for characterizing thruster operation and the impacts of facility effects on thruster operation. This setup was used for the 2024-11 and 2025-01 test campaigns using the NASA 8 cm gridded ion engine.

the beam path to cover the hole in the larger beam target plate. This protected the diagnostic behind the plate while not in use.

The layout used for most of this dissertation work is found in Figure 3.7. However, some testing was performed in a slightly older configuration that had less pumping speed. This older setup is displayed in Figure 3.8. There was only one Shimadzu turbo pump at that time and it was located downstream of the thruster. A Pfeiffer TMU 521 P turbo pump with 520 L/S-N_2 pumping speed was placed underneath the thruster for a total theoretical pumping speed of 2,620 L/s-N_2.

3.1.3.3 Telemetry and Control

Chamber pumping speed and pressure monitoring systems were controlled using LabVIEW and Python. Thruster power and control were provided using a power console originally designed at NASA Glenn laboratory for thruster testing [100]. Upgrades to the telemetry system of the power console included adding shunts and Knick high-voltage amplifier VariTrans and high-voltage DC transducer to isolate measurement signals to a Agilent 34970A data-acquisition unit. Signals were

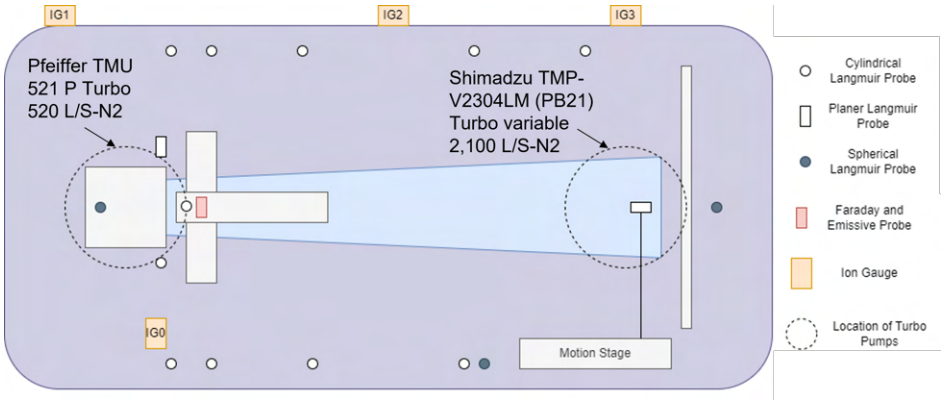

Figure 3.8: University of Michigan Rocket Chamber previous layout mid-way during chamber upgrades. Testing layout used for the 2024-05 test campaign before all upgrades were completed.

then translated into LabVIEW to the proper values at frequency of approximately 0.5-1 Hz. Additionally, chamber pressures were collected synchronously.

The feedsystem was upgraded in this work to include two additional propellant lines integrated in a manner to satisfy NASA guidelines. Flow control could be controlled manually or via LabVIEW. Two 10 sccm Alicat flow controllers were used for the cathodes and one 50 sccm Alicat flow controller for the main flow. Additionally, a 20 sccm Unit flow controller could be added to the feedsystem for additional neutral flow injection to the chamber but was controlled independently by its own controller.

To accurately capture the impact of facility effects required a plethora of diagnostics. A semi-automated diagnostic sweep was designed in LabVIEW. This allowed for the rapid capture of 21 diagnostic tools in quick succession with each probe having their own customized configuration settings via a configuration style text file. An Agilent 34970A was used as a channel switcher piping outputs to a Keithley 2450 source measurement unit (SMU), whose settings were configured for either a Faraday probe sweep with the motion stages, a Langmuir probe trace, or a heat 'n float emissive probe measurement. More sensitive current measurements for ExB or RPA probes were done using a Keithley 6517A electrometer/voltage source. Some operator actions were required for turning the emissive probe on and switching leads for the ExB and RPA probes, but an automated naming convention was adapted to limit confusion, preventing labeling errors, and to aide in tracking files and operation order of the diagnostics.

3.1.3.4 Power Densities

As aforementioned, the purpose of this smaller chamber in this work is to operate a smaller thruster in this chamber to emulate higher-power densities that one would see operating a larger 100 kW thruster in a facility such as LVTF or VTF-2. The purpose here was to gain insight into the effects

the higher background pressures and plasma densities would have on gridded ion performance. With a volume of 254 m^3, LVTF has a volume of 480 times larger than that of RC at 0.53 m^3. Thus, a 100 W thruster in RC will have the equivalent power densities as that of a 50 kW thruster in LVTF. Furthermore, a 200 W in RC would have a similar power density of 100 kW thruster in LVTF and so on.

It was expected that at these higher-power densities, there would be changes in thruster performance such as discharge impedance and thrust, beam coupling, and material sputtering. Much of this work focused on causes and potential solutions to combat and mitigate facility impacts at these emulated higher-power density conditions.

3.2 Test Articles

There are some facility effects that affect one type of thruster more than another. Hall thrusters are suspected to be impacted more on thrust [101] than for a gridded ion engines. This is due to the Clausing factor of GIEs limiting the interaction of the ambient neutrals with the discharge neutral density, where the Clausing factor is defined as the conductance loss for neutrals flowing through the grids due to the transparency of the grids. In Hall thrusters, background conditions effect the discharge since its exposed to the background and the electron neutralization, which is provided by a single cathode . Though this work mainly focuses on facility effects on gridded ion engines, insight gained here is also translatable to effects observed in Hall thrusters as well.

3.2.1 H9

Th H9 is a magnetically shield 9 kW Hall thruster developed in collaboration between JPL, the University of Michigan, and Air Force Research Laboratory (AFRL) [102]. Magnetic shielding is incorporated to improve thruster lifetime by restricting energetic electron transport to the channel wall. One major improvement over the H6 predecessor, is the improved magnetic shielding design allows of greater discharge voltages greater than 300 V, up to 800 V at the 9 kW condition. The maximum thrust is estimated to be 560 mN at 225 V and 40 A. The maximum specific impulse at 2950 s at 800 V and 11.25 A. Overall efficiency of the H9 is around 60%. Original H9 design performance numbers in Table 3.4 are using xenon. However, in experimental work presented here H9 results are using krypton. Some high-current density H9 operations comparisons between xenon and krypton are found in Tables 3.5 and 3.6 from Ref. [103].

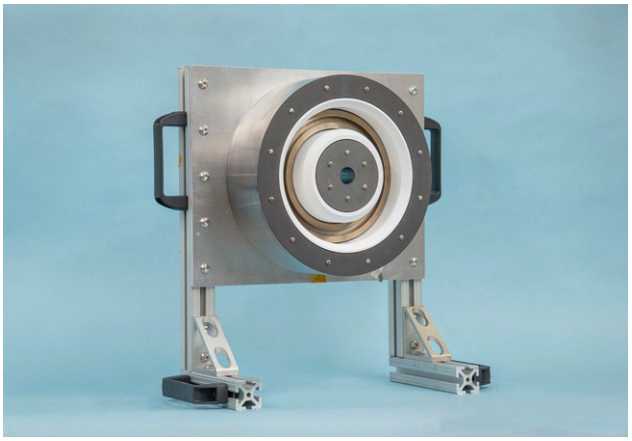

Figure 3.9: H9 Hall effect thruster used at Georgia Tech VTF-2 for investigating facility effects on Hall thruster operation [104].

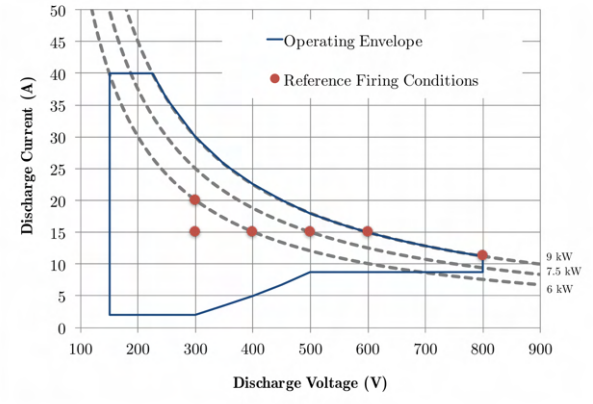

Figure 3.10: H9 Hall thruster performance and firing envelop capabilities [102]. The H9 can be operated up to 9 kW.

Table 3.4: Summarized H9 telemetry performance in SN03 at JPL on Xenon [102].

V_d [V]	I_d [A]	P_d [kW]	V_{cg} [V]	Anode [mg/s]	Cathode [mg/s]	Inner Coil [A]	Outer Coil [A]	Thrust [mN]	Total Isp [s]	Total Eff. [-]	Pressure [μTorr-Xe]
300	20	6.00	-9.8	17.88	1.25	4.5	2.97	379.1	2020	0.619	13.5
300	15	4.50	-11.4	14.18	0.99	4.5	2.97	290.1	1950	0.607	11.0
400	15	6.00	-11.5	14.86	1.04	4.5	2.97	347.7	2230	0.626	11.2
500	15	7.50	-11.5	15.28	1.07	4.5	2.97	394.7	2460	0.629	11.6
600	15	9.00	-11.1	15.47	1.08	4.5	2.97	436.2	2690	0.634	11.9
800	11.25	9.00	-13.2	12.71	0.89	5	3.3	391.0	2950	0.621	10.4

Table 3.5: High-current density operation of the H9 on xenon at 300 V discharge [103].

Current [A]	Power [kW]	Thruster [mN]	Isp [s]
15	4.5	280±8	1754±60
50	15	820±10	2174±32
75	22.5	1100±10	2244±25
100	30	1394±10	2294±20
125	37.5	1650±10	2309±17

3.2.2 NSTAR

In part, the NASA Solar Electric Propulsion Technology Application Readiness (NSTAR) program, a 2.3 kW 30 cm gridded ion engine designed for planetary science missions. This thruster was used for the Deep Space 1 (DS1) and DAWN missions. As part of a technology demonstration, DS1 mission included in-flight plasma environment measurements via onboard diagnostics. The objective of the DS1 thruster flight test was to verify that its total impulse capability and overall lifetime was compatible with deep space missions of interest. A secondary goal was to demonstrate control technology for the solar electric propulsion system. At full power, 2.3 kW the 30 cm engine could develop 92 mN of thrust with a 3100 s specific impulse at a total efficiency of 62% with an initial design goal of 87 kg of throughput [6].

Like most engines the development flows from lab model, to functional model to the flight version. The Functional Model Thruster (FMT) preceded the NSTAR Engineering Model Thruster (EMT) and the NSTAR flight thruster. The main difference between the two thruster versions is the anode material. The FMT model uses a softer aluminum material compared to the EMT comprised of aluminum and titanium [106]. FMT2 model is the version used in this work and currently resides at the University of Michigan PEPL facility. There are a few modifications of this model and thus why here it is referred to as the laboratory model (LM). Previous work using this thruster resulted in [107, 108]:

Table 3.6: High-current density operation of the H9 on krypton at 300 V discharge [103].

Current [A]	Power [kW]	Thruster [mN]	Isp [s]
15	4.5	222±17	1889±125
50	15	704±11	2184±36
75	22.5	1016±10	2331±25
100	30	1309±9	2465±19
125	37.5	1582±8	2534±15
150	45	1839±10	2567±16

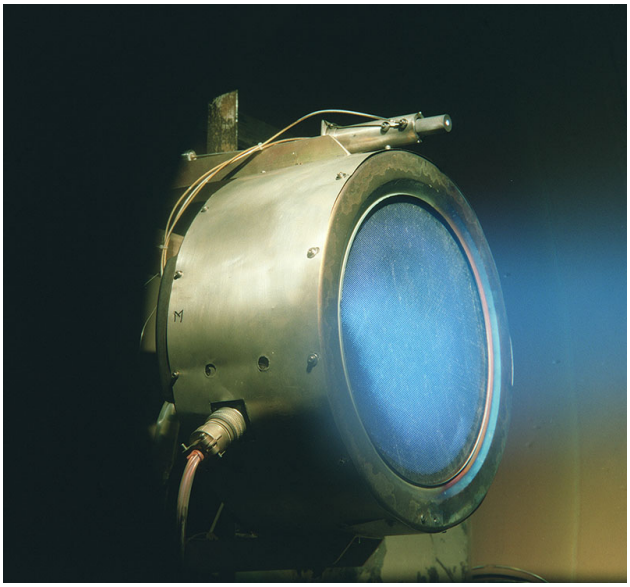

Figure 3.11: NSTAR gridded ion engine operation in a ground test environment with proven flight history used in Deep Space 1 and Dawn missions [105].

- Three holes where cut and then covered with quartz windows in the discharge chamber and plasma screen for optical access
- Modification of the high-voltage propellant isolator design
- Modified gimbal and neutralizer mounting to permit optical diagnostics
- Modification of the engineering model thrusters discharged cathode assembly design and mounting components.

In addition to the previous modifications, this work required some adjustments to neutralizer position due to hardware availability. As a result the downstream position of the neutralizer cathode was not identical to previous operations of this thruster.

An abbreviated throttle table based on Deep Space 1 (DS1) mission parameters was used as a guide for power levels to run the NSTAR engine at. Tables 3.7 and 3.8 are the performance and

telemetry results of the DS1 throttle table. The following Figures 3.12 and 3.13 are the discharge losses and beam ion cost production during the long-duration testing of the NSTAR engine.

Table 3.7: Abbreviated DS1 NSTAR throttle table performance numbers highlighting the range of the NSTAR gridded ion engine performance envelope [109].

TH Level	P_{in} [kW]	T [mN]	Total Eff. [-]	Isp [s]
TH15	2.29	92.4	0.618	3120
TH10	1.70	68.2	0.626	3177
TH5	1.09	42.5	0.574	3002
TH1	0.60	24.5	0.472	2376

Table 3.8: Abbreviated DS1 NSTAR throttle table telemetry highlighting the range of the NSTAR gridded ion engine performance envelope [109].

TH Level	V_b [V]	I_b [A]	V_a [V]	I_a [mA]	V_d [V]	I_d [A]	V_{nk} [V]	I_{nk} [A]	Main [sccm]	Cathode [sccm]	Neutralizer [sccm]
TH15	1100	1.76	-180	5.993	25.14	13.13	14.02	1.5	23.43	3.70	3.60
TH10	1100	1.30	-180	3.898	25.83	9.50	14.90	1.5	17.22	2.56	2.49
TH5	1100	0.81	-150	2.204	25.40	6.56	16.01	2.0	9.82	2.47	2.40
TH1	850	0.53	-150	1.486	25.40	4.69	17.07	2.0	5.82	2.47	2.40

3.2.3 NASA 8 cm

The NASA 8 cm gridded ion engine is a laboratory model developed for low-power missions [111, 112]. Based on NSTAR design, the 8 cm has similar grid aperture sizes and ring-cusp magnetic field configuration. However, one major difference is NSTAR utilizes a dished-out configuration whereas the 8 cm uses a dished-in. For low-power operations, the spacecraft is small and nearby components can be easily sputtered. The dished-in grids creates a beam focal point away from the spacecraft minimizing interactions with the spacecraft. Converging-diverging lens example is seen in Figure 3.15.

Target performance metrics for the NASA 8 cm are given table 3.9. The actual results obtained by Patterson are found in Table 3.10. Table 3.9 was used as the throttle table for this work and results found during testing were compared to those found in Table 3.10.

Discharge losses for the NASA 8 cm using hollow cathodes by Patterson are found in Figure 3.16. Foster et al. determined discharge losses as a variation of floating the various ring-cusp of the discharge anode in Figure 3.17. There has been a modification to the thruster since the work by Patterson and Foster et al. Due to the age and difficultly of lighting the cathodes, a keeper electrode

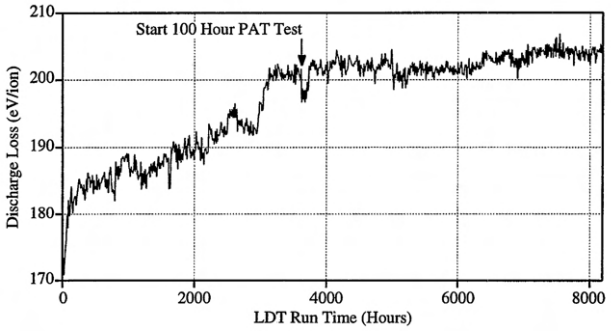

Figure 3.12: NSTAR Long-Duration Test discharge losses variation over time during ground testing. The degraded overtime highlights the need to understand if facility effects such as backsputtered wall material are obscuring results or because of thruster operation over time is the main contributing factor [110].

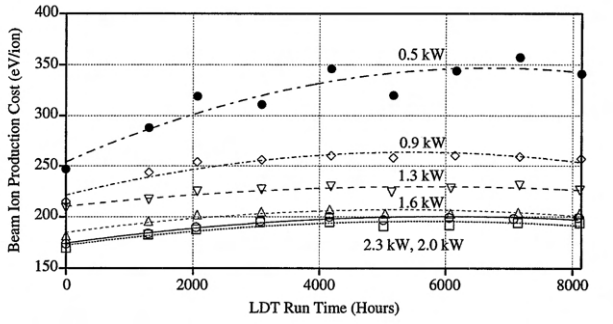

Figure 3.13: NSTAR Long-Duration Test beam ion production cost for varies power levels to indicate thruster performance will vary based on operating conditions [110].

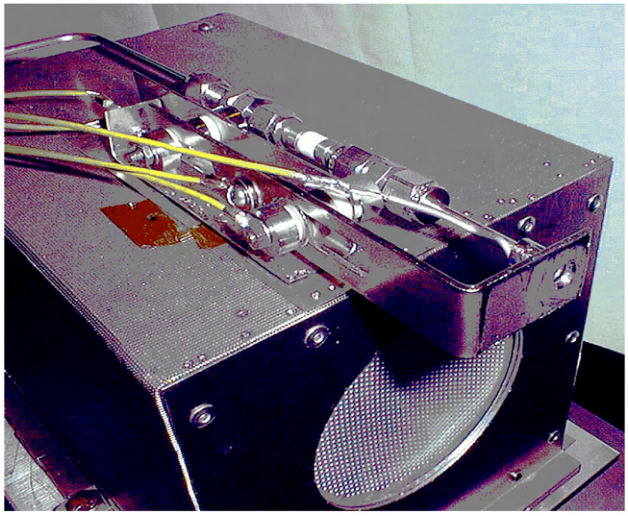

Figure 3.14: Top view of the NASA 8 cm gridded ion engine [113].

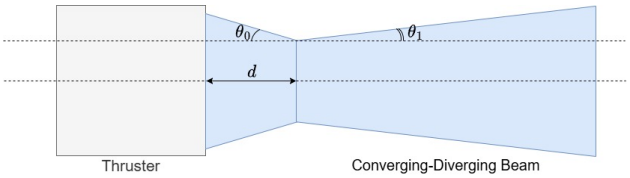

Figure 3.15: Schematic showing the meaning of the NASA 8 cm converging-diverging beam. The cross-over point d is the distance at which the converging and diverging intersect.

Table 3.9: NASA 8 cm performance targets used for setting flows and operating conditions for the 100 W, 200 W, and 300 W power levels [114].

	0.1 kW	0.2 kW	0.3 kW
Thrust [mN]	4.0	8.1	11.3
Efficiency [%]	38	48	54
Specific Impulse [s]	2,000	2,500	2,950
DISC Losses [W/A]	333	300	266
DISC Chamber Propellant Eff.	0.78	0.80	0.82
Neutralizer Coupling Voltage [|V|]	15	15	15
C [sccm]	0.78	1.39	1.69
M [sccm]	0.78	1.39	1.69
N [sccm]	0.50	0.50	0.50
NKPR [V]	20	20	20
NKPR [A]	0.1	0.1	0.1
DISC [V]	28	28	28
DISC [A]	1.05	1.71	1.90
BEAM [V]	800	960	1,200
BEAM [mA]	88.2	160	200
ACCEL [V]	200	240	300
ACCEL [mA]	0.44	0.80	1.00

Table 3.10: NASA 8cm performance Patterson results [112].

	0.1 kW	0.2 kW	0.3 kW
Thrust [mN]	3.6	7.7	10.9
Efficiency [%]	31	42	48
Specific Impulse [s]	1,760	2,260	2,650
DISC Losses [W/A]	360	290	240
DISC Chamber Propellant Eff.	0.73	0.74	0.73
Neutralizer Coupling Voltage [|V|]	17	17	17
C [sccm]	0.77	1.48	1.84
M [sccm]	0.77	1.48	1.84
N [sccm]	0.61	0.61	0.61
NKPR [V]	30	31	18
NKPR [V]	0.25	0.20	0.20
DISC [V]	26	30	30
DISC [A]	1.13	1.49	1.55
BEAM [V]	800	960	1,250
BEAM [mA]	80.9	156	194
ACCEL [V]	200	300	300
ACCEL [mA]	0.41	0.78	1.02

was placed in front of the discharge cathode. The keeper plate was tied to anode potential with a 1.5 kΩ resistor.

3.2.3.1 Discharge Hollow Cathode Characterization

Due to the addition of the keeper electrode in front of the discharge cathode and age of the cathodes, the discharge performance of the 8 cm thruster was repeated and compared to previous results. In Figure 3.18 the discharge impedance is plotted. The keeper electrode was floated in this case. All subsequent test had the keeper electrode tied to the anode via a 1.5 kΩ resistor while in operation.

Ion production cost versus corrected mass utilization of the discharge hollow cathode with simulated beam extraction outlined by Brophy [67] was performed and is displayed in Figure 3.19. The cathode flow was fixed with main flow being varied and the discharge current being adjusted to maintain the proper simulated beam current of: 88 mA at 100 W condition, 160 mA at 200 W, and 200 mA at 300 W. Data points were limited to 34 V and 2 A on the discharge cathode.

Additionally, characterizing the discharge hollow cathode with no main flow was performed. Figure 3.20 has ion production costs plotted against mass utilization (left) and simulated beam extraction current (right).

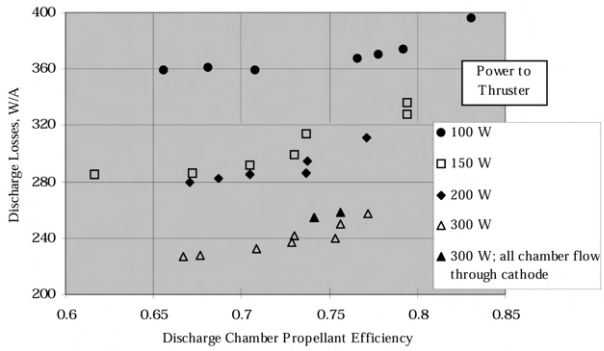

Figure 3.16: NASA 8 cm discharge losses obtained by Patterson at NASA Glenn during initial characterization of this thruster [115].

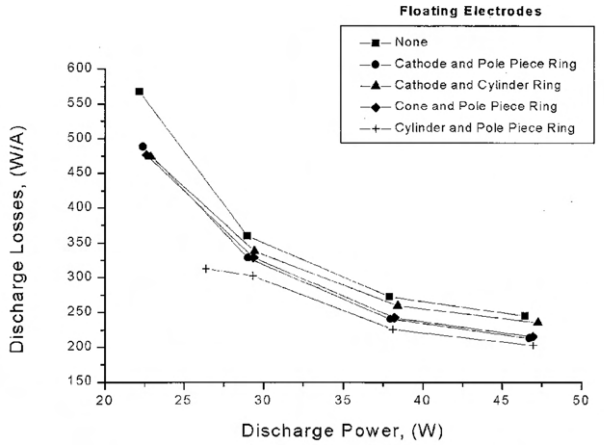

Figure 3.17: NASA 8 cm discharge losses with the impact of floating ring cusps during testing at NASA Glenn [116].

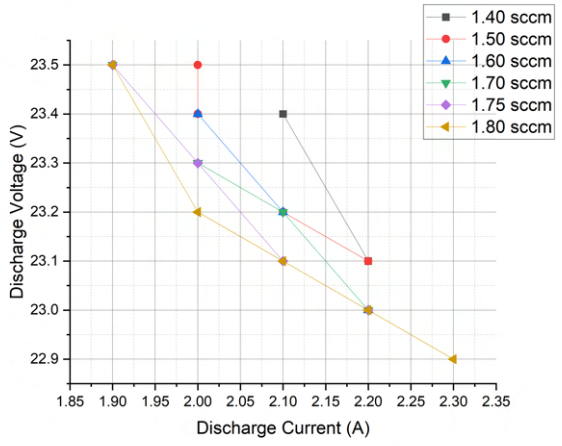

Figure 3.18: NASA 8 cm discharge hollow cathode impedance characterization for various main flows.

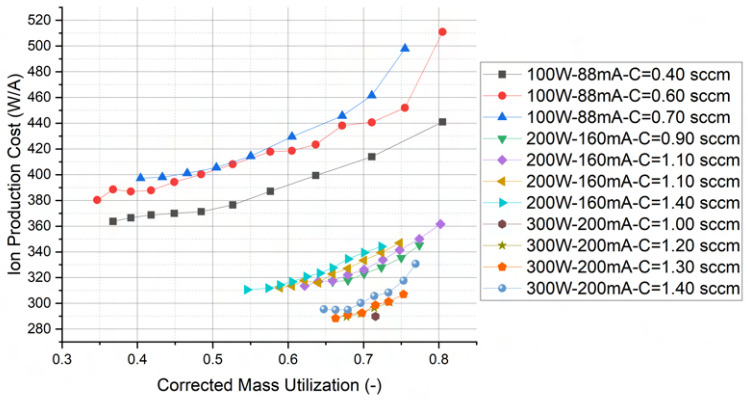

Figure 3.19: NASA 8 cm discharge hollow cathode simulated beam extraction used to characterize the thruster performance and compare to previous obtained results from NASA Glenn.

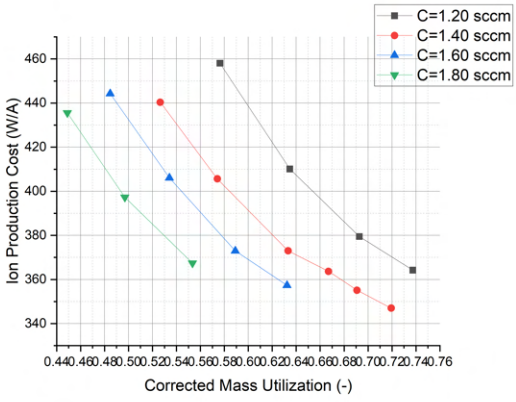

(a) NASA 8 cm discharge hollow cathode simulated beam extraction with no main flow versus mass utilization.

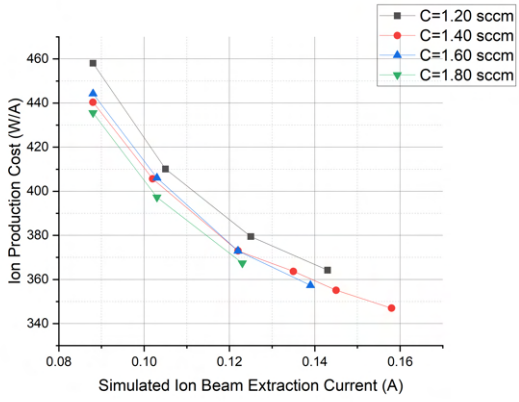

(b) NASA 8 cm discharge hollow cathode simulated beam extraction with no main flow versus extracted ion beam current.

Figure 3.20: NASA 8 cm discharge hollow cathode simulated beam extraction with no main flow to show importance of the additional flow added in the discharge chamber to produce the beam.

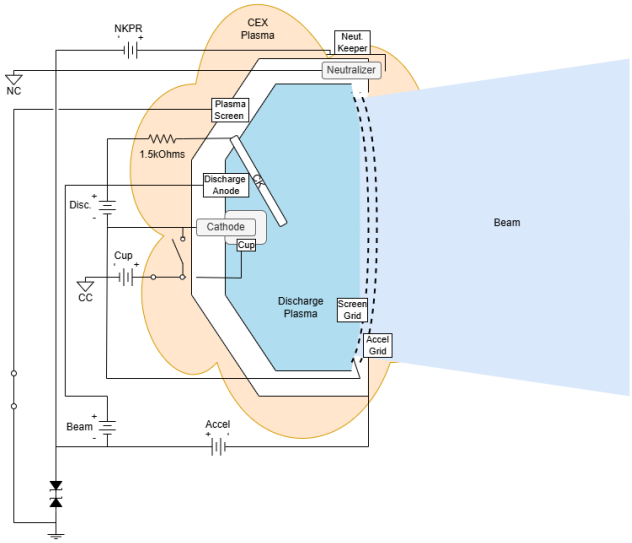

Figure 3.21: NASA 8 cm discharge scandate cathode operation circuit the cup electrode either being tied to a power supply, floating, or tied to cathode potential.

3.2.3.2 Discharge Scandate Cathode Characterization

A scandate cathode was also supplied to be used as a discharge cathode. The scandate cathode was designed, built, and supplied by Bernie Vancil and Wayne Ohlinger. To operate the scandate cathode, the typical GIE circuit found in Figure 1.1 has been modified by adding another power supply to lite the cathode using a "cup" electrode. Once lit, the power supply is removed from the circuit by shorting the cup electrode to cathode common. The cup electrode could also be floated. The resulting circuit is found in Figure 3.21.

Simulated beam extraction using the scandate cathode results are found in Figure 3.22. Similar to the hollow cathode simulated beam extraction, the flow in the cathode was fixed with main flow and discharge current varied to get a desired beam current. The scandate cathode was limited to 31 V and 4 A.

It was found during the previously mentioned simulated beam extraction that the scandate cathode performed well without main flow. Given the configuration of the cathode (button emitter) this is not surprising since the cathode serves as a type of gas injector as well. As a results Figure 3.23 has ion production costs plotted against mass utilization (left) and simulated beam extraction current (right) without main flow.

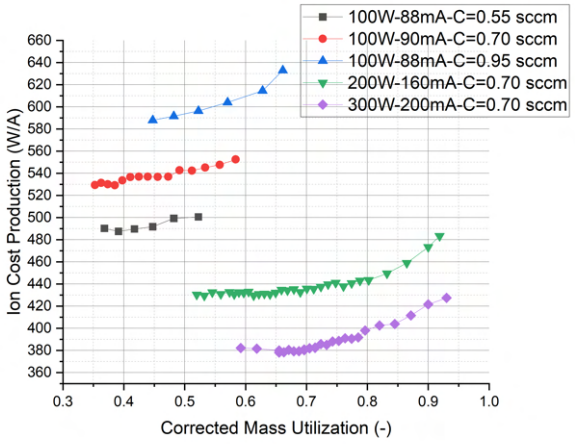

Figure 3.22: NASA 8 cm discharge scandate cathode simulated beam extraction for comparison to nominal hollow cathode operation.

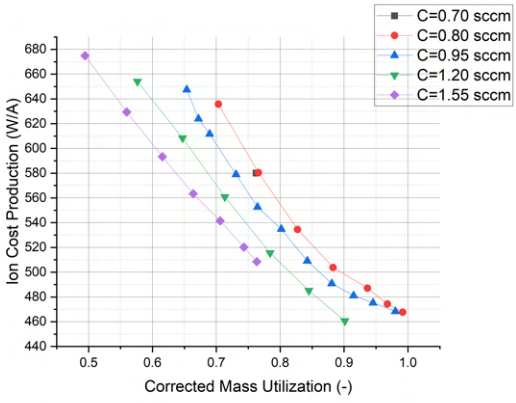

(a) NASA 8 cm discharge scandate cathode simulated beam extraction with no main flow versus mass utilization.

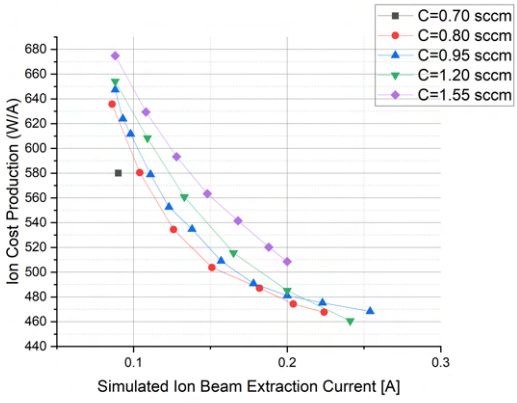

(b) NASA 8 cm discharge scandate cathode simulated beam extraction with no main flow versus extracted ion beam current.

Figure 3.23: NASA 8 cm discharge scandate cathode simulated beam extraction with no main flow to show the difference in thruster performance due to the propellant flow around the planar scandate cathode diffusing into the discharge chamber. Less propellant flow is needed in the discharge chamber.

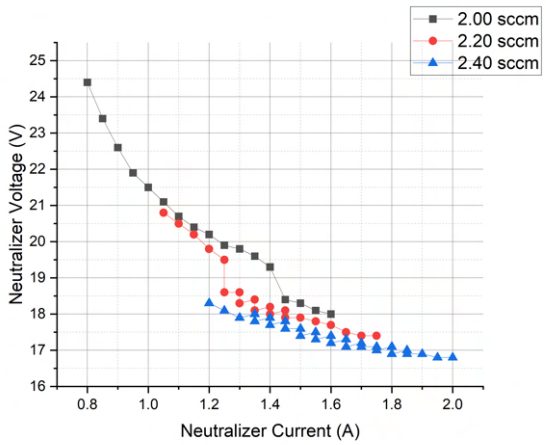

Figure 3.24: NASA 8 cm "super" neutralizer hollow cathode impedance characterization to compare to the nominal neutralizer cathode.

3.2.3.3 Neutralizer "Super" Hollow Cathode Characterization

Two types of neutralizer cathodes were used throughout the test campaigns of this work. The nominal hollow cathode with a standard orifice plate was used in later test as availability limited use early-on. Additionally, the cathode had difficulty staying on without the heater left on and additional propellant flow. A second cathode was a non-conventional hollow cathode with multiple Barium-oxide tungsten rod inserts. As a result of its geometry and capabilities, it was referred to as a "super" neutralizer cathode due to the large amount of current and plasma it could produce. Characterization of this super neutralizer cathode impedance is found in Figure 3.24. However, it was found throughout experiments that the orifice plasma can jump and couple to different inserts, resulting in slightly different performance. In other words, competition with the various insert rods at times lead to competition and unstable behavior.

3.3 Diagnostics

3.3.1 Langmuir Probe

The Langmuir probe is a simple plasma diagnostic device utilized since the early 1900's invented by Irving Langmuir. An exposed electrode is placed in a plasma and then a biased sweep is performed and resulting current to the probe is obtained. Information about the plasma characteristic can be deciphered from the IV characteristic [117, 118, 119]. Plasma properties such as, ion and electron saturation currents and densities, floating and plasma potentials, and electron temperature can be obtained. Each trace, in the case of an electropositive plasma, can be separated into three re-

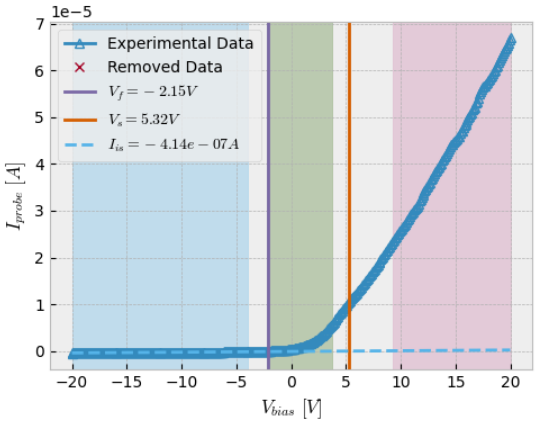

(a) Sample Langmuir linear probe IV trace

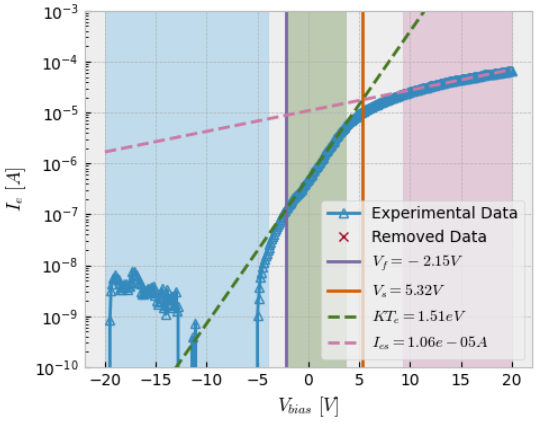

(b) Sample Langmuir semi-logy electron IV trace

Figure 3.25: Sample solved Langmuir IV trace. The left is an IV trace obtained directly from the probe. The right is the IV trace for electron current contributions after ion current has been removed from the overall probe current. Blue region is the ion saturation, green is the electron retarding region, and pink is the electron saturation region.

gions. The first being the ion saturation region located $V_{probe} << V_f$. The middle region being the electron retarding region, $V_f < V_{probe} < V_p$. Lastly, the electron saturation region, $V_p << V_{probe}$.

Although Langmuir probes are easy to implement, the analysis process is often considered complex due to orientation, probe geometry, and sheath expansion all affecting results. Recommended practices for implementations of Langmuir probes in EP testing may be found in Ref. [120]. These effects and considerations are summarized here.

There are three theories for three standard geometries: 1) cylindrical, 2) planer, and 3) spherical. Additionally, there are three sheath theories for sheath expansion: 1) thin (ideal), 2) transitional or 3) orbital-motion limited (thick). Each combination of probe geometry and sheath expansion has a slightly different analysis technique in determining the ion current. The ion current is then subtracted from the probe current to get the resulting electron current. This however, can lead to some obscurity in the tail of the electron distribution calculated from the electron retarding region as the subtraction of the ion current here may have a huge impact. If the proper ion current is not calculated based on probe geometry and sheath expansion, then a non-physical high energy electron temperature may be obtained. Additionally, other than thin sheath expansion, the ion current equations used often do not always fit well resulting in some uncertainty in the analysis process.

Furthermore, orientation of the probes can affect the obtained IV characteristic. Langmuir probe theory assumes that the $U_\infty << \sqrt{qk_BT_e/m_e}$. This assumes ions arrive at the Bohm speed



Figure 3.26: Spherical Langmuir probe example (used during the LM-NSTAR testing at LVTF to increase collected current due to low ambient background plasma densities)

and neglects preheath effects (i.e. magnetic fields). Beam ion flow to the probe are at velocities in excess of the sound speed. This can lead to ram-ion current contribution in ion saturation region, higher electron temperatures due to elongated electron retarding region, obscured plasma potential due to rounding at the knee from kinetic ion effects, and even increased ion current measurements due to secondary electron emission (SEE). Proper probe orientation has been shown to alleviate some of these issues. For an example, with cylindrical and planer probes the normal of the collection surfaces is oriented perpendicular to the ion drift flow.

3.3.2 Faraday Probe

Similar in construction to a planar Langmuir probe, a Faraday probe consist of circular collection area using an electrode typically made of tungsten to address heat loading, surrounded by a ceramic isolator. However, unlike a Langmuir probe, the Faraday probe is kept at a constant voltage to repel electrons and collect primarily ions. A spatial current profile is obtained as the probe is translated across the beam using a motion control stage. Best practice in electric propulsion testing are outlined in Brown et al. [121].

For gridded ion engines, the Faraday probe is a critical diagnostic tool. Divergence, beam flatness, and thrust can all be obtained from Faraday sweeps. The collimation of the beam can be determined from the change in the FWHM of the current profile. Flatness is defined as the peak current divided by the total integrated current. The total integrated current should be equal to the beam current in the very-near field current profile. Using the total integrated beam current, divergence half-angle, and equation (1.11) the thrust produced can be obtained.

There are few different methods in a Faraday probe construction. In plasmas where a thick



(a) PEPL LVTF Faraday probe with guard

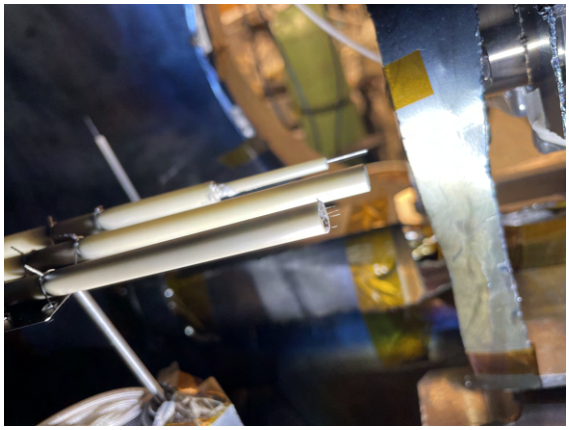

(b) PSTL RC Faraday probe no guard (middle)

Figure 3.27: Various types of Faraday probes used in this dissertation. Decisions of the type of Faraday probe used varied on easy of implementation and testing environment considerations based on recommended practices for Faraday probe use in EP testing [121].

sheath on the probe can alter results, a guard ring is placed on the outer edge of the probe to essentially flatten the sheath in the main collection area. Figure 3.27 demonstrates the ring-guard Faraday probe on the left and a smaller no-guard on the right. Additionally, some Faraday probes can have a magnetic field to act as a filter to limit SEE. In this work, the LM-NSTAR Faraday probe data was obtained using the guarded variant in Figure 3.27a while the NASA 8 cm Faraday probe was unguarded as in Figure 3.27b. No filtering was applied to either probed during data collection.

3.3.3 Emissive Probe

An emissive probe is used to obtain the potential of a plasma. Although a Langmuir probe may also be used–the knee is typically too rounded to locate the plasma potential, instead an emissive probe can be used and is more accurate as it avoids kinetic effects that can alter plasma potential measurements [122, 123, 124]. Typical construction places a thin thoriated-tungsten wire in a hair-pin loop through a double-bore alumina tube connected to thick wire leads. There are various methods used with the main two being the inflection point method and heat 'n float.

In the inflection point method an IV trace is obtained as the emitting electron current is varied. Additionally, multiple traces are taken with variations in the filament temperature. The measured plasma potential from each of the traces is then plotted versus heater power. Extrapolation the

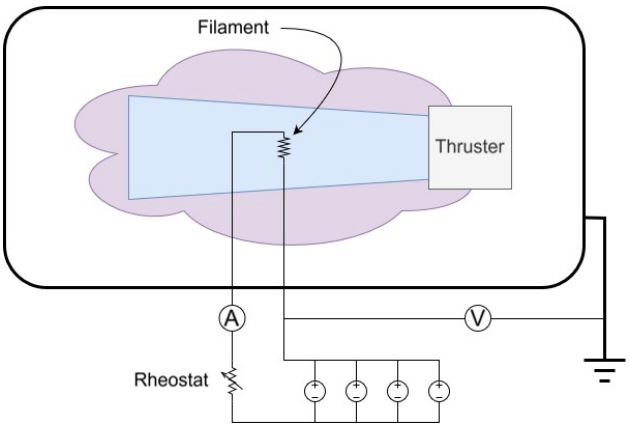

Figure 3.28: Heat 'n float emissive probe circuit to describe how plasma potentials were obtained with an emissive probe. A rheostat is used to control the electron emission current and the potential of the plasma is measured by the voltage difference of the filament to facility ground.

zero heating case yields the plasma potential. At this location space charge effects are not present to distort the IV characteristics. This method is the most accurate as it extrapolates to no sheath effects. Error for this method is $k_B T_e/10$. However, this method is slow and is not amenable to time resolved measurements unless plasma properties are well behaved and periodic.

The heat 'n float method uses a heating circuit to emit electrons from a thin filament into the plasma. The circuit is allowed to "float". Once the emitting current meets the electron saturation current of the plasma, the circuit will float at the potential of the plasma. This method has been said to have an accuracy of 1.5 -2$k_B T_e$ below the true plasma potential [122]. Using a smaller diameter filament wire can reduce the space charge effects as the field at at the probe is high. The voltage drop tends to be lower with smaller probes. This method is more advantageous over the inflection method when bandwidth or temporal measurements are needed. In this cases a probe is heated in excess of the plasma potential such that the emitting current is sufficiently in excess and deep into the electron saturation region. If not sufficiently emitting, the hot-floating potential may be far from the true plasma potential. A circuit diagram of the heat 'n float method is found in Figure 3.28.

Although Figure 3.28 displays a rather simple circuit, there are components that can be added to increase accuracy but that are also accompanied by a time response penalty. Because electrons are being emitted and collected at the filament deep into the saturation region, more accurate measurement of the plasma potential is actually at the the center of the filament. However, due to the inability to easily access and measure the potential while in use, two equal high impedance resistors may be placed between the positive and negative leads of the filament to allow an approximated measurement of the potential at the center of the filament being equal to that of which is at the center of the two high impedance resistors. However, this has a bandwidth cost. Due to

the high impedance, the reaction time of the circuit is limited. The response time frequency of an emissive probe is given as

$$f_c = \frac{1}{2\pi RC}, \tag{3.1}$$

where C is the capacitance of the wires of the emissive probe, R is the resistance in the emissive probe circuit [124]. Thus, the high impedance resistors may not capture time-resolved fluctuations. In this work, a spatially varied emissive probe was used to measure the plasma potential in the plume. The fluctuations were the primary objective and so the high impedance resistors were not used.

3.3.4 Retarding Potential Analyzer

Another electrostatic diagnostic used in this work is a retarding-potential analyzer (RPA). These devices utilize typically a three or four (or more) grid system to discriminate charge species based on potential. Peak energies and distribution functions can be readily extracted from an RPA IV characteristic. In the case of an electropostive plasma and a four-grid RPA, the first entry grid is typically floating (some older versions it was grounded but recent arguments suggest floating the grid provides more accurate results [125, 126, 127, 128]) to reduced the influx of ambient plasma into the probe. A second grid is then held at a negative potential with respect to facility ground to repel electrons. The third grid is swept with a voltage bias to discriminate the ion energy. The fourth grid is held at a negative potential to return electrons that may be emitted from the collector due to SEE. Grid alignment, spacing, and potentials are carefully selected to keep collimation, limit space charge effects, and decrease resonance time in the device to increase bandwidth of the sweep rate such that two particles with different energies are not collected simultaneously.

Unfortunately, RPAs are not able to discriminate against charge state or mass difference. As a result, a low energy doubly charge ion may appear as a higher energy singly charged ion and a ions of two species plasma are recorded simply as collected charge. High-speed RPAs are currently being developed for use in investigation of low-frequency oscillations in EP devices such as Hall effect thruster wheel-n-spoke or breathing modes [127, 126].

3.3.5 ExB

An ExB probe is used to obtain the velocity distribution and charge state by discriminating against unwanted energies with unbalanced electrostatic, $\vec{F}_Q$, and Lorentz forces, $\vec{F}_L$. The electrostatic force is determined by the voltage and gap distance between two electrodes such that the resulting force given as

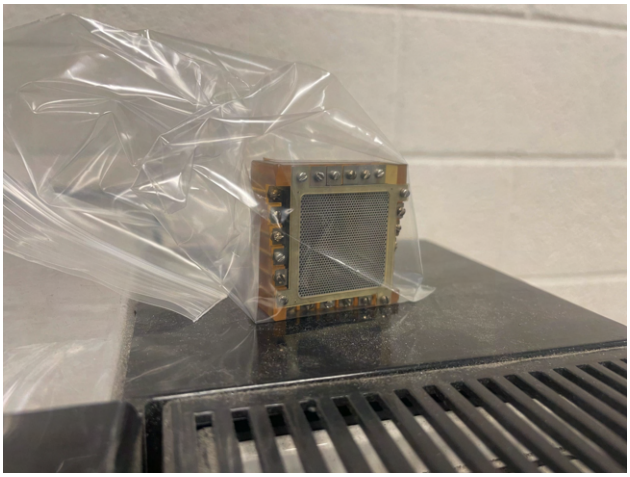

Figure 3.29: An example of a six-grid RPA like installed in the Rocket Chamber to obtain most prominent ion energy measurements.

$$\vec{F}_Q = q\vec{E}, \tag{3.2}$$

where q is the charge state and $\vec{E}$ is the electric field. The Lorentz force is

$$\vec{F}_L = q\vec{v} \times \vec{B}. \tag{3.3}$$

. Here $\vec{v}$ is the velocity vector and $\vec{B}$ is the magnetic field. Ions selectivity is determining by varying the E/B force ratios. The Wien velocity is the velocity at which the two forces are balanced written as

$$v_W = \frac{E}{B} = \frac{V/d}{B}, \tag{3.4}$$

where V is the applied voltage and d is the gap distance.

A spectra of the current as a function of bias voltage is the output from the ExB probe. Here charge species are not discriminated so the spectra of multiply charged species appears. ExB probes are used to obtain singles-to-doubles ratios for gridded ion energies. Further design considerations in collimator and drift tube lengths are discussed in Refs. [129] and [130].

3.3.6 Ion Gauge

Pressure measurements are made with a variety of different pressure gauges depending on the active pressure range. In most EP testing, the pressure is below 10^{-4} Torr. In this pressure regime, an ion gauge is often used. A hot filament emits electrons and an anode collects current. The amount of current collected can be correlated to a pressure measurement. One gauge can be used

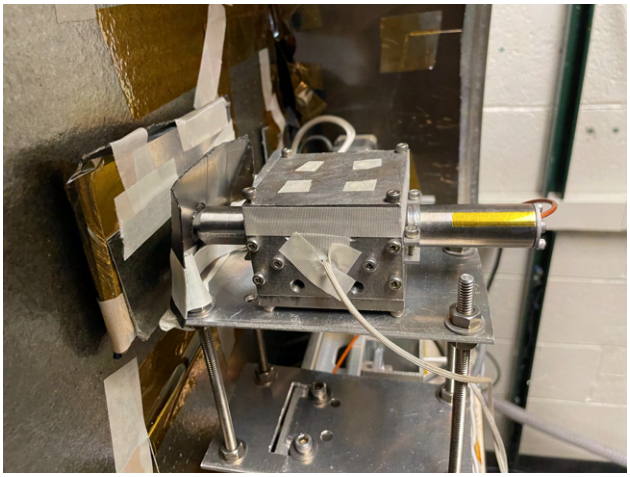

Figure 3.30: An ExB probe used to obtained doubles-to-singles ratios for thruster discharge chamber performance corrections and characterization. This probe is being designed at the University of Michigan Plasma Science and Technology laboratory to investigated doubles-to-singles ratios for the NASA 8 cm gridded ion engine.

for various gases as long as it has a correction factor from one gas to another. This correction factor is a function of the ionization potential.

Recommended practices for pressure measurements for EP testing is outlined in Ref. [42]. For thruster testing, an ion gauge is placed in-plane with the thruster about 1-1.5 beam diameters to the side to obtain reasonable pressure measurements occurring at the thruster plane. Additionally, recommended practices encourage the ion gauge to be placed in a vertical position and a neutralizer bend with a fine screen grid to be placed in front of the gauge to limit ambient plasma effects.

3.3.7 Residual Gas Analyzer

A residual gas analyzer (RGA) uses a filament to ionize the incoming gas which is then passed through a quadrupole mass analyzer separation stage which allows for mass selectivity. RGAs are used to determine the composition of the gas in the chamber. Typically, incorporated software assumes singly ionized and as a result of this assumption a doubly ionized gas particle may appear to have half the mass than expected and must be considered in analysis. An RGA used in the PSTL is seen in Figure 3.32.

3.3.8 Plasma Spectroscopy

Plasma spectroscopy uses optical emission spectroscopy to obtain line spectra of a plasma. This allows one to identify the species of the plasma and ionization states. Gas temperatures and plasma densities can also be determined based on the analysis of the structure of the line spectra (i.e.

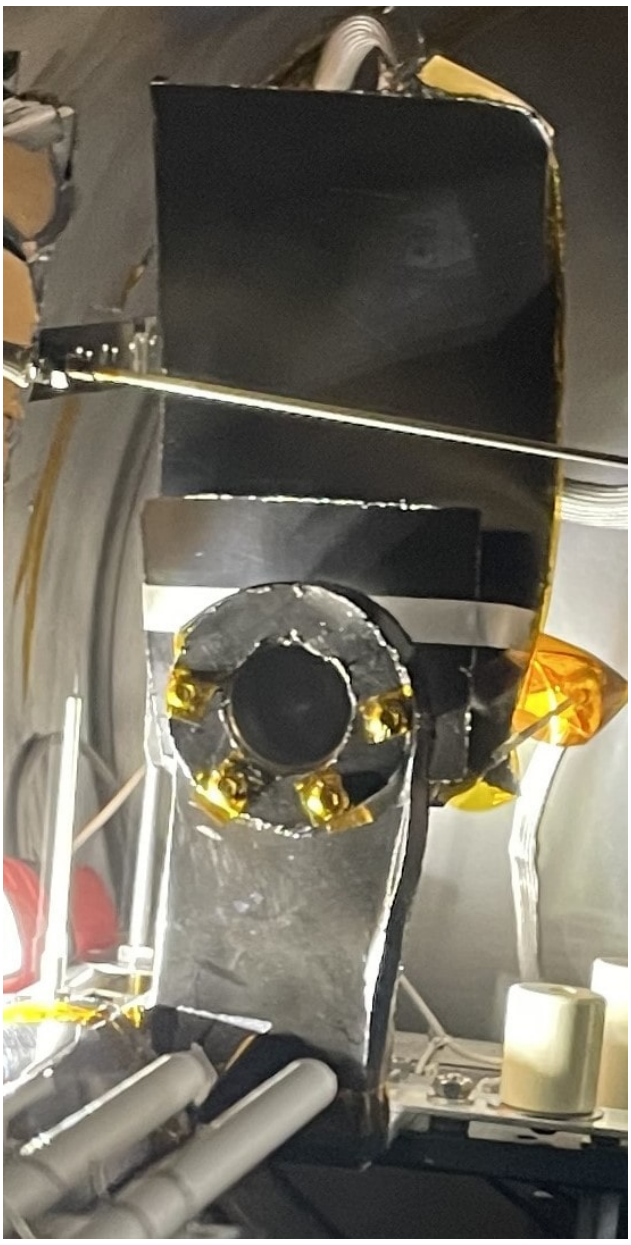

Figure 3.31: Ion gauge in the Rocket chamber to make pressure measurements.

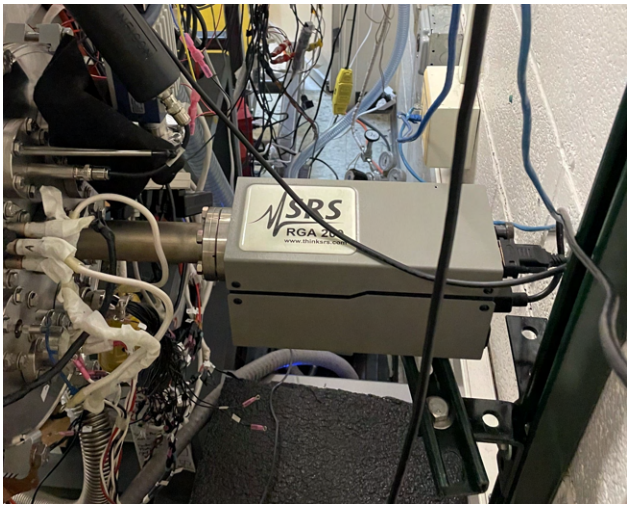

Figure 3.32: Residual gas analyzer used in the Rocket Chamber to identify potential gas species in the plasma using mass spectroscopy.

intensity ratios of two lines). This diagnostic is used in conjunction with an RGA to confirm gas and plasma species present in the system using the spectra obtained by both diagnostics.

CHAPTER 4

Low Power-Density Facility Effects

4.1 Motivation & Objectives

The objective of this work was to determine how thruster processes are impacted by the facility and how that could lead to poor predictions in actual spaceflight. This objective can be approached in essentially two ways. In one scenario the thruster operation is in a facility that is well in its capabilities of providing a reasonable spacelike environment. In the other extreme, testing is done at high-power densities where background pressure, plasma density, and potential coupling structures are present and thus thruster operation is not realistic of spaceflight. This chapter focuses on the facility effects observed in the former, in a reasonably spacelike environment. Presented here are the impacts of the facility boundary conditions on the plasma potentials in the chamber and key considerations of wall plasma potentials and their impacts on thruster operation due to their proximity to the thruster. Additionally, the effects of background neutral and ambient plasma densities on beam neutralization and coupling to the facility were explored. Measured beam current and doubles-to-singles production were also investigated. Relevance to spaceflight qualification, spacecraft design, and preparation are discussed here as well.

4.2 Experimental campaign & thruster operating conditions

The experimental setup for the low-power density test of the LM-NSTAR gridded ion engine in the PEPL LVTF is outlined in the previous chapter. Four various pumping configurations were used for three throttle conditions. The corresponding pressures during the test are located in Table 4.1.

General telemetry results during the different nominal operating conditions are presented for the three throttle conditions. Table 4.2 for TH01, Table 4.3 for TH05, and Table 4.4 for TH10. For the TH10-P1 condition, the neutralizer keeper voltage was increased during the testing. The values after the increase are designated by the "$\rightarrow$". The accelerator grid current was measured using a Fluke multimeter that only had accuracy down to the mA range.

Table 4.1: In-plane background pressures corrected for xenon approximately 1-1.5 beam diameters to the side of the thruster flats.

	TH01 (0.60kW)	TH05 (1.09kW)	TH10 (1.70kW)
Full [μTorr]	0.889	1.16	1.45
P0 [μTorr]	1.22	1.37	1.65
P1 [μTorr]	1.20	1.52	1.81
P2 [μTorr]	2.28	2.33	3.15

Table 4.2: NSTAR telemetry results in PEPL LVTF at the TH01 throttle condition.

TH01	FULL	P0	P1	P2
C [sccm]	2.50	2.50	2.50	2.50
M [sccm]	5.82	5.82	5.82	5.82
N [sccm]	3.00	2.50	3.00	3.00
NKPR [V]	25.61	26.20	25.2	19.01
NKPR [A]	2.080	2.062	2.006	2.023
DISC [V]	29.28	30.73	29.71	29.94
DISC [A]	5.348	4.300	5.442	5.372
BEAM [V]	850	850	850	850
BEAM [A]	0.532	0.523	0.533	0.524
ACCEL [|V|]	150	150	150	150
ACCEL [mA]	1	1	1	1
V_{cg} [V]	-14.75	-12.15	-14.50	-12.35

Table 4.3: NSTAR telemetry results in PEPL LVTF at the TH05 throttle condition.

TH05	FULL	P0	P1	P2
C [sccm]	2.88	2.60	2.53	2.54
M [sccm]	10.82	9.32	11.82	11.82
N [sccm]	3.00	2.50	3.00	3.00
NKPR [V]	21.82	27.40	20.61	18.47
NKPR [A]	2.080	2.052	2.015	2.025
DISC [V]	29.79	28.26	29.91	30.02
DISC [A]	6.696	8.000	6.614	6.703
BEAM [V]	1100	1100	1100	1100
BEAM [A]	0.810	0.784	0.813	0.810
ACCEL [|V|]	150	151	150	150
ACCEL [mA]	2	2	2	2
V_{cg} [V]	-14.76	-15.26	-14.23	-13.22

Table 4.4: NSTAR telemetry results in PEPL LVTF at the TH10 throttle condition.

TH10	FULL	P0	P1	P2
C [sccm]	2.52	2.35	2.54	2.54
M [sccm]	18.42	19.00	18.62	18.62
N [sccm]	3.00	2.60	3.00	3.00
NKPR [V]	19.66	22.61	18.35→17.89	17.82
NKPR [A]	2.069	2.019	1.806→2.047	2.087
DISC [V]	30.02	30.78	30.19	30.28
DISC [A]	13.022	11.825	12.931	13.481
BEAM [V]	1100	1100	1100	1100
BEAM [A]	1.291	1.310	1.294	1.305
ACCEL [|V|]	180	180	180	180
ACCEL [mA]	3	4	4	4
V_{cg} [V]	-15.41	-14.27	-13.43→-13.08	-14.90

4.3 Plasma-Facility Interactions

In this section, the ambient plasma in the facility and the effects of fixed wall potentials on thruster processes such as neutralizer margin and plume expansion were investigated. The objective of this section was to determine if the size and pumping capabilities of PEPL LVTF caused any significant facility effects on these processes. Additionally, limitations of this study were noted and used to improve the experimental design of future tests and identifying future testing objectives of interest.

4.3.1 Facility Boundary Conditions

In space, the beam plasma is allowed to expand out freely and eventually the potential will approach zero at the edges. This is in stark contrast to a ground testing environment. Most facilities are grounded directly to earth ground. As a result, this strict boundary condition in many respects compresses the beam and forces it to satisfy boundary conditions that are not spacelike. In the case of electropositive plasma, sheath formation at the walls can cause lower energy electrons to be reflected back into the bulk plasma. Only the higher energy electrons are able to overcome the retarding potential and make it to the walls. Additionally, as the sheath potential increases in magnitude (assuming the plasma potential increases with a constant electron temperature), only higher energy electrons are able to make it to the wall. As a result, more of the higher energy electrons return to the bulk plasma and the plasma potential increases until equilibrium is reached. These escaping energetic electrons create background plasma and thus their magnitude can effect the plasma that makes it back to the engine and spacecraft. How well the beam is neutralized is dependent on the magnitude of the trapped colder electrons.

It is expected that for constant plasma densities, if the plasma potential near the walls increases, then so should the electron temperature. However, these electron temperatures should be higher than to be observed in space at this distance from the beam due to the sheath-heating of the electrons via the reflection process. It is speculated from neutralization simulations that it is the lower electrons that provide the neutralization for the beam as the higher energy electrons escape the potential well created by the beam [131]. In space, these high energy electrons return due to the high potential well behind them. In a grounded test facility a sheath could elevate the plasma potential near the wall and steal these electrons by providing a different large potential well. The highest energy electrons then make it to the wall while the lower energy ones are reflected and heated by the sheath.

As a result of the sheath-heating, the returned higher energy electrons are less likely to aid in the neutralization process. From this perspective, this should limit beam neutralization from the ambient plasma. However, the increase of neutral densities from the inadequate pumping speeds increases electron-neutral collisions that cools the electrons and potentially ionizing the neutral gas. The conductivity of a plasma with the assumption that the local plasma approximation is valid and that small changes in electron temperature are negligible, then the conductivity of the plasma scales as electron density over neutral density. Thus, an increasing rate of electron density will increase the conductivity which occurs due to energetic electrons colliding with neutrals and ionizing them. Thus, high potential differences at the walls and sheath-heating increase the energy of electrons causing more ambient plasma ionization, resulting in an increase of local conductivity. This aspect is important to note as this can affect beam neutralization if the conductivity between the neutralizer and the walls increases faster than the conductivity between the neutralizer and the beam. If the impedance to the walls becomes smaller than the impedance of the plasma bridge to the beam, the beam potential will rise. In any case the potential distribution will differ from space conditions. These conditions also favor electrons collecting on the grounded surfaces of the engine for current neutrality. In any case, multiple electron populations will exist with low energy electrons trapped in the beam. These effects must be captured in the model. The walls and background plasma cannot be neglected as it impacts divergence and charge flow with implications of spacecraft engine interactions.

As a result, it is expected that a neutralizer coupled with the walls should see changes in the potential at the wall consistent of allowing more lower energy electrons to the wall to neutralize the beam but this is coupled with the ambient electrons being slowed by collisions with neutrals and getting dragged into neutralizing the beam. This process is more likely if the ambient and beam plasma densities are roughly the same order of magnitude allowing charge species to freely move between the two plasmas. Thus it is nearly impossible to track without a simulation and to determine which electrons are providing neutralization for the beam. What dominates: neutral-

izer, secondary-electron emission (SEE) and ion-induced electron emission (IIEE), or the ambient plasma? It is expected that at higher pressures that lower electron temperatures will remain in the beam and background plasma effects may not be as important in the near field but in the far field where beam potential is lower the background plasma may have a greater affect. In this respect, the neutralizer may not be the only source of neutralization and thus neutralizer margin studies in facilities may be inherently incorrect if these aforementioned processes are not accounted for. The following two subsections investigate which of theses competing mechanisms are the dominate factor in beam neutralization for low-power density ground testing.

4.3.1.1 Near-Wall Plasma Properties

Plasma boundary conditions vary from wall interactions to interactions with the engine housing. An investigation of the pressure variation on plasma properties near the wall was initially performed at the PEPL LVTF with the 2.3 kW LM-NSTAR gridded ion engine. Over the four pressure ranges and three throttle conditions. In Figures 4.1, 4.2, and 4.3 are the three throttle conditions with the four different pressures plotted against their downstream positions, respectively. These spherical Langmuir probes were approximately 7-11 cm displaced from the wall surface and with the thruster center-line located 3 m from the chamber wall. Note, that at the TH01 throttle condition, there were two sets of data for the P2 pumping configuration after a slight change occurred randomly in background pressure and thruster performance. Each figure contains these six plasma properties: 1) plasma potential, 2) floating potential, 3) electron temperature, 4) electron Debye length, 5) electron density, and 6) ion density. The P0 condition was taken on the first day of the testing campaign. Because these data points had slightly different flow rates than the subsequent runs plasma properties varied somewhat abnormally to the other data points.

Electron and ion densities in the TH01 case changed only slightly with downstream position. It was expected that the plasma density at the walls would be relatively low owing to the distance between the beam and the walls as well as the overall low-power density. This was the condition observed for the TH01 power level. In this respect or at least at low-powers, LVTF appears to be an adequate simulation of spacelike conditions.

The plasma potential and electron temperature of the wall probes were hightest for the P0 pumping configuration. On this test day, the discharge voltage was higher around 30.73 V compared to the other test conditions which were around 29.50 V. The higher discharge voltage lead to elevated doubles production and is later verified in Figure 4.25, discussed in a later section. From this it was seen that small changes in the discharge performance had an impact on the ambient plasma in the facility. The thruster and facility plasmas are coupled but here the thruster impacts on the facility were minimal.

As the pressure increased, the floating potential of the probes raised towards zero. The elec-

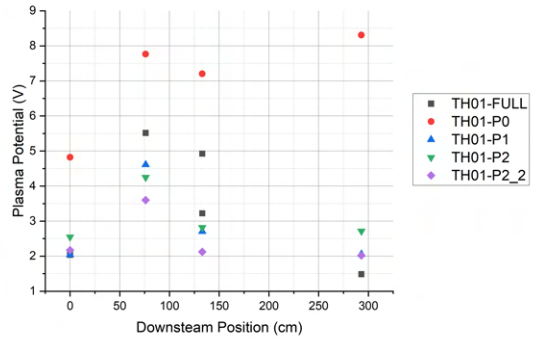

(a) Plasma potential

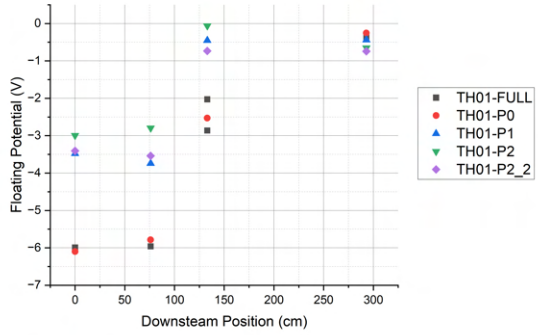

(b) Floating potential

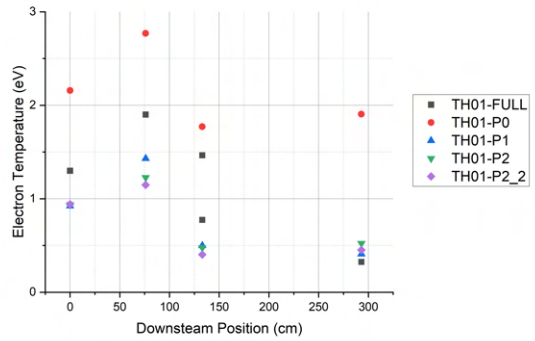

(c) Electron temperature

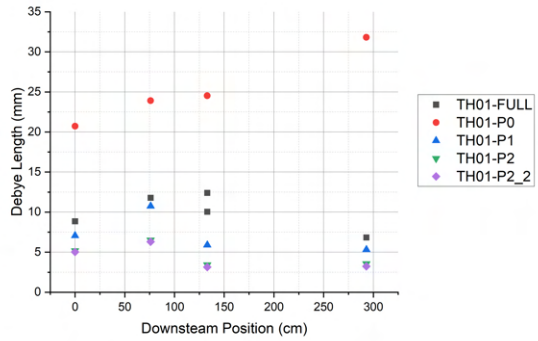

(d) Debye length

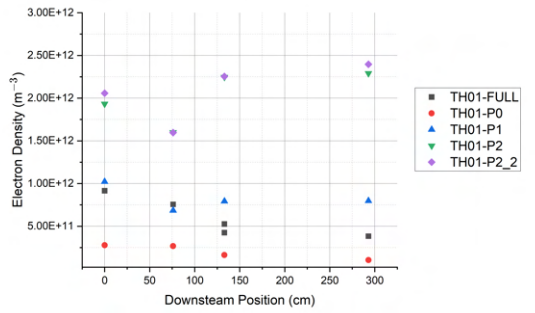

(e) Electron density

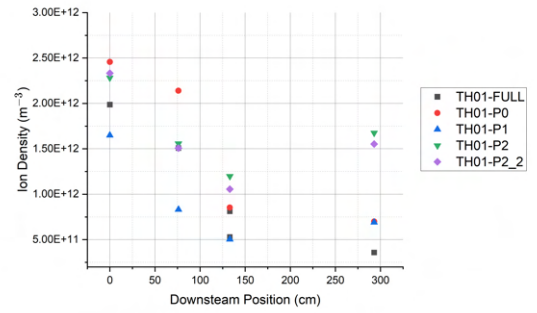

(f) Ion density

Figure 4.1: Plasma properties of the spherical Langmuir probes at the walls of the facility that are located in the ambient background plasma using the LM-NSTAR GIE operating at the TH01 throttle condition.

tron temperature also decreased with the increase of pressure. Decreasing electron temperature with increasing pressure was expected due to the increase of electron-neutral collisions cooling the electrons. As a result, the plasma and floating potentials should have decreased as well. However, the two probes closest to the thruster had similar floating potentials but there was a discontinuity between the second and third probe. As the beam became more neutralized and diffuse, the potential in the beam decreased resulting in lower plasma potentials and electron temperatures that caused the floating potentials to approach zero. The floating potential was an important parameter to observe because it gives insight to the behavior of the electrons. Because the walls were grounded and had limited electron emission, it was expected that the plasma potentials near the walls should always have been positive. The floating potential indicated the energy level of electrons that were lost to the walls. If the floating potential was negative and increasing in magnitude, an increasing amount of higher energy electrons would have been repelled back towards the beam. On the other hand, the positive floating potentials near the walls would have indicated that there was an increasing amount of lower energy electrons. The observation of a positive floating potential and more lower energy electrons would have been an important observation as it is suspected that lower energy electrons are mostly responsible for beam neutralization and can impact the neutralization process in a non-spacelike manner [131]. For the LM-NSTAR test, 1-2 eV electrons were observed in the near-field wall Langmuir probes, but downstream the electron temperatures drop to 0.5 eV. In conclusion, because the plasma densities are low at the walls at 10^{12} m^{-3} compared to the beam plasma densities of 10^{15} m^{-3} (see 4.5) the beam is allowed to expand reasonably well with limited ambient plasma or wall effects altering thruster operation such as aiding in neutralization. The NSTAR test in LVTF provides a good spacelike environment to ensure proper beam neutralization by the neutralizer and not the walls or ambient plasma.

Similar to the TH01 case, the downstream position of the wall Langmuir probes followed similar trends for the TH05 throttle level. In the near field the plasma potentials and electron temperatures, both increased and then decreased after the second probe. The floating potential also was constant for the first two probes, but then increased further downstream. Corresponding with this was the lower electron temperatures. According to the ion density, the plasma density was decreasing with probe position as expected. Only the electron density for the higher background pressure actually increased. This may be attributed to more uncertainty in locating the plasma potential, and as a result, less calculated electron density. Thus, the ion density was assumed to be more accurate for these cases in which the plasma potential measurements had more deviations and followed a less consistent trend. Overall, the TH05 power level also did not indicate large variations in the plasma properties near the walls indicating that LVTF was still an adequately sized facility for testing at this power level.

For the TH10 condition, the Langmuir probes near the wall varied similarly as the other throttle

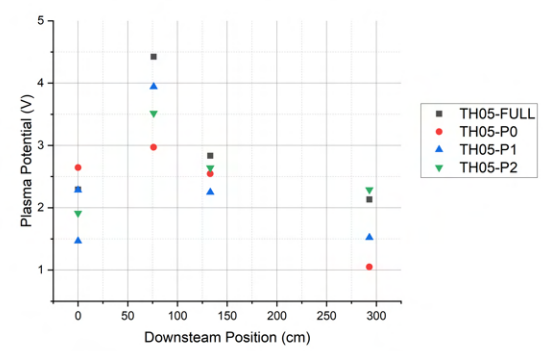

(a) Plasma potential

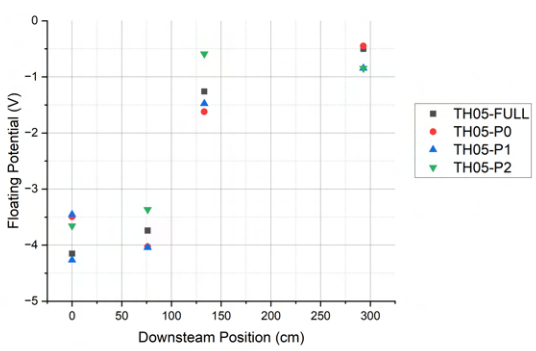

(b) Floating potential

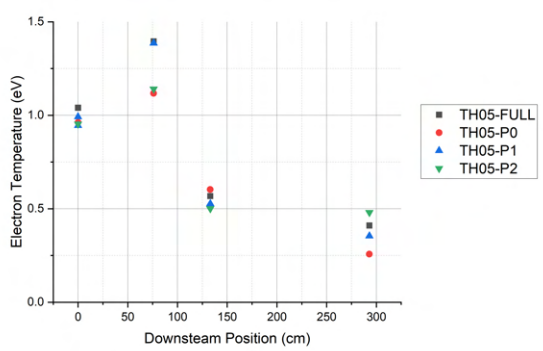

(c) Electron temperature

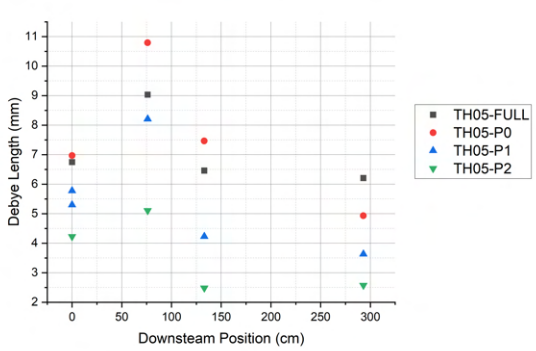

(d) Debye length

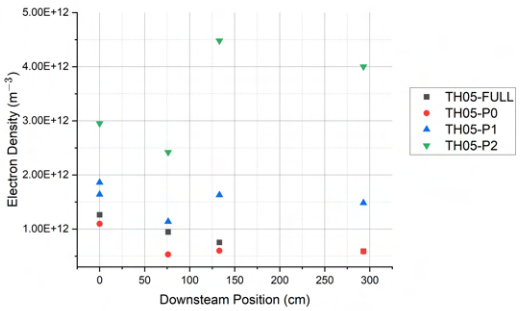

(e) Electron density

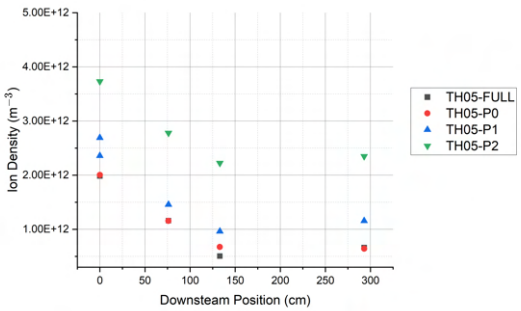

(f) Ion density

Figure 4.2: Plasma properties of the spherical Langmuir probes at the walls of the facility that are located in the ambient background plasma using the LM-NSTAR GIE operating at the TH05 throttle condition.

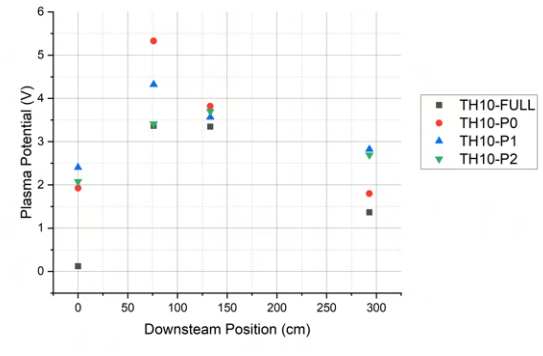

(a) Plasma potential

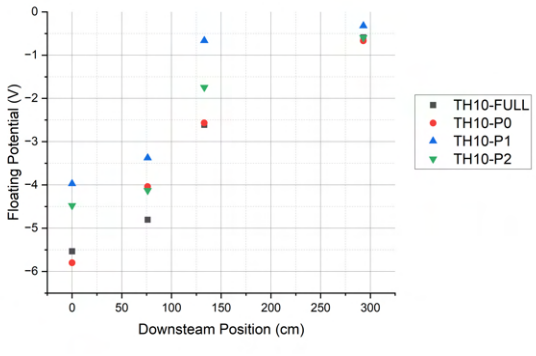

(b) Floating potential

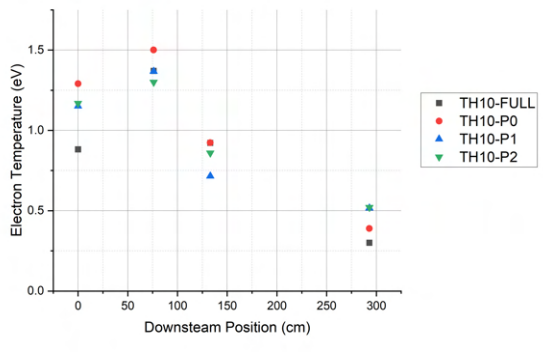

(c) Electron temperature

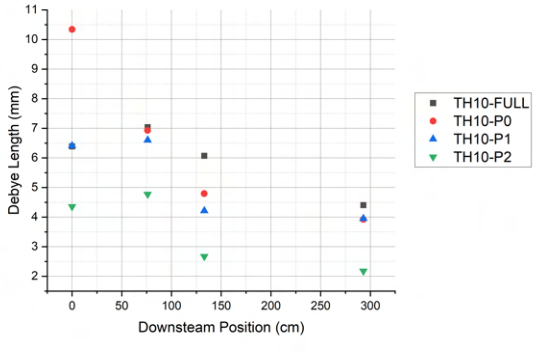

(d) Debye length

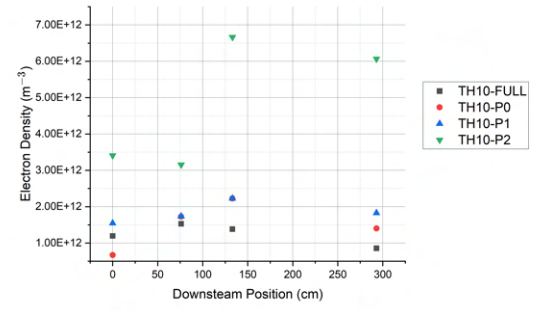

(e) Eectron density

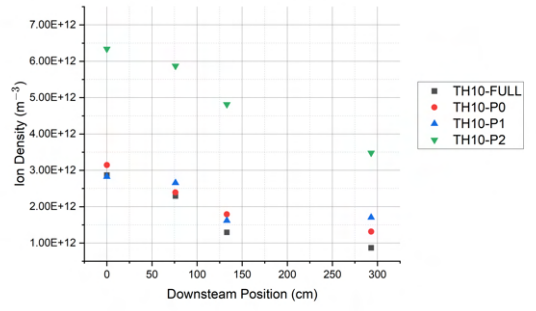

(f) Ion density

Figure 4.3: Plasma properties of the spherical Langmuir probes at the walls of the facility that are located in the ambient background plasma using the LM-NSTAR GIE operating at the TH10 throttle condition.

conditions. However the plasma potentials and electron temperatures decreased slightly downstream. There was a noticeable linear increase to the floating potential. Because the higher throttle condition and increased neutral density, cooler electrons translated into reduced floating potentials and a larger degree of neutralization in contrast to low-power case where beam decays to the background plasma density in the near field.

The plasma potential profile across the chamber is an indicator of the presence of the beam at the wall and is thus an indication of the beam dispersion. The plasma potential should have been near ground potential at the beam edge. For all three throttle conditions, it was observed that starting with the potential of the in-plane wall probe, the potential was relatively low around 2-3 V as expected. After approximately two beam diameters downstream the potential increased to about 5-6 V and then continued to decrease with downstream position. The TH01-P0 condition, which had its most dramatic difference in lower discharge current and higher discharge voltage, had the highest potentials at the walls but followed the same behavior. The plasma potential change with axial distance showed less variation downstream as the pressure increased. These variations were evidence that the PEPL LVTF may provide adequate pumping and was a decent size to emulate a spacelike environment for at least the low throttle conditions of NSTAR-like engines. These findings are consistent with space observations of the NSTAR engine used for the DS1 mission.

The electron temperature determines the plasma potential and thus its variation should mirror that of the plasma potential. This was in fact observed again as expected. It was expected that the electron temperature would decrease with neutral density due to increased collisions. This seems to be the case for the TH01 throttle condition, but not apparent for TH05 and TH10 . However, it is observed that an increase of neutral density elevated the electron density further downstream and likely suggests that the electrons were no longer Maxwellian. This behavior was enhanced and occurred at locations where the pumps were turned off. At the lowest pumping speed, most of the pumps turned off where the on the right-side of the thruster, same side as the probes. This showed that their can be dramatic change in plasma properties due to localized increases of pressure and as such it is necessary to have multiple pressure gauges throughout the chamber to understand pressure effects.

Floating potentials of the wall probes increased with downstream position. This was a different to the trend of the plasma potentials and electron temperatures. Floating potential was expected to become more positive as the electron temperature decreased (e.g. pressure increases). Reduced background plasma density would also have the effect of zeroing the plasma potential. From this study, the floating potential could be a simple guide to understand how much interaction the beam plasma could be having with the wall. The closer to zero or positive floating potentials, the more energetic ions reaching those locations.

In the following four figures, four plasma properties for the different eight Langmuir probes

plotted against pressure for the three different throttle conditions are presented. The first four are the four wall probes, followed by the Langmuir probe near the plasma screen, neutralizer, and the planar and wire probe in the plume on center-line downstream. In Figure 4.4 are the plasma potentials, Figure 4.5 are the electron densities, Figure 4.6 are the electron temperatures, and Figure 4.7 are the Debye lengths. Floating potentials and ion densities are found in the appendix B.

Plasma potential variations for the in-plane wall probe and the furthest downstream probe had the most consistent trend with increasing background pressure. For these two probes, regardless of throttle level, the plasma potential at the wall was unchanged with pressure. The other two middle probes were less consistent. The third wall probe, displayed the most significant changes over the throttle conditions, here as well it can be seen that some grouping of the plasma potentials based on the throttle condition and not background pressure. If this effect was exaggerated this could indicate the facility is not large enough for neutralization to occur in the beam before the high potentials in the beam impact the wall plasma. The planar and wire probes placed on center-line of the beam show distinct plasma potentials for the given throttle levels. Other than the outlier from the TH01-P0 condition seen in all the probes. The potential in beam varies with throttle condition and not background pressure.

Electron density at the wall probes for all throttle conditions followed a linear trend. If there was significant amounts of beam-wall interactions, then it would have been expected to see more variations in the plasma density at the walls between different throttle conditions. One would expect than at the walls that the various throttle conditions (different ion energies) would result in different rates of increase of ambient plasma density. This is not observed.

For the other probes, near plasma screen, neutralizer, and the two on center-line downstream in the beam do not scale linearly with pressure. These seem to be more effected by the throttle level of the thruster itself. The trends in these plots are dictated by the power level. This was because these probes are in closer contact with the beam plasma. It is important to note that the measured plasma density on beam center-line was approximately 10^{14}-10^{15} m^{-3} (see also Figure B.2 in appendix B) compared to the wall probes with a density of 10^{11}-10^{12} m^{-3}. Even the neutralizer plasma density seems to drop off an order of magnitude. The plasma density gradient between the beam and wall plasmas was important to prevent a strongly conductive path between the two. If the density of the ambient plasma was on the order of the beam plasma, electrons could freely flow between the two and cause ambiguity in the capabilities of the neutralizer to provide beam neutralization.

Electron temperatures in the in-plane and furthest downstream probe had the least amount of variation with background pressure. The minimal variations observed suggested that the facility background pressure did not have much of an impact at these levels. There was some small cooling of the electrons in the middle two probes, but not even that was clear for all throttle conditions.

Near the plasma screen and the neutralizer, the electron temperatures are scattered, but overall

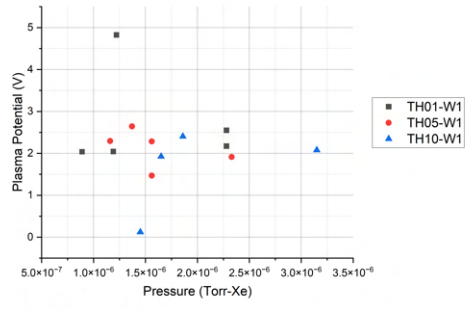

(a) Wall probe 1 at 0 cm

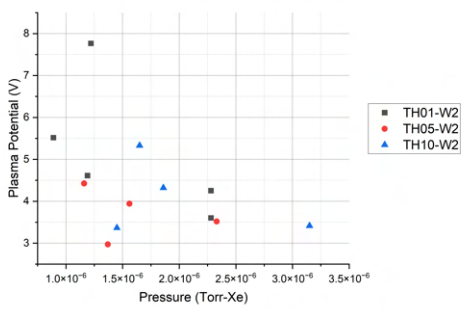

(b) Wall probe 2 at 76 cm

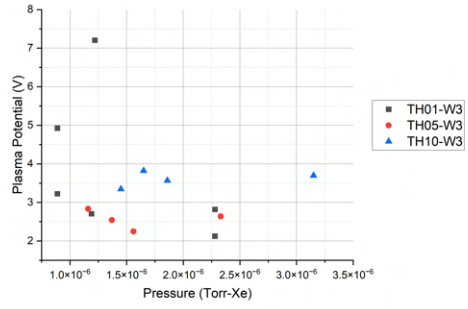

(c) Wall probe 3 at 133 cm

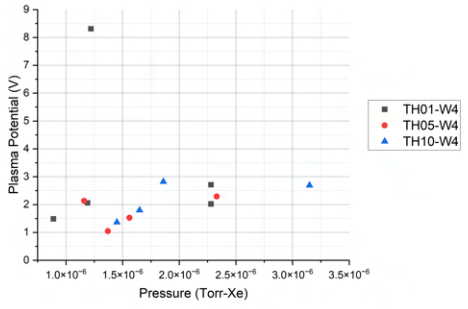

(d) Wall probe 4 at 293 cm

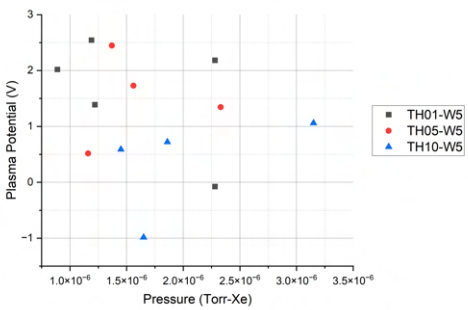

(e) Near plasma screen probe

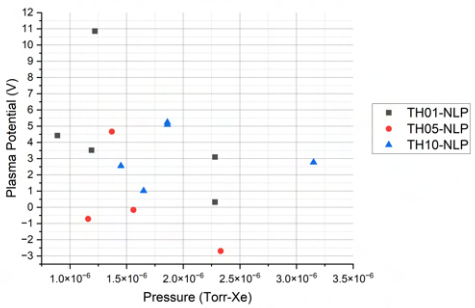

(f) Near neutralizer probe

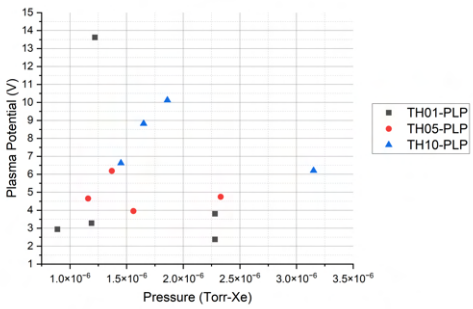

(g) Planar probe on center-line at 208 cm

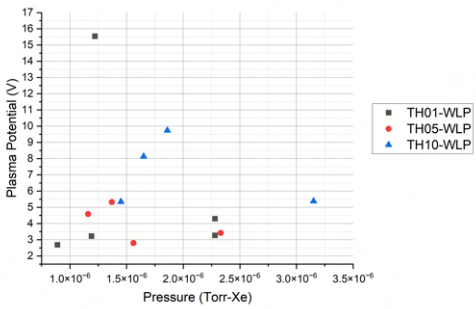

(h) Wire probe on center-line at 208 cm

Figure 4.4: Plasma potential variations measured using Langmuir probes at various locations throughout the facility as background pressure was controlled by limiting pumping speed.

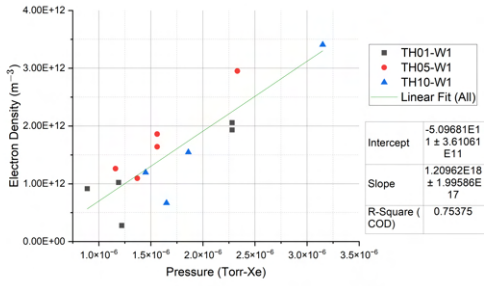

(a) Wall probe 1 at 0 cm

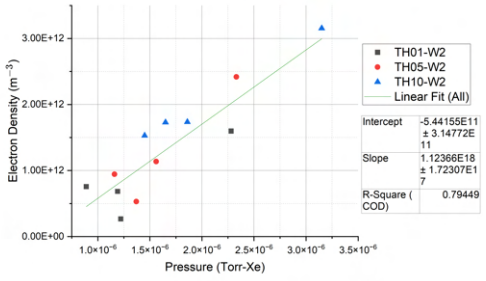

(b) Wall probe 2 at 76 cm

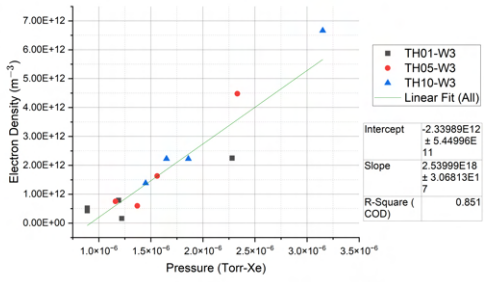

(c) Wall probe 3 at 133 cm

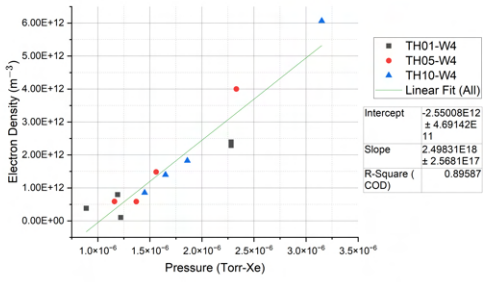

(d) Wall probe 4 at 293 cm

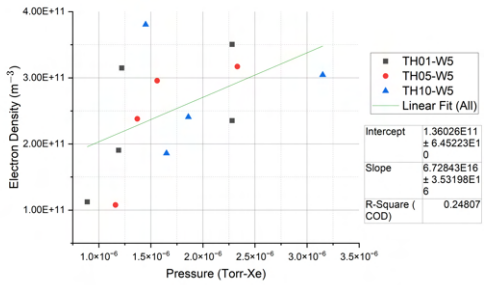

(e) Near plasma screen probe

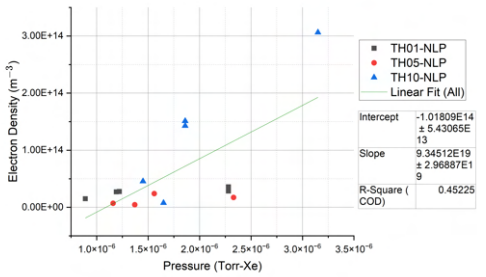

(f) Near neutralizer probe

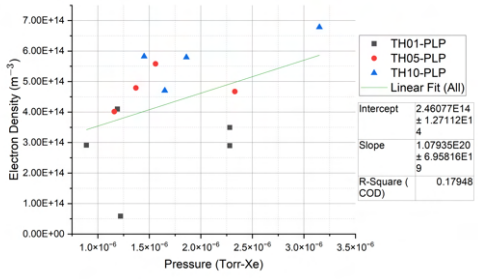

(g) Planar probe on center-line at 208 cm

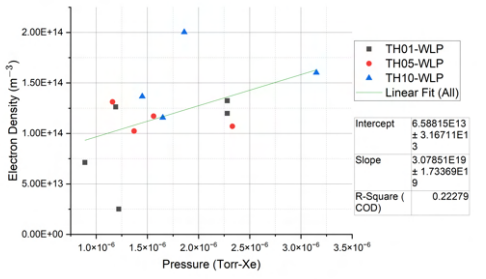

(h) Wire probe on center-line at 208 cm

Figure 4.5: Electron plasma density variations measured using Langmuir probes at various locations throughout the facility as background pressure was controlled by limiting pumping speed.

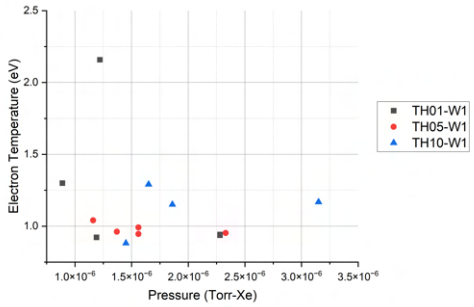

(a) Wall probe 1 at 0 cm

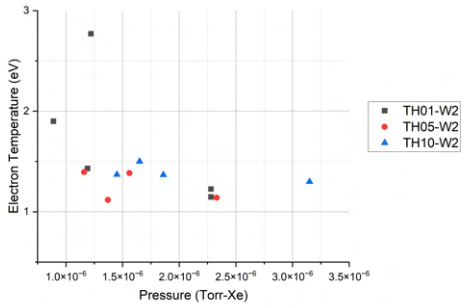

(b) Wall probe 2 at 76 cm

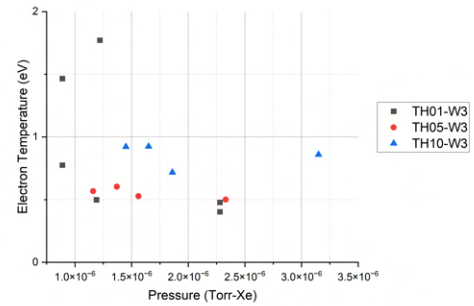

(c) Wall probe 3 at 133 cm

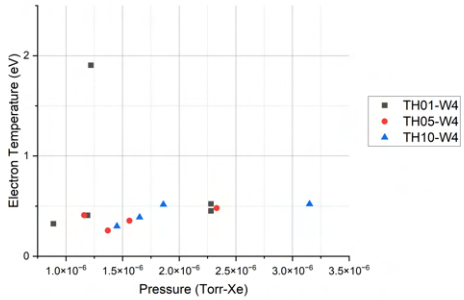

(d) Wall probe 4 at 293 cm

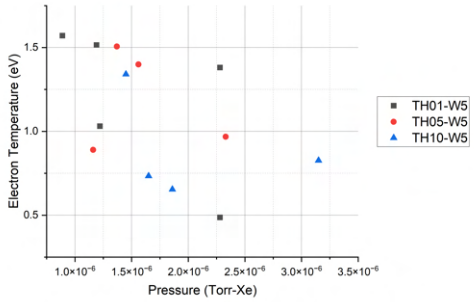

(e) Near plasma screen probe

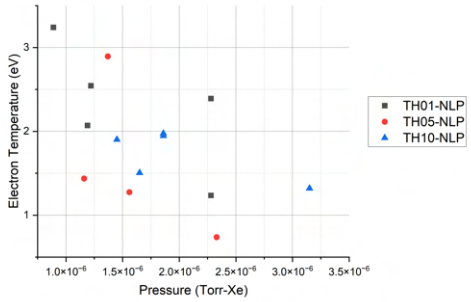

(f) Near neutralizer probe

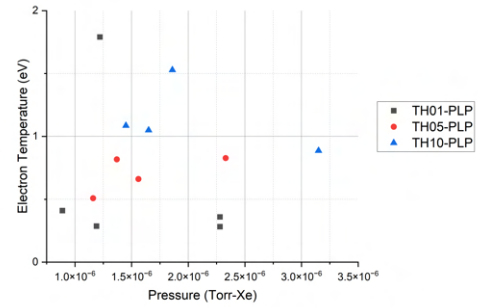

(g) Planar probe on center-line at 208 cm

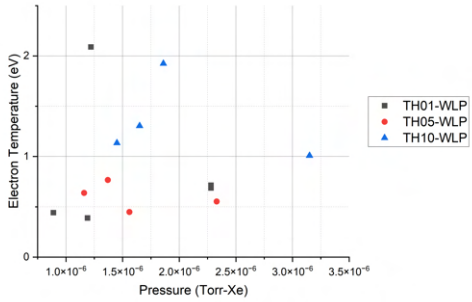

(h) Wire probe on center-line at 208 cm

Figure 4.6: Electron temperature variations measured using Langmuir probes at various locations throughout the facility as background pressure was controlled by limiting pumping speed.

did tend to decrease with background pressure. This was expected as there should have been an increase of collisions with background neutrals that should have cooled the electrons significantly as this was where higher density of neutral gas was expected to be due to non-ionized propellant flow being located there at greater densities. If additional ion gauges where available near the walls this would have probably showed that the walls had a much lower background pressure than at the thruster flats.

The electron temperatures in the beam plasma were also not only pressure dependent, but were grouped more by throttle condition of thruster. This was expected since the plasma density in the beam should be much greater than the ambient plasma density. The separation of the beam and ambient densities allowed for the electron population in the beam to increase (trapping) with the increase of beam potential at the higher throttle conditions.

Although there was not much difference in the Debye lengths of the inner two wall probes to that of the edge probes, the plasma potentials of the two probes were a lot less consistent. However, from the electron temperature plots it was observed that theses probes had much greater electron temperatures than the other two wall probes. Additionally, the fluctuations in the electron temperatures seemed to correspond with the fluctuations in the plasma potentials. Because the plasma density seemed to linear increase with pressure, the large changes in the electron temperature set the fluctuations observed in the Debye length. The Debye length trend was a non-linear decrease that appears to flatten out at higher neutral and plasma densities. As the Debye length decreased, so did the sheath penetration into the bulk plasma. The fact that the electron temperatures were not increasing (nor should they due to the increase of neutral collisions) the sheath size was determined by the plasma density. Here the Debye length converges around 3-5 mm for all wall probes. A smaller sheath is good to prevent interference with the bulk plasma but could be a future indicator that the thruster power levels are too high and the beam plasma will couple with the facility plasma leading to electron populations in the plume that are not realistic of space conditions.

4.3.1.2 Beam Plasma Plume

The facility walls do not only impact the ambient plasma, but can also impact the expansion of the beam plasma. Faraday probe sweeps were taken at 86 cm downstream. As the probe moved out to the wings, the increased plasma density due to the increased background pressure increased the measured current. This is seen in Figure 4.8 and is called plume broadening. This extra current can cause a miscalculation of thrust if it is included in the current integration of the ion beam current. This is why near field sweeps yield the most accurate thrust measurements. On the other hand, for an undersized chamber, the background plasma can extend the wings even in the near field impacting the beam profile and neutralization.

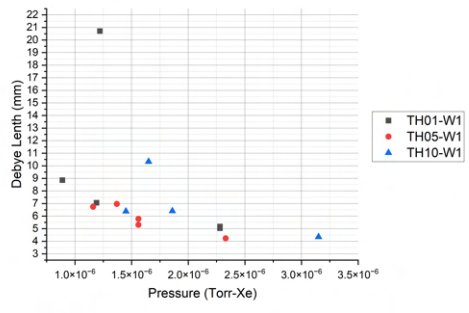

(a) Wall probe 1 at 0 cm

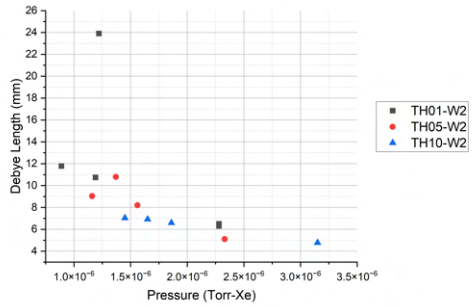

(b) Wall probe 2 at 76 cm

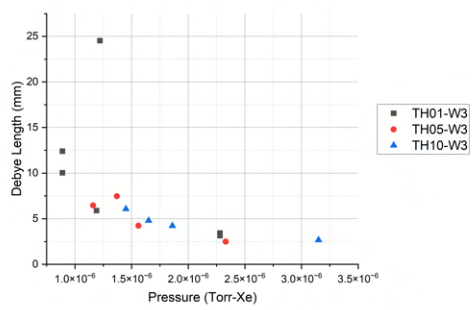

(c) Wall probe 3 at 133 cm

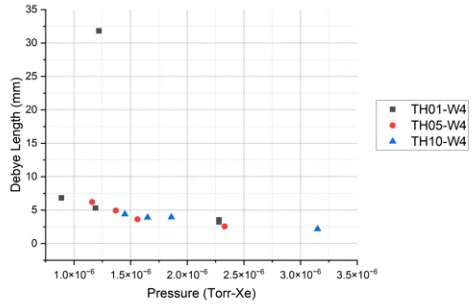

(d) Wall probe 4 at 293 cm

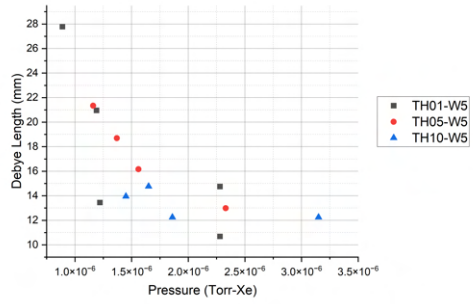

(e) Near plasma screen probe

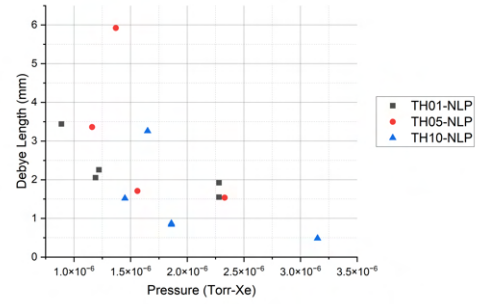

(f) Near neutralizer probe

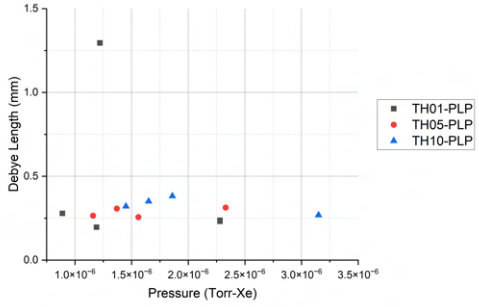

(g) Planar probe on center-line at 208 cm

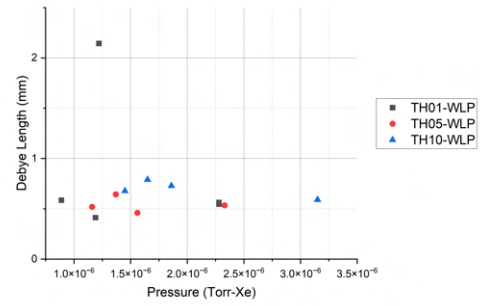

(h) Wire probe on center-line at 208 cm

Figure 4.7: Electron Debye lengths variations measured using Langmuir probes at various locations throughout the facility as background pressure was controlled by limiting pumping speed.

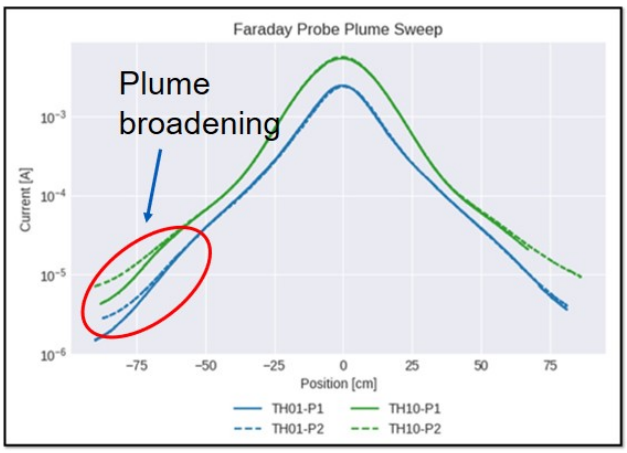

Figure 4.8: Observed plume broadening in the wings of the sweep due to elevated ambient background plasma using a lateral plume sweep via a guarded Faraday probe.

4.3.2 Electrical Coupling & Beam Neutralization

In the past, the neutralizer-facility coupling voltage, $V_{cg} = \phi_{NC} - \phi_{GRND}$, has been used as a metric to determine how well a beam is being neutralized during ground testing. This is because it has been assumed that the beam must be neutralized in a facility either by the neutralizer or off the walls. As the thruster couples more with facility to neutralizer the beam, the coupling voltage should then increase in magnitude to force more electrons from the neutralizer into the beam. However, this metric does not give insight into how the electrons from the neutralizer get to the beam. This section focuses on how the facility impacts these processes and if the assumption of using V_{cg} is always valid.

4.3.2.1 Coupling and Neutralization Variables

It was expected that the electrons from the neutralizer cool with more collisions due to the increase in the ambient background neutral density. This would than increase the impedance of the plasma bridge and so the actual electron distribution that ultimately arrives at the beam may have multiple populations–low and high energy components. If the conductivity between the neutralizer and the beam decreased due to too many electron-neutral collisions, than the potential between the neutralizer and beam needed to increase to aide the electrons in overcoming the increased impedance. This can happen by either the potential of the neutralizer decreasing (becoming more negative with respect to facility ground) or the potential of the beam increasing. If coupling between the neutralizer and the beam is very good, then the plume potential will be low, indicating that the facility is not contributing significantly more in the neutralization processes. Table 4.5 is the resulting neutralizer coupling voltages measured for the differing pumping speeds and throttle conditions.

Table 4.5: LM-NSTAR neutralizer-facility coupling voltages in LVTF for TH01, TH05, and TH10 throttle conditions and various background pressures controlled by limiting the pumping speed. The impacts of a floating plasma screen on neutralizer-facility coupling voltages are also presented with the "F" after the pumping configuration indicating a floating plasma screen was used instead of the nominal grounded plasma screen configuration used in all other cases.

V_{cg} [V]	FULL	P0	P1	P1-F	P2	P2-F
TH01	-14.75	-12.15	-14.50	-13.21	-12.35	-13.29
TH05	-14.76	-15.26	-14.23	-14.24	-13.22	-14.26
TH10	-15.41	-14.27	-15.05	-15.28	-13.10	-14.64

The "-F" indicates a test condition with a floating plasma screen.

In general, the coupling with the facility decreased (meaning the negative V_{cg} trended toward zero) as the ambient background pressure increased. The P0 condition was an outlier in this analysis because it used slightly different flows and neutralizer currents. The decrease in the magnitude of the coupling voltage was due to the increased plasma density aiding in connecting the plasma bridge to the beam. However, this was not the case for the TH10-P1. Without knowing the potentials in the beam, it is difficult to measure the true-coupling voltage, $V_{cp} = \phi_p - \phi_{NC}$. Such a measurement is a more accurate measurement of the coupling of the neutralizer to the beam. Similarly, studies in Hall thruster modeling of coupling voltage as a function of pressure show that the coupling voltage for every thruster and every facility will not vary identically. Jorns et al. highlight that there are two competing terms for Hall thrusters as well. The Boltzmann effect and a restive-drive term compete for if the coupling voltage will decrease or increase with background pressure [132]. In gridded ion engines, the conductivity between the neutralizer-beam and neutralizer to competing alternative neutralization pathways can change the behavior and trends of the coupling voltages. Thus, it is imperative that future testing involve plasma potential measurements in the plume to obtain the true coupling voltages which can be done with an emissive probe.

If the facility is aiding in the neutralization process, then the electrons from the neutralizer can go to ground to complete the circuit. Other than near-by grounded objects, the plasma screen of the thruster has been conventionally grounded. As a result, the impedance path from the neutralizer to facility ground can be decreased significantly due to the short distance between the neutralizer and plasma screen. Patterson and Mohajeri saw a decrease in the coupling voltage (more negative) of the neutralizer-facility coupling voltage while floating the plasma screen [54].

It was expected here as well that a floating plasma screen would decrease the neutralizer-facility coupling voltage further due to the beam not being as easily neutralized and so the plasma bridge potential difference must increase in magnitude to get electrons into the beam. This was observed in Figure 4.9 by the relative percent change from the nominal grounded configuration to the floating plasma screen configuration. It was observed that this effect was amplified at higher pressures.

This supports the idea that at higher background pressures, with the increase of ambient plasma density, that there was an increase in the conductivity of the neutralizer to the grounded plasma screen. As a result, the beam was being partially neutralized off a ground surface downstream. In the floating plasma screen, the path to ground had an increase in impedance and resulted in the neutralizer potential having to increase in magnitude negatively to get electrons to the beam. The change in the neutralizer-facility coupling voltage even with the floating plasma screen is unfortunate because it indicated that the beam is being partially neutralized off the facility still. A decoupled beam from the facility that is being primarily neutralized by the neutralizer would not have its neutralizer-facility coupling voltage become more negative when the plasma screen is allowed to float. A neutralizer-facility coupling voltage closer to ground potential would indicate less coupling with the facility. It would then be expected that the beam potential in the floating plasma screen case would be lower in the near field if neutralizer-facility coupling voltage was closer to zero, indicating good beam neutralization and the lack of neutralization assistance from the facility.

In space, typically the beam is the only potential well to trap neutralizer electrons. Thus, as long as the potential in the very-near field is neutralized enough to prevent a virtual anode from forming, the beam will propagate and be neutralized. In ground testing, the competing neutralization pathways will always be present and make it difficult to characterize the neutralizer operation to ensure proper good spacelike neutralization such that the flows and power requirements can be minimized. From this study, the point at which the grounded and floating plasma screen have the same neutralizer-facility coupling voltage indicates the point at which beam neutralization off the facility is constant. However, this does not mean the true-coupling voltages for both configurations are equal. A beam potential in the near field is required for this to ensure a virtual anode does not form.

4.3.2.2 Commonalities in Hall Thruster Testing

Studies on Hall thruster at Georgia Institute of Technology have also shown that near-by grounded objects can impact the coupling voltages of Hall thrusters [133]. The alternative neutralization pathways that arise in gridded ion testing can also appear in Hall thruster testing as the thruster beam can be neutralized due to cathode electrons collecting on nearby grounded surfaces and reappearing downstream at facility walls. This can lead to improper coupling voltages and effective beam voltages that lead to improper spaceflight performance predictions. During the testing of the H9 at the VTF-2 at Georgia Institute of Technology, the thruster was ran at the 4.5 kW and 9 kW throttle conditions. The corresponding plasma potentials from the hot floating potential of an emissive probe and the cold floating potential with a 1 m radial arm sweep are plotted in Figure 4.10. The true-coupling voltages were determined using the obtained plasma potentials and the

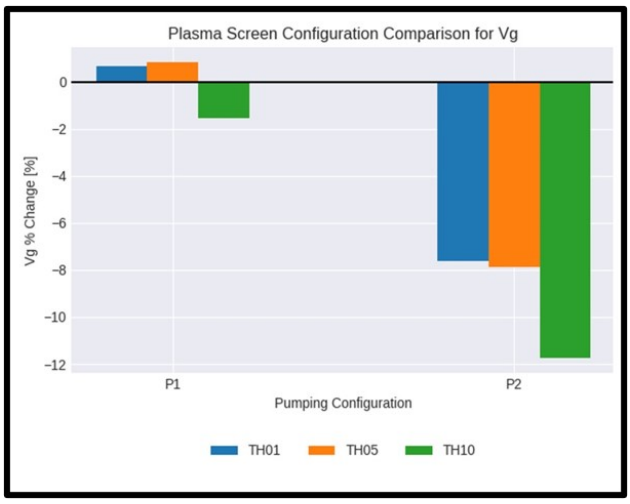

Figure 4.9: The relative percent change in neutralizer-facility coupling voltage for the LM-NSTAR GIE in LVTF between the grounded (nominal) and the floating plasma screen electrical configuration as background pressure is varied. A more negative neutralizer-facility coupling voltage (increase of coupling of the thruster with the facility) is observed with the change from a grounded to a floating plasma screen.

potential of the thruster cathode. The electron temperatures and errors are approximated using the formulas in Ref. [124], adjusting for the mass of krypton.

There is asymmetry in the measured plasma and floating potentials that should not occur. This was attributed to the geometry of the radial arm. The radial arm support structure was made of 80/20 covered by graphite. There were four probes placed on the structure. Two probes on one side of the support and two on the other. The emissive probe used to obtain this data was placed on the far end of the structure as seen in Figure 4.11. Thus, when on the negative degrees off center-line positions, the rest of the probes and radial arm structure were out of the plume, but at the positive degrees off center-line the rest of the radial arm were in the plume. As a result measured properties and calculated results were affected by the the other objects in the plume when the measurements were made. This suggested the importance of considering objects in the plume that could be affecting the measurements. Limiting the number of grounded objects and the size of these objects in the plume would limit their impact on the plasma measurements. It was also observed that the 4.5 kW test condition was more impacted by these objects in the plume because the lower plasma energies interact more with the structure and were more prone to perturbations than the higher power condition.

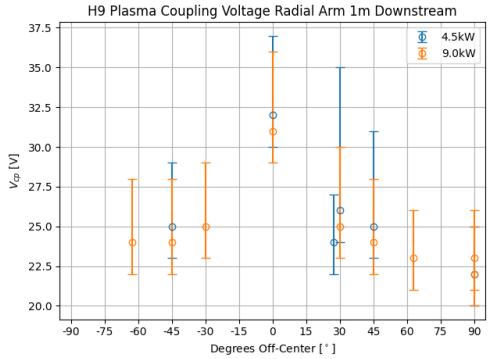

(a) True-coupling voltage

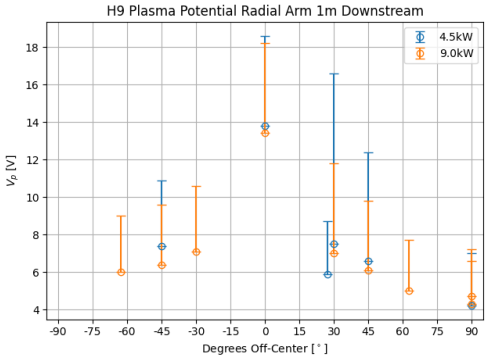

(b) Hot-floating (plasma) potential

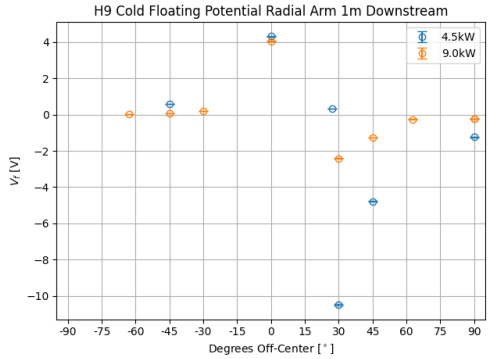

(c) Cold-floating potential

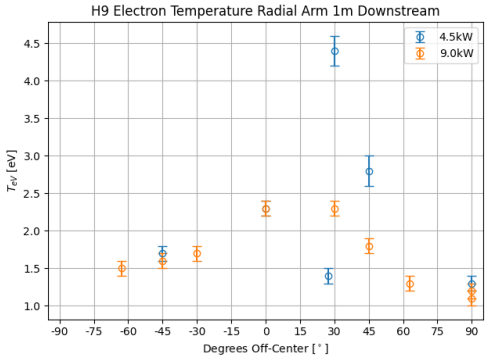

(d) Electron temperature

Figure 4.10: H9 Hall thruster heat'n float emissive probe results on a 1 m radially arm sweep of the thruster plume. Asymmetry in potential measurements.

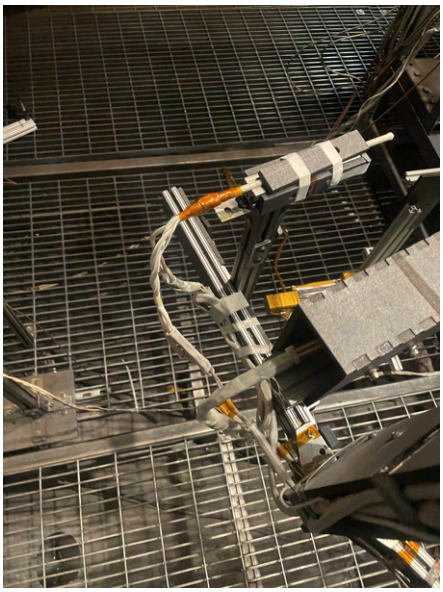

(a) Emissive probe installation on radial arm

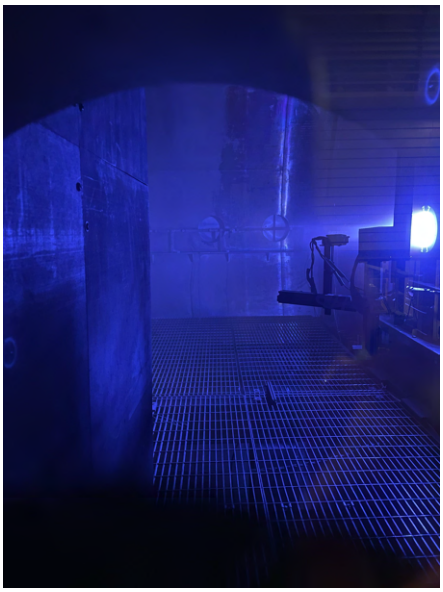

(b) Emissive probe on radial arm during testing

Figure 4.11: H9 Hall thruster radial arm probes at the Georgia Institute of Technology VTF-2 test facility.

4.3.3 Neutralizer Characterization & Margin

Characterizing the neutralizer margin in a hollow cathode neutralizer is performed by adjusting the neutral flow to the neutralizer and recording the neutralizer keeper voltage and coupling voltage till the neutralizer transitions to plume mode. Plume mode occurs when there is insufficient ion production to support the required electron emission in a plasma-bridge device [9]. In this condition an unstable sheath forms to facilitate extraction of the electrons to counter the space-charge caused by demanding an electron current which exceeds the Bohm criterion. This is typically denoted by a high peak-to-peak oscillation of the neutralizer cathode potential as the cathode becomes less stable and less quiescent. Because the neutralizer does not contribute much to thrust production, optimal operation of the thruster is met as flow is reduced to a minimum in the neutralizer without operating in plume mode. However, compared to spaceflight, the overall background neutral pressure is much higher during ground testing. This can also result in an elevated increase in the ambient plasma density. As a result, the plasma bridge formation and impedance of the bridge during ground testing differs than that of during spaceflight. Understanding the development and differences of the plasma bridge during ground testing is imperative to understand not only how to optimize the neutralizer margin for spaceflight, but also ensuring the beam is being neutralized similarly during ground testing as it would be in spaceflight. To achieve this understanding,

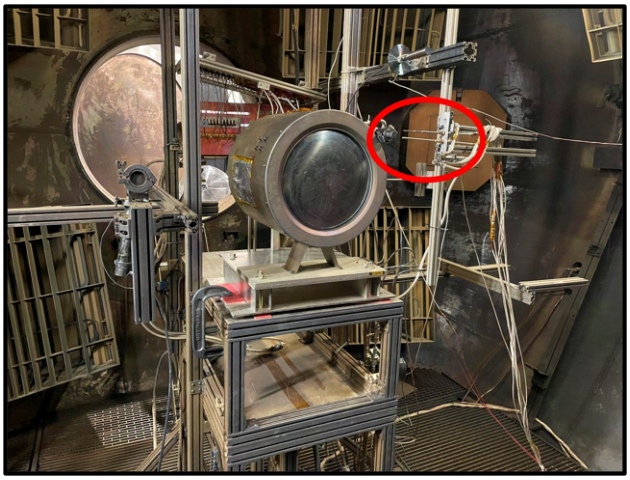

Figure 4.12: LM-NSTAR gridded ion engine and diagnostics near neutralizer (in red) used to measure plasma properties. There was a cylindrical Langmuir probe for plasma potential, electron density, and electron temperature measurements. Additionally, a retarding potential analyzer (RPA) was used to obtain the ion energy distribution function with the corresponding most prominent ion energy obtained by taking the first-derivative of the ion energy distribution function.

characterization of the neutralizer performance over a range of background pressures is needed for insight into the effects of increased neutral density on neutralizer cathode operation. Furthermore, investigation of the plasma properties near the neutralizer are obtained through a Langmuir probe and RPA. An ammeter is also placed on the grounding line of the plasma screen to measure current passing through the plasma screen to facility ground.

Further investigation into a floating plasma screen impacts on thruster performance were performed by characterizing the neutralizer. Neutralizer characterization is a measurement of the amount of gas flow necessary to flow through the neutralizer to provide the emission necessary to neutralize the beam in the so called spot mode. In the spot mode, neutralizer cathode emission is stable and low voltage, in contrast to the plume mode there the neutralizer operates in a high voltage, unstable mode, which limits neutralizer lifetime. The measurement determines the flow margin–that flow range to the neutralizer over which it operates in the spot mode. This characterization was done for only one operating condition, TH05-P2. For current characterization, current started at 2.0 A, then increased current, then returned to nominal. Following nominal current operation, the current was then decreased just before the onset of plume mode. The plume mode is so called because a luminous plume emanates from the cathode. It is typically associated with flows not adequate for desired emission current. Responses in the thruster operation were investigated via the telemetry data and the ammeter placed in-line of the plasma screen grounding lead being replaced by an voltmeter to measure the floating potential of the plasma screen with respect to facility ground. An RPA near the neutralizer is used as well to monitor energetic ion energy from

the neutralizer (a characteristic often accompanying plume mode).

4.3.3.1 Pressure Variation

Comparisons of the neutralizer margin at throttle condition TH10 over three background pressures is presented here. In Figure 4.13 telemetry data of neutralizer keeper voltage, facility coupling voltage, current to plasma screen, peak-to-peak oscillations of V_{cg} are presented. Following are Figure 4.14 are of the plasma potential and neutralizer ambient plasma potential with respect to V_{cg}, electron temperature, and plasma densities and Figure 4.15 of most prominent ion energies from the RPA.

The transition from spot to plume mode is seen in Figure 4.13d with the sharp increase in the peak-to-peak voltage oscillations. Noticeably, in spot mode the oscillations are between 4-5 V for FULL and P1 pumping configurations. This oscillation voltage increased to around 6 V for the P2 case. It was assumed to be because the neutralizer current had to be increased to 2.1 A for the P2 case as the neutralizer was consistently unstable at 2.0 A. This larger 6 V oscillation is probably because the operated flow rate for the P2 condition was at the edge of plume mode onset. In addition, this highlights that effect of background pressure on neutralizer margin. The onset of plume mode occurred at higher flow rates for higher pressures. Other background pressure affects on cathodes suggest the cathode should stabilize with increased facility pressure [134, 135]. Thus, the onset of plume mode at higher flows has nothing to do with cathode performance but rather the higher background pressures. The increased background pressure increases the neutral pressure between the neutralizer cathode and the beam which presumably effects the impedance to beam. In this case, in space, the flow margin would not be correct with plume mode occurring at a lower flow rate–a clear facility effect.

In conjunction with earlier onset of plume mode, the facility coupling voltage during plume mode was observed to decrease in magnitude with an increase of pressure. This is to say that at lower pressures, the transition to plume mode made V_{cg} much more negative than at higher background pressures. An increase in the ambient plasma density can contribute to the stabilization of the facility coupling voltage as the increase in conductivity of ambient plasma keeps the thruster interaction with the facility more constant with changes in neutralizer flow. This ambient plasma may additionally aide in the neutralization of the beam due to its increased conductivity. In plume mode, the neutralizer struggles to produce electrons to neutralize the beam, as such a measurement of plasma potential in the beam would aide in determining if the beam is being neutralized at higher background pressures by the ambient plasma. If the beam plasma potential is similar to the non-plume mode state or does not increase to an as high potential at higher background pressures, then this would be evidence that the increase in ambient plasma density is aiding in neutralizing the beam.

Alternative neutralization pathways are an important consideration and there is concerns with high amounts of current being collected on the plasma screen. There was an observed coupling between the neutralizer flow and the amount of current collected on the plasma screen. The linear correlation between the two behaves as expected, where less flow produces less plasma and as a result less current to the plasma screen. It is difficult to comment on a comparison of the magnitudes of the currents for the different pressures as it was observed that there are other factors that affect the magnitude of collected current during a constant pressure. For one, the observed discontinuity in TH10-FULL was attributed to a recycle that occurred between flows. Immediately after the recycle, the current changed drastically but then slowly recovered on the order of seconds and in some cases, even minutes. On these time scales, it was expected this was a thermal effect due to the throttling down of the discharge and beam power supplies during a recycle to prevent arc welding between grids. During this throttling down, the grids can cool rapidly and the neutralizer can vary chaotically momentarily due to the sudden changes in potentials. As the system comes back fully online, the current to the plasma screen slowly came back to normal operation. This has been seen during the NEXT-C qualification testing during their characterization of recycles in large amounts of current is emitted through the neutralizer plasma shortly after a recycle [136].

Lastly, the effectiveness of the thruster is based on the total thrust produced at a given input power required for operation. Thus, a summation of all powers required for each power supply is an important consideration. The neutralizer keeper power supply is kept in current control mode and voltage varies to meet the necessary current requirements. The TH10-P2 keeper voltage was lower than the others because the neutralizer current had to be increased to 2.1 A. TH10-FULL and TH10-P1 had similar voltages but at the boundary of plume mode it was observed for all cases the voltage increased more as the pressure decreased. This again, is attributed to the damping effect of increased local plasma density padding the changes and reducing the needed potential of the keeper to pull out electrons.

From Figure 4.14a, it was observed the ambient plasma potential near the neutralizer did not change at the onset of plume mode. However, it was seen that the potential difference between the ambient plasma near the neutralizer and the neutralizer cathode did increase sharply due to the negatively increasing coupling voltage caused by the plume mode. This large amplitude increase in coupling voltage was the result of the neutralizer not being able to expel enough electrons. It is precisely this larger negative potential that causes issues in cathode lifetimes. Not only are energetic ions known to be produced in plume mode [137], but the large negative coupling voltage can produce high energy ions that can erode thruster components, primarily the neutralizer in this situation. Additionally, the neutralizer potential, NC, serves as an overall reference point for all other thruster components. Thus, a large decrease in NC will result in the whole thruster system potential being lowered. The accelerator grid was held at a negative potential with respect to NC,

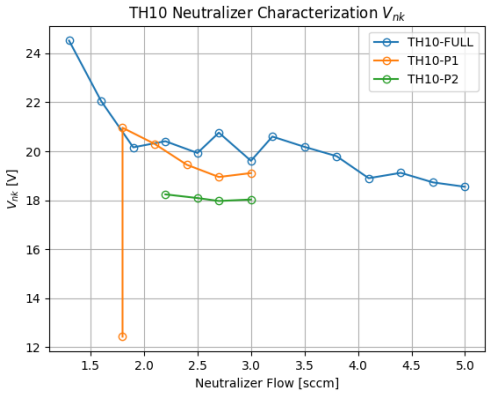

(a) Neutralizer keeper voltage

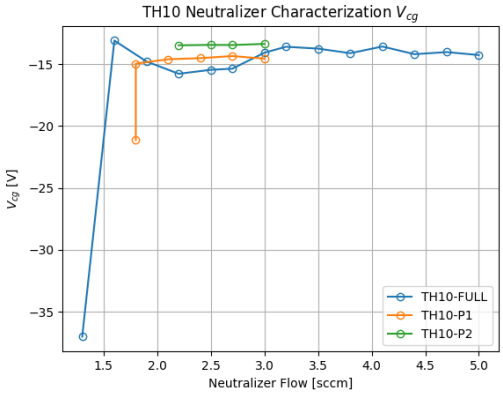

(b) V_{cg}

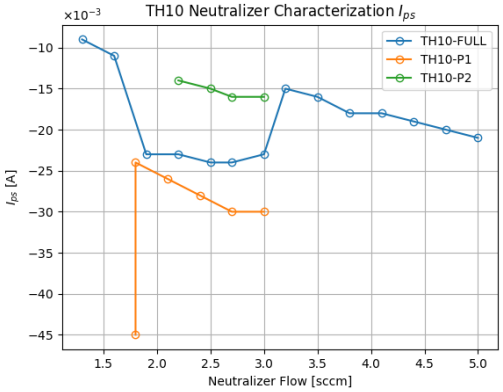

(c) Plasma screen current

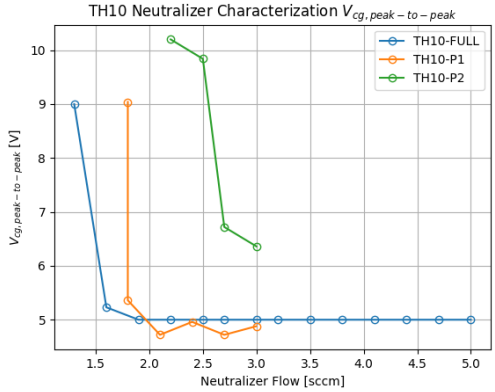

(d) V_{cg} peak-to-peak

Figure 4.13: Important thruster operating conditions during the neutralizer margin characterization of the LM-GIE in LVTF at the TH10 throttle condition for various background pressure. An indicator of the onset of an unstable high voltage mode of the neutralizer cathode is an increase in the peak-to-peak oscillations of the neutralizer cathode potential with respect to facility ground in sub-figure (d).

but care is taken in setting this value as too large of a negative value will lead to enhance grid erosion from ambient CEX ions. Considering this, a large negative NC will lower the accelerator grid potential even further with respect to the potential of the ambient plasma, enhancing grid erosion and shortening thruster lifetime. The neutralizer keeper potential was also lower and may result in enhanced erosion. Enhanced erosion like this on the neutralizer keeper was seen on Hayabusa 2 where the neutralizer was unable to expel enough electrons to keep the neutralizer from becoming significantly negative [87]. This neutralizer runaway was not observed during ground testing as as the thruster was setup with respect to facility ground, and as such, the facility was able to aid in neutralization [89]. Careful considerations are required to obtain a proper neutralizer margin such that similar issues as Hayabusa 2 are not encountered.

The electron temperature in Figure 4.14b for the TH10-FULL condition has a peak around 3 sccm of flow. At higher flows the electron temperature cools with additional collisions with neutrals. This 3 sccm corresponds with the flow rate used at the TH10 throttle condition. It appears that less cathode flow causes the electron temperature to decrease at least at around this operating condition–a local minimum. It should be pointed out that some of the noisiness may be related to a recycle which may play some role as well. In any case, local cathode conditions at this emission current and flow may explain why the electron temperatures are less consistent for the lower flows as seen by Figure 4.13c the neutralizer coupling with the plasma screen was in a different mode during this time. It was expected that there would be a local maximum for the electron temperature like in 4.14b, but for the other two condition it appears that only one side of the curve was observed. For the TH10-P1 case, the extra background pressure seems to have shifted the curve to the right, but because the onset of plume mode occurred sooner there really is no decreasing electron temperature at lower flow rates. The P2 case was interesting as it displays this decreasing electron temperature with decreasing flow rates. Albeit, the electron temperatures are much lower. Both these two affects are attributed to the increase of the neutralizer current by 0.1 A. This increase seems to have moved the curve to the right. If higher flow rates were tested, it would have been expected to see this local maximum for the electron temperature like in the TH10-FULL case.

The increase of neutralizer current did result in an increase of electron densities near the neutralizer as demonstrated in Figure 4.14c. From Figure 4.13b it was observed the coupling voltage, V_{cg}, became less negative slightly with the increased electron density. However, it was expected that the increased electron density would increase the current to the plasma screen. Figure 4.13c shows that the current is the minimum at this elevated high electron density TH10-P2 condition. Unlike the TH10-P1 condition collected higher current (25-30 mA) at the plasma screen, the TH10-P2 (15-20 mA) increased plasma production (by just under an order of magnitude in electron density) appears to neutralize the beam more by increasing the conductivity through the plasma bridge and

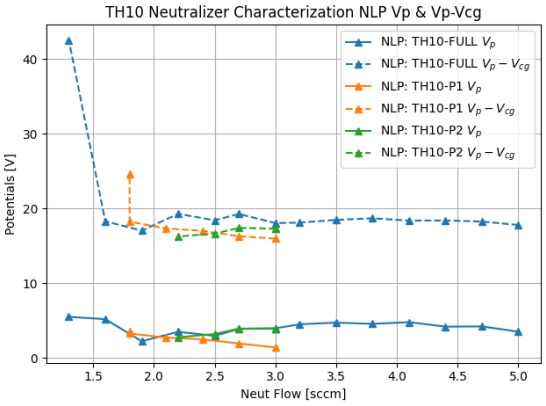

(a) Plasma potentials and coupling voltages

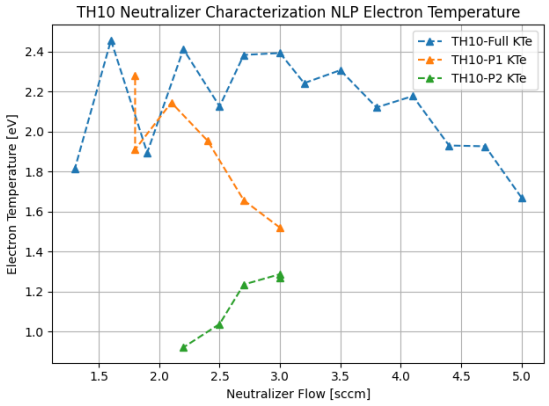

(b) Electron temperature

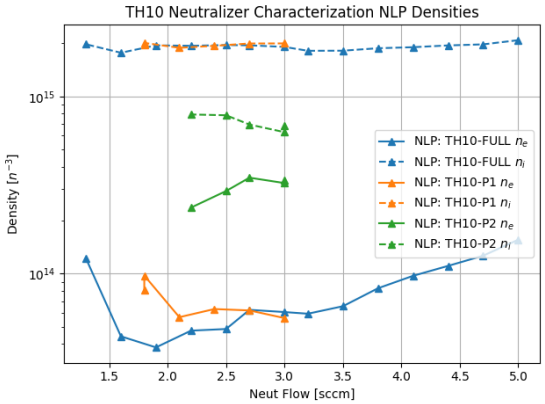

(c) Plasma densities

Figure 4.14: Plasma properties near the neutralizer using a cylindrical Langmuir probe during the neutralizer margin characterization of the LM-NSTAR GIE in LVTF at the TH10 throttle condition for various background pressures.

not the ambient plasma. Further insight to changes in the ambient plasma density near the plasma screen during this neutralizer margin testing should be considered further to determine the cause of coupling between the neutralizer and the plasma screen as these conditions ultimately determine the coupling voltage in ground tests.

Two important observations were born out from the RPA data. One, peak ion energy tended to decrease as the pressure increases. This is consistent with observations made by Goebel et al. in Ref [137]. They observed that extra flow downstream of the neutralizer keeper reduced the peak ion energies. Similarly here an increased neutral background can provide a similar effect. This finding of a decrease in peak ion energies with increased background pressure is an important consideration when running at elevated backgrounds, which will occur for high power engines. The elevated background can mask dangerous ion energies that may show up during spaceflight

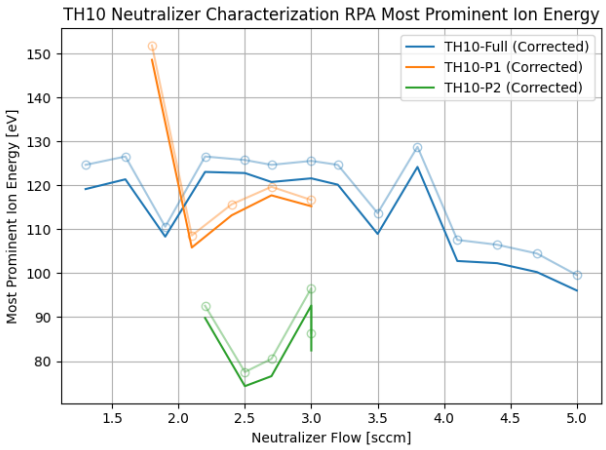

Figure 4.15: Most prominent ion energy near the neutralizer perpendicular to the direction of beam propagation using a retarding potential analyzer during the neutralizer margin characterization of the LM-NSTAR GIE in LVTF at the TH10 throttle condition for various background pressure.

that may not have been present during ground testing. As a result, increased erosion and shortened lifetimes can occur during spaceflight. This is in addition to the neutralizer performance changes that were observed and mentioned previously.

Secondly, the ion energies decreased with the increase of neutralizer current. This would seem to indicate that the ion energies are tied to the neutralizer current. However, Goebel et al. in Ref. [137] state that high energy ions just downstream of the keeper can be measured, but these typically increase in energy with a decrease in flow or increase of current. Their study primarily focused on discharge cathodes and other simulations suggest that high energy ions can be elastically scattered, even at 90° [10]. The later was suspected to be the source of these energetic ions because elastic scattering events increase with increased neutral density and ion energies will decrease with increased collisions. Elastically scattering events like CEX, increase with the increase of pressure due to more collisions with neutrals. Using the cross section for singly ionized xenon ions at 1 keV from Ref. [78] and equation 4.1, the corresponding mean free path at 1 μTorr is 65 m. Most ions travel the length of the chamber without a collision. According to the work by Pation and Wirz, those ions that do elastically scatter, scatter at the most probably angle of 88.1° [138].

4.3.3.2 Plasma Screen Configuration Impacts

Investigation of the plasma screen electrical configuration on thruster performance is done by adding a switch into the plasma screen grounding line. For the grounded configuration, the plasma screen switch is closed and current is allowed to pass through the line to facility ground. In the floating configuration, the switch is opened and no current passes through. As a result the plasma

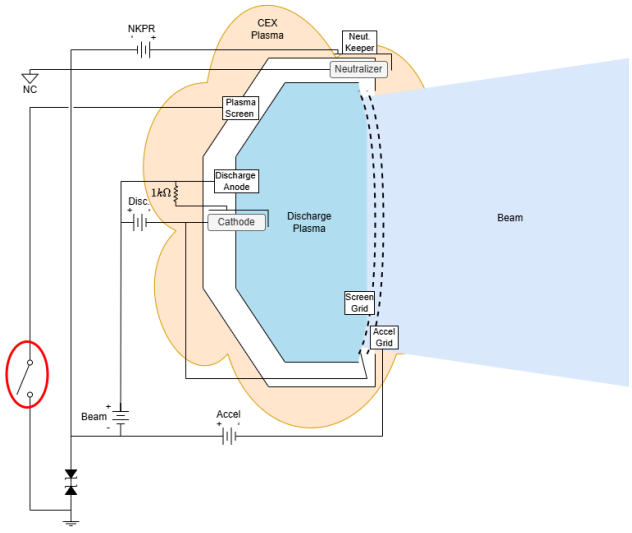

Figure 4.16: Plasma screen electrical configuration circuit diagram with an electrical switch to change between the grounded and floating plasma screen configuration.

Table 4.6: The impacts of the plasma screen electrical configuration on currents through the plasma screen (grounded) and floating potentials of the plasma screen (floating) as the background pressure is varied for different throttle conditions.

	TH01 (530 mA)		TH05 (810 mA)		TH10 (1300 mA)	
	I_{ps} [mA]	V_{ps} [V]	I_{ps} [mA]	V_{ps} [V]	I_{ps} [mA]	V_{ps} [V]
P1	-10	-8.874	-18	-9.070	-32	-8.850
P2	-9	-8.197	-17	-8.383	-18	-7.8

screen reaches a saturation point based on the balancing of the electron and ion currents to it. The plasma screen floats to the floating potential of the ambient plasma. An electrical circuit diagram is provided in Figure 4.16 the switch is circled in red. Telemetry data was obtained to investigate changes in thruster performance between transitions of the plasma screen configuration.

Langmuir probe data was taken near the plasma screen and near the neutralizer. Figures 4.17 and 4.18 show the plasma potentials, floating potentials, electron densities, and electron temperatures of the plasma screen and neutralizer Langmuir probes, respectively. A table of the plasma screen current for the grounded case, and floating potential for the floating configuration are found in Table 4.6.

The plasma potential near the plasmas screen was negative in the case of a floating plasma screen and positive in the case of a grounded plasma screen. A negative plasma potential near the plasma screen should have occurred since the plasma screen floats negatively and the Lang-

muir probe was so close to the plasma screen. Electrons were negatively charging the floating plasma screen. This can lead to an altered flux flow path of the CEX plasma compared to a facility grounded plasma screen. For ground testing this should be allowable to ensure proper beam neutralizer and decoupling of the neutralizer to the plasma screen. Electron current collection on a facility grounded plasma screen is a non-spacelike condition that can alter neutralization pathways and led to misleading neutralizer characterization and margins for spaceflight qualification as it has been mentioned previously with the changes in the coupling voltages between the grounded and floating plasma screen.

In addition there was an increase in electron density in the floating plasma screen configuration. The increase in electron densities should have occurred due to more electrons being repelled from the negatively floating plasma screen. Effectively the local loss area associated with the neutralizer plasma has decreased. An increase of electron plasma density should have allowed an increase in plasma bridge formation, to allow better conductivity between the neutralizer and the beam. In future work, more distance between the neutralizer and the grounded support structure should be considered to better isolate the neutralizer from facility ground to hopefully reduce the value of V_{cg} when the plasma screen is floated. This would determine if the facility coupling is occurring on the nearby grounded support structures due to the enhanced electron plasma density even with a floating plasma screen or if the floating plasma screen is causing higher potentials in the beam that propagate further downstream and couples the beam more with facility on downstream objects.

From the result of Figure 4.18 of the plasma properties near the neutralizer, it was determined that the floating plasma screen did not have much of an impact here. The was a small decrease in the floating potential and as such a small increase in electron temperature. These values are not outside the limits of uncertainty. It appears that the fringes of the plasma bridge were insensitive to the change to a floating plasma screen.

The impact of the floating plasma screen was further studied by characterizing the neutralizer under the floating plasms screen configuration. The telemetry data of the neutralizer current characterization with a floating plasma screen is presented in Figure 4.19. There was a large discontinuity in the plasma screen potential during the current characterization as the current started at 2.0 A and then was increased and then returned back to 2.0 A, where it was subsequently decreased. The plasma screen potential did not necessarily fully respond in time with the variations of neutralizer current. The voltage of the neutralizer varied as expected with the increase of current and resulted in the increase of voltage for more extraction of electrons. The coupling voltage and peak-to-peak oscillations also increased in magnitude as the current became too small to sustain spot mode. Further work would require plasma potential measurements in the beam to get the true-coupling voltage of the neutralizer to the beam to see how variations in neutralizer current changes the neutralization.

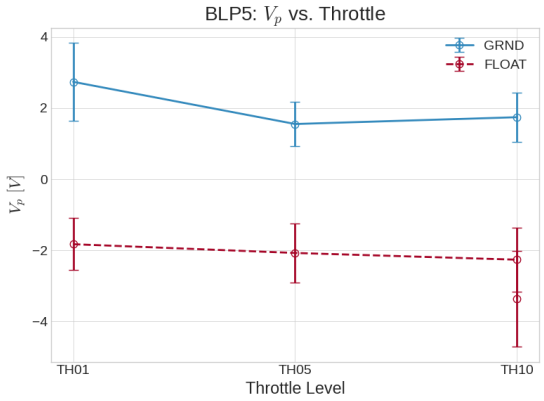

(a) Plasma potential

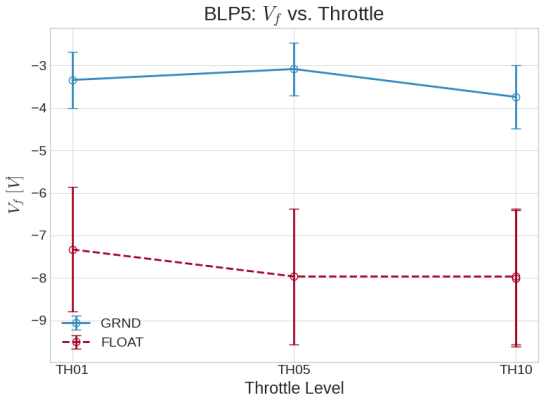

(b) Floating potential

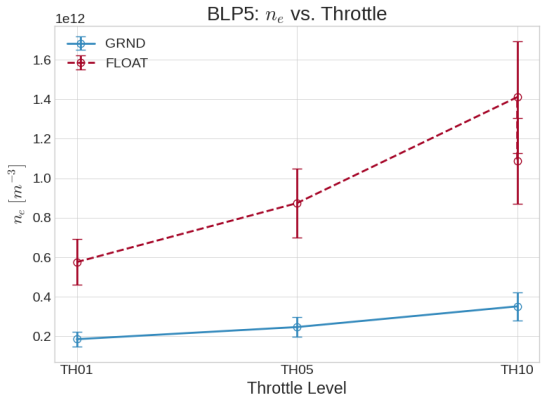

(c) Electron density

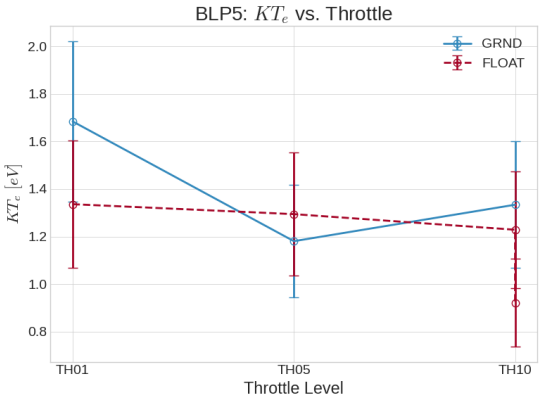

(d) Electron temperature

Figure 4.17: Comparison of the plasma properties obtained with a spherical Langmuir probe near the plasma screen between the grounded and floating plasma screen configurations at the P1 pumping speeds and corresponding background pressures for three throttle conditions: TH01, TH05, and TH10.

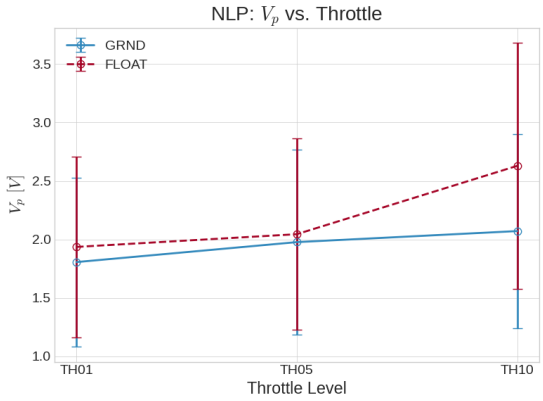

(a) Plasma potential

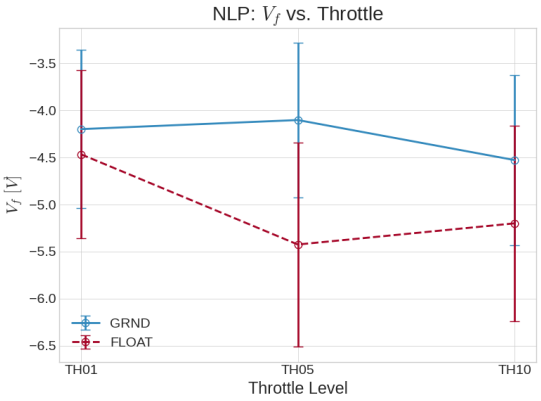

(b) Floating potential

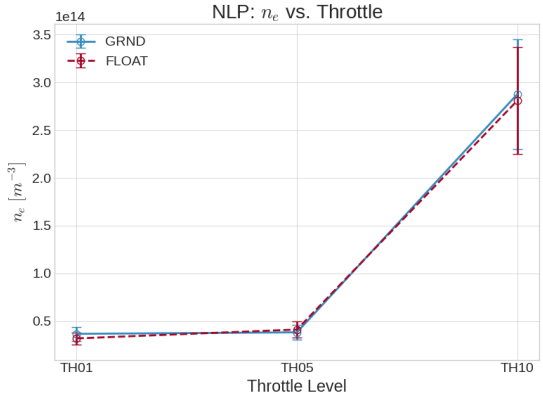

(c) Electron density

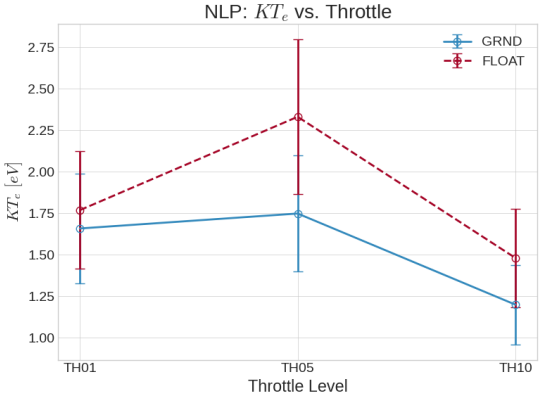

(d) Electron temperature

Figure 4.18: Comparison of the plasma properties obtained with a cylindrical Langmuir probe near the neutralizer between the grounded and floating plasma screen configurations at the P1 pumping speeds and corresponding background pressures for three throttle conditions: TH01, TH05, and TH10.

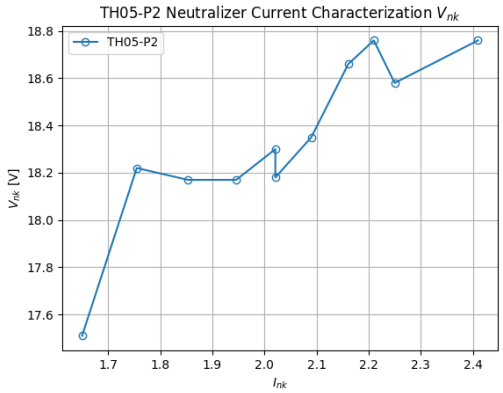

(a) Neutralizer keeper voltage

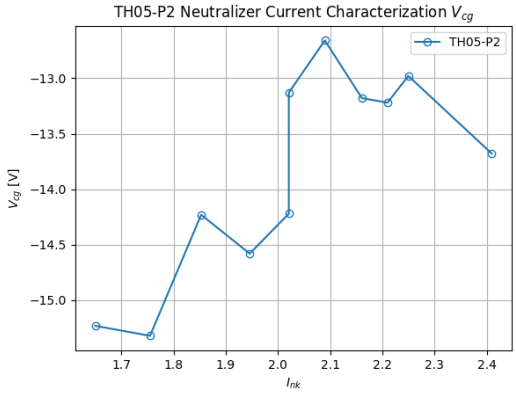

(b) V_{cg} coupling voltage

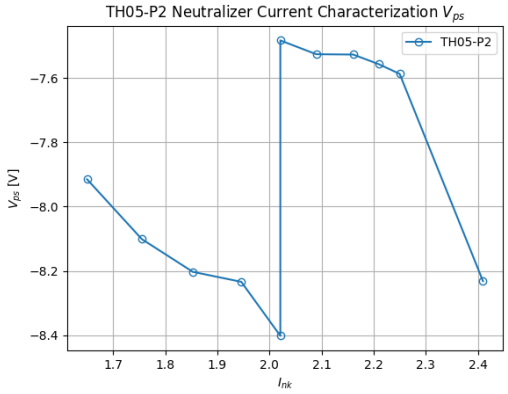

(c) Plasma screen potential

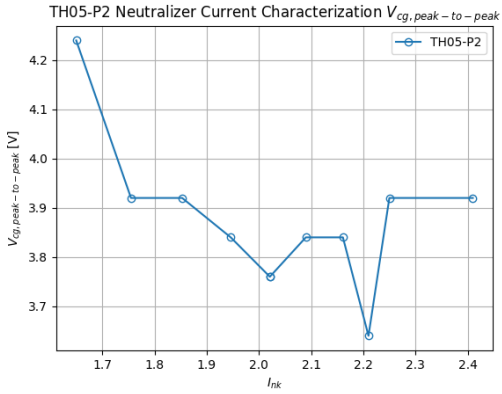

(d) V_{cg} peak-to-peak voltage

Figure 4.19: Abbreviated thruster telemetry results for the characterization of the neutralizer with floating plasma screen at the TH05 throttle condition at the P2 pumping speed configuration.

Although V_{cg} started to become increasingly more negative after increasing past 2.1 A, the peak-to-peak also increased. This is expected when the current demand begins to exceed the flow rate of the cathode. Additionally, Figure 4.20c shows that the electron temperature near the neutralizer also increased at this point, hinting the cathode was on the verge of being asked to emit a higher electron current for the given flow rate. The important takeaway here was that the floating plasma screen did not affect the neutralizer characterization in a significant way.

Plasma proprieties near the plasma screen (purple) and near the neutralizer (green) during the neutralizer characterization are found in Figure 4.20. In Figure 4.20b there was a limited amount of change in the plasma densities for both probes. Only the electron temperature in Figure 4.20c seems to vary with the change in neutralizer current and this was attributed to the increase in V_{cg} to force more electrons to the beam.

The most prominent ion energies observed during neutralizer characterization with a floating

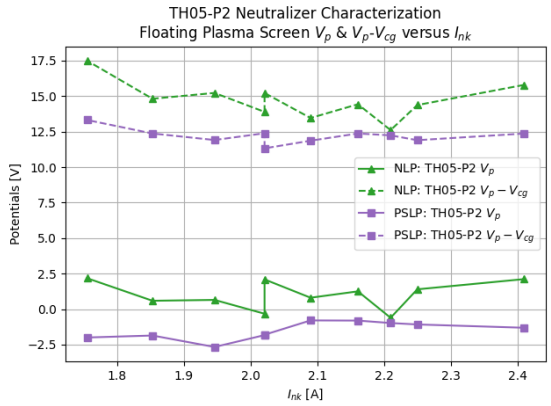

(a) Coupling voltages

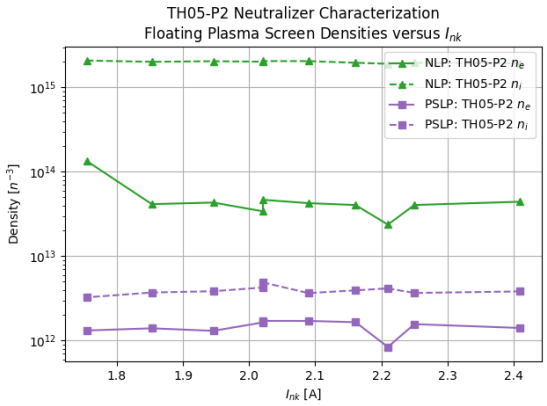

(b) Plasma densities

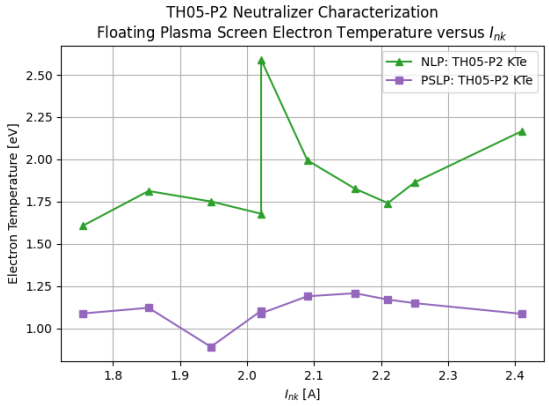

(c) Electron temperature

Figure 4.20: Near the neutralizer plasma properties from a cylindrical Langmuir probe during the characterization of the neutralizer with floating plasma screen at the TH05 throttle condition at the P2 pumping speed configuration.

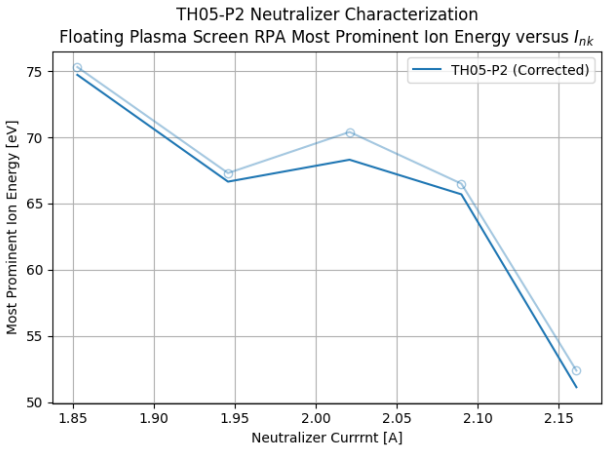

Figure 4.21: Most prominent ion energies elastically scatted from thruster beam at thruster flats measured with a retarding potential analyzer during the characterization of the neutralizer with floating plasma screen at the TH05 throttle condition at the P2 pumping speed configuration.

plasmas screen are located in Figure 4.21. Here it was observed that the most prominent ion energy decreased with neutralizer current. This is opposite to expectations from Ref. [137] state that the increase of current will increase the ion energies. However, the circumstances here are different in that this is a neutralizer cathode, not a discharge cathode placed near a strong magnetic field. From Figure 4.20b the plasma densities did not seem to vary much, but the electron temperatures did as shown in Figure 4.20c. Unfortunately, the electron temperature appeared to increase instead of decrease with increasing neutralizer current. Goebel et al. do suggest that it is the stability of the ionization fraction in the orifice plasma of the cathode along with impedance in this plasma structure that can affect the ion energies. The increase in current may have been stabilizing. Further studies by varying the grid potentials at a constant throttle condition and taking RPA measurements would help narrow the source of these energetic ions by increasing the ion energies if they are elastically scattered. If no change in energies are observed, this data would suggest that it is the neutralizer cathode that is producing these high energy ions. This is important to identify the source of these ions to take preventive measures to limit this erosion mechanism for space flight.

4.3.4 Ion Energies

Measurements of the most prominent ion energies are taken using a three-grid RPA 90° to the thruster flats near the neutralizer. Results are found in plot of Figure 4.22. From the results of the ion energies obtained by the RPA, a major concern was there are high energy ions in the very near-field, even at 90°. This can lead to sputtering and erosion of nearby components. Even more concerning was the decrease in ion energies as a function of pressure. If during ground

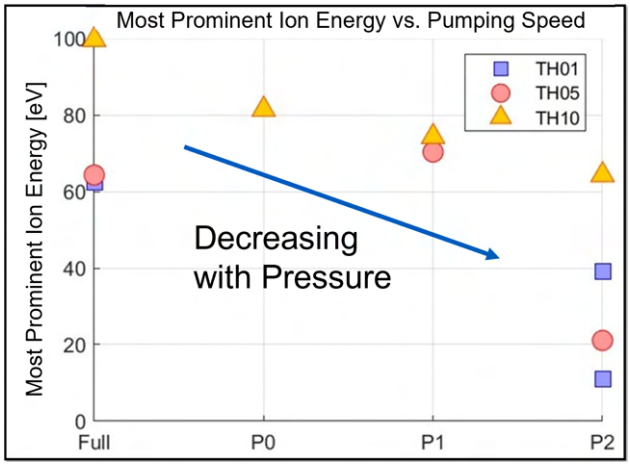

Figure 4.22: Measurement of the most prominent ion energies of the elastically scattered beam ions perpendicular to thruster flats for various pumping configurations and corresponding background pressures. Observed was a decrease in the most prominent ion energies with an increase of the background pressure.

Table 4.7: Sputtering threshold from ions [eV] for common EP materials [139].

Mo	Ti	C
39.3	40.8	70

testing the background pressure is elevated, these energetic ions may not be observed. Thus, in spaceflight where the background pressure are much lower, the nearby components on a satellites could be eroded by these high energy ions. Some sputtering thresholds for common EP materials for reference are located in Table 4.7.

The source of these ions is still not well understood. Simulations suggestion these could be elastically scattered ions [10]. Cathode experiments suggest it could be accelerated ions from the cathode [137]. As mentioned in the previous section, it is important to identify the source of these ions such that preventive measures can be in-placed to prevent erosion of the neutralizer cathode. However, it can be said that background pressure decreases this peak energy and can obscure these high energy ions during ground testing that could be damaging in spaceflight.

4.4 Thruster-Facility Interactions & Performance

In the previous sections findings regarding the facility impacting the thruster plume and characterization of the downstream thruster processes were investigated. In this section, emphasis is on the performance changes internally of the thruster due to the facility. These include how the beam current varies with a floating plasma screen and the production rate of doubles in the discharge

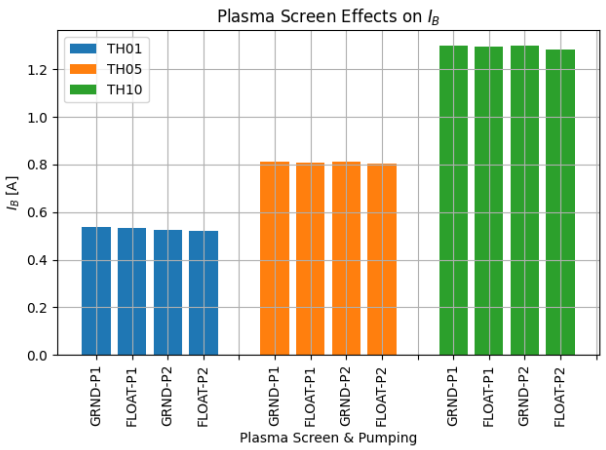

Figure 4.23: Impact of the plasma screen configuration on measured beam current from the telemetry system for the LM-NSTAR at LVTF for two background pressure (P1 and P2) and the three throttle conditions (TH01, TH05, and TH10).

Table 4.8: LM-NSTAR at LVTF plasma screen configuration impact on beam current for two background pressure (P1 and P2) and the three throttle conditions (TH01, TH05, and TH10).

TH01-P1	TH01-P2	TH05-P1	TH05-P2	TH10-P1	TH10-P2
0.19%	0.76%	0.49%	0.99%	0.15%	1.00%

chamber due to ingestion and CEX attenuation.

4.4.1 Plasma Screen Shielding

Changes in the beam current for two different pressures and three throttle conditions are presented in Figure 4.23. A relative percent change between grounded and floating is found in Table 4.8 and visually displayed in Figure 4.24. Although these changes in beam current are small, since these systems operate for long thrusting times, the losses add up over the long operation times. Additionally, the lower beam current in the floating plasma screen configurations indicate that there is plasma flow into the plasma screen in the grounded plasma screen case and collecting on the external surface of the discharge anode. The floating point of a shielding screen has shown to shield out plasma noise in plasma devices [140, 141, 127]. This could also explain the presence of burn lines by electrons often found on the outside portion of the anode at the location of the cusps. Furthermore, it is observed the differences between ground and floating plasma screen increased with the increased background pressure. These small changes in beam current and thrust production will be more of an impact at the higher background pressures with higher power engines. Thus, floating the plasma screen should be done to minimize artificial beam current.

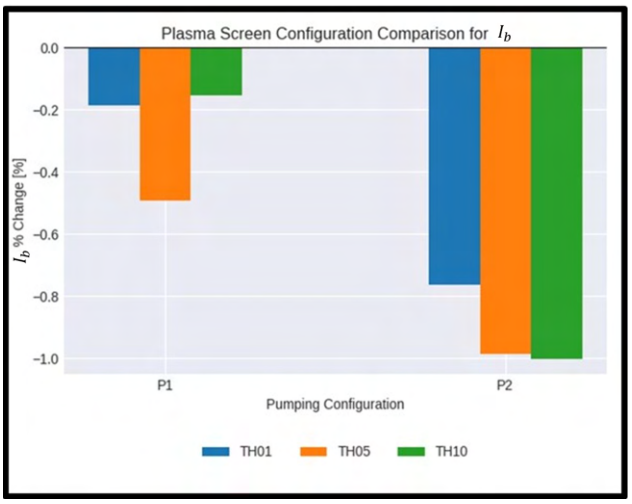

Figure 4.24: Relative percent change on measured beam current between a grounded and a floating plasma screen configuration for the LM-NSTAR at LVTF for two background pressure (P1 and P2) and the three throttle conditions (TH01, TH05, and TH10)

4.4.2 Doubles-to-Singles Production

The doubles-to-singles production ratio of a gridded ion engine gives insight into how efficiently thrust is being produced. It requires more energy to make doubles and the thrust of a single double is less than that of two singly charged ions. As a result the thrust-to-power ratio, overall efficiency of the thruster, and lifetime of components can be lowered. Figure 4.25 is a plot of the uncorrected and corrected doubles-to-singles ratio. Corrections for CEX attenuation was done using the formulas for xenon outlined in Ref. [68].

The uncorrected doubles-to-singles ratio decreased with pressure, due to the increase in singles attenuation from CEX. Additionally, the cross section for doubly charge ions is smaller. However, it was expected that after corrections that for a given throttle condition, the corrected doubles-to-singles ratio should be a flat line over any pressure range. From Figure 4.25 it can be seen that this is not observed, especially for the TH10 throttle condition.

There are two possible factors for this. One of which is there is more attenuation of singles than accounted for. Localized pumping, obstacles, stagnation zones, or pressure in the probe can create more CEX for singles than for doubles. The second, more complicated explanation, is due to ingestion. The leakage of ambient neutrals pass the grids and into the discharge chamber can have a complicated impact on the discharge performance. The impedance between the discharge cathode and anode is a function of cathode and discharge chamber flows, discharge current demand, magnetic field strength, electron temperatures, and discharge chamber geometry. The spatial distribution of ingested neutral flow can alter the discharge performance easily. However, it is expected that the extra flow would increase the neutral pressure in the discharge chamber resulting in more

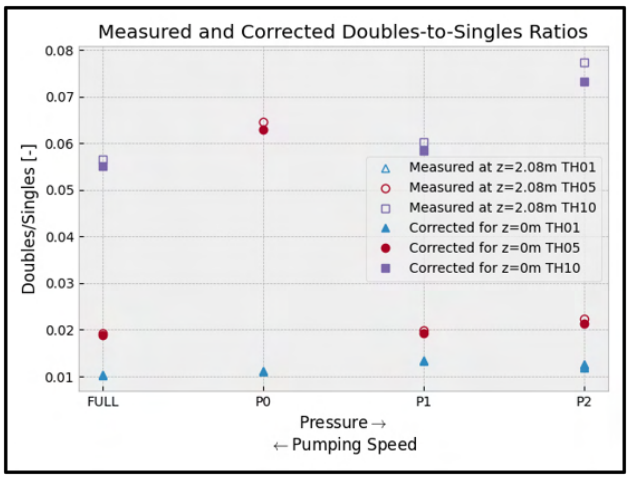

Figure 4.25: LM-NSTAR at LVTF ExB doubles-to-singles ratios measured 2.08 m downstream on beam center-line and additionally corrected for CEX attenuation to recapture the ratio at the thruster exit plane for TH01, TH05, and TH10 throttle conditions for four background pressures. Doubles-to-singles ratio increased in value with the increase of pressure even after corrections.

neutral collisions and lower electron temperatures. The decrease in electron temperature in turn would cause less doubles to be produced. Because the neutral ingestion enters the discharge chamber through the grids, it would be expected that most of the extra neutral pressure would be located near the grids. It is possible that plasma production area neutral density is not as affected and as a result the same doubles-to-singles ratio is produced but the increased neutral pressure near the grids results in increased singles attenuation near the grids which can lead to increased grid erosion. The lower doubles-to-singles ratio in space than measured during ground testing is positive as it means there should be better discharge performance there. Although it appears that it is the increased doubles-to-singles ratio is caused by localized higher background pressures and attenuation along with slight variations in discharge currents and flows, a better analysis study of the changes in discharge performance with various facilities and background pressures is warranted. For reference, the charge exchange cross sections differences for singles and doubles are given in Ref. [78] respectively as

$$\sigma_1 = 87.3 - 13.6 \log(E_{ion}), \tag{4.1}$$

and

$$\sigma_2 = 45.7 - 8.9 \log(E_{ion}), \tag{4.2}$$

where E is ion energies. Units are in Å^2. An example calculations for 1 keV xenon ions results in $\sigma_1 = 46.5\ \text{Å}^2$ and $\sigma_2 = 19.0\ \text{Å}^2$.

4.5 Conclusions

The objective of this chapter summarize gridded ion thruster testing in a moderately capable facility such as PEPL LVTF to: 1) verify and characterize facility impacts, 2) determine impacts on predicated spaceflight, and 3) identify experiments of importance for future testing of a thruster in less capable facility. This was done by looking at facility impacts on plume-facility and thruster-facility interactions. Three throttle conditions were explored. Pressure was varied during these experiments by turning pumps off and and letting the pressure relax to a steady state at an elevated background. Additionally, electrical coupling between the engine and the facility during operation was tested by varying the potential of the plasma screen of the thruster by changing from the nominal grounded configuration to a floating configuration.

The wall plasma properties give insight into how much the beam plasma plume is coupling to the facility. Wall plasma properties varying with distance and background pressure show that there is minimal effects due to the large distance from the beam to the wall and high pumping capabilities. Some cooling of electrons was observed with increasing background pressure and collisions with neutrals but less than expected. There was a linear increase in both electron and ion plasma densities for all wall probes as a function of pressure. There was no difference in the ambient plasma at the walls between the different thruster throttle conditions. This seems to indicate that there are limited beam-wall interactions. Furthermore, near the plasma screen, neutralizer and in the plume are dictated more by changes in throttle condition or thruster operation than by ambient background pressure alone. It was proposed that the floating potential of the wall probes may give insight into how much and at what point the beam plasma starts significantly interacting with the wall. A positive floating potential hints the presence of more energetic ions and results in more electron current to equate currents. These energetic ions would be expected to be sourced or scattered from the beam plasma. The spread of these ions to the wall could pull electrons with them and connect the neutralization of the beam with the walls of the facility and ambient plasma. Future experiments in less-capable facilities would include more wall probe data with a focus on the plasma properties there to determine if beam-facility coupling begins to develop.

The electrical coupling of the thruster to the facility, as well as the beam neutralization process, are important considerations in ground testing experimental design. Quantifying the electrical coupling of the thruster with the facility was investigated over various pressure ranges and electrical configurations of the thruster plasma screen. The neutralizer-facility coupling voltage, V_{cg}, generally became less negative as background pressure was increased. However, floating the plasma screen increased the negativity of the coupling voltage when compared to the nominal grounded plasma screen case. Becoming more negative, V_{cg} insinuated that the thruster was coupling more

with the facility which means the beam was not being neutralized as expected in the grounded plasma screen case. The neutralizer-facility coupling voltage in the floating plasma screen configuration occurred because the beam wants to be neutralized but was not getting enough electrons from the neutralizer directly and as such the beam increases in potential, in which this potential propagates further downstream till it terminates on the grounded facility. By so doing, this requires the facility to source electrons to the beam and increases the magnitude of the neutralizer coupling voltage. In regards to spaceflight operation, the grounded plasma screen during ground testing will under-predict the needed neutralizer performance to sufficiently neutralize the beam and allow proper beam propagation and to prevent the formation of a detrimental virtual anode. Thus, floating the plasma screen during ground testing is recommended such that realistic beam potentials will arise. Verification for future experimental would require obtaining the true-coupling voltage, $V_{cp} = \phi_p - \phi_{NC}$, where the difference in potential between the plasma potential in the beam to the neutralizer potential indicates this coupling, and smaller values mean better coupling and better neutralization. The coupling with the facility can also lead to improper spaceflight predictions for Hall thrusters due to misleading effective beam voltages due to incorrect coupling voltages.

Neutralizing the beam should be performed by the neutralizer but during ground testing this can be difficult to ensure. Characterizing the neutralizer and determine the flow and power margins are performed in ground testing to ensure maximum efficiency of the thruster. Varying the background pressure revealed that the onset of plume mode occurred at higher flow rates with elevated pressures. This seems to stem from the increase neutral density which reduces electron mobility. However, the increased background pressure and plasma damped the magnitude change and peak-to-peak oscillations of V_{cg}. Another part of the the neutralizer characterization, the most prominent ion energies near the neutralizer 90° to the thruster flats also decreased with pressure. It is speculated that the high energy ions are either derived from elastically scattered ions from the beam or energetic ions from the neutralizer cathode. Although their source has yet to be confirmed, their presence is concerning as these ions at space pressures could easily sputter, damage, and erode nearby components in space but may not even be observed during ground testing at elevated background pressures. The neutralizer was also characterized with a floating plasma screen. This process behaved as expected but at higher flow rates the V_{cg} did begin to become increasing more negative with higher temperature neutralizer electrons present as well. Future comparison studies are needed for neutralizer characterization between grounded and floating plasma screens. Additionally, better measurements of the true-coupling voltage are needed to properly characterize the effectiveness of the neutralizer.

The interactions of the thruster with facility can lead to changes in the performance of the thruster. The floating the plasma screen was shown to affect the coupling voltage by eliminating an alternative neutralization pathway, but it was also shown to decrease the power supply beam

current when the plasma screen was floating. This effect was increased as background pressure increased. As such, the grounded plasma screen did not properly shield out the higher energy electrons and can lead to artificially inflated beam currents and misleading thrust calculations.

It was expected that the doubles-to-singles ratio after corrections for charge-exchange attenuation should be invariant over a range of background pressures. However, this was not observed and the corrected doubles-to-singles ratio was higher at higher background pressures. This made ingested neutrals less likely as this would have caused the reverse affect since the discharge voltage increased only slightly with ingestion. It is suspected that localized pressures either in the chamber or in the probe have caused extra attenuation of CEX ions not accounted for. As a result, elevated background pressures may be over critical of doubles productions compared to spaceflight. There also is evidence that thruster discharge performance can have a significant impact on the plasma properties in the whole chamber and could be something to consider in future testing.

In conclusion, the PEPL LVTF provide a good of a spacelike environment for a 2.3 kW NSTAR gridded ion engine. Although some facility effects were observed and future work identified, future testing would require a much more extreme environment of elevated pressures and closer facility walls to the thruster to really emulate the high-power density of a 100 kW system. However, there is limited availability of such electric propulsion systems available. As a result, future studies will include a much smaller thruster, similar in design, that can be operated in a much smaller facility that would be classified as not a properly capable facility for emulating a spacelike environment. In this situation, better recommendations and best practices for testing future 100 kW systems could be made.

CHAPTER 5

High-Power Facility Effects

5.1 Motivation & Objectives

After the investigation in gridded ion engine testing in the PEPL LVTF test facility, it was concluded that a facility to observe high-power systems requires a higher thruster power-to-chamber volume densities to emulate the desired 100 kW power densities. This chapter focuses on the impacts of the facility on thruster testing when the facility is undersized emulating a high-power engine in an marginal to submarginal facility. This leads to elevated background neutral and plasma densities, coupling with the facility, limited beam expansion, and ingestion. Additional focus areas were added such as measurements of the true-coupling voltages. In this chapter, wall plasma properties, beam expansion, electrical coupling to the facility, and ingestion are explored. However, in addition to the background pressure being varied, the plasma screen and beam target potentials are varied between nominally grounded and floating. Localized pressure effects on plasma bridge formation are also investigated using neutral flow injection. Observations and considerations for spaceflight preparation are made and future work needed are also commented on.

5.2 Experimental campaign & thruster operating conditions

This chapter includes data from three experimental test campaigns. These test campaigns are referred to by their testing dates. For example, the first test began in May 2024 and is thus referred to as the 2024-05 test. The other test campaigns include 2024-11 and 2025-01. Although it was attempted to keep the three test campaigns similar, there are some variations that occurred.

5.2.1 2024-05 NASA 8 cm experimental campaign

Initial testing of 2024-05 used the original chamber layout descried in Figure 3.8 with a total pumping speed of 2,620 L/s-N_2. This test used a "super" neutralizer with serial number 006. A

Table 5.1: 2024-05 NASA 8 cm test campaign background pressures corrected for xenon in the Rocket Chamber while thruster is in operation at the 100 W power level with the "super" neutralizer cathode. The plasma screen configuration is defined first as either "G" for grounded or "F" for floating. The beam target configuration follows this same convention. Thus, "GF" means grounded plasma screen with a floating beam target.

100W-GG	100%	70%	40%
IG0 [μTorr]	40.02	48.37	53.24
IG1 [μTorr]	43.50	51.50	56.72
IG2 [μTorr]	36.58	43.84	48.37
IG3 [μTorr]	34.51	41.87	46.19
100W-FG	100%	70%	40%
IG0 [μTorr]	40.02	48.37	53.24
IG1 [μTorr]	43.50	51.85	56.72
IG2 [μTorr]	36.58	43.98	48.37
IG3 [μTorr]	34.51	41.36	46.19
100W-GF	100%	70%	40%
IG0 [μTorr]	40.02	48.37	52.90
IG1 [μTorr]	43.50	52.55	57.77
IG2 [μTorr]	36.58	44.66	48.67
IG3 [μTorr]	34.51	41.49	45.77
100W-FF	100%	70%	40%
IG0 [μTorr]	40.02	48.37	53.24
IG1 [μTorr]	43.50	52.20	57.77
IG2 [μTorr]	36.58	44.25	48.67
IG3 [μTorr]	34.51	41.23	45.77

reference of "N6" refers to the use of this cathode instead of the nominal cathode obtained later for other experiments. Later experiments tied a 1.5 kΩ resistor between cathode keeper and anode. In this test, the cathode keeper was allowed to float. The resulting pressures are found in Table 5.1. The plasma screen configuration is defined first as either "G" for grounded or "F" for floating. The beam target configuration follows this same convention. Thus, "GF" means grounded plasma screen with a floating beam target.

The following table, Table 5.2, contains the thruster telemetry results for the 100 W condition with a grounded plasma screen and grounded beam target. Tables 5.3, 5.4, and 5.5 are for the various other plasma screen and beam target configurations. The discharge voltage was lower than nominal as the heater was left on for part of the testing.

Table 5.2: 2024-05 NASA 8 cm test campaign telemetry results in the PSTL RC at 100 W with "super" neutralizer, grounded plasma screen and grounded beam target.

100W-GG	100%	70%	40%
C [sccm]	0.80	0.80	0.80
M [sccm]	0.80	0.80	0.80
N [sccm]	1.70	2.10	1.70
NKPR [V]	19.10	17.50	19.50
NKPR [A]	1.74	1.86	1.74
DISC* [V]	23.93	22.55	23.11
DISC [A]	1.04	1.04	1.04
BEAM [V]	801	804	802
BEAM [mA]	38.1	41.9	40.0
ACCEL [|V|]	201	201	200
ACCEL [mA]	2.13	1.82	2.27
V_{cg} [V]	-5.652	-4.815	-6.135

*Discharge heater left on for some conditions

Table 5.3: 2024-05 NASA 8 cm test campaign telemetry results in the PSTL RC at 100 W with "super" neutralizer, floating plasma screen and grounded beam target.

100W-FG	100%	70%	40%
C [sccm]	0.80	0.80	0.80
M [sccm]	0.80	0.80	0.80
N [sccm]	1.70	2.10	1.70
NKPR [V]	19.10	17.40	19.40
NKPR [A]	1.74	1.86	1.74
DISC* [V]	22.48	24.10	23.68
DISC [A]	1.04	1.04	1.04
BEAM [V]	800	805	801
BEAM [mA]	38.5	41.9	40.7
ACCEL [|V|]	200	201	200
ACCEL [mA]	2.16	1.84	2.32
V_{cg} [V]	-5.696	-4.630	-6.185

*Discharge heater left on for some conditions

Table 5.4: 2024-05 NASA 8 cm test campaign telemetry results in the PSTL RC at 100 W with "super" neutralizer, grounded plasma screen and floating beam target.

100W-GF	100%	70%	40%
C [sccm]	0.80	0.80	0.80
M [sccm]	0.80	0.80	0.80
N [sccm]	1.70	2.10	1.70
NKPR [V]	19.20	17.20	19.80
NKPR [A]	1.74	1.85	1.74
DISC* [V]	24.25	22.05	21.70
DISC [A]	1.04	1.04	1.04
BEAM [V]	801	802	801
BEAM [mA]	38.6	41.1	39.8
ACCEL [|V|]	200	200	200
ACCEL [mA]	2.15	1.93	2.18
V_{cg} [V]	-5.223	-3.941	-5.872

*Discharge heater left on for some conditions

Table 5.5: 2024-05 NASA 8 cm test campaign telemetry results in the PSTL RC at 100 W with "super" neutralizer, floating plasma screen and floating beam target.

100W-FF	100%	70%	40%
C [sccm]	0.80	0.80	0.80
M [sccm]	0.80	0.80	0.80
N [sccm]	1.70	2.10	1.70
NKPR [V]	19.20	17.20	19.60
NKPR [A]	1.74	1.86	1.74
DISC* [V]	24.15	22.17	21.09
DISC [A]	1.04	1.04	1.04
BEAM [V]	799	803	800
BEAM [mA]	38.5	41.6	39.2
ACCEL [|V|]	201	200	200
ACCEL [mA]	2.14	1.87	2.21
V_{cg} [V]	-5.091	-4.096	-5.683

*Discharge heater left on for some conditions

Table 5.6: 2024-11 NASA 8 cm test campaign background pressures corrected for xenon in the Rocket Chamber while thruster is in operation at the 100 W, 200 W, and 300 W power levels with the nominal hollow cathode neutralizer. The plasma screen configuration is defined first as either "G" for grounded or "F" for floating. The beam target configuration follows this same convention. Thus, "GF" means grounded plasma screen with a floating beam target.

100W-GG	100%	70%	40%	30%
IG0 [μTorr]	22.6	27.1	46.3	77.3
IG1 [μTorr]	24.2	28.6	48.7	N/A
IG2 [μTorr]	21.6	25.4	42.1	N/A
IG3 [μTorr]	19.7	23.6	40.0	N/A
200W-GG	100%	70%	40%	30%
IG0 [μTorr]	40.4	48.7	82.8	124.6
IG1 [μTorr]	41.1	50.1	87.7	135.4
IG2 [μTorr]	37.2	44.5	76.9	116.2
IG3 [μTorr]	34.0	41.1	73.8	114.8
200W-GF	100%	70%	40%	30%
IG0 [μTorr]	42.1	-	-	123.2
IG1 [μTorr]	45.6	-	-	135.0
IG2 [μTorr]	39.7	-	-	114.5
IG3 [μTorr]	36.9	-	-	113.1
300W-GG	100%	70%	40%	30%
IG0 [μTorr]	42.1	-	-	-
IG1 [μTorr]	42.1	-	-	-
IG2 [μTorr]	37.9	-	-	-
IG3 [μTorr]	35.8	-	-	-

5.2.2 2024-11 NASA 8 cm experimental campaign

The 2024-11 had some improvements to the chamber. The XY-motion stage used for Faraday and emissive probes was upgraded to larger sweep distances, more wall probes were added, an RGA was placed downstream, and a nominal hollow cathode neutralizer for this thruster was used. However, this cathode was very old and struggled to stay on its own and had to be operated at higher flows and currents than normally would be done. In addition, the heater was left on to aide in sustaining the plasma. The updated chamber layout is seen in Figure 3.7 with a total pumping speed of 4,200 L/s-N_2. The resulting pressures are found in Table 5.6. The plasma screen configuration is defined first as either "G" for grounded or "F" for floating. The beam target configuration follows this same convention. Thus, "GF" means grounded plasma screen with a floating beam target.

The following table, Table 5.7, contains the thruster telemetry results for the 100 W condition with a grounded plasma screen and grounded beam target. Table 5.8 is the thruster telemeter

Table 5.7: 2024-11 NASA 8 cm test campaign telemetry results in the PSTL RC at 100 W with nominal neutralizer and heater on, grounded plasma screen and grounded beam target.

100W-GG	100%	70%	40%	30%
C [sccm]	1.00	1.00	1.00	1.00
M [sccm]	0.90	0.90	0.90	0.90
N [sccm]	1.00	1.20	1.20	1.20
NKPR* [V]	25.0	25.5	26.6	25.7
NKPR [A]	0.95	0.95	0.95	0.95
DISC [V]	31.9	31.6	31.2	30.7
DISC [A]	1.064	1.058	1.061	1.049
BEAM [V]	804	805	804	805
BEAM [mA]	63.99	65.65	67.49	66.14
ACCEL [|V|]	201	201.2	201.1	201
ACCEL** [mA]	0.92	1.03	1.22	1.31
V_{cg} [V]	-7.43	-8.75	-9.06	-10.2
$V_{cg,pp}$ [V]	2.00	2.04	2.11	2.01
$V_{nk,pp}$ [V]	3.38	4.03	4.13	4.09

*Neutralizer heater left on
**Accel currents maybe incorrect

results for the 200 W condition with a grounded plasma screen and both grounded and floating beam targets. The "F" after the pumping speed percentage indicates this column is for the floating beam target case. Because the beam could not be sustained for various electrical configurations or various background pressures, the 300 W condition is not considered for most of these studies but its telemetry results are available in appendix C. Reminder that the neutralizer cathode heater was left on during testing. Additionally, the accel current telemetry had a correction factor error. Post-processing attempts were made to correct these values but some values seem to be incorrect.

5.2.3 2025-01 NASA 8 cm experimental campaign

The 2025-01 was almost identical to the 2024-11 campaign. However, this test returned back to the "super" neutralizer with serial number 006. A reference of "N6" refers to the use of this cathode instead of the nominal cathode. This was because the previous nominal cathode would temporary transition into plume mode. For more stability during testing, the "super" neutralizer cathode was used again. The updated chamber layout is seen in Figure 3.7 with a total pumping speed of 4,200 L/s-N_2. The resulting pressures are found in Table 5.9. The plasma screen configuration is defined first as either "G" for grounded or "F" for floating. The beam target configuration follows this same convention. Thus, "FG" means floating plasma screen with a grounded beam target.

The following table, Table 5.10, contains the thruster telemetry results for the 100 W condi-

Table 5.8: 2024-11 NASA 8 cm test campaign telemetry results in the PSTL RC at 200 W with nominal neutralizer and heater on, grounded plasma screen and grounded and floating beam target.

200W-GG/GF	100%	100%-F	70%	40%	30%	30%-F
C [sccm]	1.55	1.55	1.55	1.55	1.55	1.55
M [sccm]	1.75	1.75	1.75	1.75	1.75	1.75
N [sccm]	1.10	1.10	1.10	1.10	1.10	1.10
NKPR* [V]	23.7	23.6	23.9	23.9	23.7	23.5
NKPR [A]	0.95	0.97	0.96	0.96	0.98	0.97
DISC [V]	32.9	33.0	32.3	32.0	31.8	31.9
DISC [A]	1.700	1.710	1.700	1.726	1.740	1.750
BEAM [V]	960	968	969	966	970	968
BEAM [mA]	N/A	141.6	144.9	146.0	144.0	141.3
ACCEL [|V|]	241.0	242.8	243.1	242.5	243.0	243.0
ACCEL** [mA]	11.12	5.6	7.92	8.08	7.2	6.13
V_{cg} [V]	-10.0	-9.87	-10.5	-10.8	-11.7	-11.9
$V_{cg,pp}$ [V]	2.15	2.06	2.02	2.08	2.04	2.09
$V_{nk,pp}$ [V]	4.15	3.71	3.81	3.81	3.54	3.55
$V_{ck,pp}$ [V]	4.13	4.23	4.18	4.21	4.05	3.62
BT [mA or V]	43.82	1.63	44.99	37.26	30.9	1.33

*Neutralizer heater left on

**Accel currents maybe incorrect

Table 5.9: 2025-01 NASA 8 cm test campaign background pressures corrected for xenon in the Rocket Chamber while thruster is in operation at the 100 W power level with the "super" neutralizer cathode. The plasma screen configuration is defined first as either "G" for grounded or "F" for floating. The beam target configuration follows this same convention. Thus, "GF" means grounded plasma screen with a floating beam target.

100W	100%-GG	100%-FG	30%-GG	30%-FG
IG0 [μTorr]	32.29	33.09	68.21	69.25
IG1 [μTorr]	34.03	34.80	70.30	74.12
IG2 [μTorr]	29.58	29.96	60.55	60.55
IG3 [μTorr]	27.91	28.29	57.07	57.42

Table 5.10: 2025-01 NASA 8 cm test campaign telemetry results in the PSTL RC at 100 W with "super" neutralizer, grounded and floating plasma screen and grounded beam target.

100W-GG/FG	100%	100%-F	30%	30%-F
C [sccm]	0.80	0.80	0.80	0.80
M [sccm]	0.80	0.80	0.80	0.80
N [sccm]	2.00	2.00	2.00	2.00
NKPR [V]	25.6	25.9	24.2	24.2
NKPR [A]	0.70	0.70	0.70	0.70
DISC [V]	28.2	28.2	27.3	27.5
DISC [A]	1.056	1.055	1.057	1.061
BEAM [V]	801	800	801	800
BEAM [mA]	46.05	46.02	46.41	46.24
ACCEL [|V|]	200.4	200.4	200.4	200.4
ACCEL [mA]	4.931	4.562	3.002	3.558
V_{cg} [V]	-12.7	-12.8	-12.9	-12.9
$V_{cg,pp}$ [V]	2.26	2.23	2.09	2.04
$V_{nk,pp}$ [V]	4.14	4.37	3.52	3.47
$V_{disc,pp}$ [V]	5.31	5.31	5.35	5.71
PS [mA or V]	0.491	-2.431	0.569	-1.905
BT [mA]	10.61	10.58	8.20	7.75

tion with both grounded and floating plasma screen and grounded beam target. The "F" after the pumping speed percentage indicates this column is for the floating plasma screen case.

5.3 Plasma-Facility Interactions

This section contains the impacts of an undersized facility on beam-facility coupling. Investigations on the plasma properties near the wall and on the beam plume are made to determine metrics for indications of increased beam-facility coupling. Additionally, experiments on variations on both neutralizer-facility and the true-coupling voltages are performed. This is done on a wider range of background pressures and on different types of electrical configurations. Combinations of grounded or floating plasma screens and beam targets are investigated. These various configurations are tested to give better insight into potential methods to limit beam-facility coupling such that more reasonable spaceflight performance of the thruster can be done during high-power ground testing. The impact of localized increase of neutrals in the plasma bridge by injecting neutral flow directly into the plasma bridge is also performed. This gives insight into how localized pressures can affect neutralizer-beam coupling.

5.3.1 Facility Boundary Conditions

The facility walls restrict the free-expansion of the plasma and in this under-sized facility it is expected the facility will couple more with the thruster and the beam. This section investigates the plasma properties near the wall as a function of distance downstream and pressure. Potentials in the beam compared to the walls is also done to determine if pressure or electrical configuration has a large impact on facility impacting the beam.

5.3.1.1 Near-Wall Plasma Properties

In this section is the discussion of plasma properties near the wall and how it relates to beam-facility coupling. Wall probes were approximately 8.57 cm off the wall and 21.91 cm from thruster center-line. One thing to note on this presented data, it was observed that the in-plane Langmuir probes had speciously high plasma potentials and electron temperatures. Additionally, the IV traces for these probes were difficult to analyze with no clear and distinct transition from the electron retarding region to the electron saturation region. Additionally, the measured current to the probe decreased over the three different campaigns. These symptoms plus high carbon depositions on a nearby witness plate point to a dirty probe effect. It appears to really only impact the in-plane Langmuir probes as it is assumed these probes faced the brunt of the sputtering from Faraday and emissive probe sweeps. Further discussion on this is discussed in Chapter 7.

The near wall plasma properties with downstream distance for the 2024-05 100 W with grounded plasma screen and grounded beam target case are given in Figure 5.1. All variations of the configurations are found in Appendix C. Each figure contains these six plasma properties: 1) plasma potential, 2) floating potential, 3) electron temperature, 4) electron Debye length, 5) electron density, and 6) ion density. In general, the behavior trends for all configurations were similar.

Looking at the coupling voltages from the telemetry from Tables 5.2, 5.3, 5.4, and 5.5 the neutralizer-facility coupling voltage increased negatively (V_{cg} became more negative) between the 100% and 40% pumping configurations. This indicates more coupling with the facility. The higher background pressures force the thruster to couple more with the facility. The 70% case has lower neutralizer-facility coupling voltages because the plasma density for this case is much higher due to greater plasma production and increased neutralizer keeper current. This is an important factor in the case of the NASA 8 cm because it has an open keeper configuration for the neutralizer. This means the area between the cathode and the keeper is not enclosed and is connected directly with the ambient plasma.

From all four of these plots, it was observed that the 70% pumping speed configuration had the lowest plasma potentials, electron temperatures, and Debye lengths but the highest electron

and ion densities. It is important to note that these trial points all had the neutralizer running at a higher current and flow rates. As a result the background plasma in the whole chamber was generally larger. Although, the background neutral pressure was lower than the 40% pumping speed configuration, the 70% case actually had more of an impact on plasma density. In the case of smaller chambers, the neutralizer plasma can have a broad impact on the ambient plasma. Because the chamber is small, the ambient plasma can also have a large impact on the beam.

It was observed that the plasma densities and floating potentials increased from the first three probes and then began to decrease. This is expected as more beam plasma propagates downstream it increases but then diffuses out as it continues to expand and cool. This is evident in the plasma potentials and electron temperatures as well. Ignoring the potentially high values for the in-plane Langmuir probes (due to potentially dirty probe effects), these values for the second and third wall probes seem to stay constant or slightly increase, whereas the later two either stay constant or slightly decrease.

Generally, the electron and ion density were lowest during the 100% as expected, expect for the closest in-plane Langmuir probe. At this point the 70% case was the lowest. This seems to be an additional artifact of a dirty probe as data was collected in this order: 100%, 40%, and then the 70%.

The following figures are for the 2024-05 test campaigns of plasma properties for wall probes 1-4 on the left-side of the thruster, left-side of the plasma screen, and 4 cm downstream of the neutralizer. In Figure 5.2 are the plasma potentials, Figure 5.3 are the floating potentials, Figure 5.4 are the electron densities, Figure 5.5 are the electron temperatures, and Figure 5.6 are the Debye lengths. Ion densities are found in the appendix C. The plasma screen configuration is defined first as either “G” for grounded or “F” for floating. The beam target configuration follows this same convention. Thus, “FG” means floating plasma screen with a grounded beam target.

The plasma potentials do not seem to have any distinct correlating with background pressure. Most obvious is the 70% pumping configuration with the changes in the neutralizer operating conditions show the most impact on the plasma properties anywhere, including the walls, plasma screen, and neutralizer. Generally, the plasma potentials are higher for the cases when the beam target is floating. This makes sense since the beam target floats positively by about a volt. One concern in this case would be higher plasma potentials can compete for the electrons that could be used to neutralize the beam. Thus it is important to know how the potential in the beam compares to the potentials near the wall. The higher plasma potentials at the wall will create a larger sheath drop to the walls to repel more electrons such that only the higher energy electrons will make it to the wall. Thus, a higher potential at the wall is alright if the potential in beam increases as well or a separating low potential separates the two plasmas. If these do not happen, then there could be alternative neutralization pathways occurring. In this case of the floating beam target, the plasma

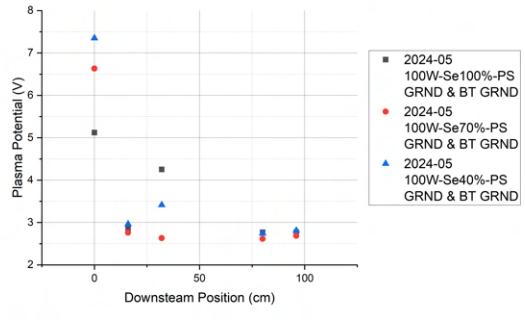

(a) Plasma potential

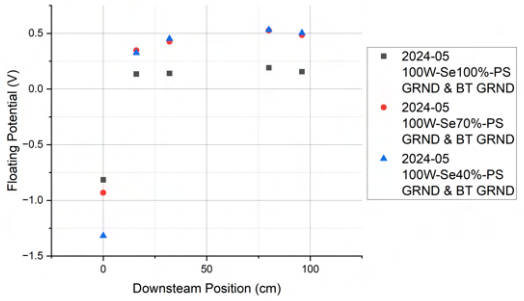

(b) Floating potential

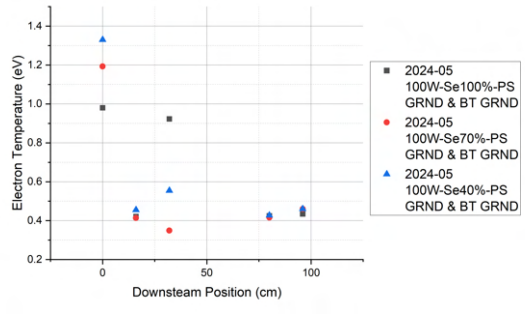

(c) Electron temperature

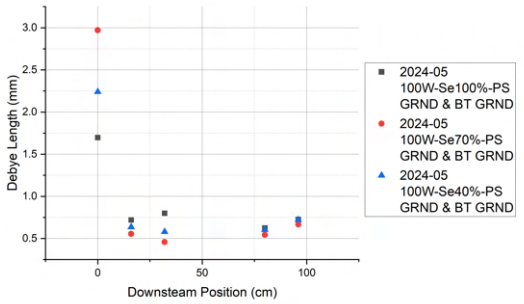

(d) Electron Debye length

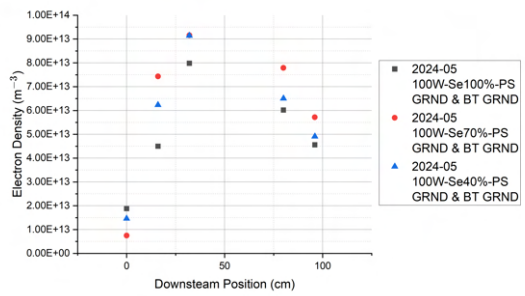

(e) Electron density

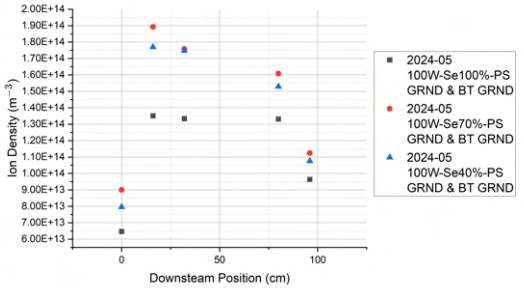

(f) Ion density

Figure 5.1: 2024-05 NASA 8 cm test campaign at the 100 W power level with the "super" neutralizer cathode, grounded plasma screen, and grounded beam target measured plasma properties in the ambient plasma near the facility walls obtained from the cylindrical Langmuir probes. Background pressure was controlled by throttling pumping speed of the downstream turbomolecular pump.

potentials seem to all raise together but a plasma potential measurement in the beam is necessary to confirm.

From Figure 5.3, the floating potentials as a function of background pressure do not seem to vary. They do vary by the 70% pumping speed case where higher neutralizer current and flow rates were used. There is however a very stark contrast between the grounded and floating beam target cases. The floating potentials of the floating beam target cases are higher. This plus the plasma potentials having a similar behavior from Figure 5.2, explains why that Figure 5.5 the electron temperatures are similar for any of the configurations. In addition the electron densities in Figure 5.4 are similar for each of the configurations. The combination of these indicate that no matter the configuration, the electron densities and temperatures are not being affected by the configuration. Thus, analysis of the true-coupling will be about how the electrons get to the beam, not by the increased conductivity due to increased plasma density or lower electrons being more easily trapped.

The floating potentials, other than first wall probe, the neutralizer, and near the plasma screen with a floating beam target, are all positive. This seems to indicate that there are either energetic ions or that the because the plasma potentials are so high and the electron temperatures so low, the floating potential becomes positive as the plasma is not truly neutralized yet at these points or that the elevation from the beam target is felt everywhere. The positive floating potentials seem to indicate when the beam has expanded to much and its presence can be felt at the walls and as a result the change in the electrical boundary condition of the beam target can and does effect the potentials in the whole system. The fact the floating potentials are positive even at only 16 cm downstream at which point the beam may not be neutralized enough or expanded enough, resulting in having significant coupling with the facility. The floating beam target elevates the whole system to limit this coupling at the walls as the floating beam target configuration limits the amount of electrons that can be reintroduced into the beam at the target by disconnecting the direct circuit connection via facility ground.

Because the electron temperature varies so little at the walls, the Debye length is predominately controlled by the plasma density. The 70% case contributed much more plasma and as such decreased the Debye even more. Because the Debye length is so affected by the plasma density, it may not be a great scaling factor in determining when a facility is too small. A ratio of conductivity and wall proximity may be a more proper choice in deciding when too much beam-facility interactions occur. Testing this system in at least two more facilities with two more ambient background plasma densities, at similar neutral pressures, would be required.

Figure 5.7 is the wall plasma properties varying with downstream distance for the 2024-11 200 W test using a grounded plasma screen and comparing both grounded and floating beam targets. Similar plots for the combination of 2024-11 and 2025-01 100 W power levels using both a

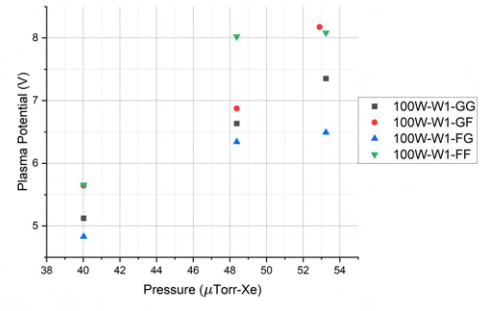

(a) Left-side wall probe 1 at 0 cm downstream

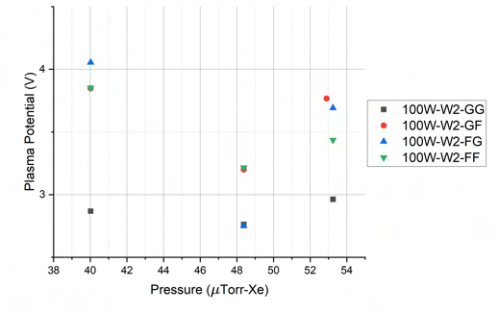

(b) Left-side wall probe 2 at 16 cm downstream

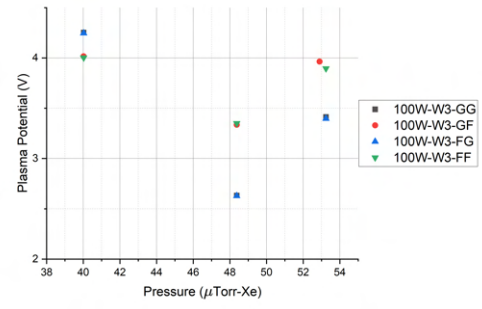

(c) Left-side wall probe 3 at 32 cm downstream

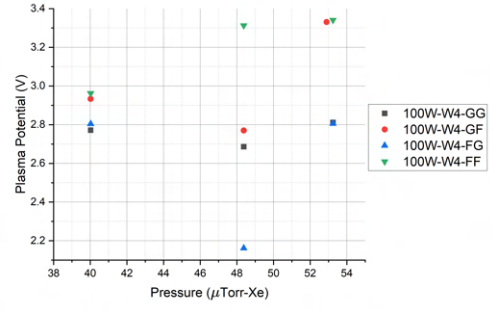

(d) Left-side wall probe 4 at 96 cm downstream

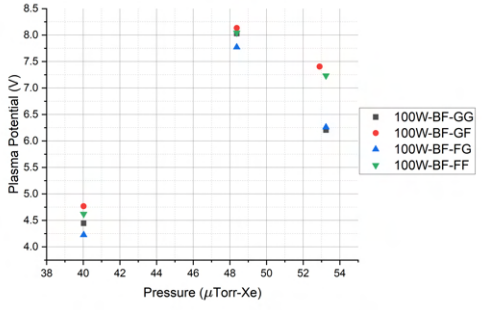

(e) Left-side of the plasma screen

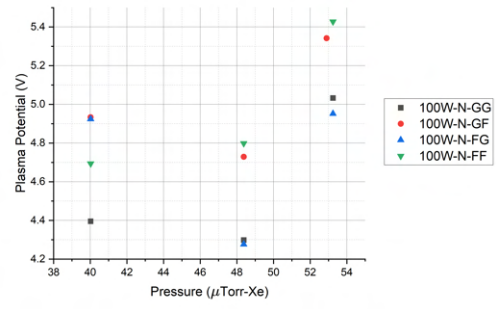

(f) Downstream 4 cm of the neutralizer

Figure 5.2: 2024-05 NASA 8 cm test campaign plasma potentials obtained from Langmuir probes in various locations in the PSTL RC using the "super" neutralizer cathode over a variety of background pressures.

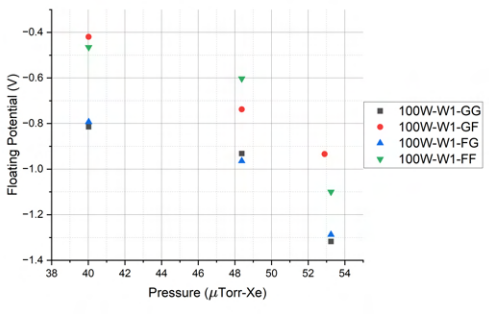

(a) Left-side wall probe 1 at 0 cm downstream

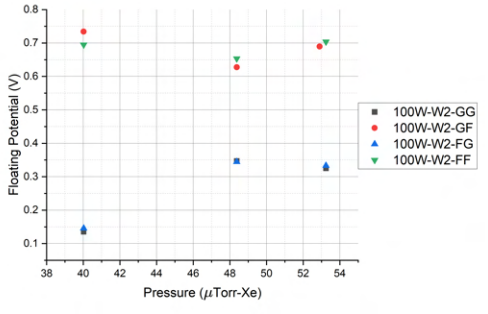

(b) Left-side wall probe 2 at 16 cm downstream

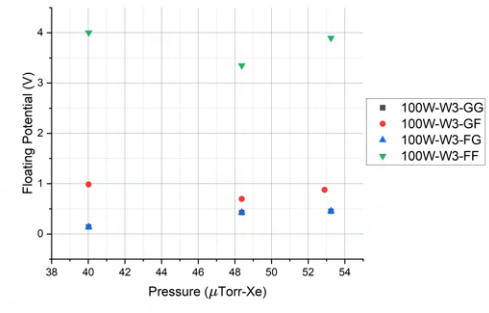

(c) Left-side wall probe 3 at 32 cm downstream

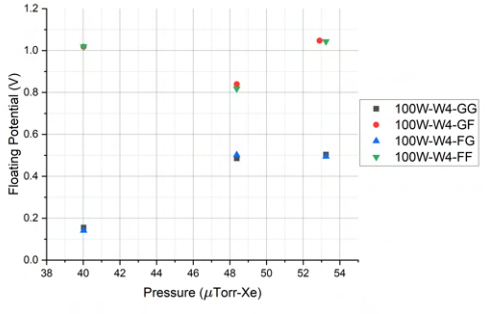

(d) Left-side wall probe 4 at 96 cm downstream

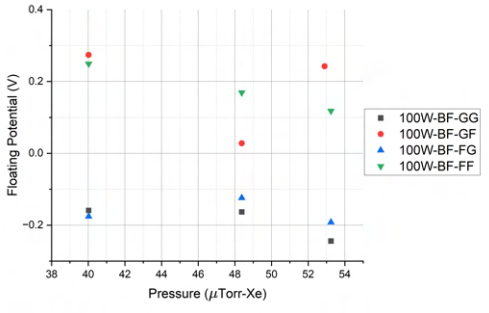

(e) Left-side of the plasma screen

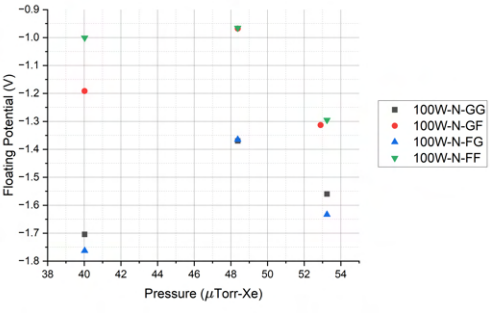

(f) Downstream 4 cm of the neutralizer

Figure 5.3: 2024-05 NASA 8 cm test campaign floating potentials obtained from Langmuir probes in various locations in the PSTL RC using the "super" neutralizer cathode over a variety of background pressures.

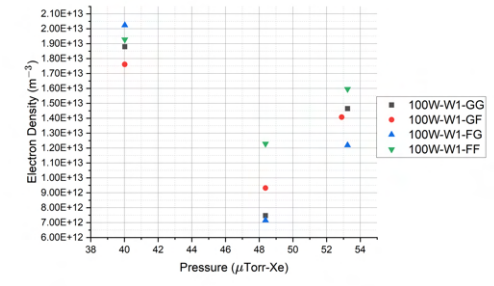

(a) Left-side wall probe 1 at 0 cm downstream

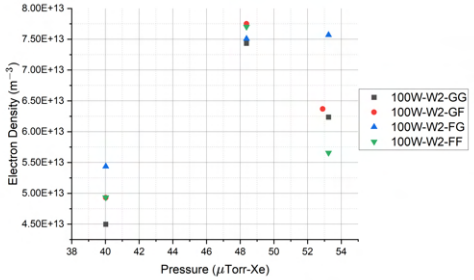

(b) Left-side wall probe 2 at 16 cm downstream

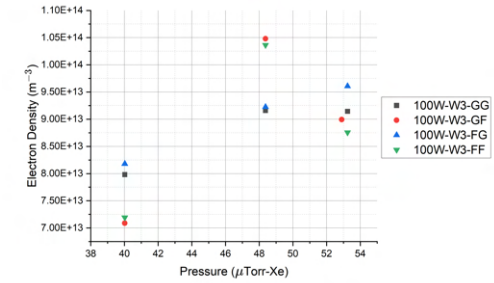

(c) Left-side wall probe 3 at 32 cm downstream

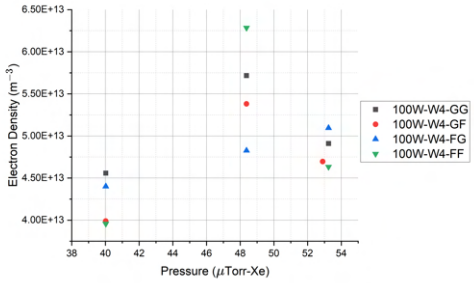

(d) Left-side wall probe 4 at 96 cm downstream

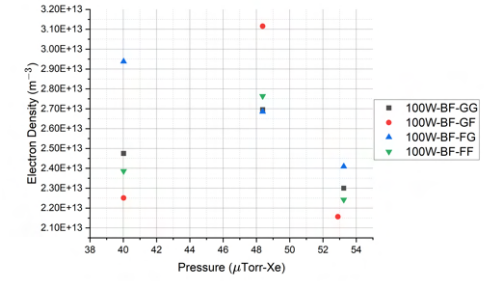

(e) Left-side of the plasma screen

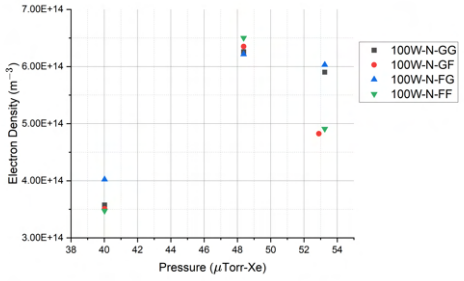

(f) Downstream 4 cm of the neutralizer

Figure 5.4: 2024-05 NASA 8 cm test campaign electron densities obtained from Langmuir probes in various locations in the PSTL RC using the "super" neutralizer cathode over a variety of background pressures.

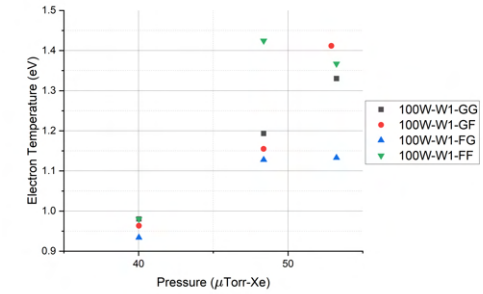

(a) Left-side wall probe 1 at 0 cm downstream

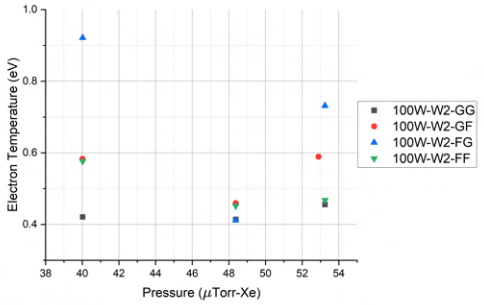

(b) Left-side wall probe 2 at 16 cm downstream

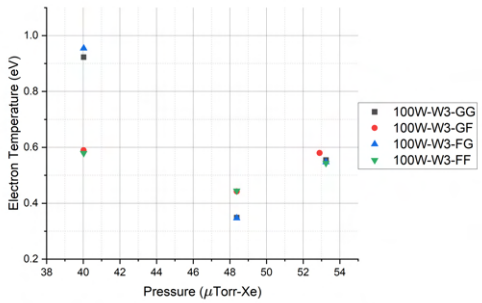

(c) Left-side wall probe 3 at 32 cm downstream

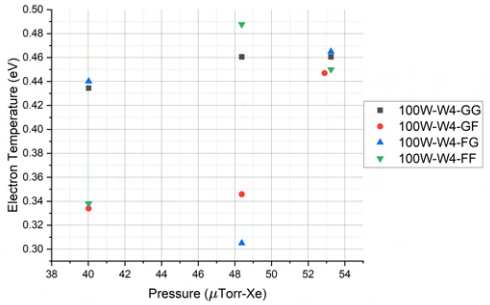

(d) Left-side wall probe 4 at 96 cm downstream

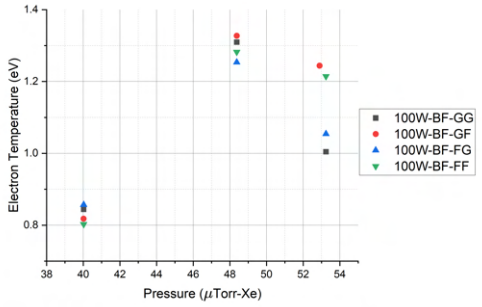

(e) Left-side of the plasma screen

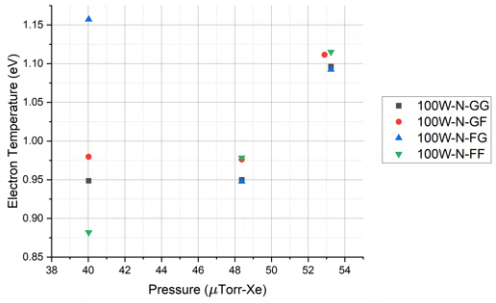

(f) Downstream 4 cm of the neutralizer

Figure 5.5: 2024-05 NASA 8 cm test campaign electron temperatures obtained from Langmuir probes in various locations in the PSTL RC using the "super" neutralizer cathode over a variety of background pressures.

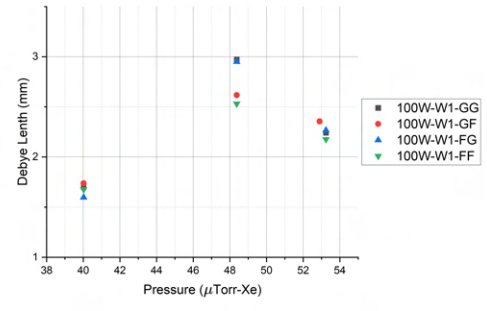

(a) Left-side wall probe 1 at 0 cm downstream

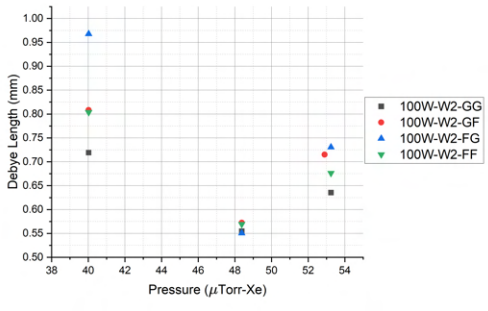

(b) Left-side wall probe 2 at 16 cm downstream

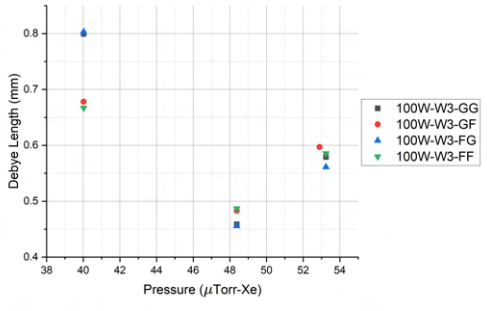

(c) Left-side wall probe 3 at 32 cm downstream

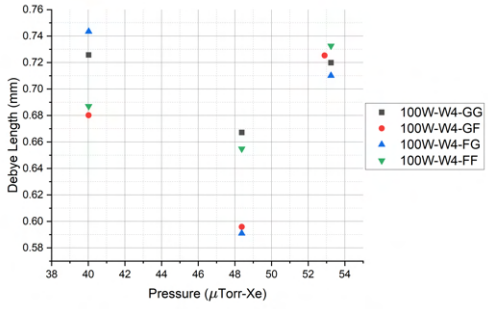

(d) Left-side wall probe 4 at 96 cm downstream

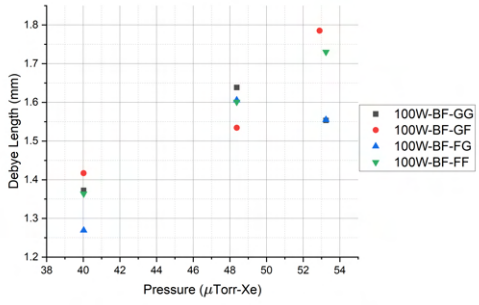

(e) Left-side of the plasma screen

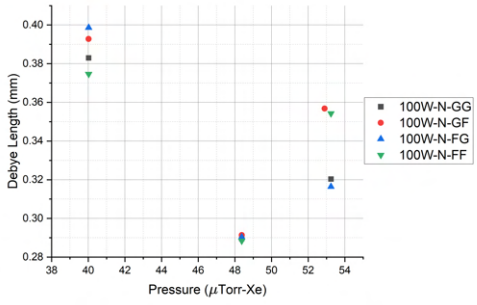

(f) Downstream 4 cm of the neutralizer

Figure 5.6: 2024-05 NASA 8 cm test campaign electron Debye lengths obtained from Langmuir probes in various locations in the PSTL RC using the "super" neutralizer cathode over a variety of background pressures.

grounded and floating plasma screen and a grounded beam target for limited pumping configurations, are given in Figure 5.8. The near wall plasma properties with downstream distance over all pumping configurations for the 2024-11 100 W with grounded plasma screen and grounded beam target case are given in Figure C.6 found in Appendix C. The 2024-11 100 W results were very similar to the 2024-05 results with the addition of one more pumping configuration and a different neutralizer. Each figure contains these six plasma properties: 1) plasma potential, 2) floating potential, 3) electron temperature, 4) electron Debye length, 5) electron density, and 6) ion density. In general, the behavior trends for all configurations were similar.

In the case of the 200 W condition with the nominal neutralizer, similar results were found in regards to trends of the plasma properties as function of downstream position. From Figure 5.7 shows that plasma potential and floating potential are greatest for the floating beam target configurations, like seen in the 2024-05 test campaign. Electron temperatures seem to be constant as well. The electron and ion densities are also more of a function of pumping speed than electrical configuration of the beam target. Thus, regardless of neutralizer or background pressure, it was observed that the floating beam target lifts the potential of the whole chamber without much impact on other plasma properties. This is good as it allows the elimination of the variables of changing electron temperatures or plasma densities from affecting later studies of beam coupling and alternative neutralization pathways.

The comparison of the 100 W condition with the two types of neutralizers but varying plasma screen potentials. In Figure 5.8 the plasma screen potential seems to have almost no impact on any plasma parameters. The only real difference is downstream plasma densities seem to be much greater for the 2024-11 test with the nominal cathode compared to the 2025-01 test with the "super" cathode. This maybe because the nominal cathode produced greater plasma densities that filled the chamber for longer distances. The nominal cathode was operated at a higher current than the "super" cathode in the 2025-01 test. This may contribute to the higher background plasmas downstream. Again, this is good as it eliminates the variables of changing electron temperatures or plasma densities from affecting later studies of beam coupling and alternative neutralization pathways.

The following figures are for the 2024-11 and 2025-01 test campaigns of plasma properties for wall probes 1-4 on the left-side of the thruster, left-side of the plasma screen, and 4 cm downstream of the neutralizer. In Figure 5.9 are the plasma potentials, Figure 5.3 are the floating potentials, Figure 5.4 are the electron densities, and Figure 5.5 are the electron temperatures. Debye length and ion densities are found in the appendix C. The plasma screen configuration is defined first as either "G" for grounded or "F" for floating. The beam target configuration follows this same convention. Thus, "FG" means floating plasma screen with a grounded beam target.

The plasma potentials are similar to the 2024-05 results in that the floating beam target has the

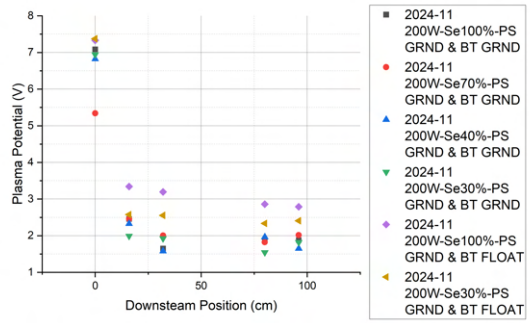

(a) Plasma potential

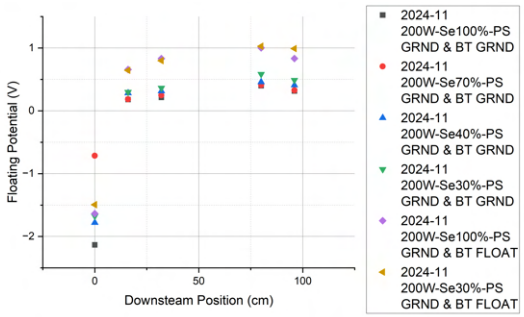

(b) Floating potential

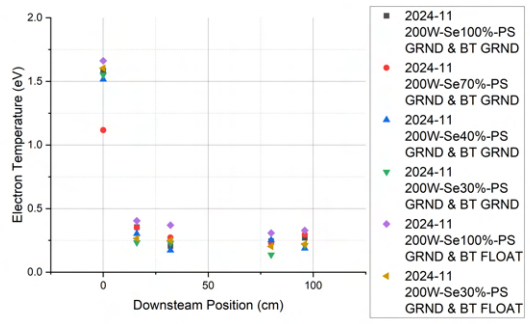

(c) Electron temperature

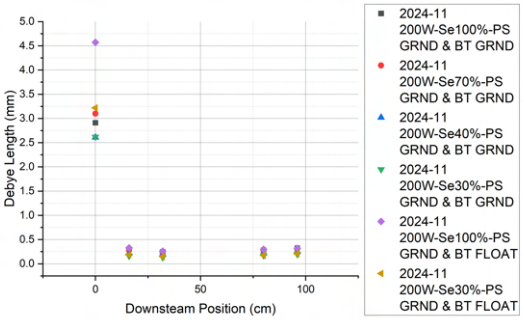

(d) Electron Debye length

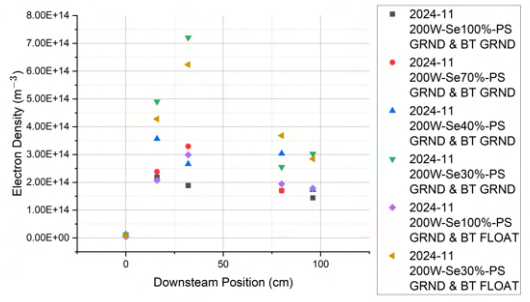

(e) Electron density

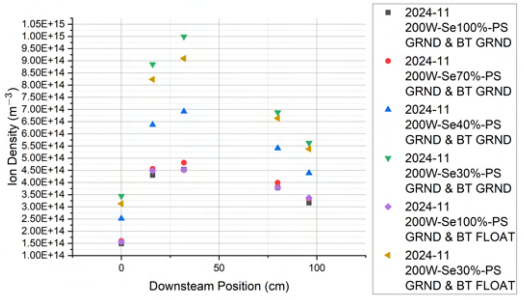

(f) Ion density

Figure 5.7: 2024-11 NASA 8 cm test campaign at the 200 W power level with the nominal hollow neutralizer cathode, grounded plasma screen, and grounded or floating beam target measured plasma properties in the ambient plasma near the facility walls obtained from the cylindrical Langmuir probes. Background pressure was controlled by throttling pumping speed of both turbomolecular pumps.

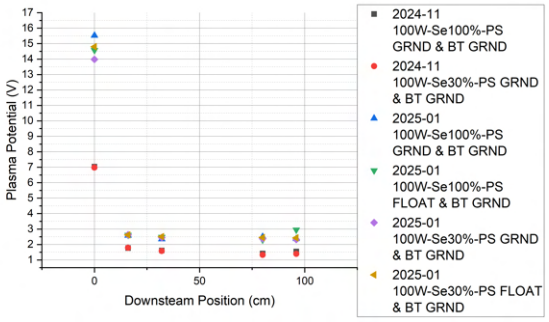

(a) Plasma potential

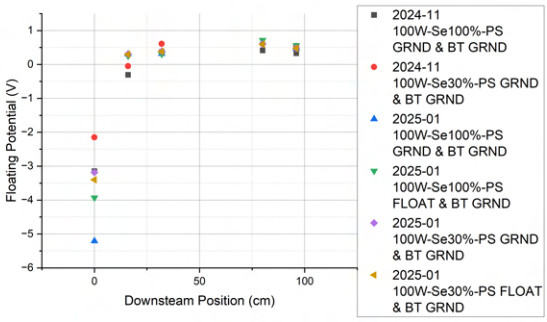

(b) Floating potential

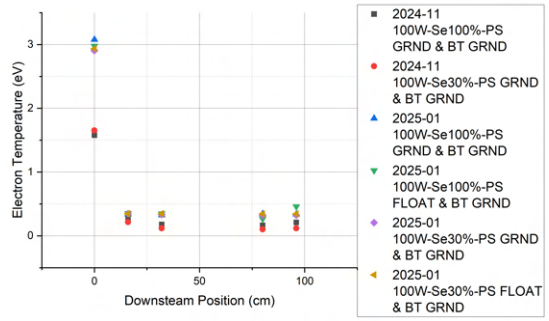

(c) Electron temperature

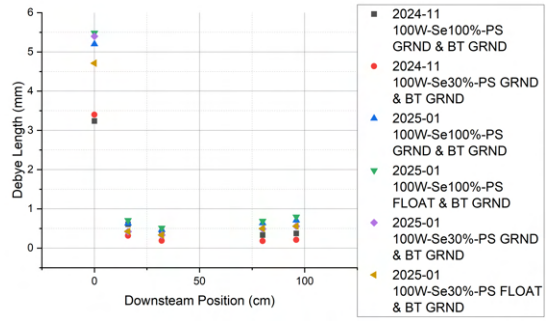

(d) Electron Debye length

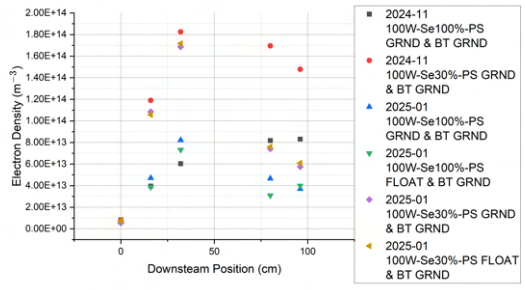

(e) Electron density

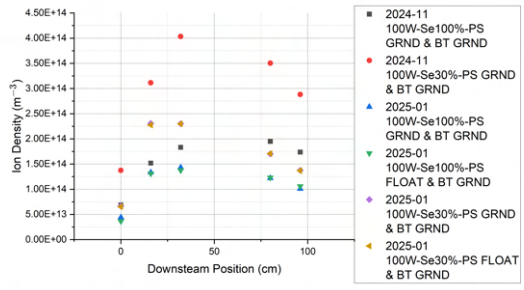

(f) Ion density

Figure 5.8: 2024-11 & 2025-01 NASA 8 cm test campaigns at the 100 W power level. 2024-11 campaign used a nominal hollow cathode for the neutralizer whereas the 2025-01 test campaign used the "super" neutralizer cathode. A combination of grounded or floating plasma screen, and grounded beam target electrical configurations were used. Plasma properties in the ambient plasma near the facility walls shown here were obtained from cylindrical Langmuir probes. Background pressure was controlled by throttling pumping speed of both turbomolecular pumps.

most impact on elevating the potentials along the walls and near the plasma screen, but not at the neutralizer. Again this elevation is from the beam target floating positive and raising the whole system.

In Figure 5.9 it can be seen that higher power beams and less neutralizer current will result in the wall probe plasma potentials being higher regardless of background pressure. For example, in Figure 5.9b, while ignoring the purple diamonds for the 200 W with floating beam target case, the plasma potentials can be grouped by either power level or neutralizer type. The 300 W case is the highest, than the 200 W, the 100 W with the less neutralizer current, and lastly the 100 W with the most neutralizer current. It was expected that there will be higher potentials in the beam due to higher power levels. It was also expected that a higher neutralizer current will decrease the potential in the beam as it neutralizes the beam better. This shows that the magnitude of beam neutralization can be felt near the walls. This is not ideal as it means the beam is most likely being easily coupled with facility and therefore the facility was impacting the neutralization process. Evidence of this was background pressure did seem to decrease the plasma potential at the wall in the 200 W cases. The decrease here was more obvious probably because the potentials in the beam were higher and the range of the background pressure was larger than the 100 W case. Unfortunately, one would want the neutralization process to not be affected by the background pressure as this can create misleading neutralization results for spaceflight.

The fact that the potential of the beam was seen at the walls decreasing with background pressure will obscure if neutralization will take place in space properly. There is a situation where the increase of background pressure is helping the neutralizer couple with the beam by increasing the conductivity between the neutralizer and the beam faster than to the walls. As a result, the neutralizer-facility coupling voltage, V_{cg}, would decrease in its negative magnitude. However, this was not the case seen in any of these test. It appears that in most cases, if it was not constant with background pressure, than V_{cg} increases in magnitude negatively. This was a difficult situation to combat as running at high-power densities of 100 kW system will be done at elevated background pressures where there will be no avoiding this. Thus, the true-coupling voltage must be used as a metric of how well a beam is being neutralized by the neutralizer.

In conjunction with the findings of increasing V_{cg} with background pressure, the plasma potential near the plasma screen did show a linear dependence with background pressure. Figure 5.9e may give insight to where the electrons are going that was causing more coupling to the facility. Unfortunately, no correlation at this time could be made to explain this phenomenon and obvious linear increase with background pressure.

In Figure 5.9f the plasma potential near the neutralizer was higher when the neutralizer current was lower with the "super" neutralizer cases. This points to the plasma potential being more positive to pull out more electrons and probably means the potential in the beam was higher as

well. This was confirmed looking at the plasma potentials in beam plume in the near-field from Figures 5.18a and 5.20a discussed later. This may be a better alternative to estimating the beam potential than having to run an emissive probe through the plume as they can be fragile and not easy to implement a full emissive sweep on spacecraft in space. A simple Langmuir probe out of the plume in front of the neutralizer may be a quick and easy alternative to getting a good estimation of the true-coupling voltage.

Floating potentials for these test campaigns were almost always positive for the wall probes starting at the second wall probe except for the 100 W super neutralizer case. The plasma screen and neutralizer floating potentials were always negative. In Figure 5.10, the planar probe made of high-density tungsten used near the plasma screen for all cases had a negative floating potential. In the previous 2024-05 test the probe was made of thoriated-tungsten TIG welding rod and had some positive floating potentials, as seen in Figure 5.3. There seemed to be some material impacts on the probe results. It was expected that the one of the tungsten probes may have experienced large secondary electron emissions or ion induced electron emission. This would explain why the floating potentials were positive as an electron emitted looks like an ion collected. However, the high-density tungsten results in Figure 5.10e for floating potential, Figure 5.12 for electron temperature, and Figure 5.9e for plasma potential all increased with background pressure. Charge-exchange or elastically scattered ions increase with background pressure as well. Since the normal of collecting area of probe was parallel with the beam propagation direction, there may be energetic ions hitting this planar probe that could have also made the electron temperature and plasma potential increase with pressure. It was expected that these two plasma properties should decrease with the increase of collisions with background neutrals.

Compared to the 2024-05 test, the electron density in Figure 5.11 all seemed strongly linearly correlated with background pressure. The neutralizer plasma seems to be less impacted by background pressure as the plasma densities here seem to be much higher than the ambient plasma near the walls. The less suitability to variation in the plasma bridge points to why the V_{cg} tends to increase in negative magnitude with increasing background plasma. The rate of increase in ambient plasma near the walls and plasma screen with background pressure was faster than in the bridge. As a result, the conductivity to the facility increases faster than the conductivity to the beam. To overcome this, the impedance to the walls and other grounded objects needs to be increased by either moving the walls further or potentially adding a dielectric barrier or insulator. Testing 100 kW systems will need to consider the ratio of conductivity over distance to the walls and to the beam. Further studies with variable wall distance and plasma densities would be needed to determine at what point does the ratios increase at the same rate, as the conductivity to the beam.

Electron temperatures in Figure 5.12 generally decreased slightly with pressure for the wall probes after the first probe. This was expected but the temperatures were already so small that the

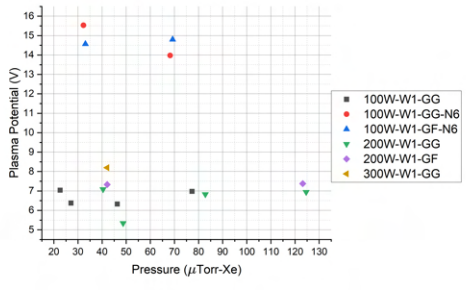

(a) Left-side wall probe 1 at 0 cm downstream

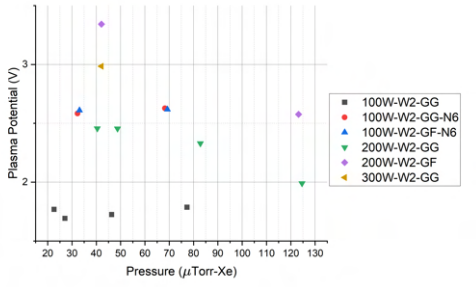

(b) Left-side wall probe 2 at 16 cm downstream

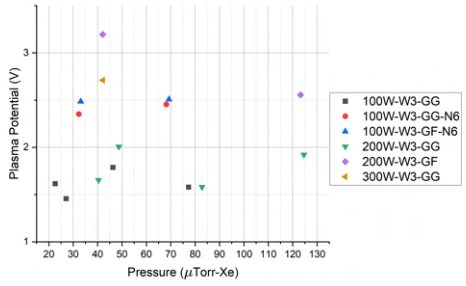

(c) Left-side wall probe 3 at 32 cm downstream

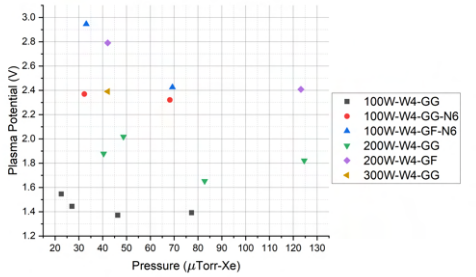

(d) Left-side wall probe 4 at 96 cm downstream

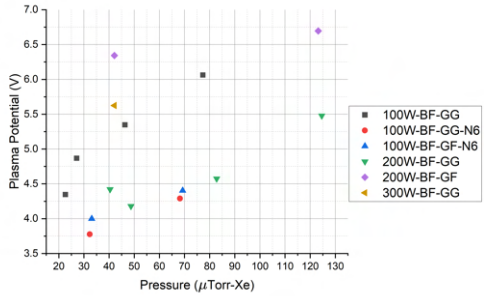

(e) Left-side of the plasma screen

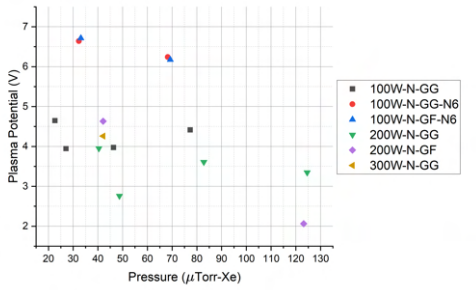

(f) Downstream 4 cm of the neutralizer

Figure 5.9: 2024-11 & 2025-01 NASA 8 cm test campaigns plasma potentials obtained from Langmuir probes in various locations in the PSTL RC. A nominal hollow cathode was used during the 2024-11 test campaign where as the "super" neutralizer cathode was used in the 2025-01 test campaign. Variations in the background pressure was done by throttling both turbomolecular pumps.

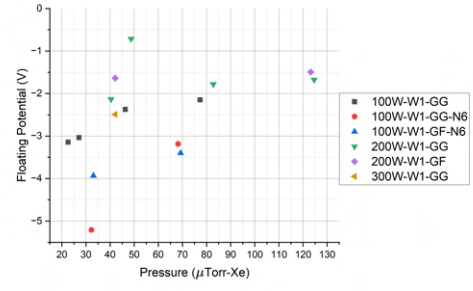

(a) Left-side wall probe 1 at 0 cm downstream

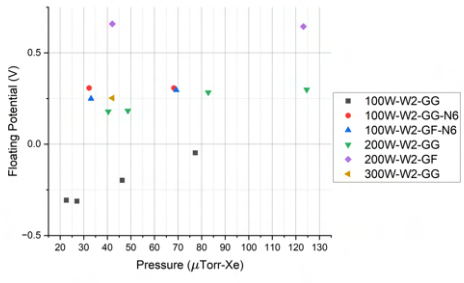

(b) Left-side wall probe 2 at 16 cm downstream

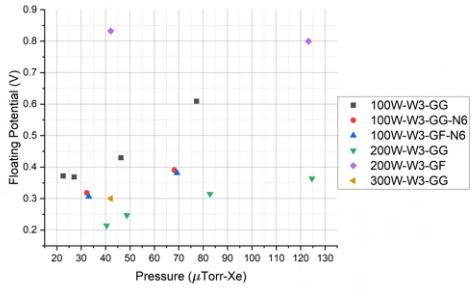

(c) Left-side wall probe 3 at 32 cm downstream

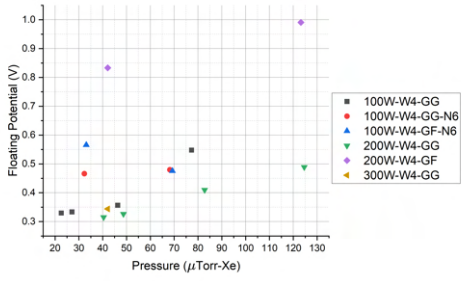

(d) Left-side wall probe 4 at 96 cm downstream

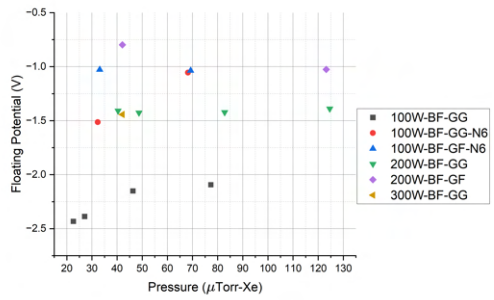

(e) Left-side of the plasma screen

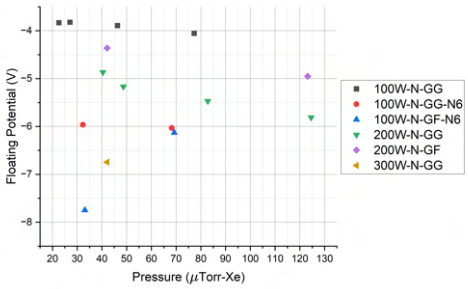

(f) Downstream 4 cm of the neutralizer

Figure 5.10: 2024-11 & 2025-01 NASA 8 cm test campaigns floating potentials obtained from Langmuir probes in various locations in the PSTL RC. A nominal hollow cathode was used during the 2024-11 test campaign where as the "super" neutralizer cathode was used in the 2025-01 test campaign. Variations in the background pressure was done by throttling both turbomolecular pumps.

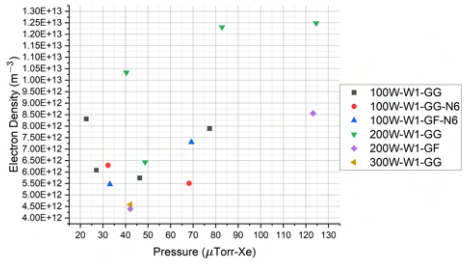

(a) Left-side wall probe 1 at 0 cm downstream

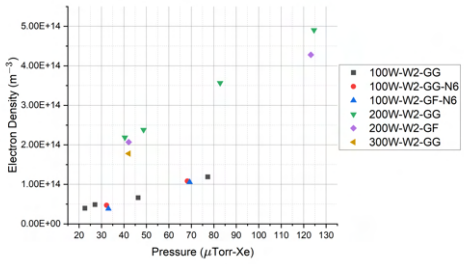

(b) Left-side wall probe 2 at 16 cm downstream

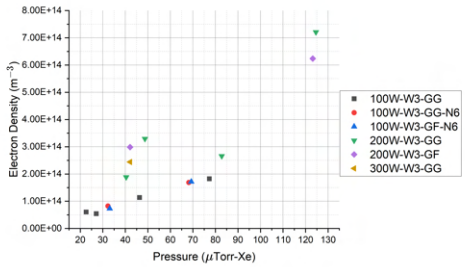

(c) Left-side wall probe 3 at 32 cm downstream

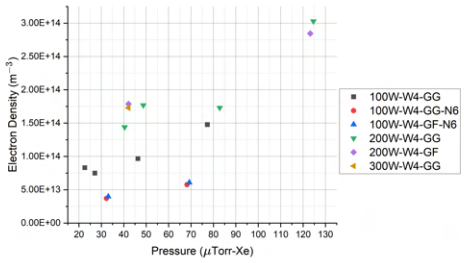

(d) Left-side wall probe 4 at 96 cm downstream

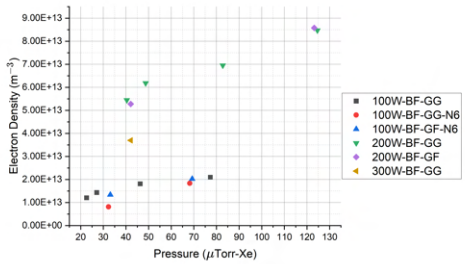

(e) Left-side of the plasma screen

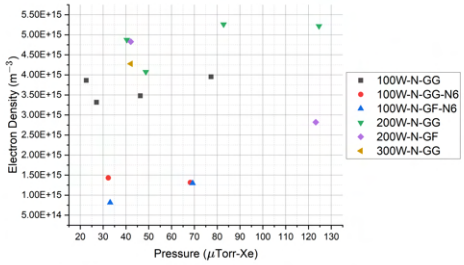

(f) Downstream 4 cm of the neutralizer

Figure 5.11: 2024-11 & 2025-01 NASA 8 cm test campaigns electron densities obtained from Langmuir probes in various locations in the PSTL RC. A nominal hollow cathode was used during the 2024-11 test campaign where as the "super" neutralizer cathode was used in the 2025-01 test campaign. Variations in the background pressure was done by throttling both turbomolecular pumps.

changes are even smaller. The increasing electron temperature near the plasma screen was still undetermined but may be due to probe materials. The neutralizer probe did not have a decreasing temperature with background pressure except for the cases where either the plasmas screen or the beam target was floating. This suggest these electrons are having an easier time getting to the beam and neutralizing it as they are not having competing potentials that were stealing them form going directly to the beam. This indicates that for high-power testing at least one of the two, the plasma screen or the beam target, should be floating to eliminate alternative neutralizing pathways. Further decisions on which is best and why are investigated in later sections of this chapter once measurements of the true-coupling voltage could be made. However, the lowering of the electron temperatures due to increased background pressure and neutral collisions was a facility effect. These were not seen in the other fully grounded cases as the alternative neutralization pathways allow the electrons to still get to the beam, thus why they were generally lower already. Higher background pressures for high-power density testing may require some sort of artificial heat of the electrons to properly determine beam neutralization. One idea is injected localized neutral flow at the plasma bridge. This idea is discussed in a later section.

Generally, it was found that the beam couples with the facility much more in the higher-power density testing. This was evident in potentials near the wall being affected by changes in the neutralization process. Additionally, either the plasma screen or the beam target needs to be floating to eliminate alternative neutralization pathways. Most importantly, true neutralizer-beam coupling can be approximated by the changes in plasma potential near the neutralizer.

Probe materials can have an impact on measurements. In addition Lobbia et al. in Ref. [120] recommend probe orientations for Langmuir probes matter as well. The following Figures 5.13 and 5.14 compare the different probe shapes and orientations for the grounded cases of 100 W and 200 W power conditions, respectively, during 2024-11 test campaign. All probes were placed approximately 80 cm downstream. “V_PLP” was a vertical planar probe, where the normal of the probe was in the vertical direction, placed on the left-side of the chamber. “WP_PLP” was planar probe with its normal in the same direction of the wall, perpendicular to the beam propagation and the normal of “V_PLP”. Also on the left-side of the chamber. The last probe on the left side was the “V_CLP” cylindrical Langmuir probe. All the the other wall probes in the study are in this orientation where the probe was vertical such that the tip of the probe points towards the ceiling of the chamber. A angled cylindrical probe and spherical probe were placed on the right-side of the chamber designated by “A_CLP” and “B_SLP”, respectively. The angled probe tip points at the thruster and the spherical probe is omni-directional.

In general, the 100 W and 200 W cases behaved similarly. Although different angles and orientations, the plasma potential should be the same for all probes as it was not directionally dependent. The “V_PLP” probe was the only probe that had a very different measurement of the

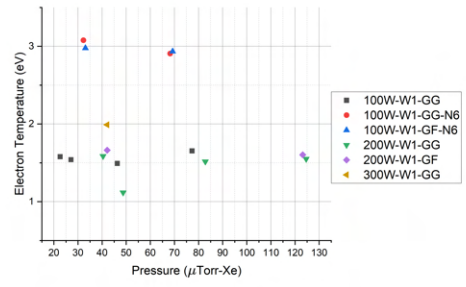

(a) Left-side wall probe 1 at 0 cm downstream

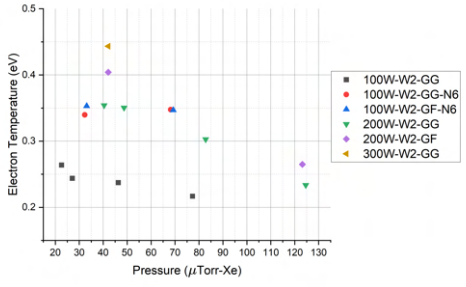

(b) Left-side wall probe 2 at 16 cm downstream

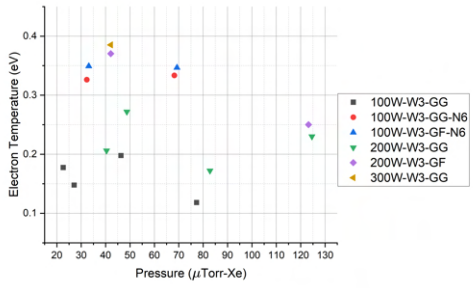

(c) Left-side wall probe 3 at 32 cm downstream

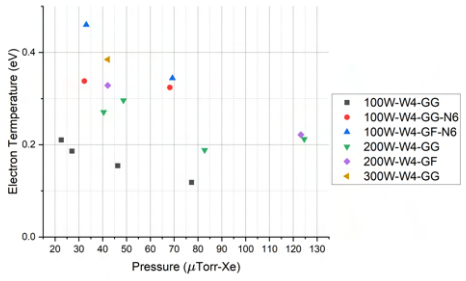

(d) Left-side wall probe 4 at 96 cm downstream

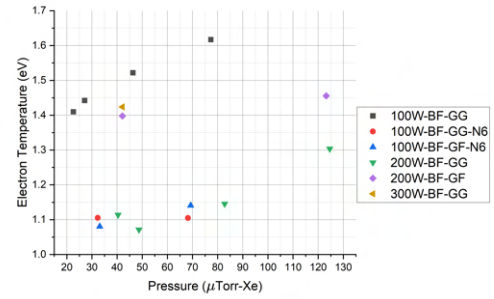

(e) Left-side of the plasma screen

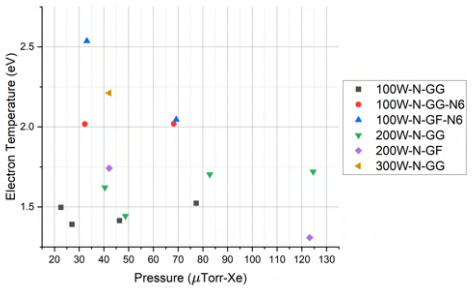

(f) Downstream 4 cm of the neutralizer

Figure 5.12: 2024-11 & 2025-01 NASA 8 cm test campaigns electron temperatures obtained from Langmuir probes in various locations in the PSTL RC. A nominal hollow cathode was used during the 2024-11 test campaign where as the "super" neutralizer cathode was used in the 2025-01 test campaign. Variations in the background pressure was done by throttling both turbomolecular pumps.

plasma potential compared to all the other probes. In addition, the measured electron temperatures were higher as well. The plasma densities were also the lowest for this probe. These are symptoms of a dirty probe. Carbon sputtered off the walls could deposit on these probes. The effects on probes with larger surface areas like the spherical probe were less impacted as some of the sides face the walls and others towards the beam. It seems the high energy ions from the beam that made it to these probes may help keep the probes clean. However, in high-velocity ion flow it is recommended in Lobbia et al. to keep the normal of the collecting surface perpendicular to the flow. Because these probes were at the walls and had limited high energy ion flows, this non-recommended orientations seems to be better as the ions that did make it keep it clean. Thus, wall probes, especially those in high-power density environments need to be cleaned before each trace by a high voltage sweep from -100 V to 100 V or have a large collecting surface facing the plasma ions.

5.3.1.2 Beam Plasma Plume

The smaller size of the chamber limits the expansion of the beam plasma. In addition, the elevated background pressure also increases the ambient plasma density as well. This section investigates how this impacts Faraday probe measurements of the plume and resulting properties of the plume such as divergence angles and total integrated current. Due to the number of plots of Faraday probe sweeps, only four are shown here as a representation of the other traces.

In the following, Figure 5.15, are four Faraday sweeps from the 2025-01 campaign. The plasma screen was floating here and the beam target was grounded. The red line is the FWHM. The purple shade was the area used for the current integration of the beam if only using the left side of the beam up to 95% of the beam radius as recommend in Ref. [121]. In the legend this is I_{left}. The brown shaded area was used for the right-side integration, given as I_{right}. Integration of the beam current over the diameter of beam using both purple and brown shaded region is the I_{full} in the legend.

There are two transitions, one was between the main part of the beam and the scattered or diverging part of the beam, the other is around 8 cm outside the beam where the plume was no longer expanding but appears to be met by the ambient plasma. This behavior was not seen in the very near-field sweeps of 0.5 cm as not much CEX or broadening has yet to occur. Thus, the sharp drop in current just outside the beam is evidence of the ambient plasma to the probe. In the very near-field sweeps, 0.5 cm downstream, the ambient current saturates in the 10^{-4} mA range where as it appears at 16 cm downstream the current seems to be approaching saturation in 10^{-3} mA range. This was expected as in the wall plasma properties section, it was found that the plasma density from 16-32 cm was increasing in plasma density. However, the fact that the plume does not seem to continue to decrease much past the width of the beam can be concerning as this can indicate high

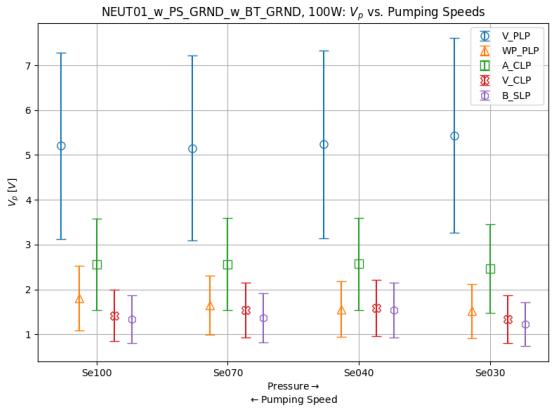

(a) Plasma potential

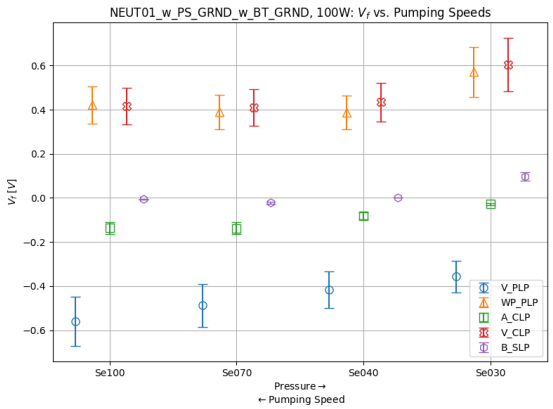

(b) Floating potential

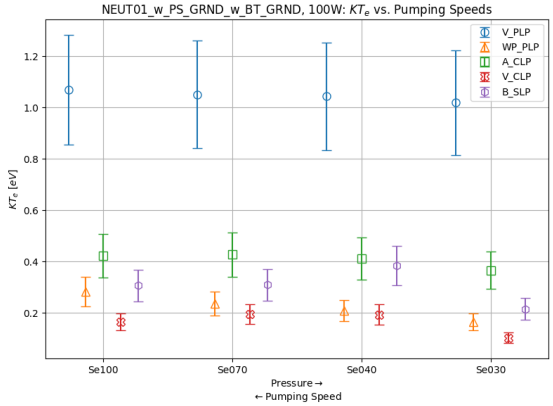

(c) Electron temperature

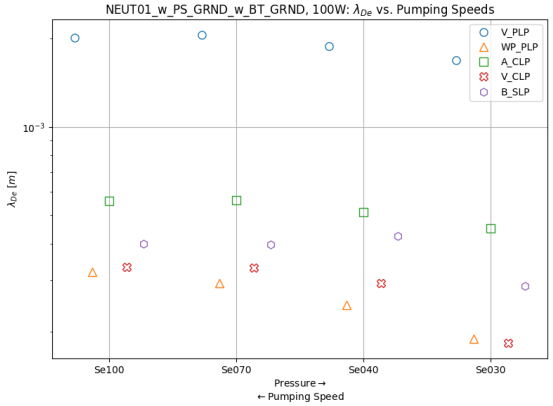

(d) Debye length

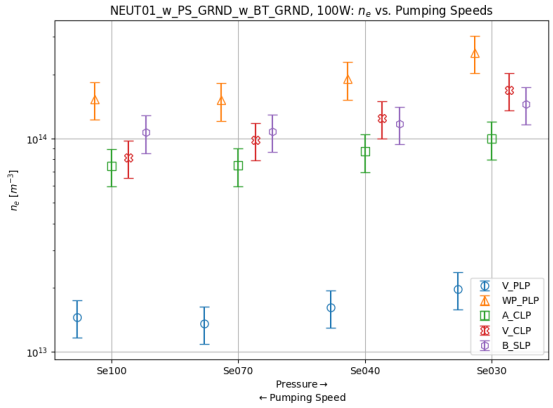

(e) Electron density

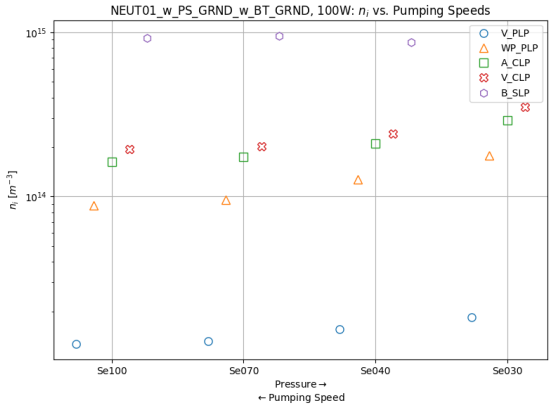

(f) Ion density

Figure 5.13: 2024-11 NASA 8 cm test campaign at the 100 W power level of the Langmuir probe geometry and orientation effects on measured plasma properties with a varying background pressure at 80 cm downstream of the thruster along the wall of the RC facility.

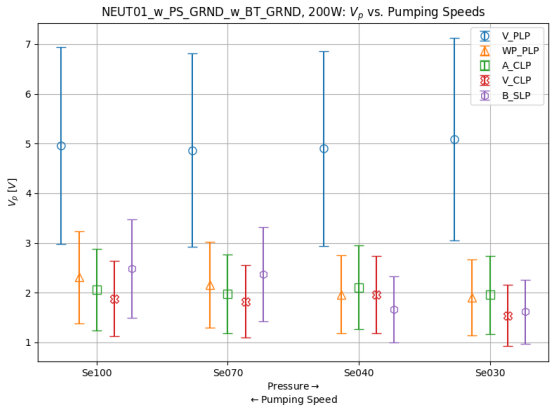

(a) Plasma potential

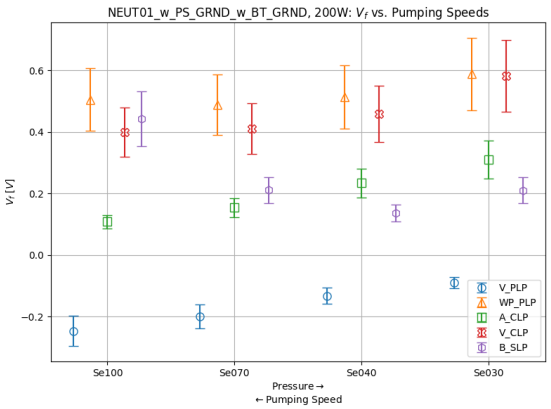

(b) Floating potential

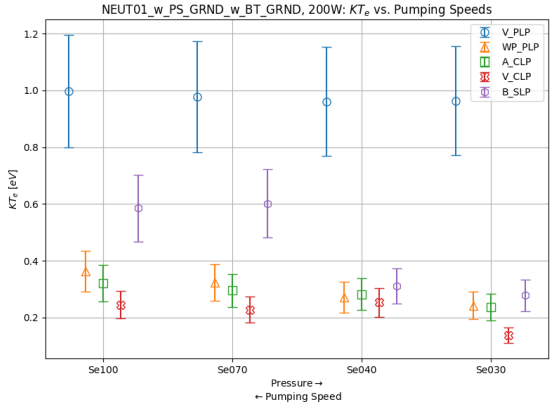

(c) Electron temperature

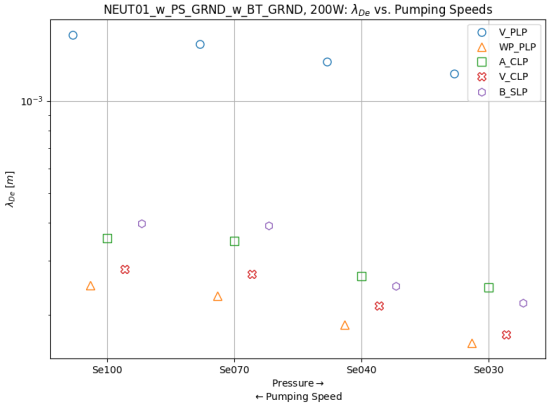

(d) Debye length

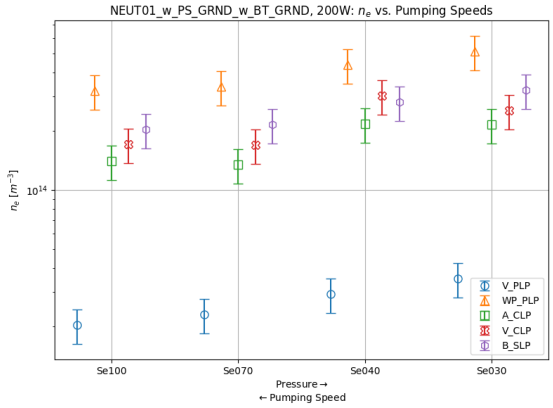

(e) Electron density

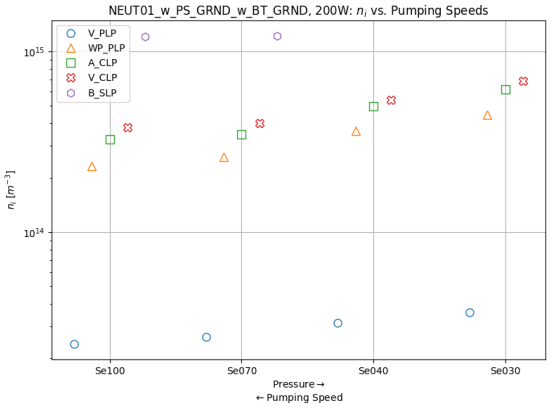

(f) Ion density

Figure 5.14: 2024-11 NASA 8 cm test campaign at the 200 W power level of the Langmuir probe geometry and orientation effects on measured plasma properties with a varying background pressure at 80 cm downstream of the thruster along the wall of the RC facility.

ambient plasma densities that can allow electrons to flow freely between the beam and ambient plasmas. This can result in neutralization from the ambient plasma electrons instead of directly by the neutralizer. The ambient plasma electrons could have much lower temperatures and more easily neutralizer the beam but this would not be present in spaceflight. The decreasing current found around 5-8 cm outside the beam in the 16 cm downstream plots was the expected behavior but should continue further. As the plasma expands it decreases in density and as such should also decrease the conductivity when there are only small changes in the electron temperatures. At these high ambient plasma densities, the low energy electrons rejected from the facility wall sheaths can be reflected back into the ambient plasma and if no retarding potential between the ambient and beam plasma exist, they can conductively make it back to the beam to neutralize it. Investigations in the plume potential profiles are needed to determine if ambient plasma electrons were aiding in the beam neutralization process. This could make operating 100 kW systems at high-power densities difficult to know proper neutralizer conditions as the beam could be naturalized via the ambient plasma and not directly from the neutralizer. As such, the neutralizer would not have to work as hard to neutralize the beam. If these neutralizer parameters are used for spaceflight, then there could be poor neutralization in space resulting in a struggling neutralizer and a virtual anode in the beam that will retard thrust or result in ion-bombardment damage of the spacecraft.

In Figure 5.16 are the converging and diverging half-angles of the beam and the cross-over distances due to the converging-diverging lens of the NASA 8 cm grids versus pressure variations. All combinations of both grounded or floating plasma screens and grounded or floating beam targets for the 2024-11 and 2025-01 test campaigns are shown. The plasma screen configuration is defined first as either “G” for grounded or “F” for floating. The beam target configuration follows this same convention. Thus, “FG” means floating plasma screen with a grounded beam target. The converging and diverging angles were determined using the variations of the FWHM of the beam peaks.

From the plots, the converging half-angle had a strong dependence on pressure, regardless of power level. Only either having a floating plasma screen or beam target did this seem to not be true. However, the diverging half-angle seem to be constant no matter pressure, power level, or configuration. It only seemed to be affected by different test campaigns, indicating that the neutralizer or neutralizer operating conditions may affect this. The calculated cross-over distance was primary affected by the converging angle. In a typical diverging grid configuration, the divergence angle was expected to increase with background pressure due to increased CEX collisions. In the case of the converging girds, the increased CEX collisions will knock ions out the beam, increasing the width of the beam. This leads to the converging angle to decrease. The back-end diverging aspect of the beam was less affected by the pressure in part that the highest amount of CEX collisions happens in the very near-field do to the highest pressures being located there. The reason

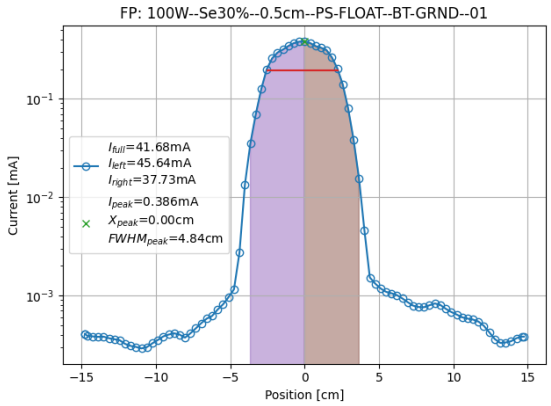

(a) 30% Pumping at 0.5 cm downstream

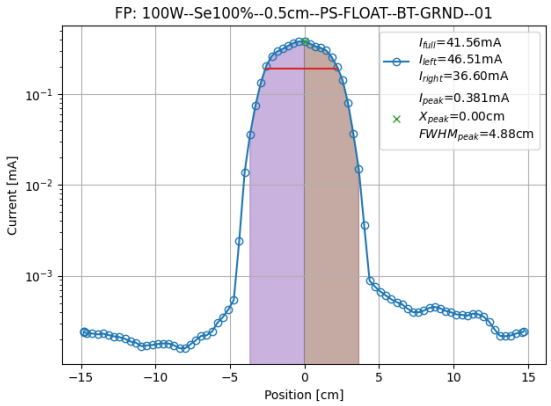

(b) 100% Pumping at 0.5 cm downstream

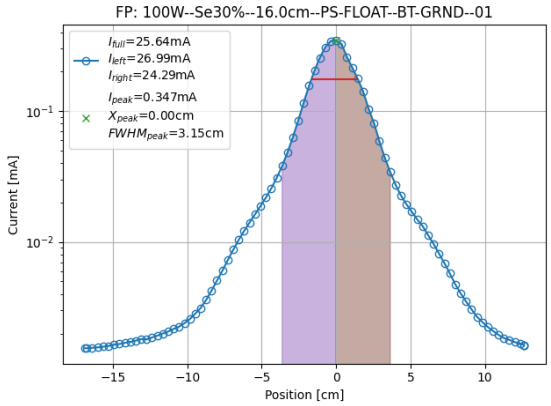

(c) 30% Pumping at 16.0 cm downstream

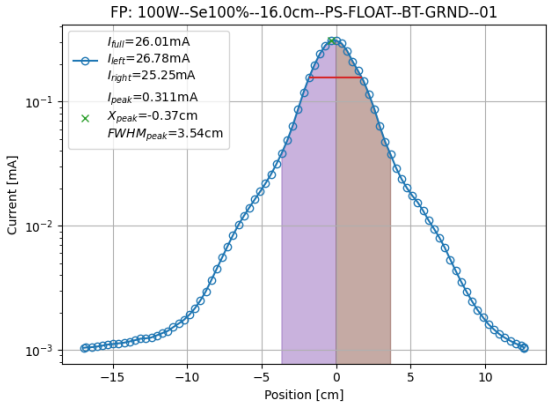

(d) 100% Pumping at 16.0 cm downstream

Figure 5.15: 2025-01 NASA 8 cm test campaign at the 100 W power level lateral Faraday probe sweep at downstream distances of 0.5 cm and 16.0 cm highlighting examples of plume broadening and high ambient background plasma densities just outside the beam plasma.

for a converging-diverging grid lenses is to create a very collimated beam in the near-field to prevent sputter erosion of near-by components. Elevated background pressures can lead to misleading converging angles and cross-over distances that would insinuate that the beam is tight for further distances than it would really be at space pressures.

The fact that the converging half-angle was less impacted by the floating plasma screen or beam target leads to suspect that the neutralization process in the beam may also affect this angle. A less neutralized beam in the very-near field may result in scattering of more ions due to the increase in potential of a virtual anode. Described in a later section, it is found the plasma potential in the beam is higher at lower background pressures with either floating the plasma screen or floating beam target increasing plasma potentials. Figures 5.19 and 5.20 in the later section demonstrate this. This effect emphasizes the importance in achieving proper neutralization to characterize a thruster. Differences in neutralization can drastically alter predicted spaceflight performance and characterization of the thruster.

The total integrated current using the full beam diameter integration method for the 2024-11 Faraday probe sweeps as a function of distance are placed in Figure 5.17. The "BT" or "PS" notation indicates either the beam target or plasma screen was in the floating configuration. Because only up to 95% of the beam diameter is used in the integration even at large distances downstream, it was expected that the beam current would decrease with distance as more of the beam diverges and becomes part of the ambient plasma. From these plots, the first observation was there is a lack of any consistent variation with pumping speed of the integrated beam current. This was ideal as it insinuates that the gridded ion engine thrust production due to ingested neutrals was limitedly affected by background pressure. This has been hypothesized since the Clausing factor of the grids helps isolate the ambient neutrals from the internal ionization chamber.

5.3.1.3 Wall-to-Beam Potentials Comparisons

Potentials near the wall compared to the plume give insight into how much coupling between the beam and facility was occurring. The following figures compare the potentials in the beam using an emissive probe using the heat'n float method with a large emission and the plasma potentials measured at the walls using cylindrical Langmuir probes. The 100 W condition from the 2024-11 test is found in Figure 5.18 and a comparison of beam target potential from the same test campaign is found in Figure 5.19. The 300 W case for the same test is located in the Appendix C. A comparison of the effect of the plasma screen configuration from the 2025-01 test is located in Figure 5.20. It is important to note that the very near-field Langmuir probes are thought to have experienced carbon deposition. As a result, the IV traces seem to show signs of dirty probe symptoms. Symptoms include high plasma potentials and electron temperatures, but lower collected current due to the restive layer of the coating. This is mostly seen in traces on the right-side of

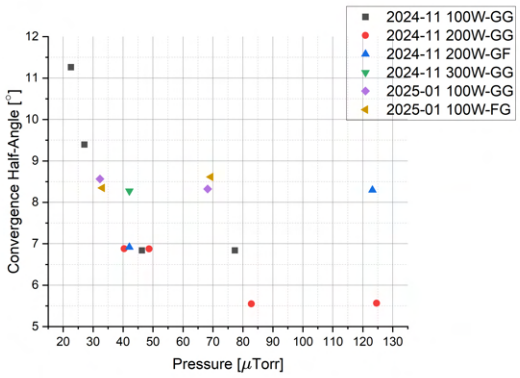

(a) Converging half-angle

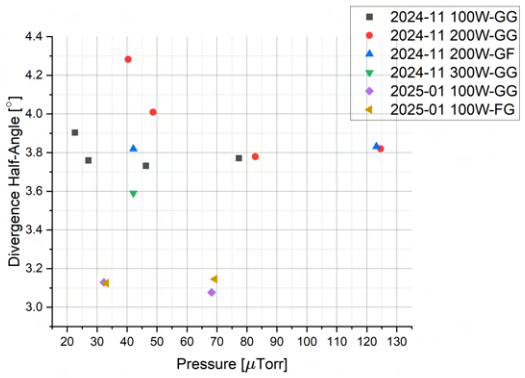

(b) Diverging half-angle

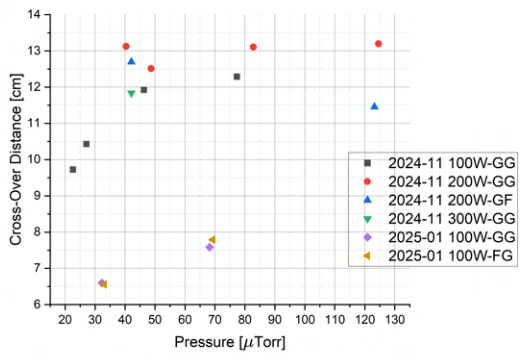

(c) Cross-over distance

Figure 5.16: 2024-11 NASA 8 cm test campaign beam converging and diverging half-angels and cross-over distance varying with background pressure.

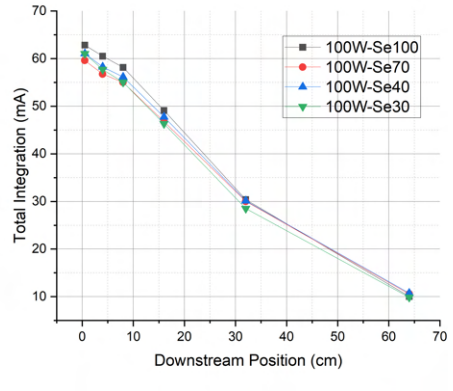

(a) 2024-11 nominal 100 W

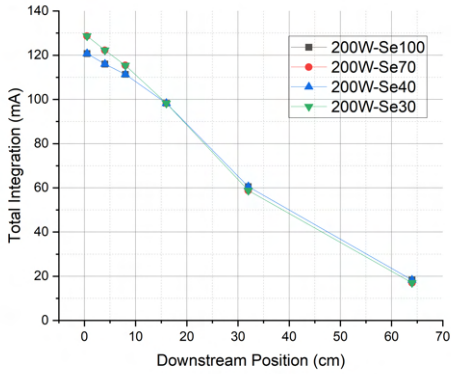

(b) 2024-11 nominal 200 W

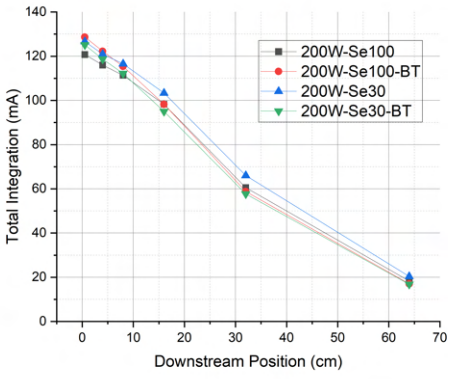

(c) 2024-11 beam target configuration comparison at 200 W

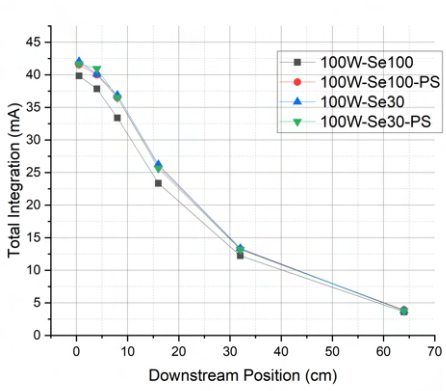

(d) 2025-01 plasma screen configuration comparison at 100 W

Figure 5.17: 2024-11 & 2025-01 NASA 8 cm test campaigns at the 100 W and 200 W power levels total integrated current from lateral Faraday probe sweeps up to 95% beam diameter with variations in downstream position.

the thruster (positive position of 21.91 cm from beam center-line) and the left-side in-plane probe. These probes are thought to be sputtered the most during the Faraday and emissive probe sweeps. Further discussion and evidence of the dirty probe effect are located in Chapter 7. Generally, the plasma potentials at the wall at 32 cm downstream of the non-dirty probes and that at this distance the beam should be have been well neutralized, there were similar plasma potentials between the ambient plasma potentials by the emissive probe and wall Langmuir probes. The changes in the beam potential with various background pressures and electrical configurations are investigated in this section.

In the 100 W cases from the 2024-11 test of Figure 5.18, generally all the plasma potentials in the beam for all pressure were about the same, especially in the closer positions. The furthest downstream position did have some small difference but these were less than 0.3 V. The peak for the lowest pressure at the 100% pumping configuration was the largest and the 30% pumping configuration being the smallest peak. This is evidence of it being easier to neutralizer the beam at higher background pressures with increase plasma density and lower electron temperatures. Looking at the telemetry in Table 5.7 it was observed the neutralizer-facility coupling voltage, V_{cg}, became increasingly negative with the increased background pressure. This, in addition to the fact that further downstream the beam potential was lower at higher background pressures indicates that the increased plasma density was helping getting electrons to the grounded facility and reemerging downstream to neutralize the beam. Thus the potentials in the near field are less affected by this downstream neutralization process. Comparing the telemetry for the 200 W case from the 2024-11 test with the height of the profiles from the left-side of Figure 5.19 also indicate the same phenomenon.

The actual structure of the plasma potential profiles in the very near-field 0.5 cm sweep in all configurations and pumping speeds of the 2024-11 have a very jagged peak in the beam and then have more horn-like structures in around one beam-diameter from thruster center-line. Around the 10 cm mark there is a dip followed by an increasing potential to the following ambient plasma. This dip followed by a raise in plasma potential can be seen in some of the profiles further downstream such as the 200 W at 100% pumping with the floating beam target of Figure 5.19d. The dip and horn-like structures seem to indicate the presence of a double-layer in-which electrons can be accelerated or de-accelerated into the beam from the ambient plasma based on their temperatures. This structure can stale the floating emissive probe potential due to energetic electrons [124]. This explains the roughness at the edges and was an indication of the presences of the beam neutralization process.

In the case of the 200 W conditions of the 2024-11 test campaign, the beam target was varied between grounded and floating configuration to determine the impact on beam plasma potentials. Table 5.8 that the beam target floats by 1-2 V positive, depending on background pressure. The

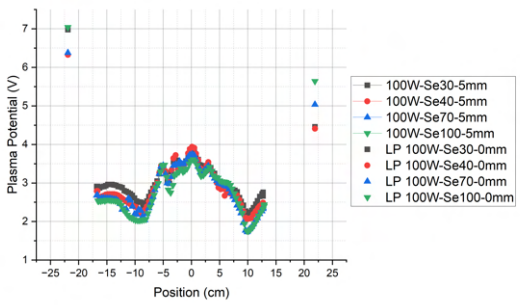

(a) Nominal at 0.5 cm downstream

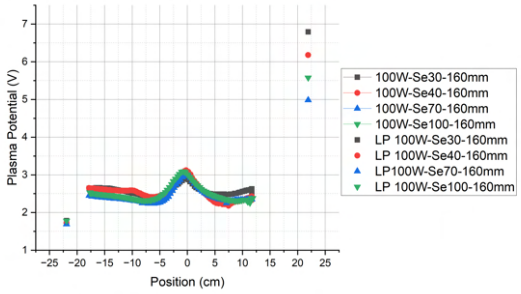

(b) Nominal at 16 cm downstream

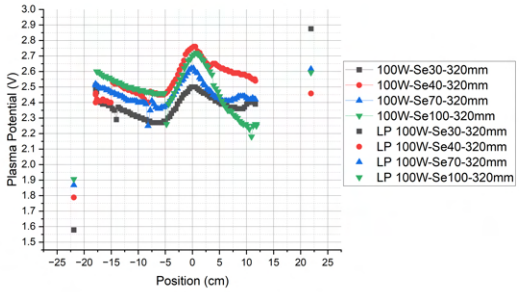

(c) Nominal at 32 cm downstream

Figure 5.18: 2024-11 NASA 8 cm test campaign at the 100 W power level comparison of the wall Langmuir probe plasma potentials to the beam heat'n float emissive probe plasma potentials. Comparisons were made at 0.5 cm, 16.0 cm, and 32.0 cm downstream of the thruster. The electrical configuration during testing included the plasma screen and the beam target being grounded. Horn-like structure at 0.5 cm downstream position show incomplete neutralization of the beam.

seemingly random spikes in the 200 W and 70% pumping in blue triangles are due to the neutralizer cathode temporarily transitioning into plume mode. As a result, the beam was less neutralized and the potential in the beam increased. Because the beam target was floating positive, it was also observed the potentials in the beam also increased in comparison to their grounded configuration. The ambient plasma potentials for the grounded cases were also closer to each others potentials than the floating cases. The grounded beam target limits the potential of the beam indicating there were electrons being emitted into the beam at the target whereas the floating target balances the currents being emitted and collected. Potentials in the beam and the potential of the target decreased with the increase of background pressure. This is due to improved neutralization of the beam and lower energy electrons. For 100 kW testing, the floating the beam target may not be manageable due to the target floating too positive or not being able to float the beam target at all. But if it was, the benefit of floating the beam target was it elevates the potential of the plasma of the whole system. This makes electrons more attracted to the beam and ambient plasmas than to the walls. The floating beam target forces electrons to get to the beam in other ways than by completing the circuit through grounded facility components. Potential concerns do arise if the potential of the target gets so high that ions are reflected back to the thruster. Further studies are needed to determine at which this process becomes too damaging to the thruster.

For the plasma screen configuration comparison study, the 2025-01 test used the "super" neutralizer but at lower currents than other test. As a result, in Figure 5.20 it can be seen that profiles are slightly different than that of the 2024-11 test. However, in the very near-field sweep at 0.5 cm there can be seem the dip and horn-like structures around 8-10 cm from beam center-line. The lower neutralizer current also resulted in much greater peaks on beam center-line. In the case of the floating plasma screen the plasma potential in the beam was much higher with a floating plasma screen. This effect was lessened at higher background pressures. The higher plasma potentials with the floating plasma screen indicated that the plasma screen was electrical connected in the neutralization process. From Table 5.10 the current to the plasma screen increased with background pressure and so does V_{cg}. This current must appear elsewhere to complete the circuit either back into the ambient plasma through the walls or at the beam target. Either way, these are alternative neutralization pathways not wanted. Floating the plasma screen and thruster chassis is a quick and easy way to get better beam neutralization characterization for high-power density testing.

5.3.2 Electrical Coupling & Beam Neutralization

For gridded ion engine operation, one key aspect is beam neutralization–a critical requirement for beam extraction and propagation. Beam neutralization was a large concern in the initial testing

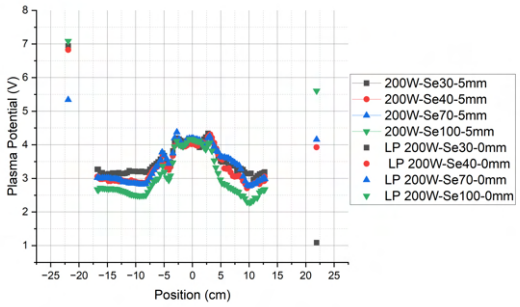

(a) Nominal at 0.5 cm downstream

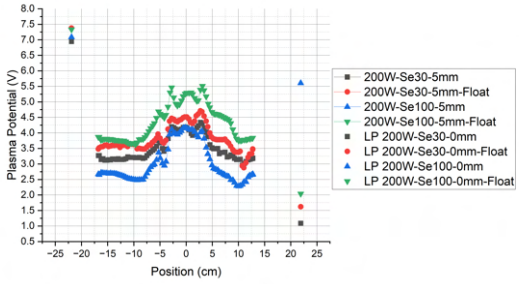

(b) Beam target configuration comparison at 0.5 cm downstream

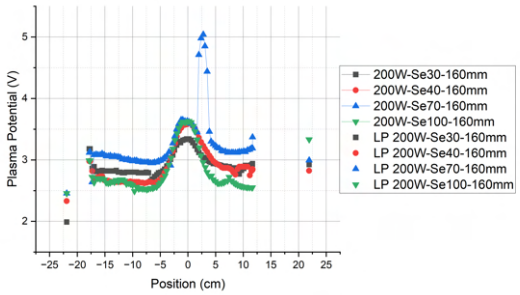

(c) Nominal at 16 cm downstream

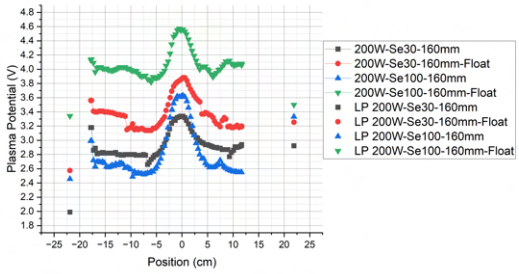

(d) Beam target configuration comparison at 16 cm downstream

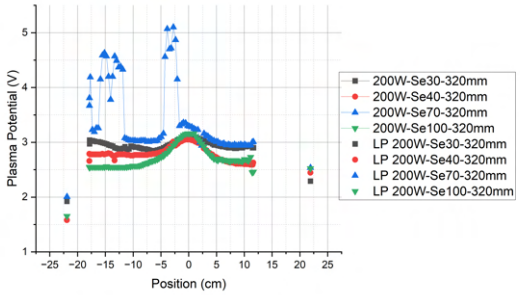

(e) Nominal at 32 cm downstream

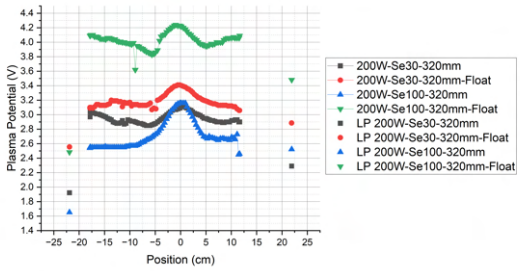

(f) Beam target configuration comparison at 32 cm downstream

Figure 5.19: 2024-11 NASA 8 cm test campaign at the 200 W power level comparison of the wall Langmuir probe plasma potentials to the beam heat'n float emissive probe plasma potentials. Comparisons were made at 0.5 cm, 16.0 cm, and 32.0 cm downstream of the thruster. The electrical configuration during testing included the plasma screen and the beam target being grounded (left column) whereas the plasma screen was grounded but comparison between a grounded and floating beam target is also made (right column). The floating beam target cases show the plasma potential in the chamber raises everywhere in comparison to the corresponding grounded beam target case.

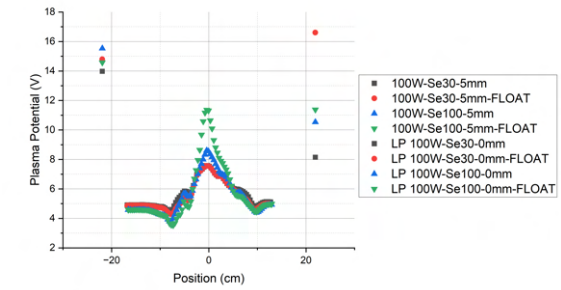

(a) Plasma screen configuration comparison at 0.5 cm downstream

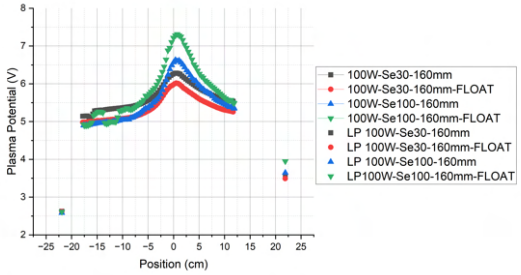

(b) Plasma screen configuration comparison at 16 cm downstream

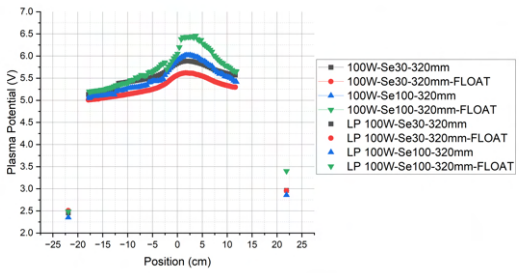

(c) Plasma screen configuration comparison at 32 cm downstream

Figure 5.20: 2025-01 NASA 8 cm test campaign at the 100 W power level comparison of the wall Langmuir probe plasma potentials to the beam heat'n float emissive probe plasma potentials. Comparisons were made at 0.5 cm, 16.0 cm, and 32.0 cm downstream of the thruster. The electrical configuration during testing included the comparison of the plasma screen being grounded or floating and the beam target being grounded. Floating the plasma screen increased the plasma potential in the very near field but higher background pressures dampens this effect.

Table 5.11: Summary and explanations of the different couplings refereed to during testing.

V_p	V_{cg}	V_{cp}	Meaning
$\uparrow$	$\uparrow$	$\rightarrow$	Less neutralization by facility and more directly from neutralizer and no changes in neutralizer-beam coupling
$\uparrow$	$\rightarrow$	$\uparrow$	Facility neutralization constant with worse neutralization by neutralizer and poorer neutralizer-beam coupling
$\rightarrow$	$\uparrow$	$\downarrow$	More neutralization by neutralizer with less neutralization by the facility resulting in better neutralizer-beam coupling
$\rightarrow$	$\downarrow$	$\uparrow$	More neutralization by the facility and less neutralization by neutralizer for poorer coupling between the neutralizer-beam

of gridded ion engines in the '60s and was one of the primary objectives of the NASA SERT missions [32, 57, 55]. Quantifying beam neutralization is done by taking the potential of the thruster reference (neutralizer common) and comparing it to the beam potential (beam plasma potential). The difference is called the true-coupling voltage, V_{cp}. During ground testing, it is easier to get the potential of the thruster reference (neutralizer common) with respect to the facility ground than the beam potential, often referred to as neutralizer-facility coupling voltage V_{cg}. It is then assumed that the beam is fully neutralized such that the potential of the beam is near ground potential. In this case, during ground testing that V_{cg} is often used as a metric to quantify beam neutralization. However, such assumption omits the physics that occurs between the neutralizer and beam that are affected by the proximity of facility walls or ambient background neutral as well as plasma densities in the plasma bridge that connects the neutralizer and beam.

In the following, Table 5.11, is an outline of the meanings of what the changes plasma potential, neutralizer-facility coupling voltage, and true-coupling voltage actually mean. Note, that neutralizer-facility coupling voltage, $V_{cg} = \phi_{NC} - \phi_{GRND}$, is typically negative and a $\uparrow$ indicates that it is increasing (becoming less negative). The true-coupling voltage, $V_{cp} = \phi_p - \phi_{NC}$, is thus typically positive but a larger number means less coupling between the neutralizer and beam.

An investigation of the impact of increased background pressure on neutralizer coupling to the beam was performed in this dissertation work. The turbopumps were throttled to vary the pumping speed. An emissive probe was used to determine the plasma potential in the beam and to obtain the true neutralizer-beam coupling. Furthermore, impacts of floating the beam target and plasma screen on the true-coupling voltage were made. Isolation of the effect of localized neutral gas flow in the plasma bridge was then also investigated by injecting neutral gas there.

5.3.2.1 Pressure Variation

Increasing the background pressure causes the ambient background plasma density to also increase. Depending on the size and shape of the facility, the rate of increases of both neutrals and plasma densities will dictate if the thruster will couple more or less with the facility. Each facility-thruster configuration needs to be characterized. This section explores this by taking true-coupling measurements for various background pressures to determine the pressure effect on thruster-facility coupling. In addition, probe data of plasma properties near the neutralizer and the plasma screen were made in addition to determine how the plasma properties in these locations vary with pressure changes. These probes gave insight into why thruster-facility interactions increase or decrease with pressure.

The coupling of the neutralizer to the beam is completed through the plasma bridge, but changes in the background pressure can cause impedance in the plasma bridge to vary. As a result, electrons can find alternative pathways to the beam. Using a passive probe, the potential of the neutralizer with respect to the facility ground was recorded in Figure 5.21. From the graph it can be seen that for all conditions where thruster operations were held constant, as the pressure decreased the magnitude of the neutralizer coupling voltage also decreased — indicating that the neutralizer may not be coupling to the beam but rather to nearby ground surfaces such as the grounded plasma screen. The middle pressure for the 2024-05 test were higher because the neutralizer current was increased resulting in better beam neutralization and less coupling with the facility. The floating beam target in the 2024-11 test did experience a smaller change in V_{cg} than the grounded case. This indicates the the floating beam target removes an alternative neutralization pathway that lessens the coupling with the facility.

In Figure 5.22 were the max beam-neutralizer coupling voltages are plotted as function of position downstream. There were a few instances where the coupling voltage was exorbitantly high due to the neutralizer cathode temporarily transitioning to plume mode. These plume mode spikes occur in the 200 W-Se70 case at 160 mm and 320 mm. The spike in the 100 W-Se100 case at 40 mm may have also resulted from a plume mode transition, but it is unconfirmed as there was a large spike in the plasma potential at the center-line that was difficult to determine if it was the natural beam potential or a fluctuation due to plume mode. The coupling profiles decreased as the beam reaches neutralization between 160 mm-320 mm.

The coupling voltage behavior trends also appear similar at all pressures except there seems to be a flatter trend in the coupling voltage in the very near field for both the 100 W and 200 W conditions at the highest pumping speed (Se100) and for the 100 W-Se70 case. This could be in part due to the instability of the neutralizer, but it could also be that at these lower pressures there was less help from the bridge and ambient plasma densities to connect the neutralizer to the beam. The later seems to be case as looking at the plasma densities near the plasma screen (left) and near

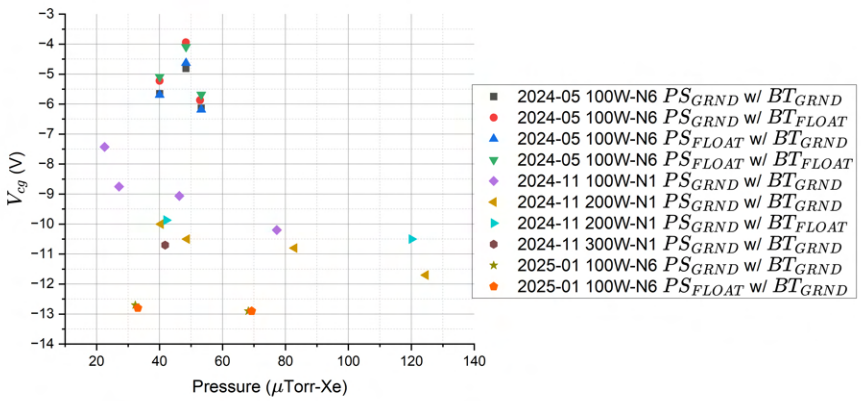

Figure 5.21: Neutralizer-facility coupling voltages for the all test campaigns in the PSTL Rocket Chamber and for all of the different electrical configurations of the plasma screen and beam targe. Additionally, all the different power levels and their variations with background pressure are plotted here. Grouping by test campaigns reveals there is a decrease in the value (increases in the negative magnitude) of the neutralizer-facility coupling voltages with background pressure resulting in more coupling with the facility at higher background pressures.

the neutralizer (right) in Figures 5.23 and 5.24 for the 100 W and 200 W conditions, respectively, it was observed that the plasma densities near the plasma screen relative change with background pressure was more than at the neutralizer. This was in part due to the fact that the neutralizer plasma was already much denser by at least a order of magnitude. In the 100 W condition, the plasma density nearly doubled its original value, where as the neutralizer plasma densities are even difficult to tell if they increased because changes were so small and inconsistent. At least for the 200 W case the plasma density increased by 1-1.5$\times 10^{15}$ m^{-3}, which at best was only 30% increase. On the other hand, near the plasma scree increases by at least 3×10^{13} m^{-3} which was a 60% increase. This also would explain why neutralizer-facility coupling voltages increase with background pressure. The increase in plasma conductivity near grounded surfaces like the plasma screen increased at a faster rate than between the neutralizer and beam plasma.

5.3.2.2 Beam Target Potential

Limiting coupling between the thruster and the facility is always advantageous in order to achieve the "test like you fly" testing condition. The increase in the magnitude of V_{cg} with the increase in true coupling voltage with higher background pressures indicates that the beam neutralization was tightly correlated to the coupling of the neutralizer to the facility. Since the beam target was directly in contact with the beam, it was decided to float the beam target at the 200 W condition to see if the true coupling voltage changed as the main contact area with the beam was disconnected from the facility.

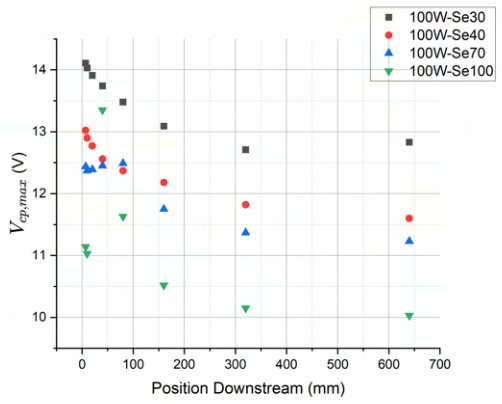

(a) 100 W

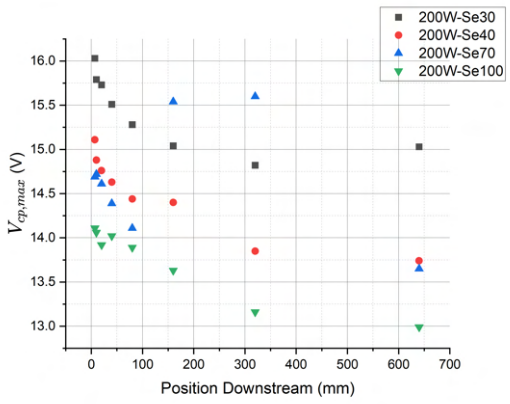

(b) 200 W

Figure 5.22: 2024-11 NASA 8 cm test campaigns at the 100 W and 200 W power levels comparison of the maximums of the true-coupling voltages as a function of downstream position from the thruster. The electrical configuration during the testing were all with a grounded plasma screen and grounded beam target. The true-coupling voltage increased with background pressure for all cases indicating poor direct neutralization of the beam by the neutralizer.

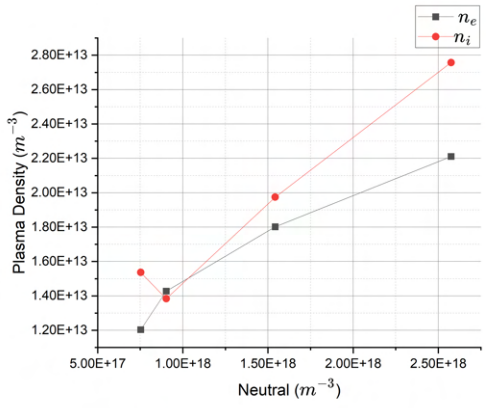

(a) Left-side of plasma screen

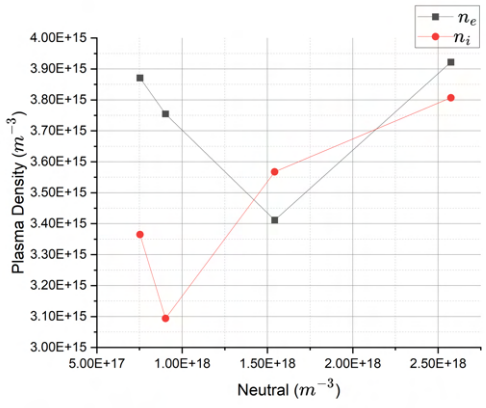

(b) Neutralizer 4 cm downstream

Figure 5.23: 2014-11 NASA 8 cm test campaign at the 100 W power level comparison of the plasma properties near the plasma screen and neutralizer. The electrical configuration included a ground plasma screen and grounded beam target.

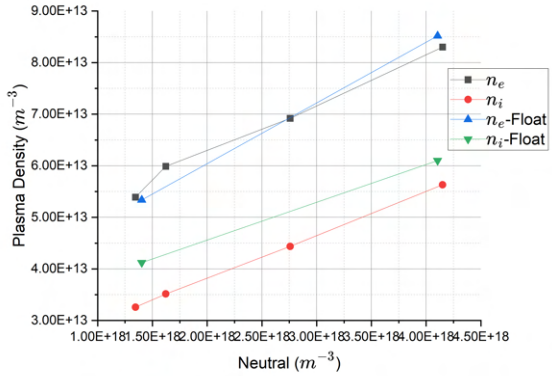

(a) Left-side of plasma screen

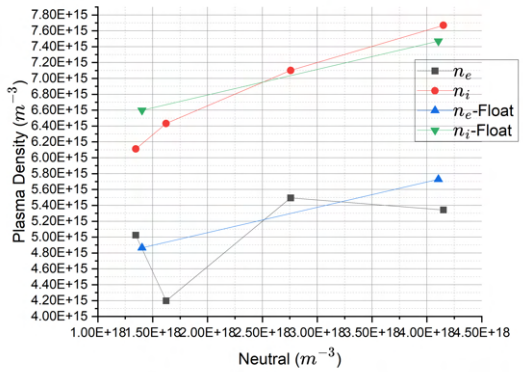

(b) Neutralizer 4 cm downstream

Figure 5.24: 2024-11 NASA 8 cm test campaign at the 200 W power level comparison of the plasma properties near the plasma screen and neutralizer. The electrical configuration included a ground plasma screen and both a grounded and floating beam target.

The neutralizer potential in Figure 5.21 shows the variation in neutralizer coupling with the facility was lessened with a floating beam target; this indicates that there was an alternative neutralization pathway through the beam target to the beam. Thus, if running at higher background pressure, it appears beneficial to minimize grounded surface area along the beam path to the target. Neutralization at the wall is an inherent facility effect. Most significantly, this indicated that limiting grounded surface area near the neutralizer would be advantageous as it increases the impedance of electrons from the neutralizer to ground. This would force electrons to remain in the beam and limit coupling to the facility.

In the beam target-floating configuration, the results of the coupling voltages as a function of downstream positions are presented in Figure 5.25. The true neutralizer-beam coupling voltages follow similar patterns to the results of Figure 5.22. The difference in true-coupling voltage at the 640 mm distance may be attributed to the increased floating potential of the beam target at the Se100 cases due to more of the beam reaching the target, resulting in a higher plasma potential further downstream closer to the beam target. The main observation is the floating beam target forces the higher and lower background pressures true-coupling voltages to match. This indicates that 100 kW testing with a floating beam target is ideal to get better matching between different background pressures because neutralization off the target is removed. However, in practice this maybe difficult as it is not so easy in larger more establish facilities to float the beam target. Covering the target with an insulating material and then placing graphite on top could be one solution to this problem.

The plasma densities near the thruster and the neutralizer are found back in Figure 5.24 and are

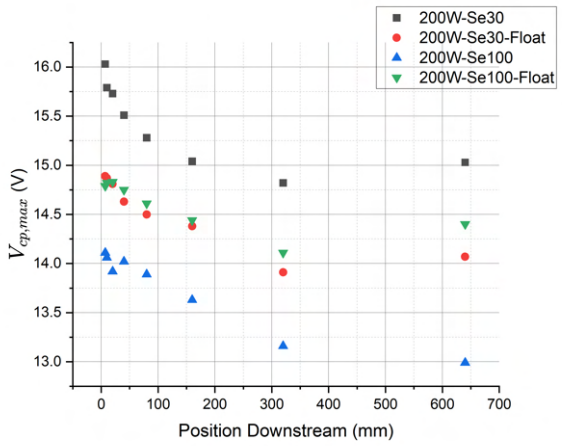

Figure 5.25: 2024-11 NASA 8 cm test campaign at the 200 W power level comparison of the maximum true-coupling voltages as a function of downstream position from the thruster. The electrical configuration during the testing were all with a with ground plasma screen and of both a grounded and floating beam target. The true-coupling voltages for the floating beam target cases match regardless of background pressure indicating that coupling in the floating beam target case between the neutralizer and the beam is less affected by background pressure.

designated by the "Float" for floating beam target. Similar to the statements made in the previous pressure variation section, the relative rate of increase in plasma density in the ambient plasma outpaces that near the neutralizer causing the neutralizer to couple more with the facility. With the floating beam target, the circuit for electrons cannot be completed, thus retarding the collection of electrons on grounded surfaces elsewhere in the facility. The higher plasma potentials in the chamber were evidence of this retarding of electrons to the walls. The higher plasma potentials created a larger sheath drop at the walls. The increasing larger sheath drop to the grounded walls respelled more of the higher energy electrons. This eliminated more of the beam from being neutralized from SEE or IIEE off the target resulting in less facility coupling.

5.3.2.3 Plasma Screen Potential

In addition to testing the impacts of a floating beam target, the plasma screen instead could be floated. The idea of floating the plasma screen was to disconnect this nearby collecting surface from the facility circuit. In the ground configuration, the neutralizer emits electrons that could be easily collected by the nearby plasma screen and reemerge at the beam target. Floating the plasma screen breaks this path but if there are other nearby facility surfaces or walls, than the floating plasma screen may not have an impact on neutralizer-beam coupling.

From Figure 5.21, the neutralizer-facility coupling voltage did not change much between the two plasma screen configurations. Instead, from Figure 5.20 there was more of a change in the

plasma potential in the very-near field. The peak of the plasma potential in the beam damped with the increase of background pressure. As a result, the true-coupling voltage between the neutralizer and beam with downstream position, found in Figure 5.26, shows an increased V_{cp} when the plasma potentials in the beam were high. The larger the true-coupling voltage the less coupled the system are and the less neutralized the beam would be. Figure 5.26 indicates that the beam was being less neutralized using a floating plasma screen at lower pressures. This is concerning as this would be a more spacelike situation. Background pressures in space are much lower and the thruster chassis and plasma screen are typically tied to spacecraft ground, which floats in the ambient plasma.

Before extrapolating the performance of this thruster in space, it is important to determine the cause of the higher plasma potentials and weaker beam neutralization. One theory would be was ions strike the plasma screen, electrons can be emitted in ion-induced electron emission. Or another explanation could be that because the plasma screen floats negative by a few volts, only the really high energy electrons were collected forcing lower energy electrons to be repelled but unfortunately there must be another high potential that was pulling the electrons away from the beam. In beams that are neutralized fully off the walls, the plasma potentials in the near-field are extremely high [142]. The plasma potential here seems to point to the floating plasma screen was limiting the supply of electrons easily collected by facility ground that can be emitted downstream at the beam target. Because the potential downstream was neutralized to the same level as the other configurations, neutralization by the ambient plasma must be occurring since the V_{cg} did not change much between the floating and grounded plasma screen, the thruster was not coupling more with the facility. Eliminating the conductive path by using floating plasma screen forces the high potential to propagate further downstream, pulling lower temperature electrons in from the ambient or residual plasma bridge plasma. As the beam expands further downstream the plasma and beam densities begin to even. The little change in neutralizer-facility coupling voltage at the higher background pressure between the two plasma screen configurations points to the increased ambient plasma densities and lower electron temperatures aiding in beam neutralization. This was not observed in the 200 W condition previously because the electron temperatures from the neutralizer were a lot lower with the nominal cathode compared to the "super" neutralizer. It has been speculated it is the lower energy electrons that provide beam neutralization [131]. Profile of the plasma potential and the height of the peak are due to the difference in the produced electron temperatures and how easily they are trapped in the beam. Further downstream the electrons cool and more easily neutralize the beam.

Generally, it would be advantageous to float the plasma screen in 100 kW test as it will reveal, to the best of the abilities of the facilities the potential in the beam in the very near-field that can reduce thrust. Proper neutralization of the plume here is key to maximize thrust and efficiency in space. Although reasons for the increase in beam potential with the floating plasma screen is

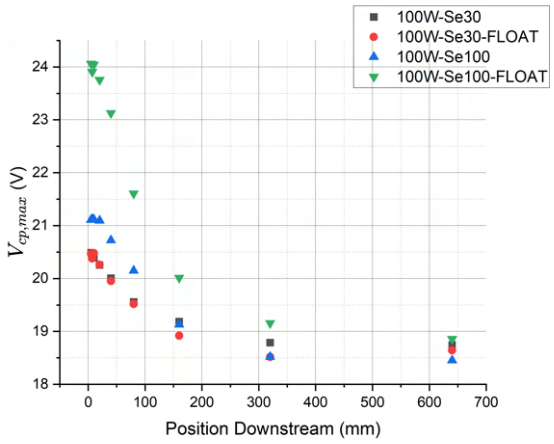

Figure 5.26: 2025-01 NASA 8 cm test campaign at the 100 W power level comparison of the maximum true-coupling voltages as a function of downstream position from the thruster. The electrical configuration during the testing were all with both a grounded and floating plasma screen while the beam target was grounded. The high plasma potential in the very near field increases the true-coupling voltage there significantly.

not fully realized but it serves to show that the extra grounded surfaces near the thruster should be minimized as they can have a direct affect on thruster processes like neutralization.

5.3.2.4 Plasma Bridge Neutral Flow Injection

In part in isolating the contributions of different elevated facility effects, neutral gas was injected near the neutralizer, approximately 2 cm downstream, to observe the changes in beam neutralization and facility coupling. The basis of this technique was as more neutral gas is injected, it is expected that the conductivity of the plasma will go down, resulting in a higher true-coupling voltage that may not be visible when compared to the facility coupling voltage. Assuming the plasma properties are only affected by local plasma properties at steady-state, then the plasma conductivity can be described as

$$\begin{aligned} \sigma_{cond.} &= \frac{q^2 n_e}{m_e \nu_{mom.}(KT_e)} \\ &= \frac{q^2 n_e}{m_e k_{mom.}(KT_e) N_g} \sim \frac{n_e}{N_g}. \end{aligned} \tag{5.1}$$

Here q is the charge constant, n_e being the electron density, m_e is the electron mass, $\nu_{mom.}$ is the momentum transfer collision frequency, KT_e is electron temperature, $k_{mom.}$ is them momentum transfer collision rate coefficient, and N_g is the neutral gas density. Assuming the rate coefficient reasonably constant over small changes in the electron temperature, the plasma conductivity should decrease with an increases of neutral gas density.

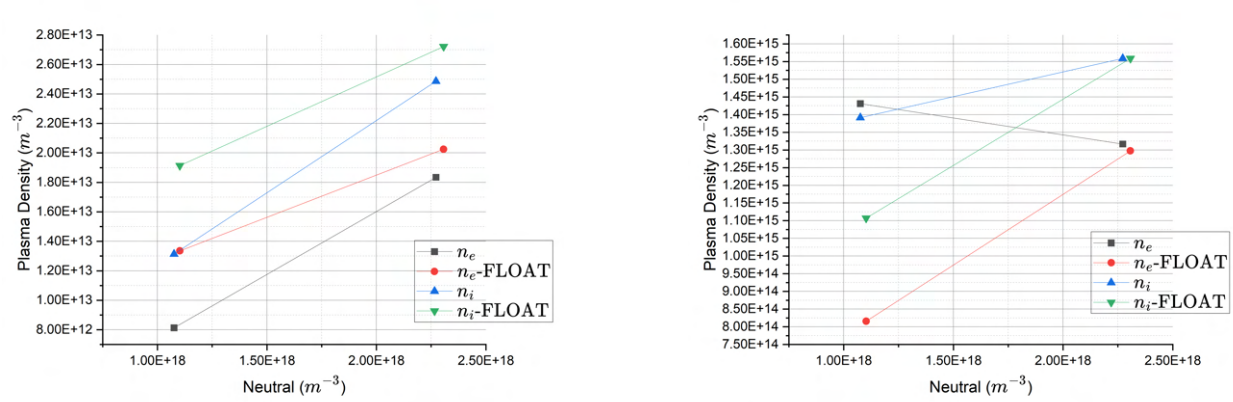

(a) Left-side of plasma screen

(b) Neutralizer 4 cm downstream

Figure 5.27: 2025-01 NASA 8 cm 100 W plasma properties comparison of grounded and floating plasma screen with a grounded beam target.

In Figure 5.28, analysis of a comparison of facility coupling voltage and true-coupling voltages were made using plasma potential measurements obtained from a linear emissive probe sweep 11.0 cm downstream of an 8 cm gridded ion engine operating over various neutral flow injection rates at 2 cm downstream of the neutralizer for the grounded plasma screen and beam target at 100% pumping speed only. Note, that $V_{cath.}$ is equivalent to V_{cp}. For all configurations and pumping speeds, only the neutralizer-facility coupling voltages and plasma properties near the neutralizer and plasma screen were obtained. The neutralizer-facility coupling voltage, V_{cg}, for the various flow rates, configurations and pumping speeds is found in Figure 5.29. Plasma potentials, electron temperatures, and electron densities measurements by a Langmuir probe located 4 cm downstream of the neutralizer were also made and presented in Figures 5.30 and 5.31, respectively. These same values for near the plasma screen are also presented in Figures 5.32 and 5.33. The floating potentials, electron and ion densities, and Debye lengths for both probes are located in Appendix C. In general, these behaved as expected. The floating potentials and plasma densities increased with neutral flow and the Debye lengths decreased.

Neutral flow injection localized to the plasma bridge impacts on coupling voltage for the ground plasma screen and beam target at full pumping speed of Figure 5.28 provides insight into how better neutralization can be achieved with out coupling more to facility. The magnitude of neutralizer-facility coupling voltage, V_{cg}, increased only slightly with injected flow. This limited increase indicated that the change in plasma potential, V_p, must be mainly due to direct neutralization from the neutralizer and not from the facility. As a result, the true-coupling voltage, $V_{cath} = V_{cp}$, decreases in magnitude as an indication of better coupling. This goes against initial expectations. The increase of neutral flow here was suspected to increase the impedance of the bridge and make

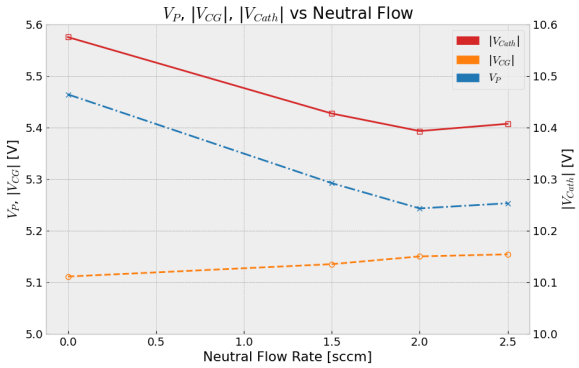

Figure 5.28: 2024-05 NASA 8 cm test campaign at the 100 W power level and 70% pumping speed measured values of V_p, V_{cg}, and V_{cp} for grounded plasma screen and beam target as neutral gas is injected into the plasma bridge.

it more difficult for electrons to get to the beam. However, from Figures 5.31a, and C.12a of the electron temperatures and densities there was a drop in electron temperatures and an increase of electron densities for the 70% pumping speed as additional flow was added. The drop in electron temperature allows for the electrons to be more readily captured by the beam and the increased plasma density increases the conductivity of the bridge. So although there was more neutral collisions because the electron temperatures were high enough, they ionized more of the neutral gas such that the plasma density to neutral density ratio stayed relatively constant. However, lower temperature electrons can be more easily captured by the beam. The balance between neutralizer operating conditions and the background neutral density set how coupled the neutralizer was to the beam. Thus, testing at higher background pressures during 100 kW operations may lead to better neutralizer-beam coupling than would occur in space if the plasma screen and beam target are grounded.

The behavior of all the different configuration with background pressure for the different pumping speeds gives insight into how changing the electrical setup of the chamber could potential give better in-space performance predictions. Figure 5.29 shows that for any pumping configuration, the change in V_{cg} was limited when the plasma screen and beam target are grounded. All other configurations had some variation with neutral flow injection. There was less change when only the plasma screen was floating at higher background pressure or lower pumping speeds. This was consistent with the observations in the true-coupling voltages for the 2025-01 test. There as well the facility coupling voltage did not change much with pressure but the plasma potential in the beam did. It was expected that the higher background pressures and higher plasma density near the plasma screen and other grounded support stand objects was high enough that coupling did not vary with plasma screen configuration. Additionally, the 2024-05 test had only the one variable

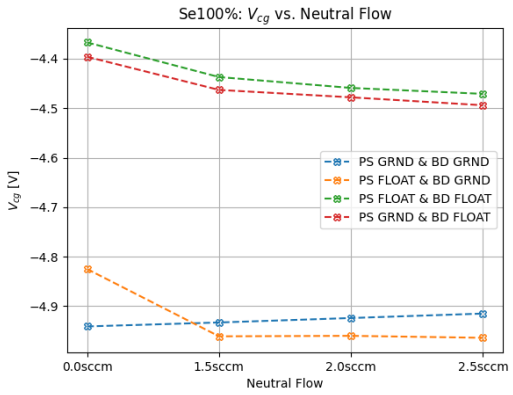

(a) 100% pumping speed

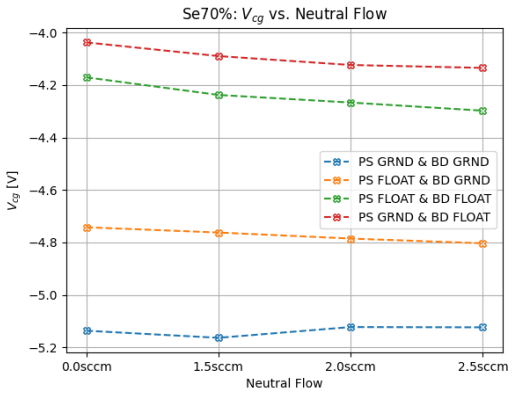

(b) 70% pumping speed

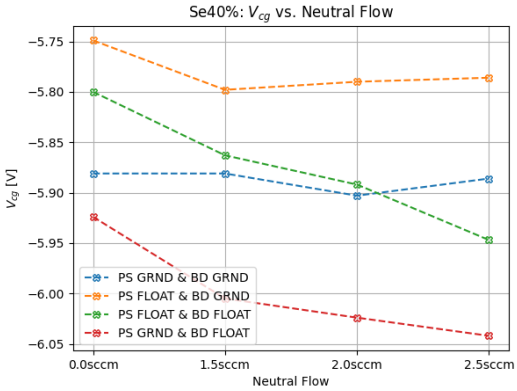

(c) 40% pumping speed

Figure 5.29: 2024-05 NASA 8 cm test campaign at the 100 W power level impacts of neutral flow injection in the plasma bridge on the measured neutralizer-facility coupling voltages.

pumping speed pump which was located downstream at the beam target. Variations in pumping speed affected the plasma and neutral density more there. This was probably also why the beam target floating V_{cg} become more negative at the lowest pumping speeds compared to the 2024-11 test where there was less facility coupling with the floating beam target compared to the grounded case. In this regard, localized pressure effects can have a large impact on facility coupling.

The plasma potentials near the neutralizer for the various configurations and neutral flow injection at the plasma bridge were relatively unchanged for the 70% pumping speeds. However, in Figure 5.30 the lowest background pressure had the largest increases in plasma potentials and this increase was present in all the configurations except the floating plasma screen and ground beam target case. Here the plasma potential decreases for both the 100% and 40% pumping speed cases. The changes in the plasma potentials were almost in direct correlation with electron temperatures in Figure 5.31 for all configurations. Additionally, the increase in electron temperature and plasma

potentials follow a similar behavior as the facility coupling voltages in Figure 5.29 for the 100% and 40% pumping speeds. As facility coupling voltages increases in magnitude, so did the plasma potentials and electron temperatures. This was not seen for the 70% case. Here the changes were much smaller in the first place, but it appears the electron temperatures did drop with increasing facility coupling. The increased neutralizer current in the 70% pumping configuration seemed to dominate over the impacts of the facility. This unfortunately, was not a normal cathode or at the much lower nominal operating conditions. It was expected that the beam neutralization process will be much more greatly impacted by the lower operating conditions of the neutralizer. Generally, the different configurations did not change the electron temperatures but the plasma potentials where higher by approximately a volt in the floating beam target configurations. This was similarly observed in the 2024-11 tests that the floating beam target raises the whole system in facility. This was in order to limit electrons collected at the walls as they can no longer reemerge at the beam target as SEE and IIEE.

The plasma properties near the plasma screen are much less impacted by the injected neutral flow as hoped for. The idea of the neutral flow injection in the plasma bridge was to artificially only change plasma properties there. From Figures 5.32, 5.33, and those found in Appendix C, the plasma properties were not disturbed much. This allowed for the plasma properties near the neutralizer to be more isolated and for better understanding of increased neutrals effects there and their impact on the neutralization process.

5.4 Thruster-Facility Interactions & Performance

In the previous sections, the facility impacts on the thruster plume, neutralization,and coupling processes were investigated. In this section, the performance changes internally of the thruster due to the facility such as ingestion are explored.

5.4.1 Neutral Ingestion

Ingestion of background neutrals will occur in space and in ground testing. However, in ground testing because the background pressures are elevated, it is expected that the rate of ingestion will be higher. A schematic of ingestion is given in Figure 5.34. The ingestion rate is given as

$$Q_{ingestion} = 7.82 \times 10^{8} \frac{p \cdot A \cdot \eta_{Clasusing}}{\sqrt{T_{gas} M_{gas}}} [sccm], \tag{5.2}$$

where p is the background pressure in Torr, A is the total open area fraction of the grids, $\eta_{Clausing}$ is the Clausing factor or the conductance correction factor, T_{gas} is the temperature of the ingested

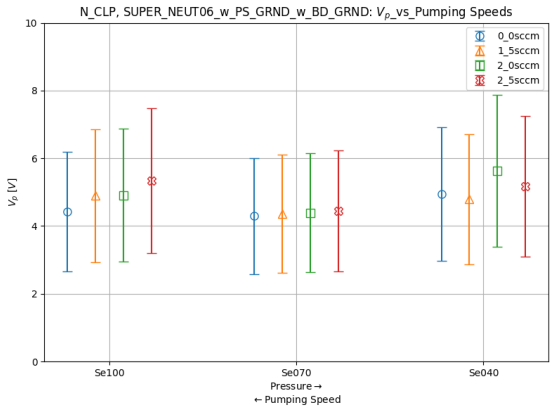

(a) PS grounded & BT grounded

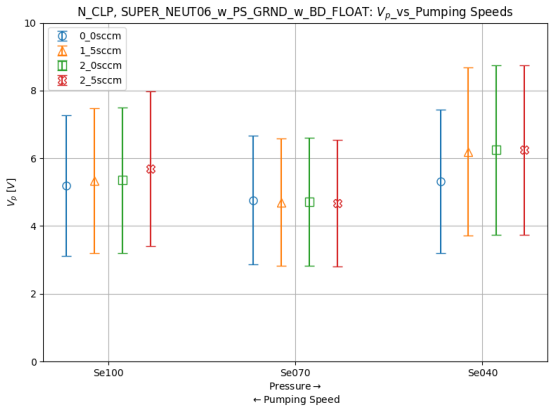

(b) PS grounded & BT floating

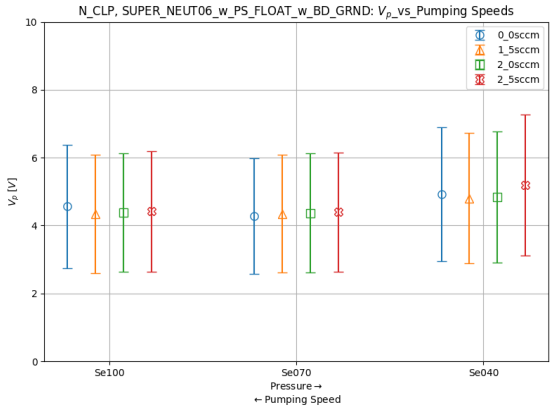

(c) PS floating & BT grounded

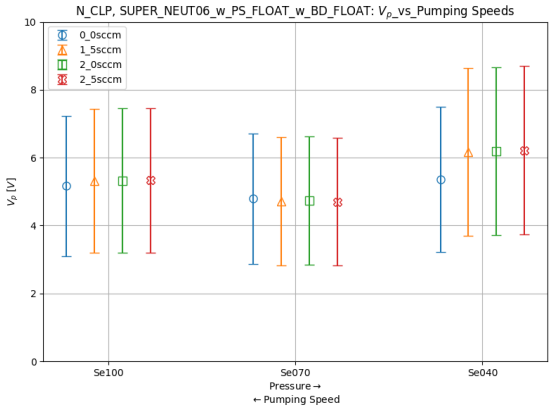

(d) PS floating & BT floating

Figure 5.30: 2024-05 NASA 8 cm test campaign at the 100 W power level impacts of neutral flow injection in the plasma bridge on the measured plasma potentials using a cylindrical Langmuir probe approximately 4 cm downstream of neutralizer.

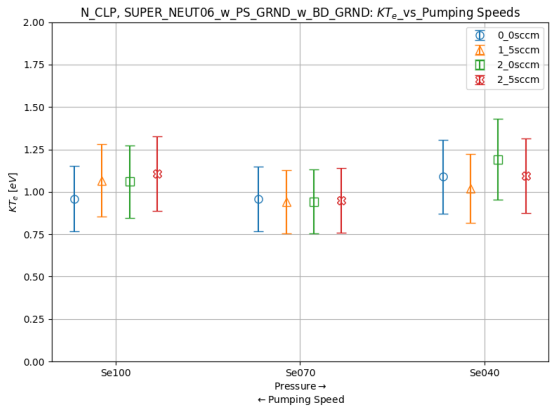

(a) PS grounded & BT grounded

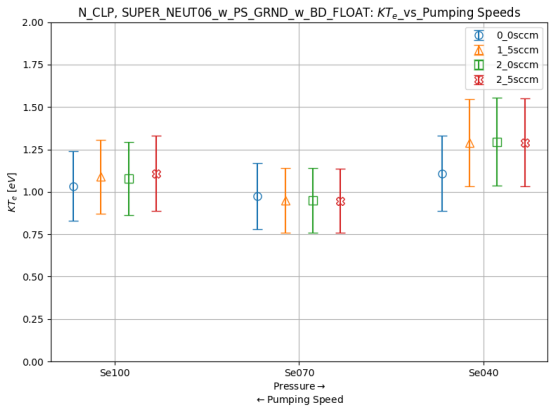

(b) PS grounded & BT floating

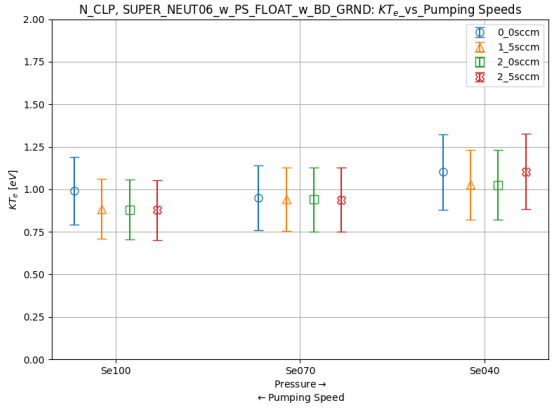

(c) PS floating & BT grounded

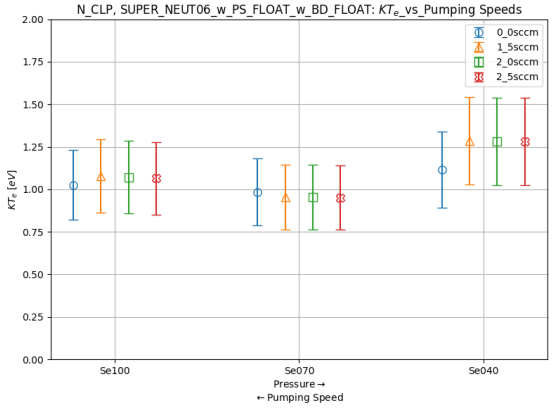

(d) PS floating & BT floating

Figure 5.31: 2024-05 NASA 8 cm test campaign at the 100 W power level impacts of neutral flow injection in the plasma bridge on the measured electron temperatures using a cylindrical Langmuir probe approximately 4 cm downstream of neutralizer.

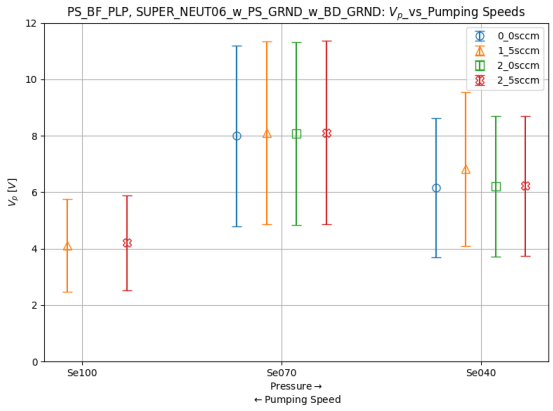

(a) PS grounded & BT grounded

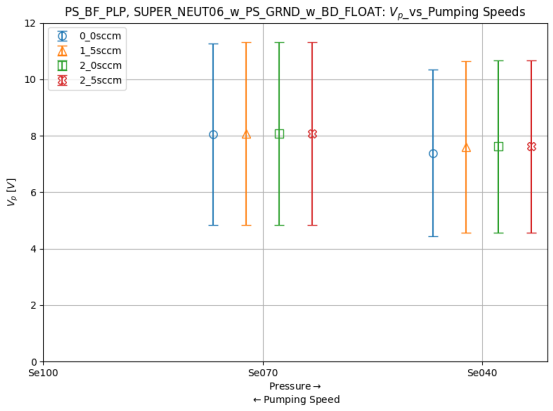

(b) PS grounded & BT floating

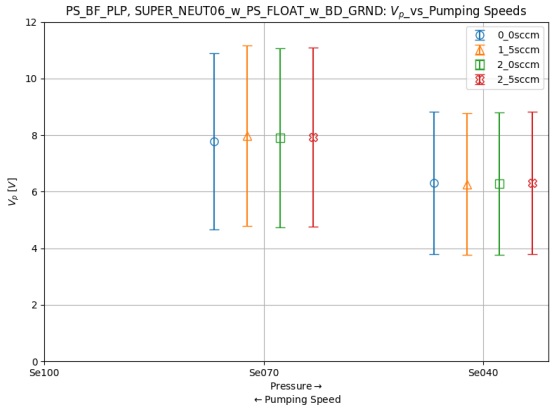

(c) PS floating & BT grounded

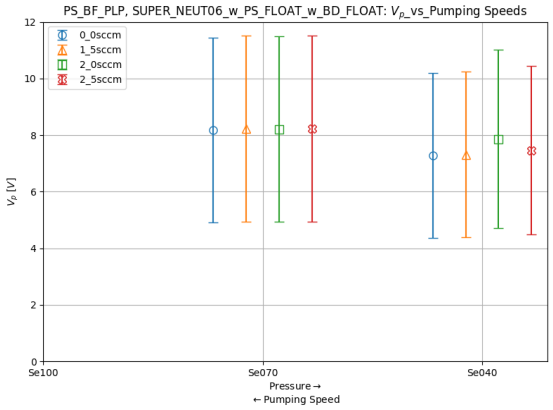

(d) PS floating & BT floating

Figure 5.32: 2024-05 NASA 8 cm test campaign at the 100 W power level impacts of neutral flow injection in the plasma bridge on the measured plasma potentials using a planar Langmuir probe near the plasma screen on the left-side of the thruster.

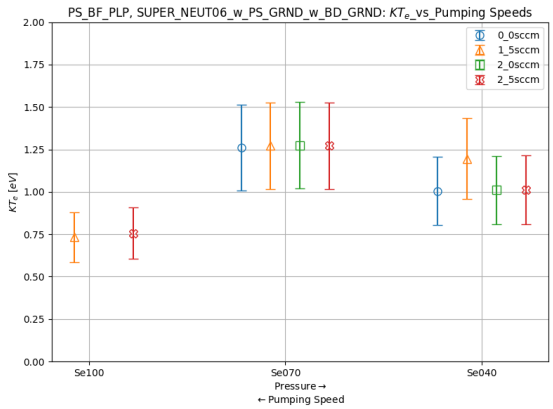

(a) PS grounded & BT grounded

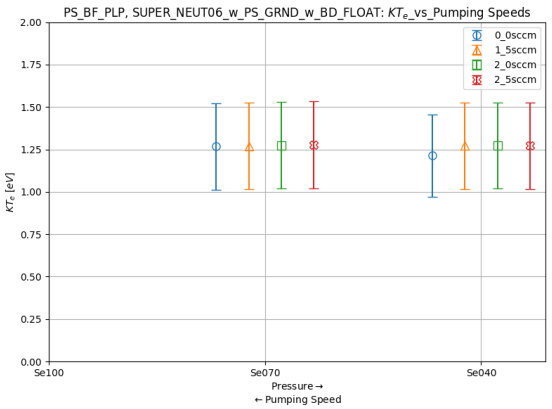

(b) PS grounded & BT floating

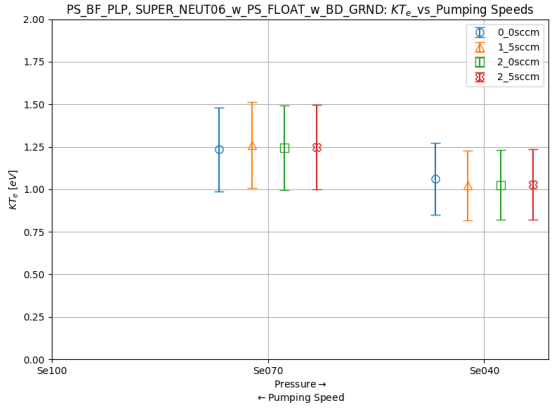

(c) PS floating & BT grounded

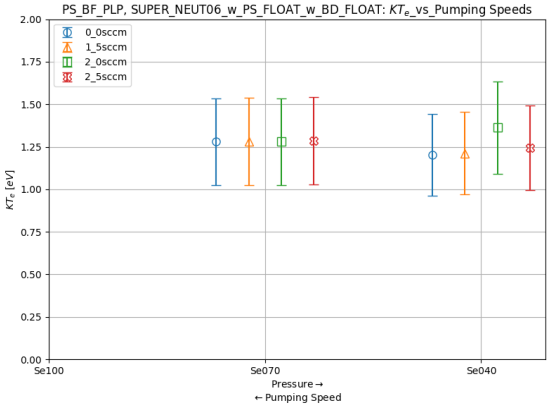

(d) PS floating & BT floating

Figure 5.33: 2024-05 NASA 8 cm test campaign at the 100 W power level impacts of neutral flow injection in the plasma bridge on the measured electron temperatures using a planar Langmuir probe near the plasma screen on the left-side of the thruster.

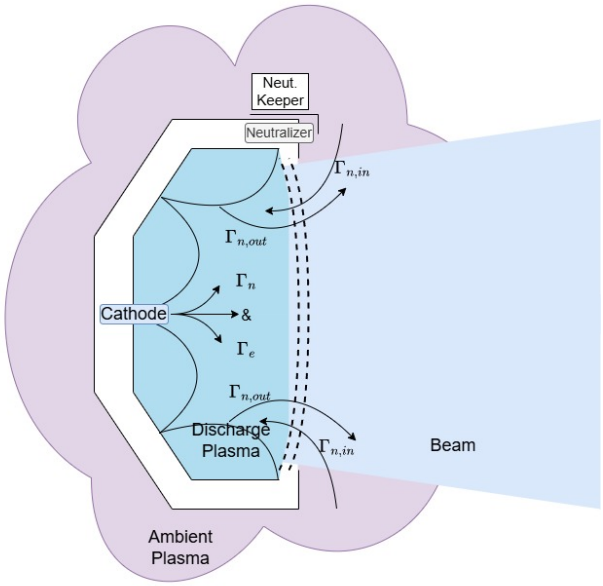

Figure 5.34: Schematic of gridded ion ingestion. Ambient neutral gas leaks through the grid holes and alters the discharge performance.

neutral gas in Kelvin, and M_{gas} is the mass of the ingested neutral gas in AMU.

The total flow for the thruster is then the summation of all the flows supplied to the thruster plus the neutrals ingested resulting in

$$Q_{total} = Q_{cathode} + Q_{main} + Q_{neutralizer} + Q_{ingestion}. \tag{5.3}$$

Here Q is the flow rates of the discharge cathode, main discharge chamber, neutralizer cathode, and ingested neutrals. The total flow in the chamber plus the neutral spatial profiles can have a large impact of the discharge performance. The additional ingested neutrals can decrease the number of doubles produced or change in the impedance between the cathode and anode of the discharge chamber. The discharge impedance is defined as

$$Z_{DISC} = \frac{V_{DISC}}{I_{DISC}}, \tag{5.4}$$

where V_{DISC} and I_{DISC} are discharge power supply voltage and current, respectively. The voltage of the discharge is a function of cathode and main flow rates, electron temperatures, magnetic field strength, and the neutral spatial density. In addition, changes to flow rates or neutral spatial density can cause a domino effect and alter electron temperatures as well. Thus, understanding performance changes during ground testing can help prepare for spaceflight predictions based on impacts on discharge performance and the resulting produced beam. Ingestion impacts on thruster

performance were carried out in the 2024-11 test campaign and are presented here.

Expectations were that increased background neutral density should decrease the discharge voltage and increase the beam current. Figures 5.35a and 5.35c indicate the discharge voltage drops with increasing pressure, but the beam current was fairly unchanged. As pressure increased, the discharge voltage seemed to be flattening at the 200 W condition. For both power conditions, the change was only about 1.5 V for a 3.5× increase in background pressure. The change was less than 5% over the overall voltage. It appears that high-power gridded ion engines may be well-behaved with ingestion effects than previously expected allowing for better spacelike extrapolation.

Figure 5.35b is a plot of the neutralizer keeper voltage as a function of pressure. The neutralizer keeper voltage showed an increase originally followed by a decrease in voltage as the background neutral pressure increased for both conditions. The exact cause is currently unknown, but it was hypothesized that it was connected to the ratio of plasma density to background neutrals. The 200 W condition had a less obvious change than the 100 W condition. There are two contributing factors: 1) the neutralizer keeper current was increased resulting in creating more plasma, therefore increasing the plasma to neutral density ratio and 2) the amount of plasma produced in the 200 W condition is much more than the 100 W condition and again contributing to more plasma creation. The additional plasma may have mitigated the potential partial low performance of an aged cathode by simply increasing the plasma density in the gap and allowing more electrons into the beam and reducing the required keeper voltages.

The relative change of the discharge impedance with the lowest background pressure being the normalizing value, shows a linear decrease in impedance with background pressure. This linearity can be correlated to the ingestion rate of equation (5.2) also varying linear with background pressure. The change was also less than 6% over 3.5× change in pressure. In addition the amount of the ingested flow over the total flow rate is shown in Figure 5.37. This increased linearly as well with background pressure but was dependent on the throttle condition and its corresponding flow rates. The linearity of the relative change in impedance with pressure and the small changes over a large pressure ranges will alow for better predictions of spaceflight.

Thrust is produced via the emitted beam ion current. But the efficiency of the production of that beam is defined by the ion production cost given as

$$Ion\ Production\ Cost = \frac{V_{DISC} I_{DISC}}{I_{BEAM}}, \tag{5.5}$$

where I_{BEAM} is the beam current and V_{DISC} and I_{DISC} are discharge power supply voltage and current, respectively.. The ion production cost as the amount of power to produce an ion of thrust. This equates to the discharge power over the beam current. Figure 5.38 includes relative changes normalized to the lowest pressure value. This includes, thrust, mass utilization, ion production

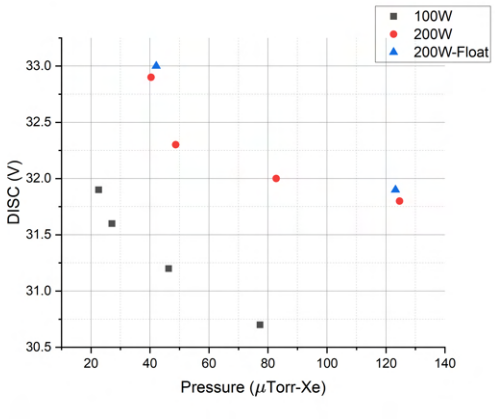

(a) Discharge voltage

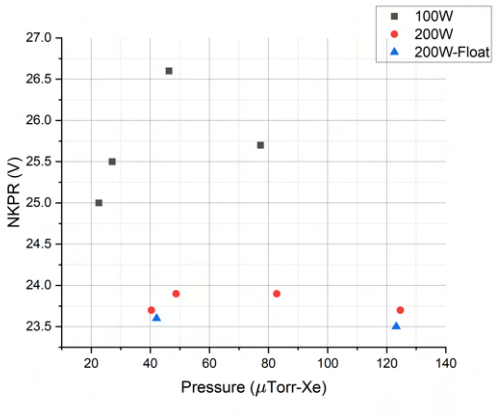

(b) Neutralizer keeper voltage

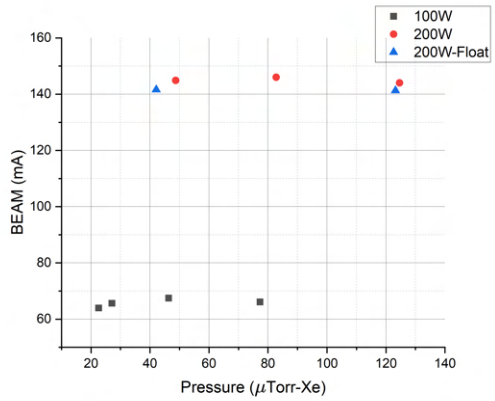

(c) Beam current

Figure 5.35: 2024-11 NASA 8 cm test campaign ingestion impacts on discharge voltage, neutralizer keeper voltage, and beam current background pressure is varied by throttling the turbomolecular pumps.

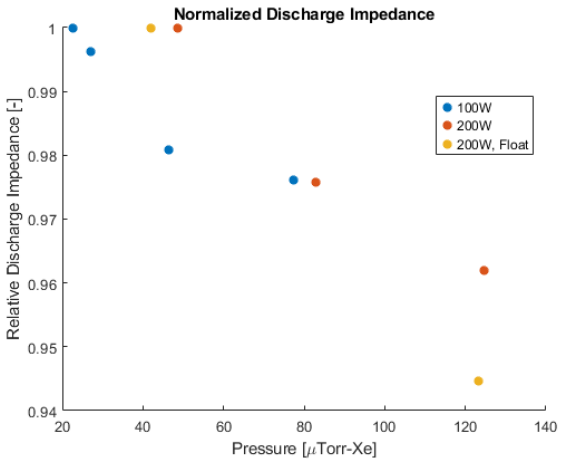

Figure 5.36: 2024-11 NASA 8 cm test campaign ingestion impacts on discharge impedance with varying background pressures normalized to lowest pressure.

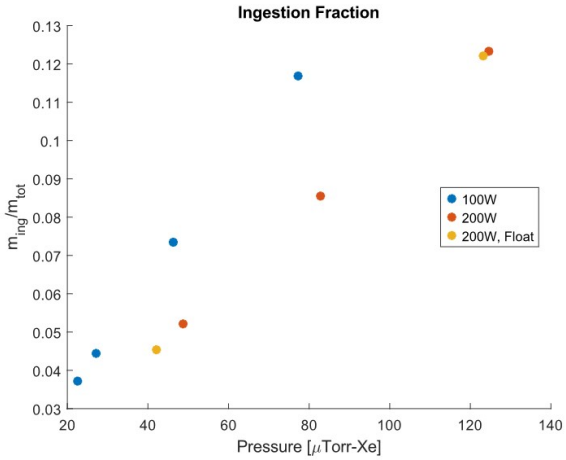

Figure 5.37: 2024-11 NASA 8 cm test campaign ingestion flow ratio to total flow with varying background pressures.

cost, and total efficiency. Thrust is calculated using equation 1.11, however doubles and divergence corrections are neglected here. Mass utilization is determined using equation (1.19). Total efficiency is found using equation (1.26). Thrust, mass utilization, and total efficiency are predominately all dependent on beam current. As such, they all have similar trends to that of found in Figure 5.35c. The ion cost production is effectively Figure 5.35a divided by Figure 5.35c. It would appear based on the ion cost production that higher powers like the 200 W case were less affected by ingestion than at low powers. However, this is because the beam current was changing at the same rate as discharge power. It was expected that the increase of ingested neutrals will decrease the required discharge power to maintain the same beam current as in the 100 W case. Because there were a number of factors in the discharge impedance, the non-expected behavior due to neutral ingestion for the 200 W case needs to be explored further for changes in the doubles-to-singles ratio. Just because the ion production cost appears invariant, does not mean the efficiency of the thruster due to changes in doubles-to-singles ratio was unaffected. For testing 100 kW systems, the doubles-to-singles ratio at higher background pressures needs to be varied as ion production cost could appear invariant due to the high ingestion rates affecting both discharge impedance and beam current linearly.

5.5 Conclusions

In this chapter, the impacts of an undersized and inadequately equipped facility on high-power density ground testing of a gridded ion engine was explored. Areas of focus included plasma properties near the wall, restrictions on plume expansion, potentials and coupling of the beam, impacts of electrical configuration of the plasma screen and beam target, localized increased neutral flow in the plasma bridge, and background neutral ingestion on performance of the thruster. Discussions on applicability and recommendations for running 100 kW systems in similar high-power densities were also made.

Plasma properties near the walls give insight into how much the beam plasma was coupling to the facility. The most obvious change with increasing background pressure was the increase of plasma densities with pressure. There showed little variances in plasma properties with electrical configurations of the plasma screen and beam target other than the plasma and floating potentials being elevated with the beam target as it floated positively. Because electron temperatures and plasma densities did not change, it was concluded that the floating beam target was the reason for the elevate the plasma potentials observed that in the floating beam target configuration that limited the amount of electrons collected at the walls. Limiting the collected electron current at the walls in the floating beam target occurred because the circuit of emitted electrons via SEE or IIEE at the target could not happen with the disconnection of the beam target from facility ground.

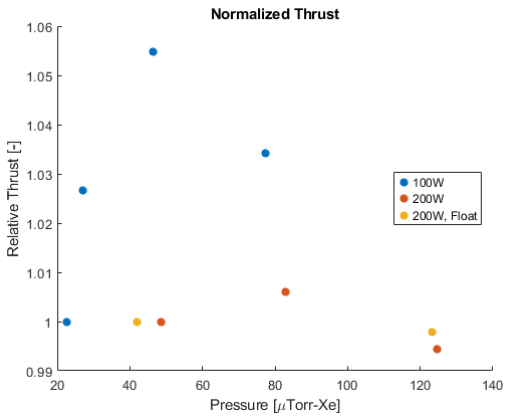

(a) Normalized thrust

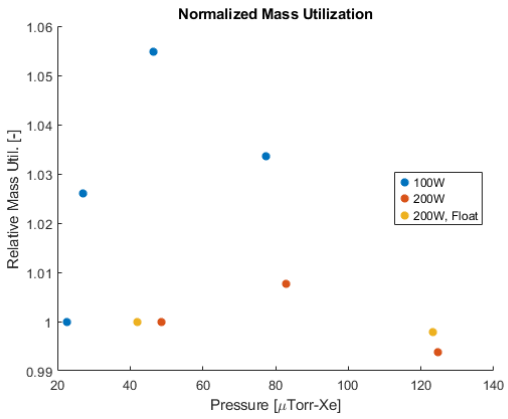

(b) Normalized mass utilization

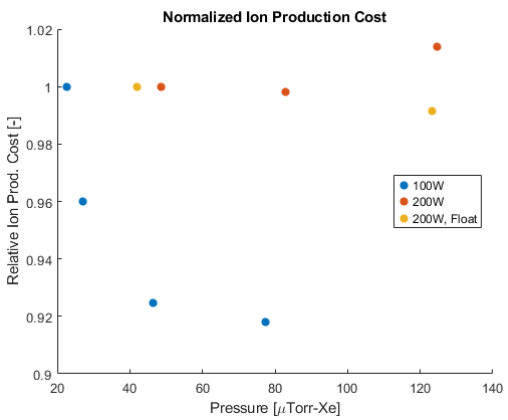

(c) Normalized ion cost production

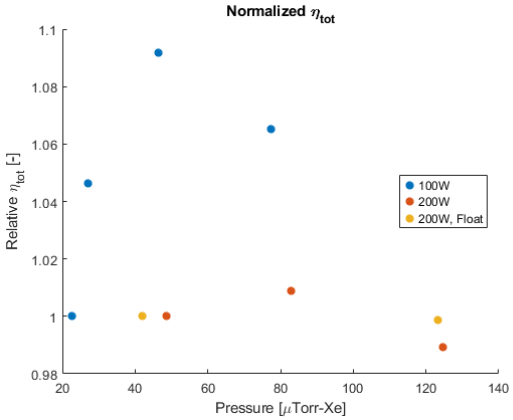

(d) Normalized total efficiency

Figure 5.38: 2024-11 NASA 8 cm test campaign ingestion impacts on performance with varying background pressures normalized to lowest pressure.

Additionally, it was found that the floating potentials of the wall probes were often positive starting at 16 cm downstream of the thruster. Because the plasma potentials were typically only 2-3 V with positive floating potentials the resulting electron temperatures were very low often less than 0.5 eV. This, in combination with the plasma densities being relatively high around 10^{13}-10^{14} m^{-3}, there can be strong coupling of the beam with the facility walls through this wall plasma. Neutralization of the beam can be altered as these low energy electrons of the wall plasma make it to the beam due to the densities of the ambient and beam plasmas being similar. This can make decoupling neutralization from the facility for 100 kW testing more difficult to decipher in high-power density testing; leading to misleading neutralizer characterizations for spaceflight.

The high density ambient plasma effects can also be seen in the beam plasma current profiles. In the very near-field, Faraday probe current sweeps around 0.5 cm downstream reveal two distinct regions: the beam and the ambient plasma. The ambient plasma current saturated instead of continuing to drop-off with distance. This is also seen further downstream at 16 cm at higher currents due to the higher ambient plasma densities. However, at the 16 cm profiles also show the expected decrease starting from about 1 beam radius from thruster center-line to 2 beam radii. The restriction of beam expansion and high background plasma densities are more evidence of non-spacelike neutralization. This neutralization is trickier to observe because it will not necessarily appear as an increase of facility-coupling voltage since the electrons are not being directly sourced from the facility. However, this ambient plasma properties are affected by the facility wall processes such as sheath heating of the electrons or the electrical potentials of the facility. Thus, the plasma potentials in the beam as a function of downstream position are critical to understand the amount of neutralization from the ambient plasma.

Hot emissive probe profile sweeps in the beam at various downstream positions revealed that the neutralizer type along with electrical configuration of the plasma screen and beam target can have significant impacts on beam plasma potential profiles. The positive floating potential of the beam target elevated the plasma potentials all along the beam. A floating plasma screen increased the plasma potential peak in the very near-field but downstream was more or less equivalent to the grounded plasma screen case. The plasma potentials in all cases decreased significantly when the background pressures were increased. The high plasma potential peak in the floating plasma screen was severely decreased and was almost identical to the grounded plasma screen case. The floating beam target plasma potentials increased due to the positive potential the beam target floated to. The changes in plasma screen potentials are less understood. The neutralization in the very near-field is being altered as the plasma screen is floating. There were changes in the plasma properties near the neutralizer such as increased electron temperatures with the "super" neutralized used in the plasma screen test campaign that may explain why the plasma potentials profile here was more peaked on center-line compared to the floating beam target test campaign using the nominal cathode that had

lower electron temperatures and greater plasma densities.

In addition, the plasma potential profiles in the very near-field revealed dip and horn-like structures in the profiles, reminiscent of double-sheath potential profiles. These structures give evidence of this being the neutralization zone. This double-layer can either accelerate or de-accelerate electrons into the beam. As this double-layer dissipates down stream, the ambient low temperature electrons can easily be drawn into the beam better neutralize it. This is potentially the mechanism aiding neutralization downstream for the floating plasma screen case as its downstream potentials match that of the grounded case. The impact of the double-layer sheath are better understood after comparing the changes in facility coupling voltages for these different configurations.

As a measurement of the interaction of the thruster with the facility, the neutralizer-facility coupling voltage, V_{cg}, has been typically used as a metric of how well the beam is being neutralized. This assumes the beam is fully neutralized and is at or near ground potential. In this testing, the facility coupling voltage increased in negative magnitude, which previous thought conventions would insinuate that the beam is being less neutralized. It was found however in the emissive probe plasma potential profiles that the plasma potentials decrease with increasing background pressure, meaning better neutralization. The facility coupling voltage is not a good metric of beam neutralization as by its definition is a metric of the amount of coupling of the thruster to the facility itself. The better measurement of the neutralizer-beam coupling has always been the true-coupling voltage, V_{cp}, defined as the difference between the beam plasma potential and the neutralizer potential. As this value decreases in magnitude, the better coupling between the neutralizer and the beam. However, measurement of this value is not trivial to obtain as emissive probes can be fragile and set objects in the plume are not desired. But it was found that the plasma potential on center-line of the neutralizer via a cylindrical Langmuir probe proved to follow trends of the beam plasma potential under various pressures and electrical configurations.

Further investigations of the true-coupling voltage were explored over various background pressures and electrical configurations. The increase in facility coupling voltage with background pressure was negated by floating the beam target. The floating beam target raised the plasma potentials everywhere in the chamber such that collection of electrons at the walls was decreased, reducing facility coupling. The true-coupling voltages for the floating beam target matched over the lowest and highest background pressure. Testing of high-power systems can get better neutralizer characterization at higher-background pressures by floating the beam target such that the neutralization of the beam is dependent on the neutralizer performance and not the background pressure. Caution must be advised as there is still unknowns with a floating beam target including at what level is the positive floating value of the beam target too high that a high flux of ions are retarded or turn around and impact on the thruster.

The floating plasma screen impacts are localized to the near-field. The true-coupling voltage in

the near field increases drastically with lower background pressures and floating plasma screen due to the increased plasma potential. The facility coupling voltage did not change with the floating plasma screen and barely changed with the increased pressure. Because the plasma potentials downstream matched between the two plasma screen configurations, it is assumed that the floating plasma screen is changing the neutralization process in the near field but the ambient plasma and residual plasma bridge quickly neutralize the beam downstream. Since the plasma screen is tied to the spacecraft chassis in space and floats in the ambient plasma, it is recommended to float the plasma screen during testing to ensure the high potentials in the near field will appear, as they would in spaceflight. There are some challenges in doing this during ground testing as the increase of background pressure obscures this high potential in the near field. Artificially heating of electrons somehow may be required to replicate these high potentials as this would keep electrons from being so easily trapped by the beam. Previous thoughts were that by adding increased impedance in the plasma bridge by neutral flow injection. However, this was later to be found ineffective for the floating plasma screen with a grounded beam target and dependent on neutralizer operating conditions more so than background pressure. Alternative ideas for artificially heating electrons to explore maybe controlling the potential of the thruster with respect to facility ground or changing potentials of grounded objects near the thruster and the walls.

Although some preliminary testing was done with the floating plasma screen and beam target the overall impact of both of them floating has yet to be fully quantified. Plasma potential measurements in the beam as a function of background pressure are needed to determine the changes in true-coupling voltages. Because the floating beam target increases the potential of the whole system and as a result the plasmas screen can float positive with respect to facility ground. This may alter the near-field neutralization process opposite of that observed in the plasma screen comparison tests. Using current knowledge, it is recommended to use a floating plasma screen, especially at lower pressures to capture accurate beam potentials in the near field. But to characterize the neutralizer, the floating beam target should be used as it is less susceptible to pressure affects. It thus may be needed that one of these should be floating at all times. This goes along with recommendations found in Ref. [49].

The impacts of neutral ingestion have been thought to be less on gridded ion engines due to the separation of the ambient neutrals to the ionization chamber due to the grids. This was found to be true, even at these higher pressure during high-power density testing. The impedance in the discharge chamber varied linearly with pressure and varied less than 6% over a pressure change of $3\times$. The linearity over this large pressure range gives a good estimate of extrapolated discharge performance at lower background pressures. Reliability of this estimate is given by the total ingestion fraction, meaning the amount of ingested flow over the total flow. This ingestion fraction is expected to be linear due to its dependence on pressure, but it shows that at increasingly small

ingestion fractions, the affect on discharge impedance is still linear. Beam current, the thrust production mechanism, were also fairly well-behaved with ingestion. It was found that higher power conditions were varied less with pressure. One caveat is the beam current can vary in a similar fashion to discharge power which can be misleading. Additionally, discharge operation is complex and although the powers and performance seem insensitive, the doubles-to-singles ratio could be altered and needs further exploration as high doubles can lead to lower thrust or enhanced erosion on the grids.

Generally, operating at high-power densities is not the issue, but decoupling the impacts of the facility on beam neutralization and coupling become extraordinarily difficult at higher background plasmas. Additionally, the wall plasmas is not appear to dependent purely on charge-exchange and can be greatly impacted by the neutralizer plasma. There are some avenues for better spaceflight predictions such as floating the plasma screen or beam target, but one potential challenge is determine the proper amount of neutralization in the very near-field such that a high potential virtual anode does not form and decrease thrust or cause damage to the spacecraft.

CHAPTER 6

Low & High-Power Density Ground Testing

6.1 Motivation & Objectives

This chapter is a compilation of the finding from Chapters 4 and 5 for low and high-power density ground testing facility effects. Here, the differences and similarities are discussed and compared. Furthermore, highlights of what matters most in these test is commented on. After-which, outlines of the guidelines and recommendations for ground testing of gridded ion engines is put forth. The last section highlights current gaps and potential future work that can be explored to deepen the knowledge and understanding obtained through this dissertation work. Short of flying high-power systems in space in substitute of ground testing, this work aims at providing the framework and expectations of ground testing gridded ion engines.

6.2 Low & High-Power Density Comparison

A comparison between the low and high-power density ground testing facility effects is made in this section. First, some limitations of this comparison are explained. Then a list of the meanings of the differences between the two ground test facilities and the causes of the differences are then explained. A general overview of the observed differences is given. Lastly, ending statements and conclusions on if high-power density gridded ion engine ground testing is feasible for accurate spaceflight qualification.

Limitations of the comparisons of low and high-power density facility effects is outlined here. It was previously desired after the LM-NSTAR low-power density test at LVTF that the high-power density test would include neutralizer characterization and margin studies as a function of background pressure. Unfortunately, due to hardware availability, stability, and operating conditions of these neutralizer cathodes this study could not be done in a way that would be meaningful for extrapolation studies to spaceflight conditions. The stability of the nominal cathode temporarily would transition to plume mode and then back again, making it extraordinary difficult to determine

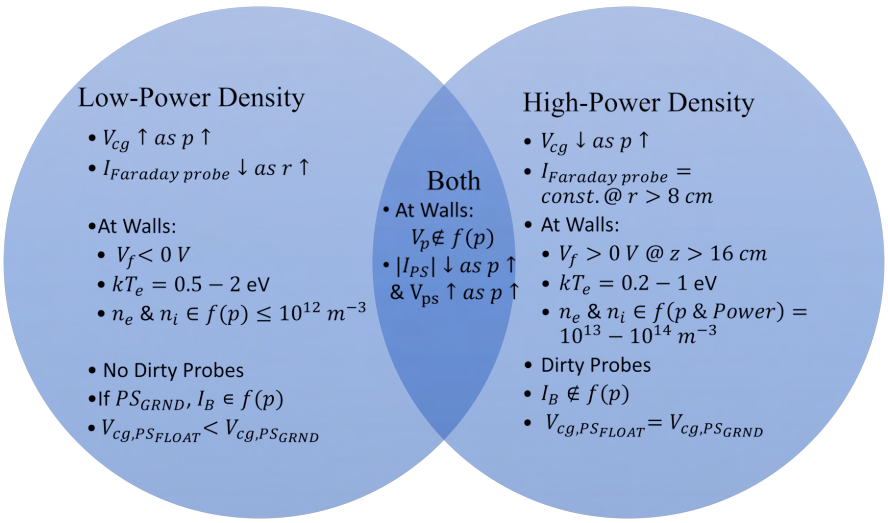

Figure 6.1: Venn diagram comparison of low & high-power density ground testing facility effects.

the true transition. In addition, the heater for the nominal cathode had to be left on, obscuring even more the true transition point. In conjunction, both the nominal and super neutralizer cathodes were operated at high flow rates and currents above that which would nominal be done. As a result, these would not be actual power levels and flow rates for spaceflight.

Another limitations of the low-power density test was the beam target could not be easily floated as in the high-power density test. In addition, the low-power test only partially investigated the floating plasma screen condition to determine if this facility effect was worth investigation in future test. As a result, there is less data with the floating plasma screen configuration at low-power densities than there was available at the high-power densities. One of these important values was the plasma potential in the beam such that the true-coupling voltage could be determined. Some estimates could be made for the low-power density case base on observations in the high-power density case and plasma potential measurements of the low power-density case further downstream. Lastly, hardware malfunctions during the LM-NSTAR test resulted in Faraday Z-direction motion stage failing and no current profiles as a function of downstream position could be obtained. Additionally, a more rigorous study of ingestion at low-power densities is needed for more accurate comparisons to the high-power density cases. The high-power density case is also missing doubles-to-singles measurements for better discharge chamber characterization. Regardless of these limitations, there is ample data available for reasonable comparisons to be made between the low and high-power density facility effects and the understand of the importance of these differences. A summary of these comparable difference observed between the low and high-power density ground test are displayed in a Venn diagram in Figure 6.1.

From the Venn diagram, there are limited similarities between the two power densities. It was

observed that the plasma potentials near the walls were reasonably unaffected by the change in background pressure, p. However, both power densities did experience a decrease in the magnitude of the current collected on the plasma screen as pressure increased. The plasma screen potentials were negative for all grounded beam target cases and increased in potential (becoming more positive) as the pressure increased. The increase collisions of neutrals and the decrease of electron temperatures at high background pressures causes the decrease in the magnitudes of the plasma screen current or floating potentials. This is generally where the similarities end.

The facility coupling voltage, V_{cg}, is a measurement of the coupling of the thruster with the facility and is typically negative in value. In the low-power density case, the facility coupling voltage became less negative as the background pressure increased. This insinuates that the thruster couples less with facility and one would expected better beam neutralization is occurring using the conventional interpretation of V_{cg} of the community. However, in the high-power density case, the V_{cg} would increase in magnitude (become more negative) as the facility pressure increased. The more negative V_{cg} would mean the beam is coupling more with the facility conventional interpretation would insinuate the beam is being less neutralized as the beam potential increases and propagates downstream such that more of the beam needs to be neutralized by the facility. Similar to the findings in Hall thrusters by Jorns et al., the coupling voltage of the cathode does not vary directly with pressure but is a function of the thruster and the facility size as well [132]. For gridded ions, the change in conductivity between neutralizer-facility and neutralizer-beam determines how V_{cg} will vary. This conductivity for small changes in electron temperatures is primarily a function of the ratio of the plasma density over the neutral density. However, the overall impedance due to distance between neutralizer-facility and neutralizer-beam is also an important factor. In the case of the low-power density, the plasma density connecting the neutralizer to the facility does not increase fast enough with background pressures to overcome the larger impedance due to the large distances to grounded surfaces in this case. Whereas the high-power density case their is a lot of grounded surfaces nearby due to support structures and the close proximity of the walls. Additionally, the plasma density in the plasma bridge varies slowly with pressure in comparison to that of the ambient plasma density near grounded structures. Thus, at higher-power density ground testing, separating the coupling of the thruster system from the facility is one of the main challenges.

Current profiles using radial Faraday probe sweeps are crucial diagnostic tool for understanding the behavior of the propagating beam. It was expected that their would be plume broadening in the wings of the obtained current profiles as the background pressure increases. This is due to the increase rate of CEX at these elevated pressures. This plume broadening was observed in the low-power density case. Unfortunately, it was not expected that in the high-power density test the plume broadening in the current profiles would be so dominated by the ambient plasma density.

Measured current is a function of density and charge particle velocity. The saturation in the very near wing of the current profiles indicate that the plasma densities just outside the beam plume plasma are very comparable to that of the beam itself. This can have very negative impacts such as electrons from the ambient plasma easily flowing into the beam to neutralize it. This neutralization pathway in space would not exist until much further downstream when the beam is much more diffused already. Additionally, this ambient plasma density will keep the beam plasma from freely expanding as it would in space. The effects of confining the beam may artificially elevate the peak beam potential on center-line, changing how and what energy electrons actual neutralize the beam. As it is, the beam neutralization process is known to occur but the exact how is still an active area of investigation [131].

In the case of the wall plasma properties, there were the similarities in plasma potentials but that is where commonalities end. In the low-power density case, the floating potentials are all negative with respect to ground and the electron temperatures range from 0.5-2 eV. The high-power density case the floating potential after 16 cm downstream are almost all positive and electron temperatures are much lower between 0.2-1 eV. The lower electron temperatures are expected due to the increased neutral collision at higher background pressures. The floating potentials being positive is more complicated phenomenon. Floating potentials are defined as the potential at which the positive and negative charge species currents are equal. In the case of an electropositive plasma, the floating potential is typically set by the more mobile free electrons. However, energetic beam ions can charge an emersed conductor positively. However, this positive floating potential can also occur in instances where the plasma potential is very positive and the electron temperatures are low that the potential difference between the plasma potential and floating potential is very small such at that the floating potential ends up still being positive. This can easily happen in situations where the floating conductor is placed in a plasma between to DC potentials above ground potential. Either situations would indicate that the beam plume potentials are being affected by the close proximity of the walls in not being able to freely expand. Additionally, the magnitude of the plasma densities are an order of magnitude or two higher in the high-power density test. Evidence of the ambient plasma densities approaching comparability of the beam plasma.

During the data analysis of the high-power density test, the Langmuir probes in the very near-field appeared to have impurities on the probe causing improper analysis of the plasma properties. This effect was not really observed in the low-power test. Deposition of carbon species in the high-power density ground test facilities can be more impact-full in the smaller volumes because more sputter of nearby components have less surface area to land on. Thus, in high-power density testing probes need to be cleaned more often with a high-voltage sweep or proper probe orientation to be consistently bombarded by some energetic ions.

Lastly, the plasma screen configuration has more of an impact in the low-power density ground

testing than the high-power density tests. The beam current decreased between the transition between the nominal grounded to floating plasma screen. This was not observed in the high-power density case. There are two contributions to this. In the low-power density case the plasma screen holes were much larger allowing more electrons to enter through the gaps in the grounded plasma screen case. Secondly, it was observed that a large potential in the very near-field of the high-power density test appears with a floating plasma screen at lower background pressures. It would then be expected that something similar would occur in the floating plasma screen in the low-power density case at a much large extent. This could not be confirmed as there was no plasma potential measurement in the very near-field of the low-power density test. If a high plasma potential in the very near-field does occur and a virtual anode appears, then this can retard the beam ions and reduce produced thrust.

Overall, there are general difference observed between the low and high-power density facility effects. Coupling of the beam plasma to the walls was observed more in the high-power density test due to the smaller distance to the walls. However, the increased background pressures do decrease the beam potentials overall due to assistance of the ambient background plasma. At the same time, this is a more difficult affect to decouple from the beam neutralization process. The increased plasma density aides in the beam neutralization process, mostly downstream. This limits the beam potential from propagating downstream unlike in the low-power density testing where high potential could still be measured downstream. Additionally, evidence of high ambient plasma densities confining the beam can be seen in the radial current probe profiles taken at the high-power density tests which is in contrast to the free expansion observed in the low-power density test. As a whole, the grounded plasma screen should be floating in both low and high-power density tests as the grounded plasma screen seems to aide in neutralization process somehow as this is more realistic of a spaceflight configuration.

To answer the question, can gridded ion engines be operated at high-power densities to qualify for spaceflight? The answer is a cautioned yes. Thrust and overall thruster performance does not seemed to be as affected by increased background pressures as previously suspected. However, beam neutralization is still very coupled with the facility and this coupling is not so easily seen in V_{cg} or V_{cp} measurements. Rather, the ambient plasma density can have a significant impact on the neutralizing of the beam before the beam potential can propagate downstream and make contact with the target or the facility walls. To make it even more convoluted, the neutralizer operating parameters significantly alter the ambient plasma at these high-power densities. As a result, neutralization is in part a function of the neutralizer operating conditions but also through a process that is not realistic of spaceflight. Characterization of a small thruster at high-power densities, then at low-power densities, and then in spaceflight is needed to full understand how tangled and if it can be untangled, the beam neutralization process is with the facility.

6.3 Guidelines & Recommendations

There are two sets of guidelines and recommendations that can be made. One set is geared towards those building a facility from scratch or having the time and means to adjust their current facility for best high-power density testing. The other is for those that may want the "quick & dirty" method of not necessarily being the best, but being better than before.

First is the best recommendation for the experimental layout of the test facility. The grounded reference of the plasma screen is not going to be present in space and as a result will not aide in the neutralization process in the near-field. For accurate beam potentials and to ensure a virtual anode does not arrive in space, a floating plasma screen will provide better and more accurate spaceflight results. A floating beam target elevates the whole potential of the facility and thruster system. The breaking of the electron circuit at the beam target limits the amount of electrons collected at the walls. Floating the beam target is appropriate in determining how well the neutralizer is coupled to the beam as floating the beam target revealed that the true-coupling voltage did not change with pressure. However, it is currently unknown the effect of floating the beam target and the plasma screen at the same time and what it will do to the neutralization process as the plasma screen in this case may actually float positive with respect to facility ground. As a result the current recommendations for high-power density testing are, for operating the thruster and determining thrust, the plasma screen should be floated as the higher potential in the very-near field will determine how much thrust in space will be achieved. Caution is advised however at high pressures around 5×10^{-5} Torr dampened out this potential severely and is not representative of spaceflight. However, a proper neutralizer may improve the pressure range of operation as the amount of background plasma produced by the neutralizer decreases. During the characterization of the neutralizer and neutralizer margin test, the beam target instead should be floated as the neutralizer is best coupled to the beam in this configuration.

If testing at low-power densities, either the plasma screen or the beam target can be floated, but most likely it will be better to float the plasma screen. This is because the high potentials in the beam are not damped by the ambient plasma downstream. As a result the potential propagates further coupling the thruster more with the facility as the beam is more neutralized by the facility. The higher potential in this case can cause the beam target to float very positive, resulting in higher energetic ions be reflected back to the thruster causing damage. The increase in magnitude of V_{cg} for low-power densities can be a suitable guide of direct beam neutralization by the neutralizer if the the increase of background pressure lessens the facility coupling. In the case of high-power testing where this is reversed or does not vary much with pressure, V_{cg} as an indication of beam neutralization is false as the potential in the beam does not really propagate downstream to increase coupling with the facility, but the increase of neutralization is from the ambient plasma.

As mentioned previously, for understanding and achieving better spacelike beam neutralization and potentials, the lower the background pressure the better. In looking at thruster performance, ingestion impacts seem to be easily corrected for as discharge impedance depends linearly on the ingestion fraction. The ingestion fraction can be up to around 10% and the behavior on discharge impedance is linear. In addition, beam current seem relatively unaffected by ingestion. However, there are two caveats here. One, the doubles-to-singles production ratio for high-power density has yet to be full investigated as this can be majorly affected by changes in discharged voltage due to ingestion. Secondly, beam neutralization can have a big impact on beam current. The dampened potentials in the near-field at higher background pressures may obscure impacts on beam current in space.

Lastly, more care is advised for probe measurements in high-power density situations. Due to the increased sputtering and deposition of impurities in the near field, probes need to be clean before ever trace via a high-voltage ramp of -100 V to 100 V. Additionally, placing probes that have the normal of their collecting surface perpendicular to the beam flow but that are also not directly in the main flow, can help keep collecting surfaces cleaner.

For best practices, gridded ion engine operation at high-power densities can be done, but validation of very near-field beam neutralization needs to be done either in a low-power density environment or adjustments in spaceflight will probably need to be made. A few background pressures of at least 4-5 different values, more of which should be done at the lower pressures, for estimated tend changes in the very-near field beam plasma potential with a floating plasma screen could give a more accurate prediction of spaceflight. Currently, lifetime qualifications have yet to be determined. In short, the "quick & dirty" methods would involve at least floating the plasma screen and keeping probes clean. Incorporation of a floating beam target may be too time consuming or impractical for large facilities. Care should be involved though in design in limiting localized pressure spikes and deflection angles of downstream objects as these to can have impacts on the thruster although not explicitly investigated here [143, 95].

6.4 Future Work

The guidelines here are made with the communities current knowledge of gridded ion ground testing. There are many unanswered questions still needed to be explored. For one, a more in-depth study comparison between ingestion affects at low-power densities to high-power densities is needed. Furthermore, an understanding of the impact of floating both the plasma screen and beam target simultaneously still needs to be addressed. The impact on neutralizer characterization and margin at high-power densities also needs to be investigated for improved spaceflight preparation. Additionally, the role of the double-sheath observed in the very near-field needs to be understood

and its presence at low-power densities needs to be confirmed. It is unconfirmed if this double-sheath forces a separation between the beam and ambient plasma or if it acts more of a bridge. Lifetime impacts at high-power densities due to sputtering and deposition have yet to be tackled.

Future work also requires real testing of a 100 kW system in a facility like LVTF to see if the comparisons found here hold true. Additionally, the gold standard would be to have a thruster travel through all the stages for more accurate comparisons. This would mean the same thruster tested in a high-power density situation, than a low-power density test, and ultimately have its behavior in space investigated. This would not yet need to be a 100 kW system, but even a sub-10 kW system would give great insight to if high-power density testing can be a viable option in the future for reduced cost and opening up the use of the more numerous smaller facilities.

CHAPTER 7

Target Plasma & Impurities

7.1 Motivations & Objectives

In ground testing of gridded ion engines, it is not only the background pressure and electrical coupling that affect operation but also sputtered materials and impurities in the plasma. Investigated here is "target glow" that has been witnessed in this work and works of others. Here, the objective is to determine that composition of this target glow such that relative impacts can be considered. Plasma impurities can have other major impacts as well. Probes and other diagnostics can give misleading results if the impurities are not considered. The impact of sputtered material into the plasma on probes and diagnostics is documented with recommended correction procedures where possible.

7.2 Investigation of Target Glow

During the LM-NSTAR testing at PEPL LVTF, a unusual white glow was observed around the near field graphite structures when placed in the beam. Figure 7.1 is a snapshot with extra exposure time to enhance the captured light. Circled in red is graphite probe shield that is source of the witnessed target glow.

Original suspicions were that the white glow is due to carbon clusters being sputtered off either as metastables or ions. To investigate this, during the operation of NASA 8 cm at PSTL RC, plasma spectroscopy was performed but poor single-to-noise ratios prevented conclusive results. Instead a mock-up of the beam ions was produced in a separate vacuum facility where better optical access and higher current densities on the target could be performed. Testing was done in the Gaseous Electronics Conference (GEC) Reference cell, a standardized test cell for micro-electronics manufacturing research developed in the 90's [144]. The inner diameter of the chamber is 25.1 cm with an overall height inside of 22.2 cm. In this test setup, a DC glow discharge plasma is created with argon. A Poco graphite carbon sample (same as in PEPL LVTF) is then placed



Figure 7.1: Target glow during LM-NSTAR operation at PEPL LVTF. Reveals a whitish glow around the target of unknown composition that is suspected to not be the xenon propellant. A non-spacelike condition to have this material sputtered off and enter the plasma environment.

below the plasma and biased negatively by 300 V with respect to facility ground to accelerate ions to the sample. The experimental setup is displayed in Figure 7.2. Due to the GEC limitations and DC plasma breakdown in the chamber, background pressures are much higher than experienced at PEPL LVTF or PSTL RC at 320 mTorr. A photo of the Poco sample is found in Figure 7.3

The resulting obtained spectra using a Czerny–Turner type spectrometer (Acton Series, SP 2300i) with an 1800 grooves/mm holographic grating and a fast intensified CCD detector (PI MAX3, Princeton Instruments) with some identified peaks is found in Figure 7.4. A list of line spectra of interest found in Figure 7.4 is located in Tables D.1 and D.2 of Appendix D.

There the obvious strong Ar I lines starting at 696.54 nm to 842.46 nm in Figure 7.4. Additionally, the strongest ion argon lines at 458.98 nm and 472.68 nm. However, there are a plethora of lines between 400 nm to 500 nm that are not nitrogen lines. Carbon and carbon clusters can be found between 370 nm up to almost 700 nm. These lines are not as intense as the argon lines. A few of this carbon and carbon clusters are highlighted in Figure 7.4. Hydrocarbon species were also observed in significant quantities as well. Some of which include ionized species as well such as CO II.

The presence of hydrocarbons was unexpected and can be a topic of concern. Carbon on its own is conductive and can act as a low impedance resistor. Adding reactive water species alters the electrical properties of carbon and some species such as carbon chains can be reactive to metals. At high-power density testing, the current density to the walls and sputtered materials will be increased. These reactive hydrocarbon species can be anywhere in the chamber. They not only deposit on the probes and mess-up their traces, but these hydrocarbon reactive species can make

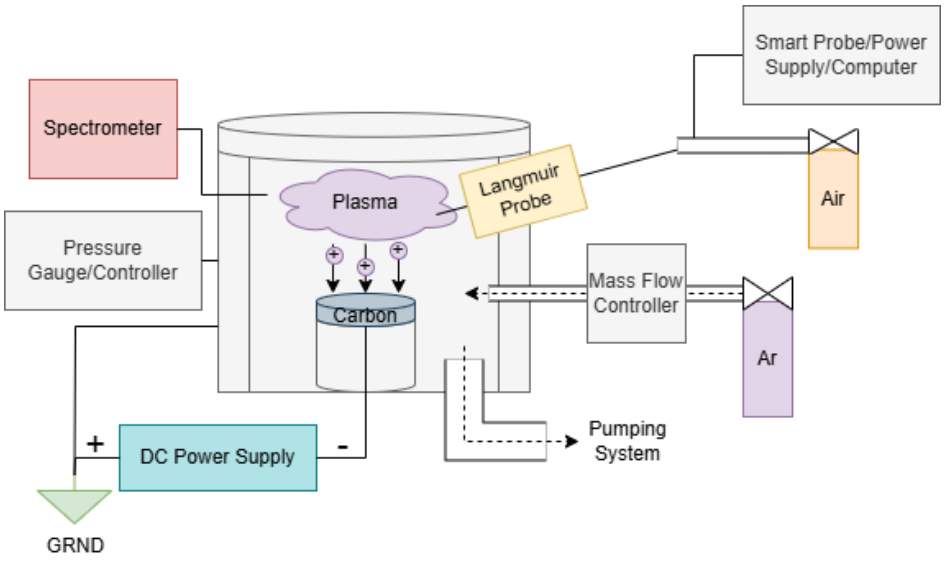

Figure 7.2: GEC bell jar test chamber plasma spectroscopy experimental setup.

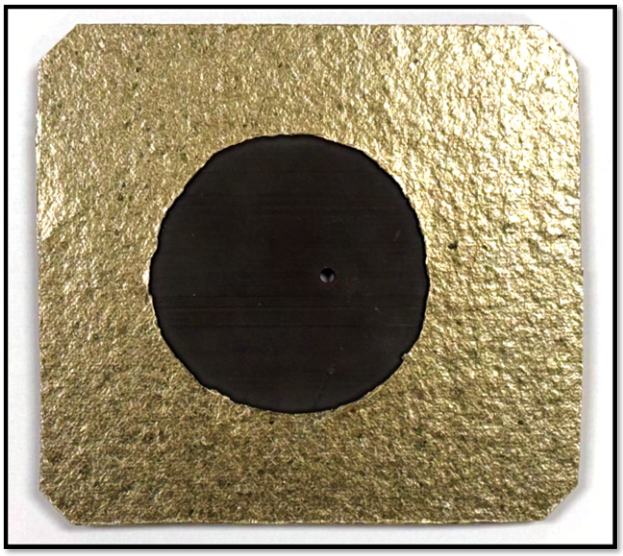

Figure 7.3: GEC bell jar test chamber Poco carbon sputtering test sample to emulate the target glow seen in thruster testing.

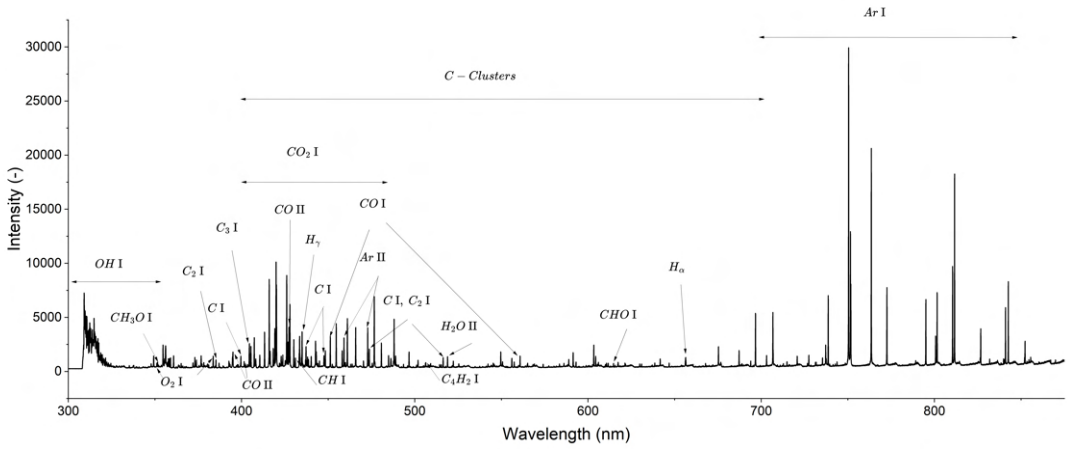

Figure 7.4: Sputtered carbon spectra with some identified peaks using the emulated thruster ion beam in the GEC bell jar chamber.

it back to the thruster as well. The deposition of hydrocarbon species on the thruster can do a number of things such as mislead thruster lifetimes, weaken the metal, coat the anode resulting in changing the impedance, or cause more recycles by shortening out the grids. These effects can lead to improper thruster characterization for spaceflight. These hydrocarbon reactive species can be neutral or ions. As a result they can drift through the plasma screen and deposit on the anode and magnet rings. The burn lines sometimes observed on the magnets may in-fact be due to energetic electrons cracking these hydrocarbon chains, resulting in the blackening discoloration observed. Furthermore, these reactive species can get inside the discharge chamber and degrade the cathode overtime. Other possibilities include negative ions changing the beam neutralization processes as well. These species can be everywhere and are currently unaccounted for.

The reactive hydrocarbon species are produced from energetic ions sputtering off carbon and the trapped water vapor in the sample. The change in water concentration overtime can be seen in Figure 7.5. After only 30 minutes, a noticeable decrease in OH concentration was observed as the water vapor began to outgas and be pumped out. However, this is not a new phenomenon. The fusion community has been aware of the water vapor issue in graphite for years and has made many attempts at conditioning the material or adding a chemical layer [145, 146, 147, 148, 149, 150, 151, 152]. At the higher-power densities desired, this affect will become more important to the electric propulsion community. To minimize the sputtered hydrocarbons, conditioning processes on the carbon must be done beforehand. Also, limiting chamber exposures to atmospheric air and conditioning chambers before testing maybe required.

Although these hydrocarbon species were observed in the mock-low power beam setup, they were also verified during actual thruster operation. Figure 7.6 is the partial pressure mass spec-

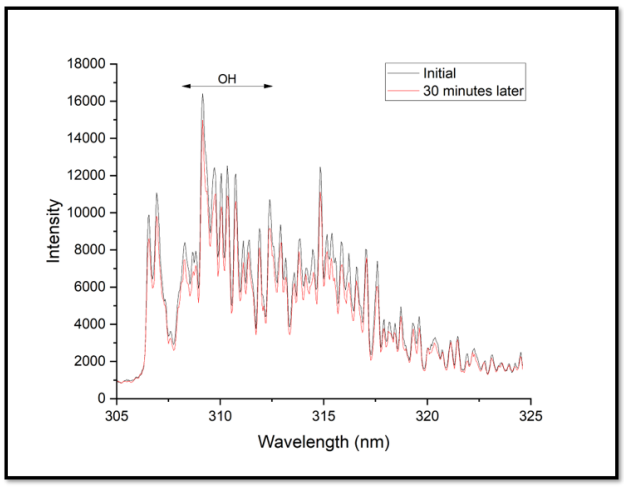

Figure 7.5: Sputtered carbon spectra OH bands over time after exposure to the emulated thruster ion beam in the GEC bell jar chamber after 30 minutes. An observed decrease in the OH levels after the 30 minutes of outgassing.

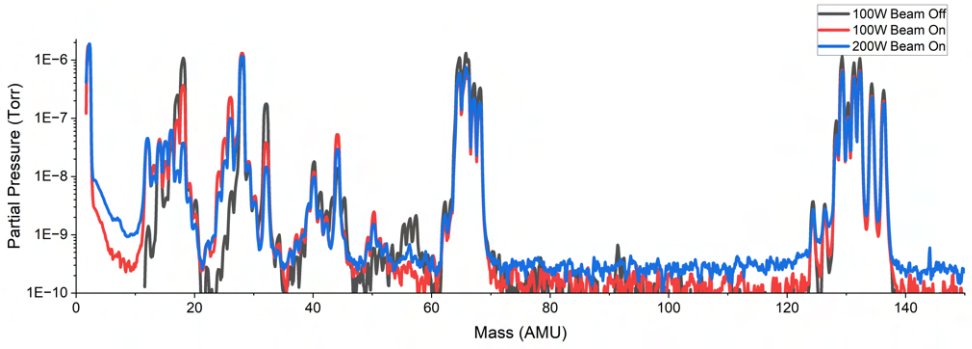

Figure 7.6: 2024-11 NASA 8 cm test campaign mass spectroscopy using a residual gas analyzer on sputtered material in the ambient plasma in the Rocket Chamber near the beam target.

troscopy measurement using an RGA with a mass per charge, m/z, for the abscissas using the setup from the 2024-11 test of Figure 3.7. Three conditions were obtained. The first was with the discharge mode only (no beam extraction) at the 100 W power level (black). Then, the beam was extracted at the 100 W level (red). Lastly, the power was increased to the 200 W (blue). The peaks around 132 AMU are for xenon and all its isotopes. Around 66 AMU is half the mass of xenon is again xenon but due to the doubly ionized atoms from the RGA ionizer. The whole RGA trace is seen in Figure 7.6 and the lower masses show significant increases with power level with beam extraction where ions of smaller monoatomic species will be. The lower partial range of 10 AMU to 30 AMU is found in Figure 7.7a. The middle partial range of 30 AMU to 60 AMU is in Figure 7.7b. Both of these figures have annotation marking most probably species. Tables of these values are located in Appendix E in Tables E.1 and E.2.

From both figures, there are both noticeable increases and decreases in certain species. Noticeable increases occur for C (12 AMU), CH_3 (15 AMU), C_2 (24 AMU), C_2H (25 AMU), and C_2H_2, CN, B_2H_6 (26 AMU). As more sputtering occurs, carbon and carbon cluster densities increase as well. Additionally, hydrocarbons begin to form such as C_2H. But at higher power levels with beam extraction, there are decreases in OH, NH_3 (17 AMU), H_2O (18 AMU), and O_2 (32 AMU). As beam power increases, the production of hydrocarbons increases and depletes the exposed water vapor. In addition, as time passes it is expected that the water vapor would decrease overtime. Testing began with 100 W no beam, then 100 W with beam, and lastly 200 W with beam over the span of two days. The partial pressure of these hydrocarbons is not negligible either. In some cases, comparing the xenon partial pressure to that of the hydrocarbons, the hydrocarbons begin to make up a significant portion of the partial pressure and are only an order of magnitude lower than that of xenon. Because of their lower mass, the same amount of pressure for a small species will require greater densities. Thus, the densities of these hydrocarbons maybe on the order of xenon. A future study to determine the density of these hydrocarbons will be critical to determine the quantity of their impact on thruster ground testing, especially at high-power densities.

7.3 Plasma Impurities

Impurities in the plasma can be deposited throughout the chamber causing problems for probes and other diagnostic tools. This was observed during the post-analysis of the NASA 8 cm test campaigns mainly on the in-plane wall Langmuir probes. The right-side wall probes also experienced significant impurity deposition. This can lead to dirty probe traces with misleading plasma properties [153]. Typically dirty probes lead to increases in the measured plasma potential and electron temperatures by the stretching of the electron retarding region. If a resistive layer builds up overtime, then the measured current will also decrease overtime resulting in an error propagating of a lower calculated electron density.

Evidence of the dirty probe affecting the IV traces of the wall Langmuir probes can be seen in Figure 7.8. The top row contains the semi-logy plots of the wall probe on the left-side of the thruster over the three test campaigns. The bottom row is the mirrored Langmuir probe on the right-side. All traces shown here are under the 100 W with grounded plasma screen and beam target. The used neutralizers and overall background pressures are slightly different but changes in the IV traces can be observed overtime that resemble a dirty probe effect. In the later test campaigns, the electron retarding region elongates and results in more difficulty in determining the plasma potential. Carbon is conductive with low resistance and should have resulted in lower measured currents but somewhat similar electron and ion temperatures. But the fact that values were drastically different overtime insinuates that the impurities are more likely to be some sort of

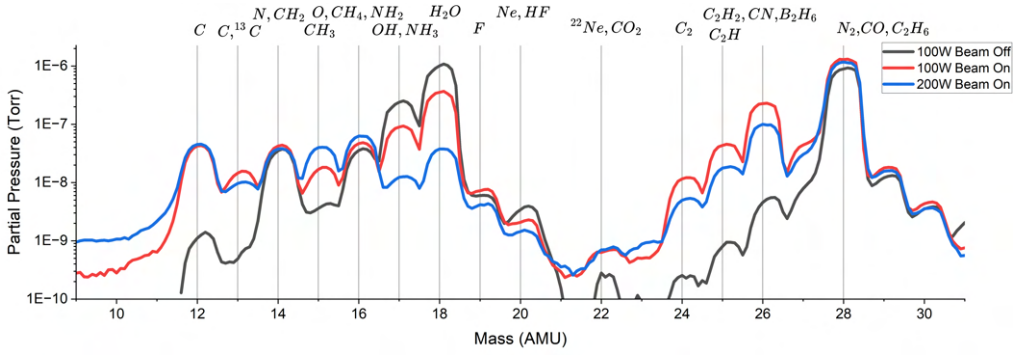

(a) Annotated 10-30 AMU

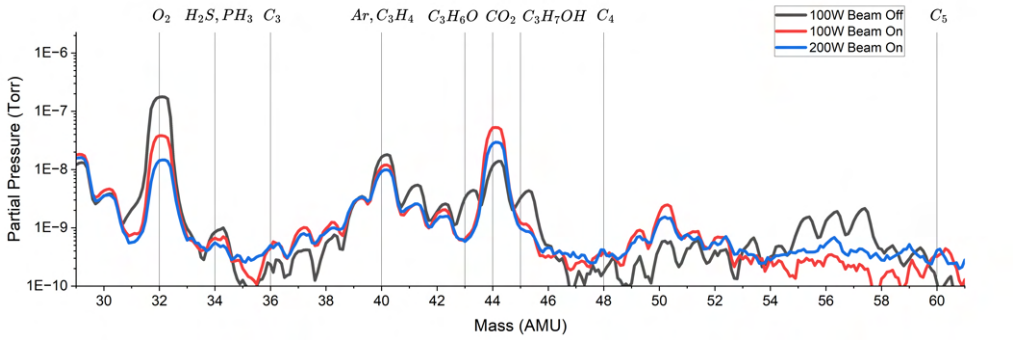

(b) Annotated 30-60 AMU

Figure 7.7: 2024-11 NASA 8 cm test campaign mass spectroscopy using a residual gas analyzer in the Rocket Chamber near the beam target for two focused ranges. Shows increases in carbon species and hydrocarbon species found in the plasma spectroscopy results as the thruster power level is increased.

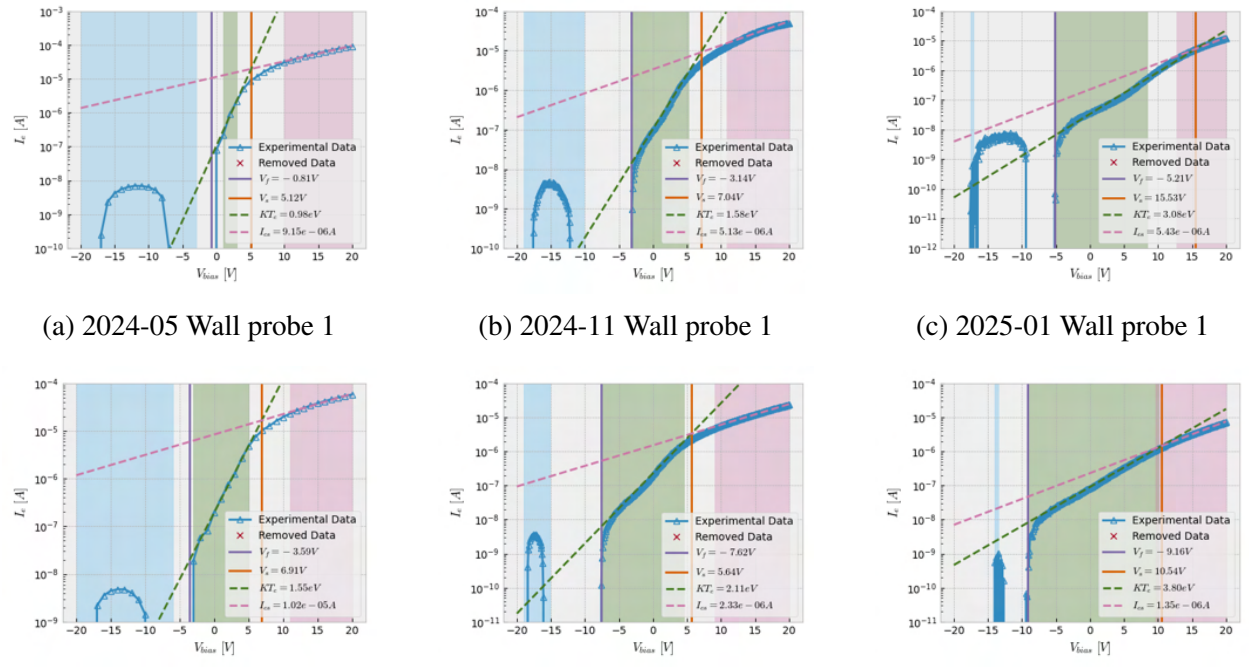

(a) 2024-05 Wall probe 1 (b) 2024-11 Wall probe 1 (c) 2025-01 Wall probe 1

(d) 2024-05 Wall probe 5 (e) 2024-11 Wall probe 5 (f) 2025-01 Wall probe 5

Figure 7.8: Rocket Chamber in-plane wall cylindrical Langmuir probes 1 (left-side) & 5 (right-side) IV trace changes during test campaigns that became more dirty over time.

hydrocarbon with more capacitive or inductive electrical properties. Future testing should involve a -100 V to 100 V bias sweep before the actual probe trace is taken to burn off the impurities.

It is expected that the in-plane probes suffered the most deposition due to their locations. The in-plane probes received a lot of carbon deposition every time the Faraday probe or emissive probe were operated on the motion stage with multiple very-near field sweeps being made. Because these probes were not further downstream, there was limited ion energy ions impacting on these probes to clean the surfaces. In Figure 7.9, the top two photos highlighted in red point out a glass witness plate placed perpendicular to the thruster off to the right-side, in the direction of the in-plane wall Langmuir probe. The bottom photo is the deposition on this witness plate after only a few days of testing. It is easy to see that large amounts of sputtered material are heading towards the probe. This rate of deposition, along with the hydrocarbons found in the previous section, suggest that large amounts of impurities are disrupting the in-plane Langmuir wall probes. At these high-power densities and the small confines of the chamber, special care is needed in running diagnostics like Langmuir probes to ensure accurate measurements are made.

In the low-power density facility effects of Chapter 4, there was a short discussion on the asymmetry observed in the plasma potential of the H9 Hall thruster. This was determined to be caused by the geometry, size, and location of the rest of the probe arm when measurements were made.



(a) Thruster operation with witness plate first view angle

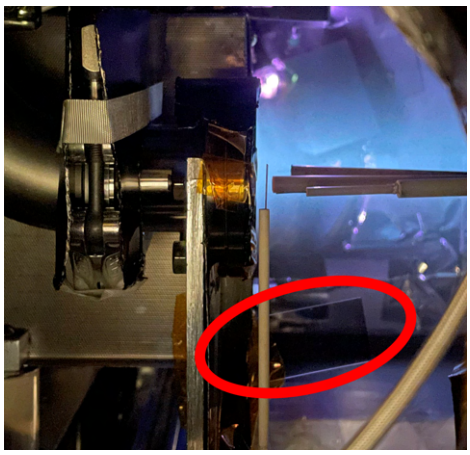

(b) Thruster operation with witness plate second view angle



(c) Witness plate

Figure 7.9: Rocket Chamber glass witness plate in front of one of the in-plane wall cylindrical Langmuir probes that had an increase in deposited material overtime. Shows location and resulting deposited material on the glass witness plate after only two days of testing.

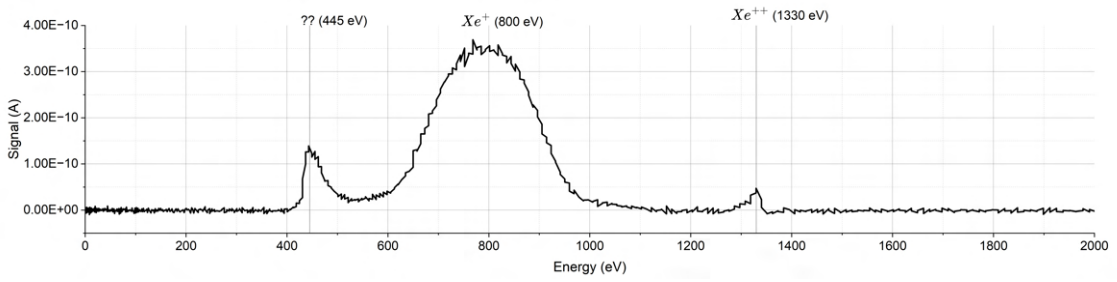

Figure 7.10: 2025-01 NASA 8 cm test campaign at the 100 W power level ExB spectra with unusual peak before the main singly ionized beam ions. Suspected to be attributed to CEX ions.

As more of the probe arm was located in the plume (when emissive probe measurements were at positive angles) the electron temperatures and plasma potentials where lower than on the other-side. As has been seen here, impurities in the plasma can lead to all sorts of issues and having that large of an object in the main part of the beam can lead to poor measurements of how the plasma plume would really be in space. Impurities in plasmas cannot be ignored and care in experimental design must be taken.

There are other issues that arise with plasma impurities that can affect probe measurements. After the LM-NSTAR test, an ExB probe for the Rocket Chamber was designed and built to characterize the impact of neutral ingestion under high-power densities. Unfortunately there has been difficulty in the post-test analysis of the traces and is why this information was not apart of the previous chapters. Figure 7.10 is the ExB current signal plotted against the calculated ion energies. The largest peak being the 800 eV singly ionized ions of the 100 W power condition. At approximately double this value should be the doubly ionized ions at 1600 eV, however, current refinement errors have these doubly charged ions at 1330 eV. Oddly, there was another peak detected below the singly charged ions at approximately 445 eV. This peak was unexpected but has been thought to be either elastically scattered ions or CEX ions. Currently it suspected that this peak is from the CEX ions as this peak increases with background pressure while the singles peak decreases. Additionally the peaks begin to blend more as the background pressure increases. This follows trends outlined by King in Ref. [154]. Currently it is undetermined if the increase of CEX is because of the increase in background pressure in the vacuum facility itself or in the probe. Other suspicious is that because the ExB is behind the beam target with a hole cut out, that there is an increase of pressure here due to neutralized beam ions off the target and sputtered material. In general, information from probes and diagnostics can be compromised due to facility effects and as a result can make spaceflight preparation even more difficult to prepare for.

7.4 Conclusions

The goal of this chapter was to highlight the importance of materials in high-power density ground testing of gridded ion engines. It was determined that the target glow witnessed is not carbon or carbon clusters alone, but hydrocarbons and other reactive water species that stem from the water absorbed in carbon lattices. A mock-beam was first used to obtain the optical emission spectra of these species in this mock-beam test but later mass spectroscopy verified the presence of these species during actual thruster beam testing. These impurities from carbon materials have been a known issue in the fusion community for decades but is starting to have more relevance to the electric propulsion community. These impurities in the plasma can deposit and create problems for cathode lifetimes, discharge impedance, and probe traces to name a few. Future studies on density measurements and the magnitude of their effects on thruster operations are needed for these plasma impurities.

There has already been evidence of the plasma impurities causing problems on probe traces as seen in the NASA 8 cm wall probes. Dirty probes can lead to invalid measurements of electron temperatures, plasma potentials, and electron densities. Especially for probes not hit by high energy ions, a cleaning bias sweep of -100 V to 100 V should be done prior to the actual Langmuir trace in an attempt to burn off the impurities. A witness plate near the wall probe should huge amounts of sputter material deposited there only over two days of testing. Additionally, an ExB probe measurement was attempted but revealed some suspected increased CEX altering the trace. Additionally, previous result from the H9 Hall thruster plasma potential measurements show that objects in the plume and impurities in the plasma can have significant impacts on plasma measurements that would not be observed in space.

At high-power density testing of gridded ion engines, or an electric propulsion deceive for that matter, can be impacted greatly by sputtered materials and impurities in the plasma. This stems largely from probes behaving differently than as expected due to these impurities. Some best practices are needed for probe operation and facility design to mitigate these effects. However, at high-power densities and confined spaces, the transport of and density of these plasma impurities increases but the extent of their effects is not yet known and needs to be investigated further.

CHAPTER 8

Conclusion

This chapter summarizes ending conclusions and future work needed from this dissertation. Before this discussion, a brief overview of the important data and their relevance/limitations from each of the gridded ion engine test campaigns is outlined in the following tables. Table 8.1 summarizes the data from the low-power density testing results from 2023-02 test campaign with LM-NSTAR in LVTF. Tables 8.2, 8.3, and 8.4 are for the high-power test in the Rocket Chamber using the NASA 8 cm for the 2024-05, 2024-11, and 2025-01 campaigns, respectively. These tables are to serve to highlight important findings and provide connections back to the results embedded in this dissertation work. As a database for model validation, this dissertation work includes a plethora of data and these tables aim to connect readers to the appropriate sections in the previous chapters or in the appendices. Summary tables of the objectives of each test campaign and diagnostics available in each test can be found back in Chapter 3 in Tables 3.1 and 3.2.

Table 8.1: 2023-02 low-power density LM-NSTAR gridded ion engine testing summary at LVTF.

Section & Parameters Investigated	Methods & Variations	Relevance & Limitations
Sec. 4.3.1.1: Plasma properties in ambient plasma near the walls V_p, n_e, kT_e, and λ_{De} (V_f, n_i in Appendix B)	Obtained from Langmuir probes with variations in: • Background pressure (4 pressures) • Throttle level (3 throttle levels) • Downstream position along the wall	• Database for model validation • Verified limited beam-wall interactions
Sec. 4.3.1.2: Thruster plume expansion $I_{beam}(r, z)$	Obtained by lateral Faraday probe sweep with variations in: • Background pressure (2 pressures) • Throttle level (2 throttle levels)	• Database for model validation • Verified plume broadening in the wings behaves ideally with continues expansion towards plasma density and potentials approaching zero at the wall
Sec. 4.3.2.1, 4.4.1, and 4.3.3.2: Impacts of floating the plasma screen I_{beam}, V_{cg}, and thruster telemetry results	Obtained by voltmeter (V_{cg}) and thruster telemetry with variations in: • Background pressure (4 pressures) • Throttle level (3 throttle levels) • Between grounded and floating plasma screen	• Determined floating plasma screen has impacts on V_{cg} and on thruster performance but needs more investigation • Limitation was no measurement of plasma potentials in the beam for V_{cp} measurements

Sec. 4.3.3.1 and 4.3.3.2: Characterization of neutralizer V_{cg}, $V_{cg,peak-to-peak}$, V_{nkpr}, I_{ps} or V_{ps}	Obtained by passive oscilloscope probe (V_{cg} & $V_{cg,peak-to-peak}$) and thruster telemetry with variations in: • Background pressure (3 pressures) • Between grounded and floating plasma screen	• Determined that higher backgrounds causes higher neutralizer flow margins, thus in space the neutralizer flow rates can be lower • Limitation was one throttle condition and no measurement of plasma potential in the beam
Sec. 4.3.4: Ion energies perpendicular to beam propagation at thruster flats E_{ion}	Obtained using a retarding potential analyzer (RPA) with variations in: • Background pressure (4 pressures) • Throttle level (3 throttle levels)	• Database for model validation • Potential sputtering can occur do to high energy ions scattered at the thruster exit that decrease in energy at higher background pressures • Limited data points at lower throttle conditions
Sec. 4.4.2: Discharge doubles-to-singles production J^{++}/J^{+} (uncorrected, measured at z=2.08 m downstream) & J_0^{++}/J_0^{+} (corrected)	Obtained using an ExB probe and corrected for attenuation with variations in: • Background pressure (4 pressures) • Throttle level (3 throttle levels)	• Database for model validation • Corrected doubles-to-singles values not constant over a pressure range for a constant throttle condition as expected • Limited understanding of localized pressure effects

Table 8.2: 2024-05 high-power density NASA 8 cm gridded ion engine testing summary in the Rocket Chamber.

Section & Parameters Investigated	Methods & Variations	Relevance & Limitations
Part of Sec. 5.3.1.1: Ambient plasma properties near the wall V_p, V_f, n_e, kT_e, and λ_{De}	Obtained at 100 W power level using Langmuir probes with variations in: • Background pressure (3 pressures) • Between a combination grounded and floating plasma screen/beam target (4 combinations) • Downstream position along the wall	• Database for model validation • Impacts of the combinations of grounded/floating plasma screen and/or beam target on wall plasma properties were limited • Limited data for various power levels and smaller range of background pressures
Sec. 5.3.2.4: Neutral flow injection effects on the plasma bridge formation V_{cg}, V_p, and kT_e (V_f, n_e, n_i, and λ_{De} are found in Appendix C)	Obtained at 100 W power level using passive oscilloscope probe for V_{cg} and all other properties using Langmuir probes with variations in: • Background pressure (3 pressures) • Between a combination grounded and floating plasma screen/beam target (4 combinations) • Near plasma screen and neutralizer	• Controlling the formation of the plasma bridge revealed balancing neutralizer electron temperatures and neutral density can impact conductivity and coupling more than neutral density alone • Limited data for various power levels and smaller range of background pressures from data from near the plasma screen • Limited measurements of V_p in the beam to get accurate measurements of V_{cp}

Table 8.3: 2024-11 high-power density NASA 8 cm gridded ion engine testing summary in the Rocket Chamber.

Section & Parameters Investigated	Methods & Variations	Relevance & Limitations
Part of Sec. 5.3.1.1: Ambient plasma properties near the wall V_p, V_f, n_e, and kT_e (λ_{De}, n_i in Appendix C)	Obtained using Langmuir probes with variations in: • Power evel (2 levels) • Background pressure (4 pressures) • Between grounded and floating beam target (2 pressures and 200 W power level only) • Downstream position along the wall	• Database for model validation • Floating the beam target elevated plasma potentials everywhere in the chamber to limit electron current collection on the walls due to the higher sheath drop • Evidence of beam-wall interactions due to changes in throttle conditions affect the plasma densities at the walls for different electrical configurations • Limited data over the pressure range for floating beam target
Last part of Sec. 5.3.1.1: Probe shape and orientation effects V_p, V_f, n_e, kT_e, λ_{De}, and n_i	Obtained using Langmuir probes with variations in: • Power Level (2 levels) • Background pressure (4 pressures)	• Determining which probe type is best for ambient plasma measurements and least susceptible to error revealed a collecting surface that is facing incoming scatted beam ions is best to help keep the probe surface clean • Limited downstream position variations

Sec. 5.3.2.2 and part of Sec. 5.3.1.3: Coupling and plasma potentials in the beam V_{cg}, V_{cp}, $V_{p,wall}$, and $V_{p,beam}$	Obtained using passive oscilloscope probe (V_{cg}), Langmuir probes ($V_{p,wall}$), and heat'n float emissive probe ($V_{p,beam}$) with variations in: • Background pressure (2 pressures) • Between grounded and floating beam target • Downstream position along the wall	• Database for model validation • Floating beam target had little effect on thruster performance • Floating the beam target allowed for the same V_{cp} to be determined regardless of background pressure, thus floating the beam target is ideal to determine proper neutralizer-beam coupling • Limited data over the pressure range and power levels
Sec. 5.4.1: Ingestion effects Various thruster performance metrics such as thrust and discharge impedance	Obtained using telemetry system with variations in: • Background pressure (4 pressures) • Power level (2 levels)	• Database for model validation • Ingestion at high-power densities on thruster operation was limited and some avenues for extrapolating spaceflight performance seem viable • Limited data on doubles-to-singles production ratio

Table 8.4: 2025-01 high-power density NASA 8 cm gridded ion engine testing summary in the Rocket Chamber.

Section & Parameters Investigated	Methods & Variations	Relevance & Limitations
Part of Sec. 5.3.1.1: Ambient plasma properties near the walls V_p, V_f, n_e, and kT_e (λ_{De}, n_i in Appendix C)	Obtained at 100 W power level using Langmuir probes with variations in: • Background pressure (2 pressures) • Between grounded and floating plasma screen	• Database for model validation • Floating the plasma screen seems to have little effect on the ambient wall plasma properties • Limited data over the pressure range and power levels
Sec. 5.3.2.3 and part of Sec. 5.3.1.3: Coupling and plasma potentials in the beam V_{cg}, V_{cp}, $V_{p,wall}$, and $V_{p,beam}$	Obtained using passive oscilloscope probe (V_{cg}), Langmuir probes ($V_{p,wall}$), and heat'n float emissive probe ($V_{p,beam}$) with variations in: • Background pressure (2 pressures) • Between grounded and floating plasma screen • Downstream position along the wall	• Database for model validation • Floating plasma screen had little impact on thruster performance • Floating plasma screen especially at low background pressures revealed a high plasma potential in the very near field that extrapolating to space can result in lost of thrust if the potential grows • Limited understanding in differences in plasma potential profiles in the very near field • Limited data over the pressure range and power levels

8.1 Summary

To advance current state-of-the-art power levels of EP devices from 10s of kW to 100s of kW, ground testing and qualification of these devices is necessary. Gridded ion technology is one option that can be used for high-power operation on nuclear electric propulsion missions supporting science, cargo, and human missions to the Moon, Mars, and beyond. Exploring such high-power operating conditions on the ground while maintaining the conditions necessary to replicate operations in space is beyond the capabilities of current vacuum facilities. As such, ground testing is performed under non-ideal situations. Diagnostics and models together may be able to correct the performance data such that spacelike operation can be recovered. But first, an understanding of the mechanisms underlying these facility effects is required to determine the thruster processes impacted that are of relevant importance for obtaining proper spacelike operation. The focus of this dissertation research was to capture the changes in thruster behavior and performance under a variety of induced facility effects with a range of magnitudes from low to high-power density thruster operation. Because 100 kW and greater systems will need to be ground tested in undersized facilities with insufficient pumping speeds, understanding the differences of these facility effects between low and high-power density operation is crucial to determine if high-power density testing can accurately provide meaningful insight into a systems spaceflight performance.

Three areas of interest were explored. Initial understanding of facility effects on gridded ion engine operation was investigated in a low-power density test of the NSTAR-like engine at the University of Michigan PEPL Large Vacuum Test Facility (LVTF). Here the objective was to explore pressure effects over a range of power levels and to categorize areas of future interest. The second area of interest was based on findings from the NSTAR low-power density test. Changes in facility effects were explored by operating a smaller engine in a undersized facility with insufficient pumping speeds to emulate high-power density operation of a 100 kW engine at PEPL LVTF. This was done using the NASA 8 cm gridded ion engine at the PSTL Rocket Chamber (RC). Similar testing variables to the low-power density test such as a variety of background pressures and throttle conditions were also done in this high-power density testing. Other parameters were also investigated based on findings from the low-power density test such as further exploration into beam neutralization and coupling by altering the plasma screen and beam target potentials from their nominal grounded state to allowing them to electrically "float" in the plasma. A comparison of the plasma properties, coupling and neutralization, and thruster performance were then made and formatted into a guidebook and recommended practices for gridded ion engine ground testing operation in both low and high-power density situations. Finally, investigation of "target glow" composition was performed and the implications of impurities in the plasma on thruster performance, probes and diagnostics, and extrapolation of ground testing results to spaceflight predictions.

Currently there are no ground test facilities that can adequately provide the ideal "test like you fly" testing environment such that an accurate spaceflight performance of high-power gridded ion engines can be predicted. Thus, one is left to deal with the facility effects impacting testing results. True spaceflight performance can then only be recovered by correcting for these facility effects via validated models. These models need experimental data to be validated. This work accomplishes two things: 1) operating thrusters under both high and low power densities to characterize the impacts of facility effects at these two extremes and 2) provide a wide range of experimental data for model validation for a larger range of power densities than has been previously done. Results from this dissertation work show that in the absence of a fully qualified ground test facility for high power electric propulsion testing, gridded ion thrusters can be operated at high-power densities with a potential path of recovering spaceflight performance via validated model corrections. However, there are some aspects such as beam neutralization at high-power densities that need further investigation.

8.1.1 Low-Power Density

In the initial low-power density operation of LM-NSTAR at LVTF, the facility effects were limited but were observed. There was little variation of the plasma properties observed near the walls of the facility other than a linear increase in plasma density with increasing background pressure. The limited changes in the ambient plasma at the walls with changes in throttle conditions seemed to indicate limited beam-wall interactions. Changes in throttle condition or thruster operation were found to alter the plasma properties near the plasma screen, neutralizer and in the plume more than by ambient background pressure alone. It was proposed that the floating potential of the wall probes may give an insight into how much and at what point the beam plasma starts significantly interact with the wall. If there are high energy ions or a large amounts of low energy electrons present at the walls, than this could indicate too much beam plasma interaction with the facility.

The electrical coupling of the NSTAR thruster to the facility as well as the beam neutralization processes are important considerations in ground testing experimental design. Quantifying the electrical coupling of the thruster with the facility was investigated over various pressure ranges and electrical configurations of the thruster plasma screen. The neutralizer-facility coupling voltage, V_{cg}, for the most part, was less negative as the background pressure was increased. It was observed that floating the plasma screen increased the negativity of the coupling voltage (meaning V_{cg} became more negative). A more negative V_{cg} insinuated that the thruster is coupling more with the facility. This means the beam is being less directly neutralized by the neutralizer or an increase in beam potential is causing the thruster to couple more with the facility to neutralize it. Future measurements of the true-coupling voltage and the differences between beam potential and

neutralizer common potential will verify this. In regards to spaceflight perpetration the grounded plasma screen during ground testing will under-predict the needed neutralizer operating conditions to sufficiently neutralize the beam and allow proper beam propagation to prevent the formation of a detrimental virtual anode. Thus, floating the plasma screen during ground testing is recommend such that the real beam potentials will arise.

Pressure effects on the neutralizer characterization and margin were observed indicating that the onset of plume mode will occur at higher flow rates with an increase of background pressure. Furthermore, increased background pressure and plasma densities damped the magnitude changes and peak-to-peak oscillations of V_{cg}. It was also observed the most prominent ion energies near the neutralizer 90° to the thruster flats also decreased with pressure. It is speculated that the high energy ions are either elastically scattered ions from the beam or energetic ions from the neutralizer cathode. Although their source has yet to be confirmed, their presence is concerning as these ions at space pressures could easily sputter, damage, and erode nearby components in space but may not even be observed during ground testing at elevated background pressures. The neutralizer was also characterized with a floating plasma screen were everything behaved as expected. However, at higher flow rates the V_{cg} did begin to become increasing more negative with higher neutralizer electron temperatures measured as well.

Interactions of the thruster with facility can lead to changes in thruster performance and should be limited as much as possible. Floating the plasma screen affected the facility coupling voltage by eliminating an alternative neutralization pathway. Additionally a decrease in the power supply beam current was observed when the plasma screen was floating. As background pressure increased, so did the magnitude decrease in beam current. Thus, the grounded plasma screen does not properly shield out the higher energy electrons and can lead to artificially inflated beam currents and misleading thrust calculations.

Doubles-to-singles ratios determined after corrections for charge-exchange attenuation were applied did not behave as expected. There should have been a flat line over the range of background pressures as long as the throttle condition and operating parameters were held constant. The corrected doubles-to-singles ratios were higher at higher background pressures. This ruled out ingested neutrals as this would have caused the reverse affect. Suspicions are that localized pressures either in the chamber or in the probe have caused extra attenuation of CEX ions that are presently not accounted for in this correction procedure. As a result, elevated background pressures may be over critical of doubles productions compared to spaceflight.

Overall, the PEPL LVTF provided a too good of a spacelike environment for a 2.3 kW LM-NSTAR gridded ion engine. Although some facility effects were observed and future work identified, it was concluded that future testing would require a much more extreme environment of elevated pressures with facility walls in closer proximity to the thruster to really emulate the high-

power density of a 100 kW system. With limited availability of such electric propulsion systems available, future studies were designed to include a much smaller thruster, similar in design, that can be operated in a much smaller facility to emulate high-power density operation in an effort to make better recommendations and best practices for testing of future 100 kW systems.

8.1.2 High-Power Density

The next stage of testing involved operating a smaller thruster in an suboptimal facility to emulate high-power density operation of a 100 kW system in a facility like PEPL LVTF. To do this, the NASA 8 cm gridded ion engine was operated at the 200 W power level at the PSTL Rocket Chamber. Background pressures and throttle conditions were varied. In addition, the plasma screen and beam target were either grounded nominally or allowed to float to the plasma floating potential. During these test, not only were the facility effects observed but could be dominating over the thruster processes.

Plasma properties near the walls increased with increasing background pressure as in the low-power density case. There showed little variances in plasma properties with electrical configurations of the plasma screen and beam target other than the plasma and floating potentials being elevated when the beam target was floating positive with respect to ground. The collected electron current at the walls in the floating beam target was limited because emitted electrons via SEE or IIEE at the target cannot occur since the target was disconnected from facility ground. Floating potentials of the wall probes were often positive starting at 16 cm downstream of the thruster. Because the plasma potentials were typically only 2-3 V and with positive floating potentials, the electron temperatures were very low, often less than 0.5 eV. These in combination with the plasma densities being relatively high around 10^{13}-10^{14} m^{-3}, there appeared to be strong coupling of the beam with the facility walls through this wall plasma. Neutralization of the beam could have been augmented with low energy electrons from the wall plasmas making their way to the beam. They could accomplish this due to the densities of the ambient and beam plasmas being similar in magnitude. Decoupling neutralization via the facility from the neutralization via the neutralizer for a 100 kW testing may prove to be extremely difficult to decipher. Obscurity in the correct neutralization process leads to improper neutralizer characterizations for spaceflight.

The impact of high density ambient plasma was also seen in the beam plasma current profiles. In the very near-field, Faraday probe current sweeps around 0.5 cm downstream reveal two distinct regions: the beam and the ambient plasma. The ambient plasma current quickly saturated instead of continuing to drop-off with distance as seen in the low-power density case. Further downstream at 16 cm, the saturated currents were observed again but were now at much higher magnitudes due to the higher ambient plasma densities. The restriction of beam expansion and high back-

ground plasma densities were more evidence of non-spacelike neutralization. This non-spacelike neutralization by the increased ambient plasma is trickier to observe in ground testing because it will not necessarily appear as an increase of facility-coupling voltage. As a result, the plasma potentials in the beam as a function of downstream position are critical to understand the amount of neutralization from the ambient plasma.

To obtain the beam potential at various downstream positions, hot emissive probe profile sweeps of the beam were made. This process revealed that the neutralizer type along with electrical configuration of the plasma screen and beam target can have significant impacts on beam plasma potential profiles. The positive floating potential of the beam target elevated the plasma potentials all along the beam. A floating plasma screen increased the plasma potential peak in the very near-field but downstream potentials were more or less equivalent to the grounded plasma screen case. The plasma potentials in all cases decreased significantly when the background pressures were increased. The high plasma potential peak in the floating plasma screen was severely decreased and was almost identical to the grounded plasma screen case. The floating beam target plasma potentials increased due to the positive potential of the floating beam target. The changes in plasma screen potentials are less understood. The neutralization in the very near-field is being altered as the plasma screen is floating. There were changes in the plasma properties near the neutralizer such as increased electron temperatures with the "super" neutralized used in the plasma screen test campaign that may explain why the plasma potentials profile here were more peaked on center-line compared to the floating beam target test campaign using the nominal cathode that had lower electron temperatures and greater plasma densities. The plasma potential profiles in the very near-field also revealed dip and horn-like structures in their profiles that were reminiscent of double-sheath potential profiles. As this double-layer dissipates down stream, the ambient low temperature electrons can easily be drawn into the beam better neutralize it.

The neutralizer-facility coupling voltage, V_{cg}, has been typically used as a metric of how well the beam is being neutralized. This assumes the beam is fully neutralized and is at or near ground potential. In contrast to observations in the low-power density testing, the facility coupling voltage here became more negative with an increase of pressure. Previous thought conventions would insinuate that the beam was being less neutralized. However, the emissive probe plasma potential profiles reveal that the plasma potentials decrease with increasing background pressure, meaning better neutralization. As a result, the facility coupling voltage is not a good metric of beam neutralization. By its definition is a metric of the amount of coupling of the thruster to the facility itself. The better measurement of the neutralizer-beam coupling has always been the true-coupling voltage, V_{cp}. However, measurement of this value is not trivial to obtain as emissive probes can be fragile and set objects in the plume are not desired. But it was found that the plasma potential on center-line of the neutralizer via a cylindrical Langmuir probe proved to follow trends of the beam

plasma potential under various pressures and electrical configurations.

Further investigations of the true-coupling voltage were explored over various background pressures and electrical configurations. The increase in facility coupling voltage with background pressure was negated by floating the beam target. The floating beam target raised the plasma potentials everywhere in the chamber such that collection of electrons at the walls decreased, reducing facility coupling. The true-coupling voltages for the floating beam target matched over the lowest and highest background pressures. Testing of high-power systems can get better neutralizer characterization at higher-background pressures by floating the beam target such that the neutralization of the beam is dependent on the neutralizer performance and not the background pressure. Caution is advised as there is still unknowns with a floating beam target such as at what positive floating value is too high that a high flux of ions are returned to the thruster.

The floating plasma screen impacts were localized to the near-field. The plasma potential in the near field increases drastically with lower background pressures but causes are currently unknown. The facility coupling voltage did not change with the floating plasma screen and barely changed with the increased pressure. It is assumed that the floating plasma screen was changing the neutralization process in the near field but the ambient plasma and residual plasma bridge quickly neutralize the beam downstream. Since the plasma screen was tied to the spacecraft chassis in space and floats in the ambient plasma, it is recommended to float the plasma screen during ground testing to ensure the high potentials in the near field will appear as they do in spaceflight.

Artificially heating of electrons may be required to replicate the high potentials observed at lower background pressures. The idea would be to keep electrons from being so easily trapped by the beam. Neutral flow injection into the plasma bridge was thought to increase the impedance. However, this was later to be found ineffective for the floating plasma screen with a grounded beam target and was mainly dependent on neutralizer operating conditions more than the background pressure.

The impacts of neutral ingestion are more well-behaved on gridded ion engines due to the separation of the ambient neutrals to the ionization chamber due to the grids. The impedance in the discharge chamber varied linearly with pressure and varied very little over a large pressure range. A reasonable estimate of extrapolated discharge performance at lower background pressures are assumed to be plausible as result. Reliability of this assumption is given by the total ingestion fraction showing that at all ranges of ingestion fractions the affect on discharge impedance is still linear. Beam current, the thrust production mechanism, was also fairly insensitive to ingestion. But discharge operation is complex and although the powers and performance seem insensitive, the doubles-to-singles ratio could be altered and needs further exploration as high doubles can lead to lower thrust or enhanced erosion on the grids.

Generally, operating at high-power densities was not the issue, but decoupling the impacts of the

facility on beam neutralization and coupling became extraordinarily difficult at higher background plasma densities. The wall plasmas were also not purely charge-exchange and could be greatly impacted by the neutralizer plasma at these high-power densities. Better spaceflight predictions can be achieved by floating the plasma screen or beam target. One challenge of testing at high-power densities was determine the proper amount of neutralization necessarily in the very near-field as a high potential virtual anode does form at lower background pressures and can decrease thrust or cause damage to the spacecraft if not appropriately accounted for.

8.1.3 Target Glow & Impurities

The goal of this chapter was to highlight the importance of materials in high-power density ground testing of gridded ion engines. For ground testing of gridded ion engines sputtered materials and impurities in the plasma can impact thruster operation and the proper interpolation of data. Investigations of the composition of the witnessed "target glow" was performed to gather information on potential impacts of this plasma could be on thruster ground testing. Plasma impurities can have other major impacts as well. Probes and other diagnostics data can be interpreted incorrectly due to impurities affecting the measurements. The impact of sputtered material into the plasma on probes and diagnostics were documented with recommended correction procedures where possible.

It was determined that the target glow witnessed is not carbon or carbon clusters alone, but hydrocarbons and other reactive water species that stem from the water absorbed in carbon lattices. A mock-beam was first used to obtain the optical emission spectra of these species in this mock-beam test but later mass spectroscopy verified the presence of these species during actual thruster beam testing. Issues stemming from carbon materials have been known in the fusion community for decades but are now starting to become more relevant to the electric propulsion community as high-power density testing begins. These impurities in the plasma can be found everywhere in the chamber. They can deposit and create problems for cathode lifetimes, discharge impedance, and probe traces, etc. Future studies on density measurements and the magnitude of their effects on thruster operations are needed for these plasma impurities.

There was evidence of the plasma impurities derived from sputtered efflux and gas phase chemistry. Dirty wall probes lead to invalid measurements of electron temperatures, plasma potentials, and electron densities. It was observed that probes not impacted by high energy ions or using a cleaning bias sweep of -100 V to 100 V, suffer from dirty probe symptoms. A witness plate near the wall probe should huge amounts of sputter material deposited there only after two days of testing. ExB probe measurements were also attempted but revealed some increased CEX altered the obtained traces. The H9 Hall thruster plasma potential measurements also showed that objects in the plume and impurities in the plasma can have significant impacts on plasma measurements

making these impurities an issue for all EP devices.

8.2 Recommendations & Future Work

Recommendations and guidelines for gridded ion thruster ground testing can be made for both low and high-power density operation. These are more fully defined in Chapter 6. One set of guidelines is geared towards considerations that should be taken into account in building a new facility. In addition, guidelines are suggested for modifications that can be made to existing facilities including diagnostics to correct performance data.

There are some knowledge gaps in the interpretation of thruster operation in the low-power density conditions that are worth revisiting after what was learned in the high-power density testing cases. Acquisition of plasma potential profiles in the very-near field under various background pressures and plasma screen configurations provides insight into understanding the very-near field neutralization processes not well understood in the high-power density testing. Such measurements would also give better insight into the changes in true-coupling voltages under these conditions.

Although some preliminary testing was done with the floating plasma screen and beam target, the overall impact of both the plasma screen and beam target floating has yet to be fully understood. The near-field neutralization process may be drastically altered by potentially a positive floating plasma screen with a positive floating beam target. Using current knowledge, it is recommended to use a floating plasma screen, especially at lower pressures to capture accurate beam potentials in the near field. But to characterize the neutralizer, the floating beam target should be used as it is less susceptible to pressure affects.

Furthermore, due to hardware availability and stability, neutralizer characterization and margin tests were not performed at the high-power density conditions. Such data would go a long way to understanding the changes in neutralization and coupling under these conditions and determine if such measurements can be reliably done to qualify a thruster for spaceflight or if facility effects dominate. Improved double-to-singles measurements as a function of ingestion is also needed to better understand discharge performance under the high-power density operation conditions.

Measured plasma properties generated with in-plume probes can be impacted greatly by sputtered materials and impurities in the plasma. Materials such as graphite can store water and thus probes measure plasma not only due to the beam but also a background plasma consisting of water and carbon along with plasma-chemically generated hydrocarbons. This augmented plasma is usually derived from the shielding material of the probes themselves. The probes therefore measure this plasma chemical "soup" along with the beam. Coatings derives from such a plasma contaminate collecting surfaces leading to error in the interpretation of the plume plasma. This stems largely from probes behaving differently than as expected due to these impurities. Some best prac-

tices are needed for probe operation and facility design to mitigate these effects. Quantification of the densities of these impurities is also needed. Recommendations for best practices and designs to minimize these effects for facilities with confined spaces will need to be made.

Future work also requires actual testing of a 100 kW system in a facility like LVTF to see if the comparisons found here hold true. Additionally, the gold standard would be to have a thruster travel through all the stages for more accurate comparisons. The same thruster should be tested in a high-power density situation, then a low-power density test, and ultimately have its behavior investigated in space. This does not necessarily have to be a 100 kW system, as even a sub-10 kW system would give great insight into whether or not high-power density testing can be a viable option in the future for reduced costs.

APPENDIX A

Review of Beam Neutralization of Gridded Ion Thrusters

A.1 Abstract

Gridded ion engines have been a concept since the 1950s and utilize the rocket equation to produce thrust via an exhausted ion beam. To prevent space-charge drag and loss of thrust, electrons are also emitted from the spacecraft to neutralize the beam. Although beam neutralization of a non-relativistic beam has been demonstrated, the current mechanics of the neutralization are not well understood. In addition, beam neutralization in space versus ground testing has exhibited consequential differences. Understanding and obtaining beam neutralization is the upmost importance in preventing loss of thrust and beam divergence. This paper reviews the modeling attempts since the 1960s to capture and validate experimentally the beam neutralization process of a gridded ion engine. Results show that although much progress has been made, there are still unexplained and unaccounted for phenomenon in the neutralization process.

A.2 Introduction

Plasma is the fourth state of matter. As energy is added to a system the solid turns to a liquid, liquid to a gas, and a gas to a plasma. A plasma can be either partially or fully ionized gas that consist of positive and negative particles, that as a whole, follow a collective behavior. However, in a plasma, individual particles are affected by localized electric and magnetic fields. Although not necessary, typical plasmas consist of positive ions and free electrons. For this paper, references to a plasma will follow this standard convention of positive ions and free electrons. Plasmas have a range of applications such as fusion energy, semiconductor manufacturing, electric propulsion, medical, water treatment, etc. In each application, the density and temperature of the plasma used varies, and as a result, so does the mathematical equations used to model plasmas. Due to the

collective behavior exhibited by plasmas, while also maintaining individual particle actions, there are multiple models used to model plasma behavior based on the temperature and density of the plasma regime. The main three regimes that could be involved in electric propulsion modeling are discussed here. Following the model descriptions, a section on gridded ion engine operation is presented.

A.2.1 Modeling Theories

In the limit that the ion and electron distributions cannot be assumed to be thermalized/Maxwellian velocity distribution, or in other words, because the mean free path of particles is very large and particles may not interact with one-another over very large time scales, kinetic theory is applied. This is done by integrating over all the individual particles to solve for each particles individual Lorentz force based on proximity to other particles. There are two typical cases for kinetic theory, collisionless and collisional. In the collisionless case, the Vlasov equation is solved. In the collisional case, particle-to-particle interactions are not frequent but occur enough that it changes the collective behavior of the plasma and thus the Boltzmann equation is solved instead. Because of the tracking of individual particles, this method is the most computational expensive simulations, especially when modeling of collisions is incorporated. Both collisionless and collisional kinetic theory could be coupled with an electron fluid assumption to develop a hybrid model. In the hybrid model, an electron fluid approximation is made assuming electrons have a Boltzmann distribution. If ions could also be considered to have a separate Boltzmann distribution, then they too could be modeled as a fluid and the two-fluid model is produced. In the limit that electrons and ions thermalize and couple together, the magnetohydrodynamic (MHD) equations can be used. This is typically only in a very collisional case where the the mean free path of ions and electrons is much smaller than the system length.

A.2.2 Gridded Ion Engines Operation

Gridded ion engines (ion thrusters or ion rockets) are an electric propulsion devices used in space for exploratory space missions, orbit keeping/transfer, etc. They leveraging the rocket equation to produce thrust by electrostatically accelerating ions to produce a high velocity ion beam. These devices are known to have some of the highest specific impulse (an efficiency measurement of thrust per unit of mass) of any propulsion device. Ion engines are in their element in space as currently they typically produce less than a Newton of thrust, but in the absence of drag forces and with the incremental compounding of thrust over time leads to continuous spacecraft acceleration and spacecraft velocities that can reach to the order of 10,000 mph! However, if one were to expel only ions to produce the beam, the spacecraft would charge negatively and could lead to

beam turnaround, the expelled ions returning to the spacecraft, and space-charge drag. This would result in the nullification of thrust produced. As a result, beam neutralization must occur for both charge and current in order to maximize thruster and efficiency of the engine. In this regard, charge neutralization refers to equal amounts of electrons and ions in the beam and current neutralization referring to equal emissions of electrons and ions from the spacecraft to prevent charge build up. Neutralization is done by a separate neutralizer subsystem that injects electrons into the beam.

A.3 Scope of the Problem

First most, as one may see, it is upmost importance to choose the right governing equations when developing a computational model for an plasma simulation. In electric propulsion, more specifically gridded ion engines, typically the ion mean free path ($\lambda_{mfp,i}$) in the ion beam plume is much greater than the ion Debye length (λ_{Di}) due to the electrostatic heating, but the $\lambda_{mfp,i}$ is less than the overall system length, the length of the beam. However, the electron mean free path ($\lambda_{mfp,e}$) is typically smaller than the length of the beam. In this limit, the ions are collisionless in respect to other ions, where as the electrons are original assumed to be collisional in most cases. It will be discussed further that his not always the case and electrons are sometimes semi-collisional. In the presence of a background neutral gas, the ions mean free path to neutrals is relatively small and these collisions need to be accounted for. In this regard, two-fluid and MHD are not ideal, however some studies have been performed [155]. On the other hand, collisionless kinetic theory is not really applicable either as there are enough collisions to cause deviation. In this limit, a it seems kinetic theory with collisions solving the Boltzmann equation would be ideal, however, this is the most computational expensive method. Some work has been done in using hybrid methods of kinetic ions with fluid electrons, but some would argue certain electron kinetic effects are still missing and is the investigation of this review.

As of current, beam neutralization of a gridded ion engine is known to exist in space, but its mechanisms not fully understood nor does neutralization process during ground test match within reason to that of actual space flight. The limitations in computational cost and complexity of experimentally simulating space during ground test has partially accounted for the current gap of understanding and identification of the predominate beam neutralization processes. Although beam neutralization in other fields has been achieved through background gas ionization[156], this is not the case in space flight due to lack of background neutrals and the fact that the beam is also non-relativistic. In addition, flight data of previous ion engines show discrepancies in thruster performance and differences in beam neutralization mechanics are not well understood when compared to ground test data [32, 157, 158, 159, 109]. This makes it difficult to understand how an ion beam in space is actually neutralized without testing in space as ground test do not seem to be

sufficient.

As such, the best understanding of the mechanisms of beam neutralization in space can be best gleaned from computational models. However, these results are only trustworthy if these models can be validated with experimental data. Thus, modeling of beam neutralization in ground facilities must be modeled and validated via experimental data to substantiate beam neutralization in space results. However, in such domains manifest the computational issues and costs of large domains having to resolve small mesh cell sizes to fully capture all kinetic effects and collisions. This review, although not exhaustive, tries to summaries work since the early 1960s to model beam neutralization of gridded ion engines with supporting experimental findings. The aim is to summarize the effects of key assumptions made in regards to their effects on observed neutralization mechanisms. In addition, key models and experiments needed to understanding/validating neutralizing process are also touched upon.

A.4 Results

The following sections are separated into two categories, model development and environment replication. Model development entails the how advancements in computational abilities allowed for more physics to be modeled and observed. The environmental replication section describes the attempt and effects of modeling to actual test environments such as chamber walls and neutralizer location. Differences in models between simulations of beam neutralization in space versus ground testing and how specific parameters can affect the neutralization process are also discussed.

A.4.1 Model Development

A.4.1.1 Governing Mathematical Equations and Solvers

Earliest modeling work in regards to ion thruster beam neutralization used a particle-in-cell (PIC) method to track macroparticle electrostatic interactions with one another [160, 161, 162, 163]. Due to computer memory restraints, the marcroparticles are used to represent large amounts of particles, sometimes 10^7 or even larger. This allows for a relatively ideal likeness of true amount of particle modeling but lower memory cost while still maintaining a sense of individual particle motions. In the electrostatic (ES) case, typically the Poisson's equation is solved for charge density and in turn, electric fields. This can be done both explicitly or implicitly. Explicit schemes decouple the particle movement and field solver [164]. Gridded ion engines are considered an electrostatic device and do not necessarily need to be modeled by electromagnetic (EM) PIC, but can be done in for cases such as spacecraft charge [34, 165].

Due to the large ion-to-electron mass ratio, the time steps of each solver iteration has to be resolved at electron time-scales in a full-PIC model. This can be very computational expensive. Alternatively, a hybrid-PIC may be used where electrons are assumed to follow Boltzmann distribution. This allows for electrons to be treated as a fluid instead of individual particles. In this case, only ion particles have to be tracked and ion time scale can be used for the time step. Although this method is much faster and less memory, there is a trade-off in accuracy of electron motion if electrons do not follow a Boltzmann distribution, and in beam neutralization cases, this may not be an acceptable assumption [166, 167, 34, 168, 169, 170, 164, 171]. Some modeling work has been done using other models such as PIC-MHD electrons [155] or particle-particle codes [172] but are often specialized or validation cases only.

A.4.1.2 Model Dimensions

The diode modeling of Lomax [160], and Birdshall and Bridges [161], along with beam neutralization models of Buneman and Kooyers [162], and Dunn and Ho [163] were only capable of running 1D models. Their models were first developed to prove beam neutralization of an ion thruster was possible and such a thruster could produce thrust in space. In their models they witnessed electrons where trapped by the potential well of the beam and oscillated back and forth between the beam front and electron source. Their work was validated by experiments done by Bernstein and Sellen [173] and later the SERT I test showed neutralization of the beam and thrust were possible in space [82]. Progress quickly expanded to 2D models and eventually 3D. This allowed for experimental modeling of not only an electron source inside the beam, but also externally [174].

As more dimensions were utilized, changes in results was observed by Wadha et al. it was found that in comparison to 1D cases of Buneman et al. and Dunn et al., the required electron current to neutralize the beam was less than the 1D scenario [174, 175]. They speculated it was the extra degree of freedom that allowed energy to be in other directions. In addition, 2D effects lead to observations of electron solitary waves (ESWs) in beam neutralization [176]. The ESWs are essential moving electron holes or in other words, moving electron potential wells. Unfortunately, ESWs are thought to impede beam neutralization as they can heat and eject electrons out of the beam. As the third dimension was added, it allowed observations of other Trivelpiece–Gould (TG) surface waves excited by the ESWs which also tend to slow down beam neutralization [177]. Although the added dimensions give raise to more observed physics, the mechanism of neutralization seems to be non-linear due to raise of ESWs and TGs charge mixing and their impedance on neutralization process. Furthermore, longer time studies on these non-linear mechanics are needed to understand their dampening process and stabilization to a steady-state.

A.4.1.3 Resolving Debye Lengths and Time Scales

Assuming an ion is a proton, the mass is 1836 times larger than an electron. As a result, electrons typically account for the movement in a plasma and thus why the plasma frequency is defined by the electron oscillations around the ions. Because of the greater electron mobility, for effective PIC codes, the electron Debye length must be resolved to ensure all electron kinetics are captured. Early models typically used only a proton as an ion instead of the real ions such as cesium or xenon, which can be orders of magnitudes larger. The mobility of the ion increases and approaches that of an electron as the mass of the ion gets closer to the mass of an electron. Thus, while resolving electron time scales one would observe more ion movement in that same time step as the ion mass approaches that of an electron. This can significantly decrease the number of time steps needed to achieve a steady-state solution.

In regards to beam neutralization, this assumption of lowering the ion mass was thought to have very limited effects on the observed physics of ions. However, the work of Jambunathan and Levin indicated that the mass of the ions does change beam neutralization [164]. As expected, the divergence of the beam itself was less due to the decreased in ion mobility and trapping electrons in the beam when the true mass of xenon atoms was used. In addition, because the electrons are trapped in a tighter beam, electron temperatures are higher when true ion masses are used. This can affect the efficiency of beam neutralization as higher energy electrons are shown to be ejected out the beam [176, 178, 179]. On the other hand, higher energy electrons maybe trapped more effectively because of the higher mass ions.

Othmer et al. used a true xenon mass, but for the computational limits of their time, the computational cost were too high and thus they had to use higher velocities for both electrons and ions. These inflated velocities allowed them to use a larger grid mesh cell sizes and speed up the simulation such that the using true xenon mass could be possible. They found that the ratio of electron thermal velocity to ion bulk flow velocity to be important. This was not a new concept as other works have also found this ratio to be of importance [163]. In Othmer et al., they found that if the ratio of electron thermal velocity to ion bulk flow velocity was greater than 1.7, than two-stream like instability appears whereas below 1.7 results in a shock-like front in which the "shock" thermalizes the electrons to a Maxwellian velocity distribution. Othmer does mention that this shock-like feature is not seen in current thrusters as the electron thermal velocity to ion bulk velocity ratio in thrusters is typically greater than this critical 1.7 value. Wheelock et al. did not use the true xenon mass as they suspected that the increased velocities affected the physics when collisions are considered [180]. Their results indicated that it is not necessarily the ratio of the velocities but the temperature of the electrons. This continues to raise questions to what is the controlling parameter that effects neutralization,the ratio of velocities or electron temperature?

A.4.1.4 Collisions

PIC models work well for collisionless plasmas with non-Maxwellian velocity distributions. But when collisional effects begin to occur more frequently, no longer is a simple PIC model enough to capture all the kinetic effects. To capture the collisional effects, typically for background neutrals, PIC is often coupled with either a Monte Carlo Collision (MCC) or Direct Simulation Monte Carlo (DSMC). In MCC there is no pairing of particles for collisions like in DSMC, therefore, unlike DSMC, MCC is non-energy conserving. MCC is easier and faster to implement and is typically a valid assumption when collisions with neutrals is very small. However, in the limit that momentum exchange (MEX) and charge exchange (CEX) factors become influential, DSMC should be incorporated.

Fluctuations in the beam potential where seen to regulate electron supply and demand to the beam via a virtual cathode electron sheath emitter in early studies [174]. Wadhwa mentions that in the presence of readily available electrons in the case of an externally located neutralizer neutralizes the beam very effectively. It seems this virtual cathode regulates the flow of electrons into the beam. Similar results are found in other studies involving pooling of electrons due to overshoot [34]. Neither study accounted for background neutral effects. Experimental work of Intrator et al. indicated that virtual cathode is destroyed by CEX ions and thus background neutral density is important for understanding beam neutralization [181]. Simulations done by Jambunathan and Levin which do have an external neutralizer and background neutrals shows a bimodal electron velocity that eventually resolves around zero does appear during neutralization [164]. Their results indicate that their is this virtual cathode like affect at first but is destroyed as time continues maybe an affect of CEX ions returning as stated by Intrator. Usui however did mention that they wished to perform longer simulations to see a steady-state. Thus, further time studies are needed to understand the destruction of the virtual cathode in beam neutralization with regards to CEX plasma affects.

Another reported issue that limits beam neutralization a is the formation of a virtual anode even in the presence of CEX plasma. A virtual anode was formed in the work of Wheelock et al. when not enough electrons are present or high velocity electrons are not properly trapped [180]. This virtual anode causes the beam to turn around or reflect, and as a result indicates poor neutralization. Later work by Wheelock explored the variation of in electron-to-ion current ratios. They found they were unable to achieve current neutralization [182]. Wheelock again investigated velocity-drag and two-stream instability in current coupling of the neutralizer to beam but do not find a sufficient correlation of the current coupling mechanism [183]. These findings indicating that although CEX is important, the supply and temperature of electrons may have more of an impact on beam neutralization.

A.4.2 Environment Replication

A.4.2.1 Facility Chamber Modeling

In some of the earliest beam neutralization simulations, the typical study was only allowed to run in transit state due to the computational time step limits of the time and unrealistic boundary conditions [162, 163]. Original boundary conditions used were field-free space, which works while in startup and propagation into space but cannot resolve stead-state situations nor explain the neutralization process in a chamber. In addition, the beam must be terminated before reaching the boundary or numerical instabilities could arise in full-kinetic simulations [166].

A new boundary condition is needed not only to prevent numerical instabilities, but to also allow beam neutralization simulations up to steady-state. In Brieda et al., they explain that full-kinetic PIC models can develop an "electron jet" numerical instability. This occurs at absorbing boundary conditions where there the potential is very sensitive to changes in charge distributions. If an electron is removed from the system at this absorbing boundary condition by random-walk, there suddenly develops a large positive potential where the electron was evacuated from. Because of the greater mobility of electrons, electrons are accelerated to this potential to charge neutralize it. However, as they accelerate towards this positive potential, they too pass the potential and get absorbed by the boundary conditions, increasing further the issue until an exiting "jet" of electrons is created. Brieda corrects for this with a conservation of energy boundary condition that corrects for this instability by filtering if electrons are absorbed or reflected by the boundary. The difference in kinetic and potential energies are used to determine if electrons would be trapped by the exiting beam and thus be absorbed by the boundary, or those that would random-walk out of the domain are instead reflected back into the domain [166]. Other works develop similar and expand on this new boundary condition [170, 184, 185, 171].

The use of conservation of energy boundary condition works for replicating a space, however beam neutralization replication during ground test also needs to be investigated and validated. Field-free space and boundary conditions cannot be used as the walls of ground test chamber are typically grounded and as a result prematurely terminate the plasma plume expansion [186, 187]. In the work of Chang et al. and Wang et al., they found that chamber wall proximity increased the potential of the plasma outside the beam expansion. The beam in both causes is still neutralized, however, the large potential in outside the beam indicates there is more coupling to the facility as expected. Later, Hu et al. determined that the beam target or beam dump need to be at least 20 times the radius of the thruster beam downstream of the thruster or its presence would affect beam expansion[188]. However, in both these cases the ion-to-electron mass ratio was 1836, ions being represent by protons. Because the mass of typical propellants is much larger, the ions should not be as mobile and beam expansion would be less. Not directly neutralization, the plasma plume

expansion from the beam is important to consider as it can alter the magnitude of the coupling effect of the beam plasma to the facility and as a result, the neutralization mechanics.

A.4.2.2 Neutralizer Location Effects

Due to the short life-times of immersed or wire neutralizers located in the beam, modern gridded ion engines typically have an external cathode used to provide a source plasma of electrons for the beam neutralization process. Early work by Buneman et al., Dunn et al. and others typically modeled an immersed or co-located neutralizer as that was the initial design for SERT I. After the successful neutralization demonstrated by SERT I and general agreement with models, work began on improving lifetime of the neutralizer. This spurred experimental work on externally located neutralizer in regards to the SERT II engine testing [189, 49, 190, 191, 192, 193].

As mentioned in a previous sections, the introduction of 2D and 3D models added some new physics to be observed and it allowed for testing of external neutralizer. Initial studies continued to show oscillations in potential and electrons reflecting back in forth in the beam as explained previously [174, 175]. Wadhwa indicates that neutralization of the beam with an external neutralizer performs better when a more sufficient electron current is emitted. Later work by Usui et al. using a full-PIC actually showed electrons accelerated by the beam potential create high energy electron pools as these electrons overshoot the beam. These overshooting electrons then get pulled back into the beam as they cool [34]. These bimodal electrons simply cannot be modeled correctly using a hybrid fluid electron approximation. Similarly, Jambunathan and Levin found that hybrid-PIC cannot be used for modeling electron dynamics in plume expansion and beam neutralization for an external neutralizer for similar reasons [194]. Furthermore, they expect that the deviations in ground test to space-like simulations are contributed to background neutral density and chamber wall boundary conditions. As such, models of varying background neutral density in bounded boundary conditions should be explored and validated with experiments.

A.5 Summary

In order to capture the proper dynamics and mechanisms of beam neutralization of a gridded ion, a 3D full-PIC/DSMC with proper ion-to-electron mass ratio is needed and any assumption of anything less will leave out some necessary physics. Models must also account for boundary conditions in replicating space or ground test, as plasma plumes do vary and in turn, the beam neutralization process. Although significant progress has been made in understanding the mechanisms of beam neutralization thanks to computational improvements and advanced models, there still is a large gap of understanding of what are the most driving factors and how steady-state neutralization

is achieved in both space and ground test conditions. Further investigation into long-duration and steady-state beam neutralization in the onset of ESWs and TG waves is needed to understand their impedance effects on beam neutralization and their damping. In addition, future insight into the prominent parameter of beam neutralizer, whether that be the ratio of electron thermal velocity to bulk ion velocity, electron temperature, or something else. The differences in ground test to space flight also need to be more thoroughly characterized via boundary conditions, background neutral density, and effects of plume expansion on neutralization. In conjunction, more experimental work is needed in order to validate these models such that ground test models can be used to extrapolated to space flight performance with better degree of accuracy.

APPENDIX B

Additional NSTAR Data

B.1 Wall Probe Pressure Study

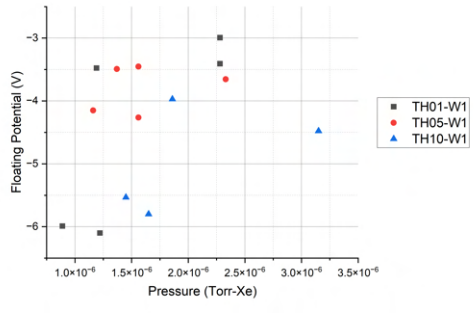

(a) NSTAR wall floating potential 0 cm

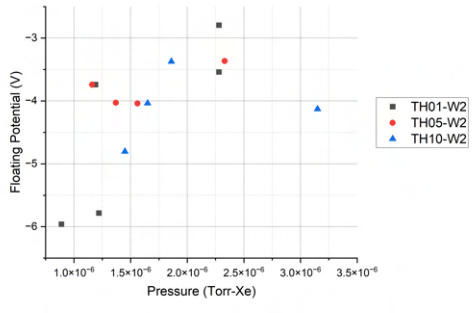

(b) NSTAR wall floating potential 76 cm

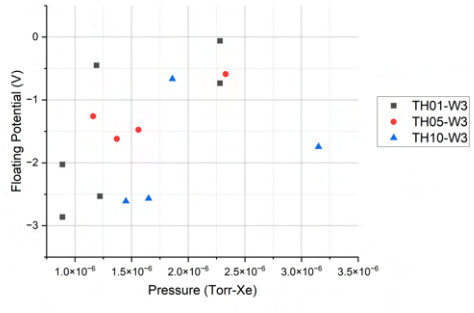

(c) NSTAR wall floating potential 133 cm

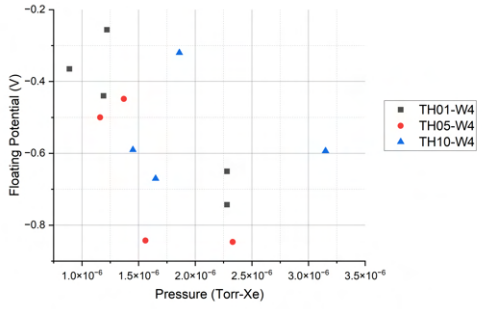

(d) NSTAR wall floating potential 293 cm

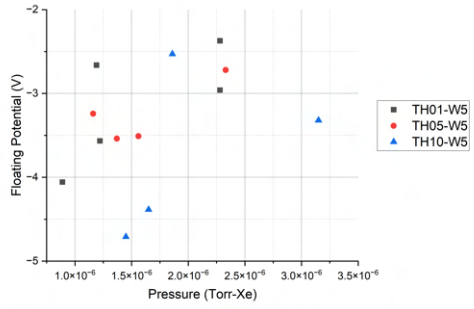

(e) NSTAR near plasma screen floating potential

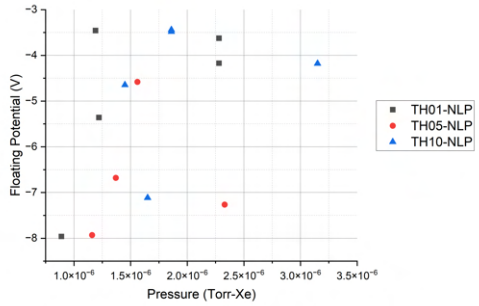

(f) NSTAR neutralizer floating potential

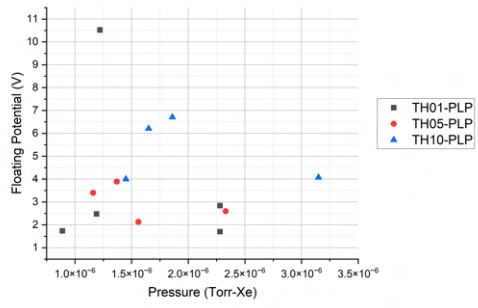

(g) NSTAR planar probe floating potential on centerline 208 cm

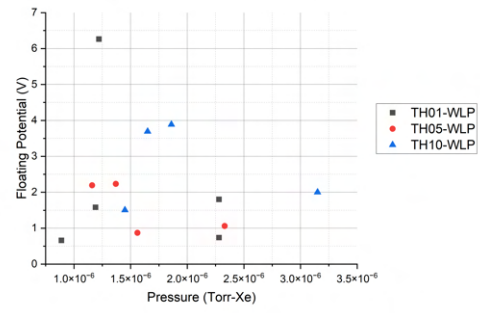

(h) NSTAR wire probe floating potential on centerline 208 cm

Figure B.1: NSTAR probes floating potentials pressure study

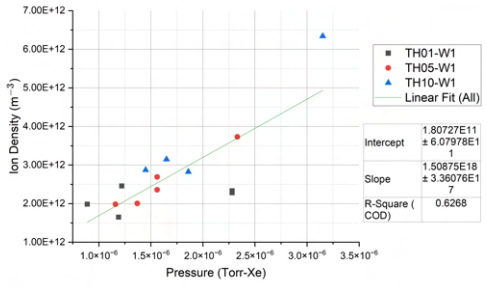

(a) NSTAR wall ion density 0 cm

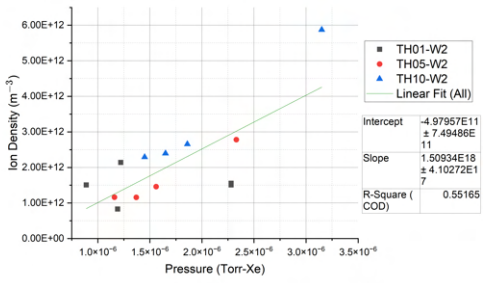

(b) NSTAR wall ion density 76 cm

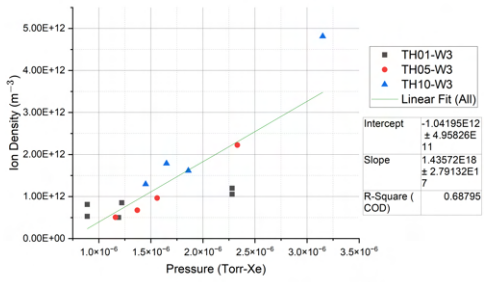

(c) NSTAR wall ion density 133 cm

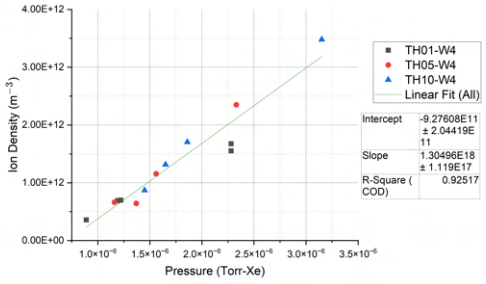

(d) NSTAR wall ion density 293 cm

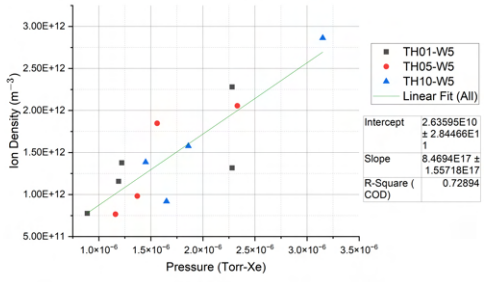

(e) NSTAR near plasma screen ion density

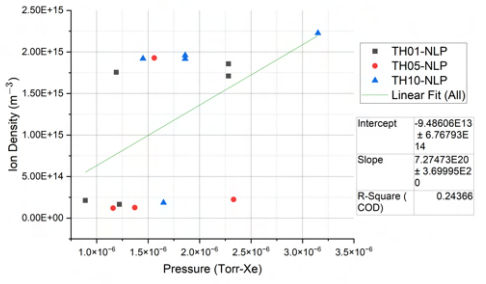

(f) NSTAR neutralizer ion density

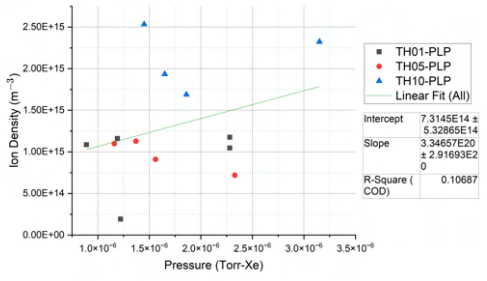

(g) NSTAR planar probe ion density on centerline 208 cm

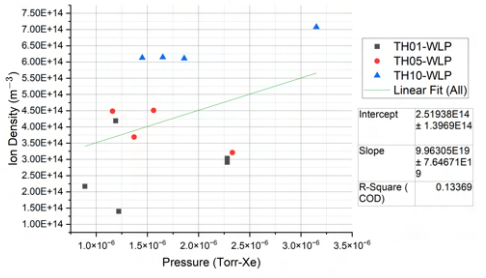

(h) NSTAR wire probe ion density on centerline 208 cm

Figure B.2: NSTAR probes ion density pressure study

APPENDIX C

Additional NASA 8 cm Data

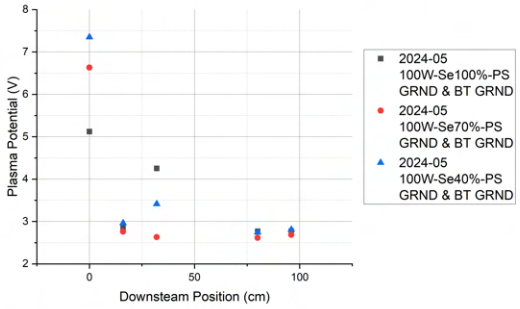

(a) Plasma potential

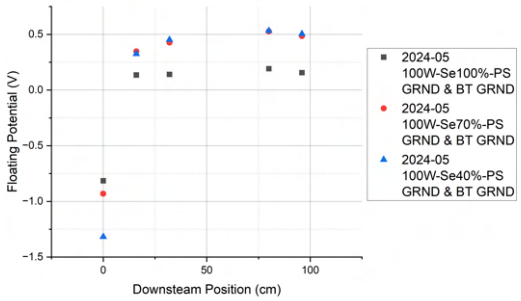

(b) Floating potential

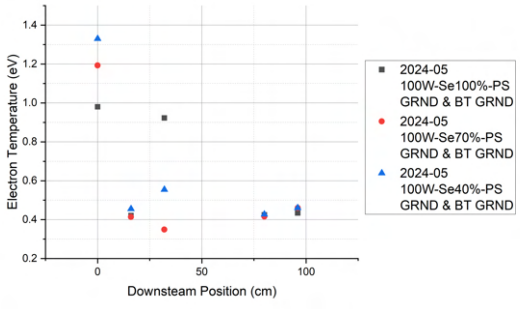

(c) Electron temperature

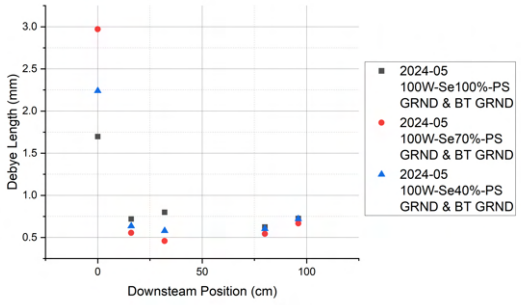

(d) Electron Debye length

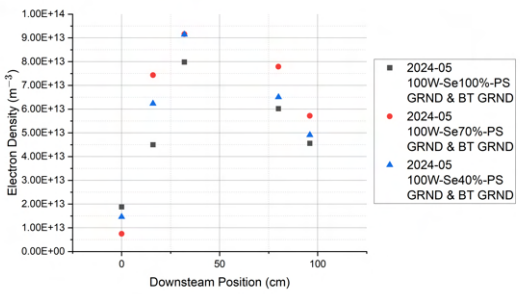

(e) Electron density

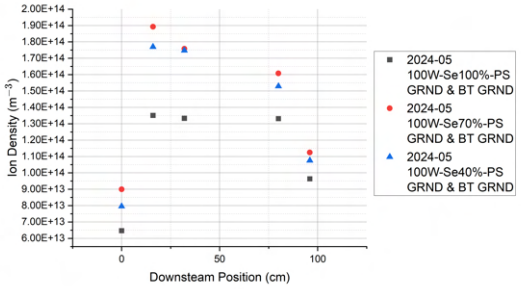

(f) Ion density

Figure C.1: 2024-05 NASA 8 cm 100 W with “super” neutralizer, grounded plasma screen, and grounded beam target wall probes pressure study

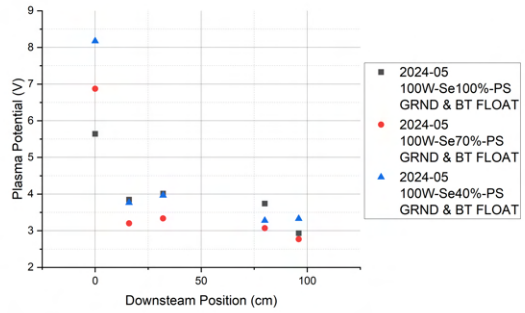

(a) Plasma potential

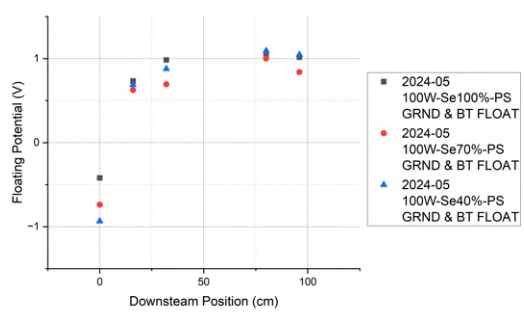

(b) Floating potential

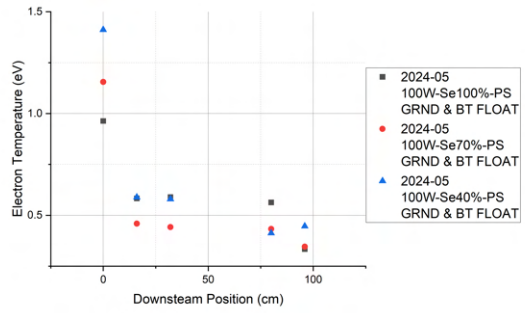

(c) Electron temperature

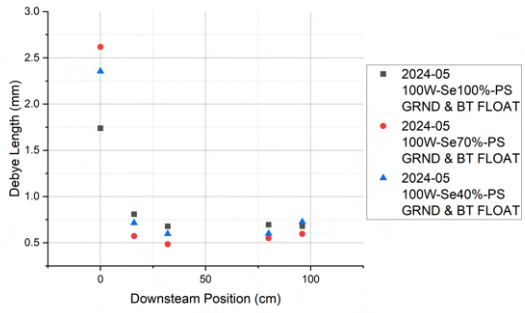

(d) Electron Debye length

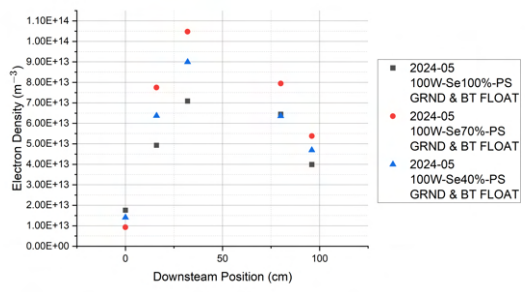

(e) Electron density

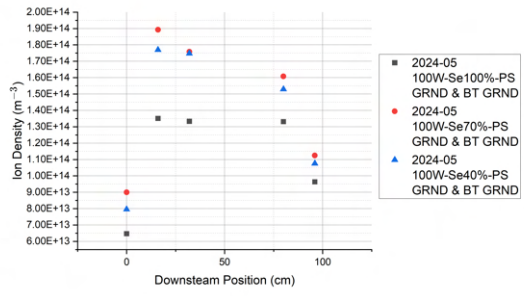

(f) Ion density

Figure C.2: 2024-05 NASA 8 cm 100 W with "super" neutralizer, grounded plasma screen, and floating beam target wall probes pressure study

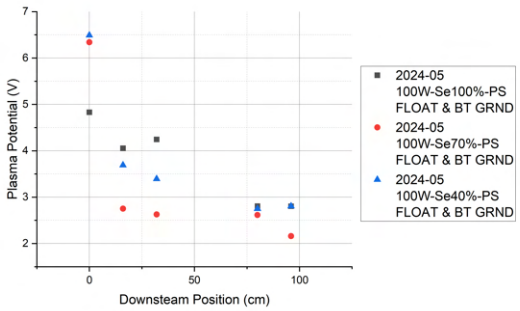

(a) Plasma potential

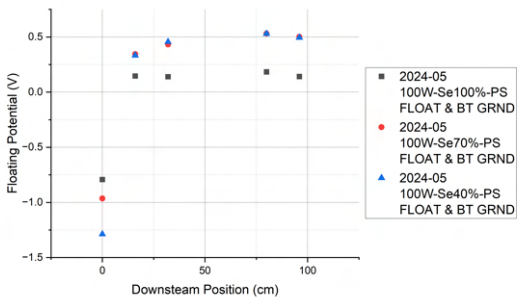

(b) Floating potential

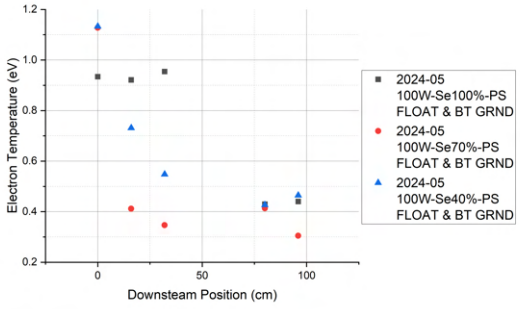

(c) Electron temperature

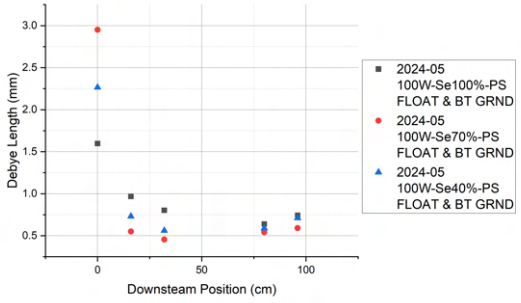

(d) Electron Debye length

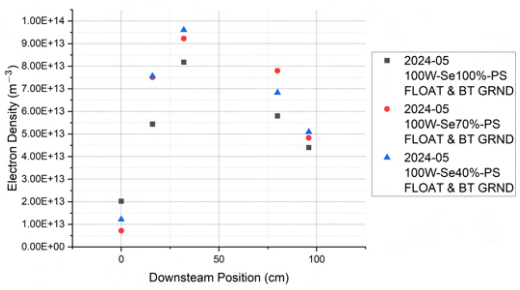

(e) Electron density

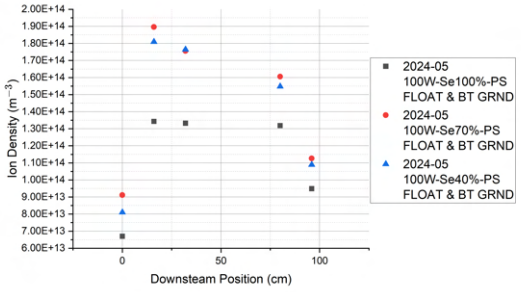

(f) Ion density

Figure C.3: 2024-05 NASA 8 cm 100 W with "super" neutralizer, floating plasma screen, and grounded beam target wall probes pressure study

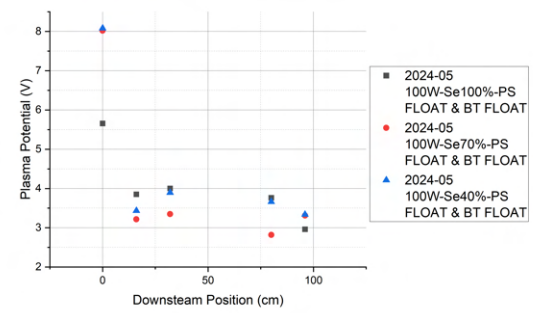

(a) Plasma potential

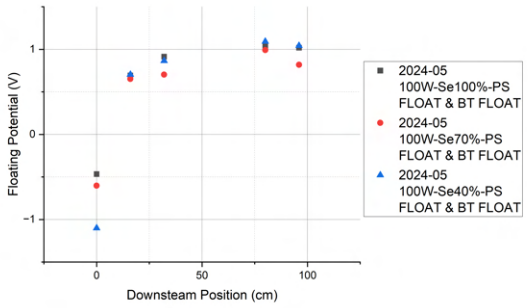

(b) Floating potential

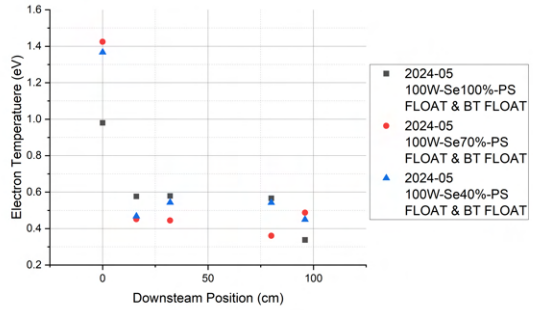

(c) Electron temperature

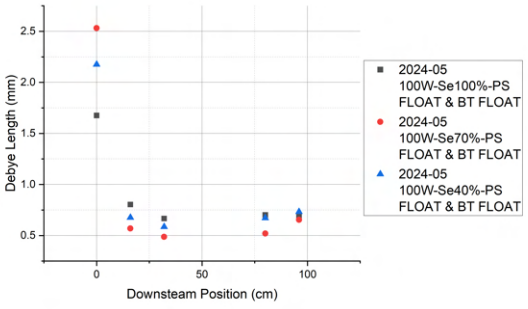

(d) Electron Debye length

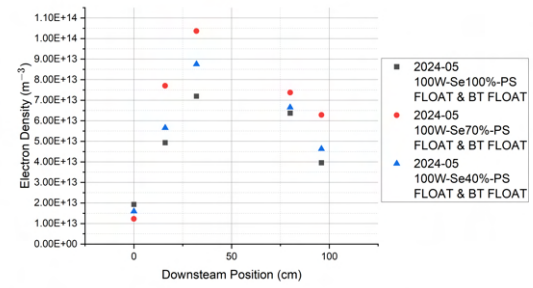

(e) Electron density

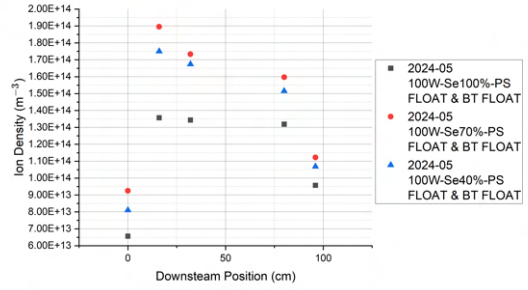

(f) Ion density

Figure C.4: 2024-05 NASA 8 cm 100 W with “super” neutralizer, floating plasma screen, and floating beam target wall probes pressure study

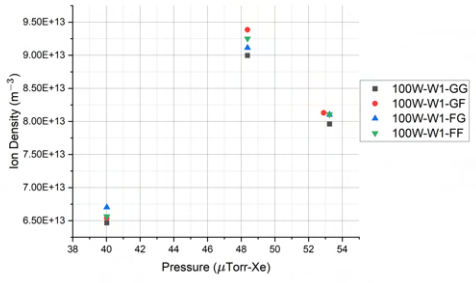

(a) Left-side wall probe 1 at 0 cm downstream

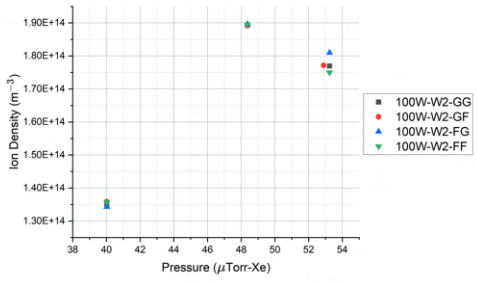

(b) Left-side wall probe 2 at 16 cm downstream

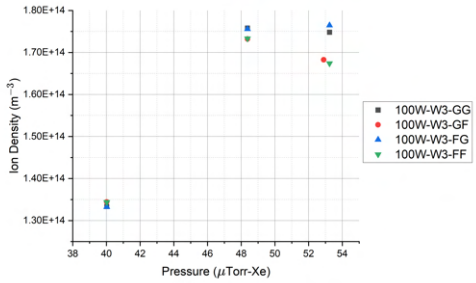

(c) Left-side wall probe 3 at 32 cm downstream

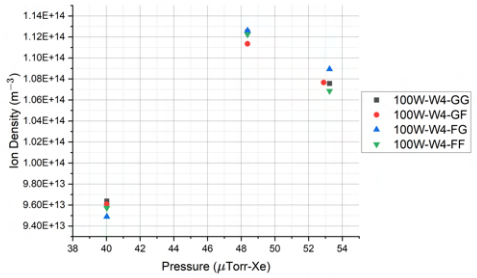

(d) Left-side wall probe 4 at 96 cm downstream

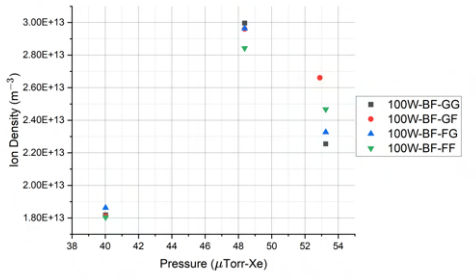

(e) Left-side of the plasma screen

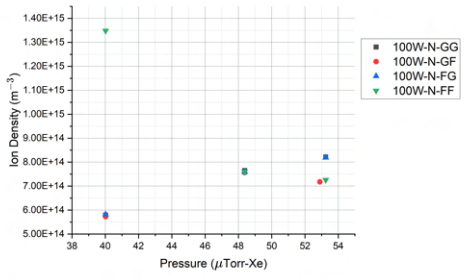

(f) Downstream 4 cm of the neutralizer

Figure C.5: 2024-05 NASA 8 cm with "super" neutralizer ion density pressure study

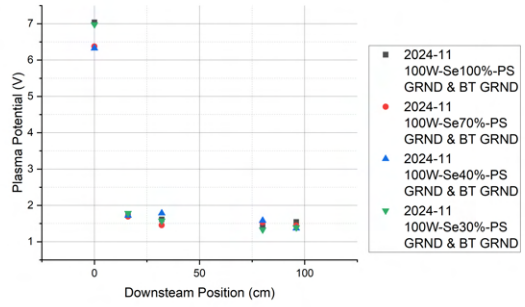

(a) Plasma potential

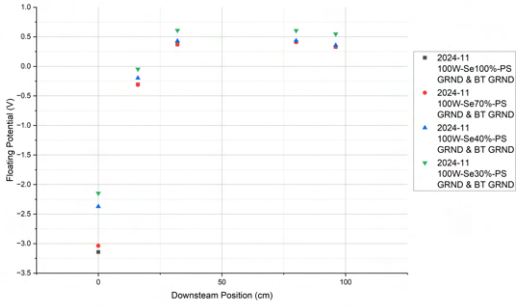

(b) Floating potential

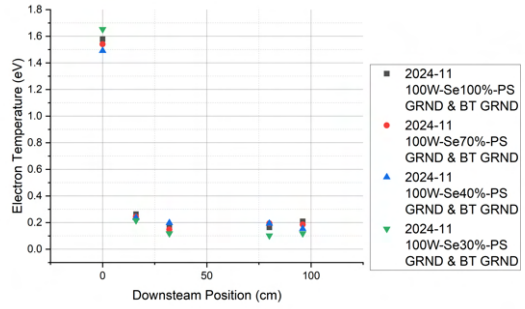

(c) Electron temperature

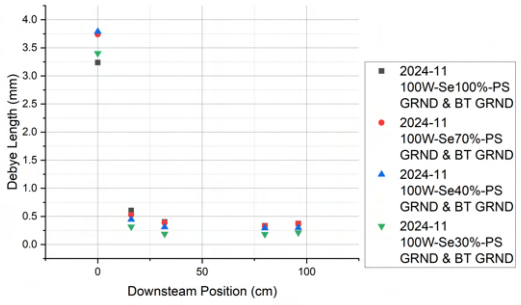

(d) Electron Debye length

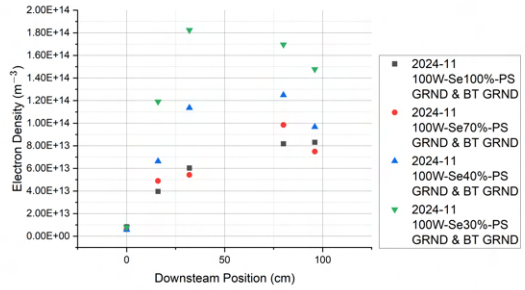

(e) Electron density

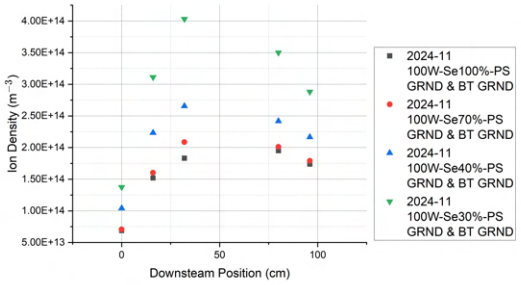

(f) Ion density

Figure C.6: 2024-11 NASA 8 cm 100 W with normal neutralizer, grounded plasma screen, and grounded beam target wall probes pressure study

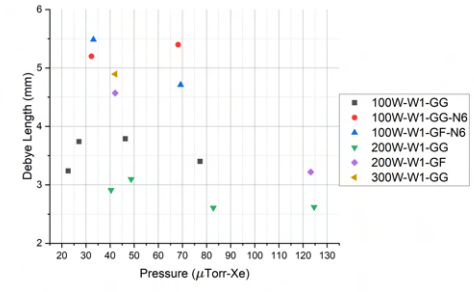

(a) Left-side wall probe 1 at 0 cm downstream

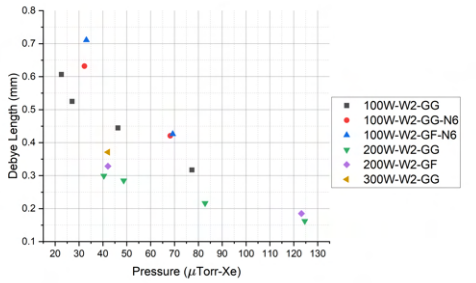

(b) Left-side wall probe 2 at 16 cm downstream

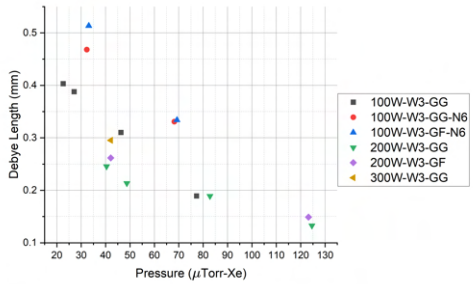

(c) Left-side wall probe 3 at 32 cm downstream

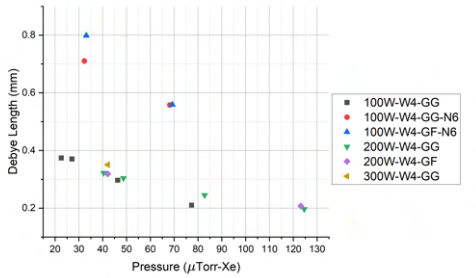

(d) Left-side wall probe 4 at 96 cm downstream

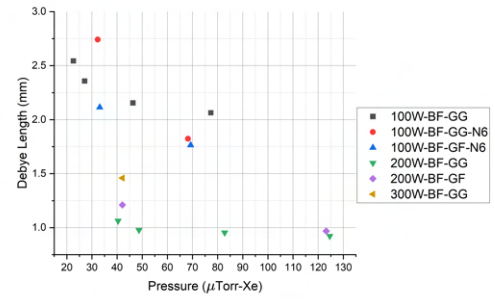

(e) Left-side of the plasma screen

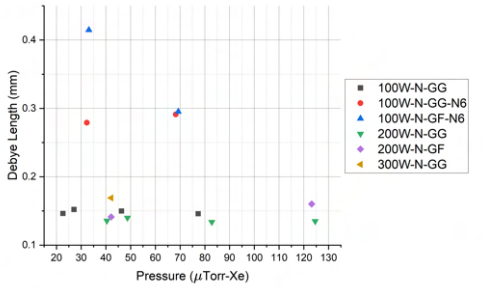

(f) Downstream 4 cm of the neutralizer

Figure C.7: 2024-11 & 2025-01 Debye length pressure study

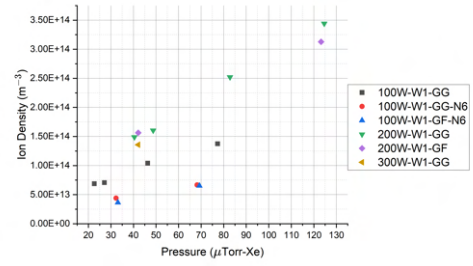

(a) Left-side wall probe 1 at 0 cm downstream

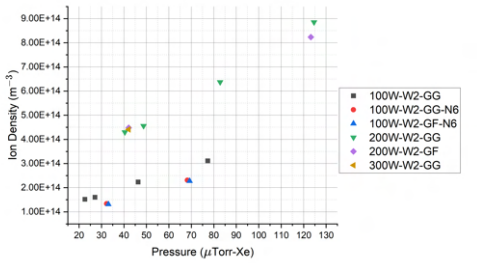

(b) Left-side wall probe 2 at 16 cm downstream

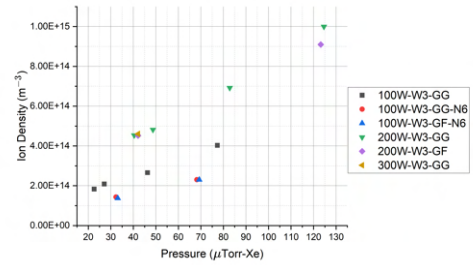

(c) Left-side wall probe 3 at 32 cm downstream

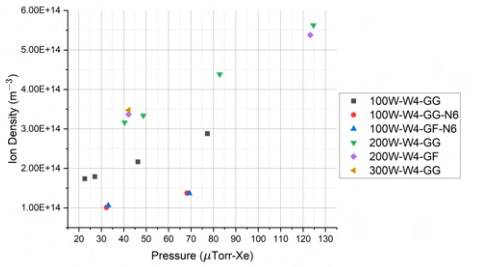

(d) Left-side wall probe 4 at 96 cm downstream

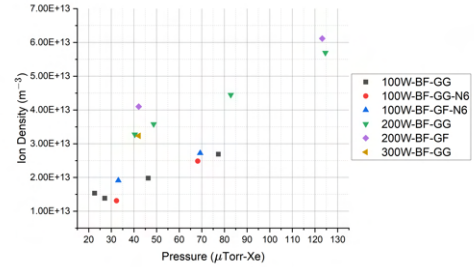

(e) Left-side of the plasma screen

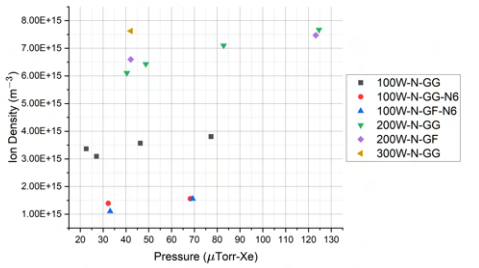

(f) Downstream 4 cm of the neutralizer

Figure C.8: 2024-11 & 2025-01 ion density pressure study

Table C.1: 2024-11 NASA 8 cm at PSTL RC at 300 W with nominal neutralizer and heater on, grounded plasma screen and grounded beam target

300W-GG	100%
C [sccm]	1.75
M [sccm]	1.95
N [sccm]	0.75
NKPR* [V]	26.7
NKPR [A]	0.97
DISC [V]	31.4
DISC [A]	1.906
BEAM [V]	1200
BEAM [mA]	157.0
ACCEL [|V|]	299.6
ACCEL [mA]	2.488
V_{cg} [V]	-10.7
$V_{cg,pp}$ [V]	1.74
$V_{nk,pp}$ [V]	3.55
BT [mA]	53.17

*Neutralizer heater left on

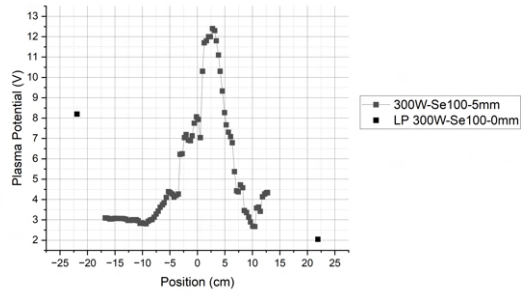

(a) Nominal at 0.5 cm downstream

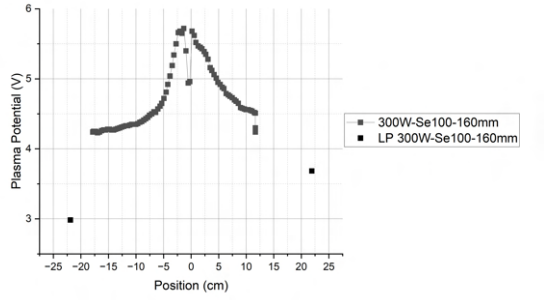

(b) Nominal at 16 cm downstream

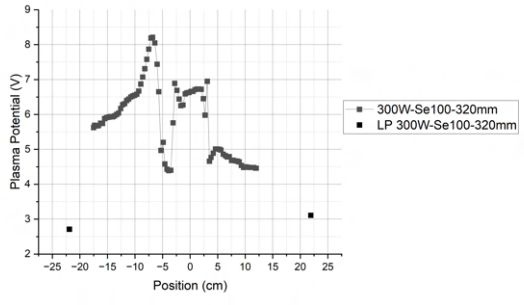

(c) Nominal at 32 cm downstream

Figure C.9: 2024-11 NASA 8 cm 300 W wall probe to beam emissive probe potentials comparison

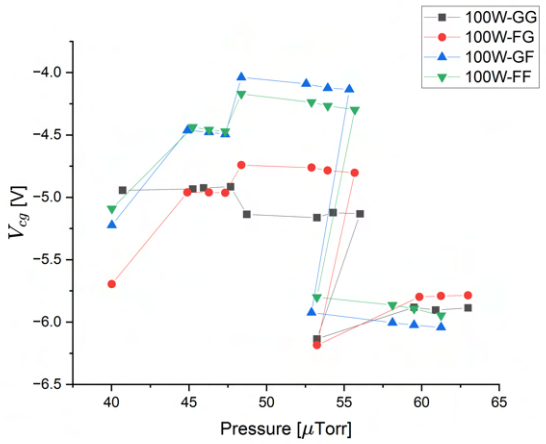

Figure C.10: 2024-05 NASA 8 cm 100 W neutralizer-facility coupling voltage with ground plasma screen and compression of grounded floating beam target and injected neutral flow versus pressure

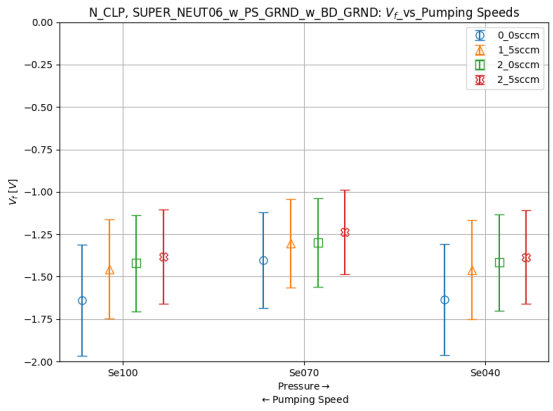

(a) PS grounded & BT grounded

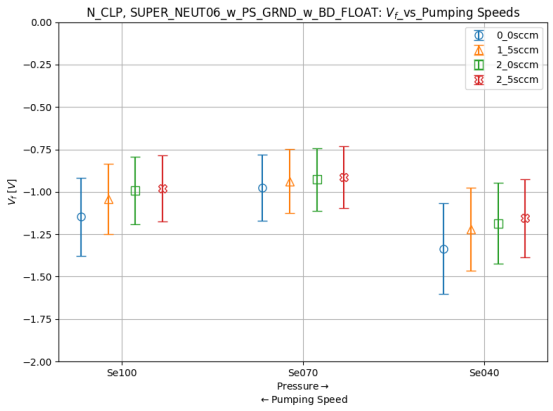

(b) PS grounded & BT floating

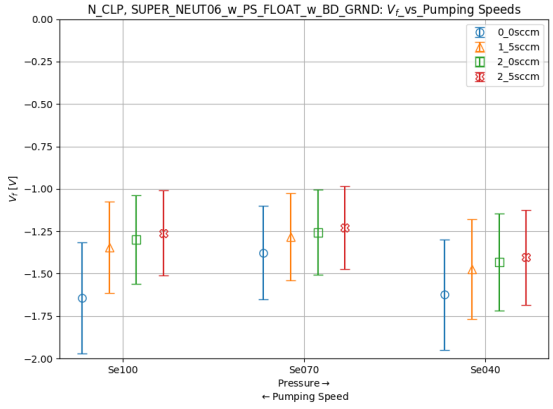

(c) PS floating & BT grounded

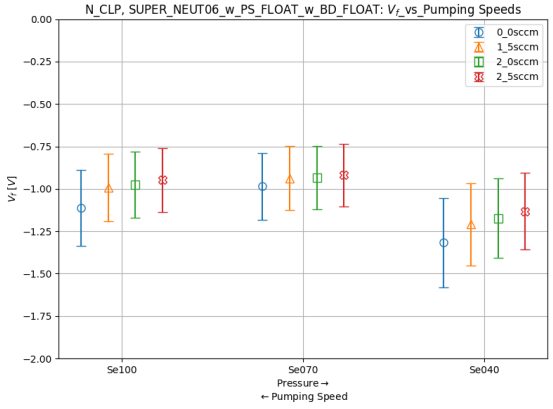

(d) PS floating & BT floating

Figure C.11: 2024-05 NASA 8 cm 100 W neutral flow injection floating potentials 4 cm downstream of neutralizer

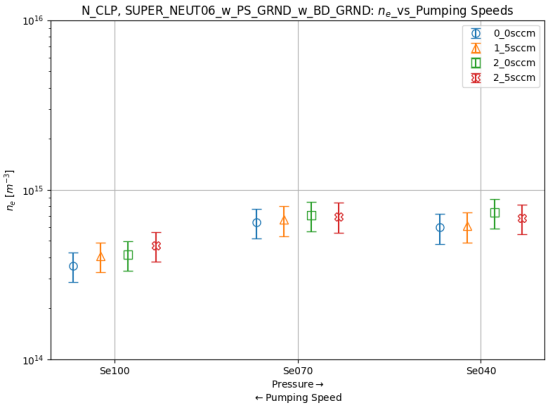

(a) PS grounded & BT grounded

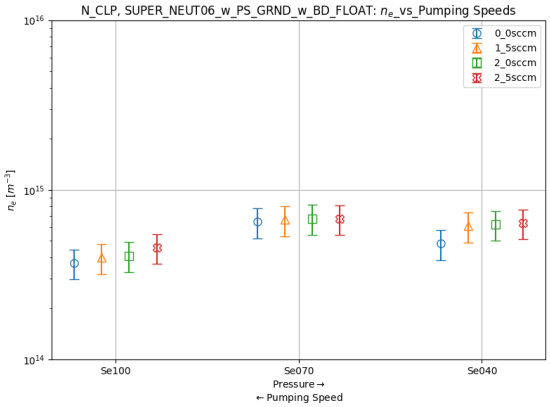

(b) PS grounded & BT floating

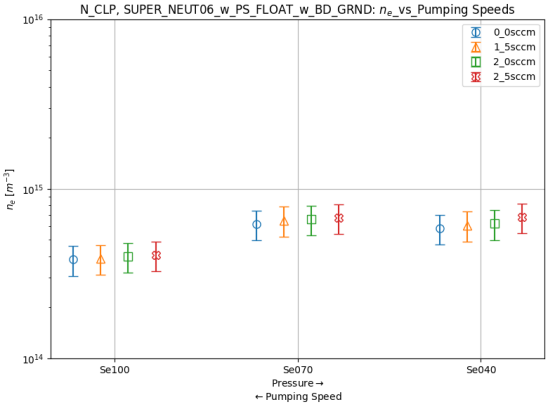

(c) PS floating & BT grounded

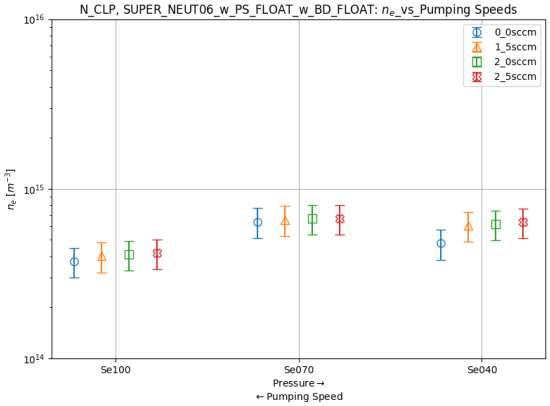

(d) PS floating & BT floating

Figure C.12: 2024-05 NASA 8 cm 100 W neutral flow injection electron density 4 cm downstream of neutralizer

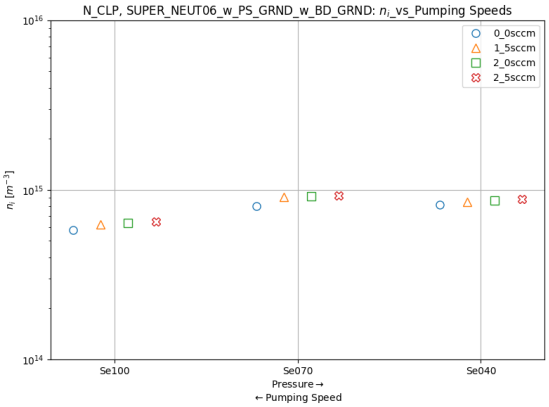

(a) PS grounded & BT grounded

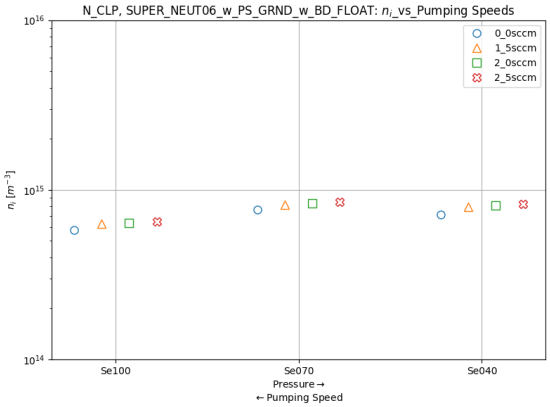

(b) PS grounded & BT floating

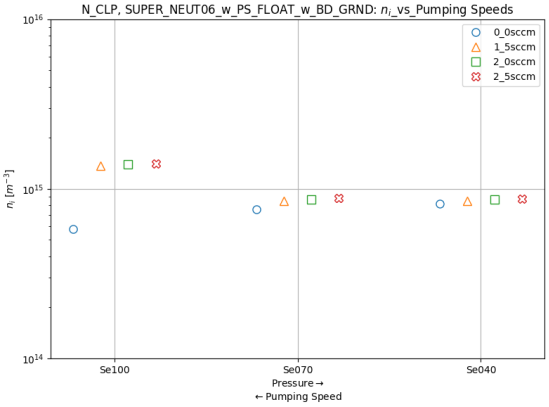

(c) PS floating & BT grounded

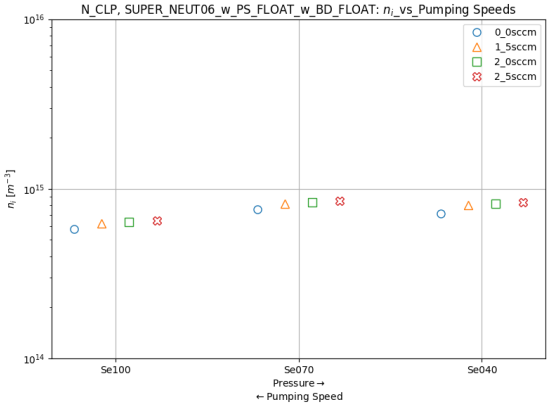

(d) PS floating & BT floating

Figure C.13: 2024-05 NASA 8 cm 100 W neutral flow injection ion density 4 cm downstream of neutralizer

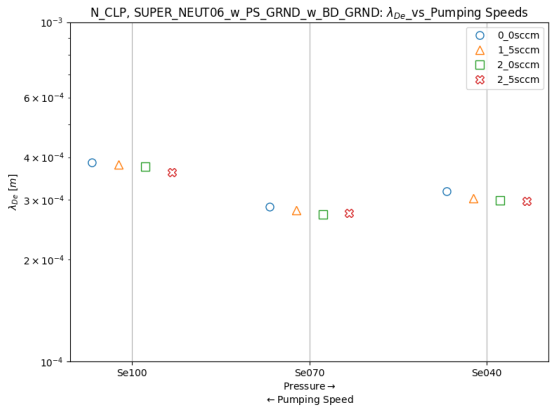

(a) PS grounded & BT grounded

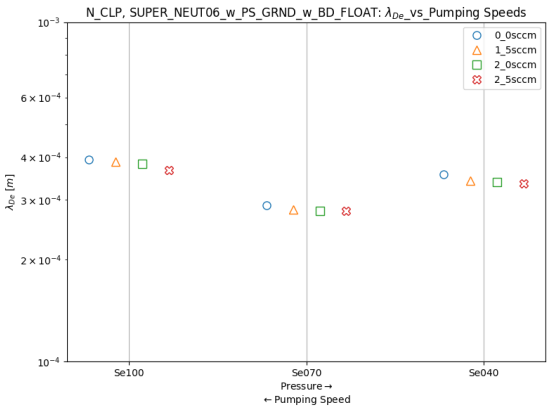

(b) PS grounded & BT floating

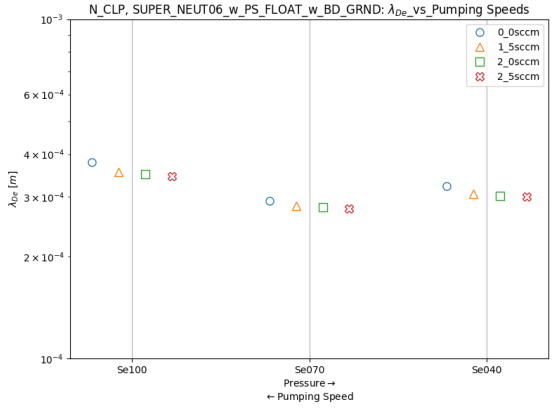

(c) PS floating & BT grounded

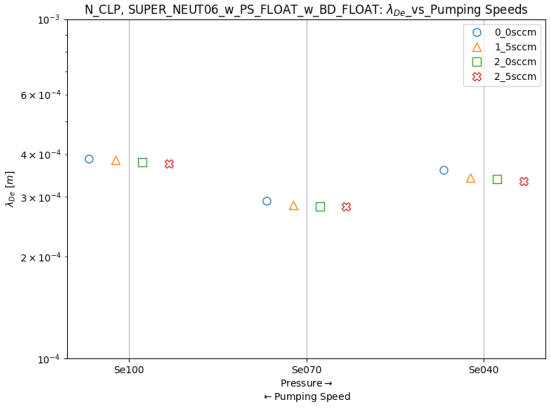

(d) PS floating & BT floating

Figure C.14: 2024-05 NASA 8 cm 100 W neutral flow injection Debye length 4 cm downstream of neutralizer

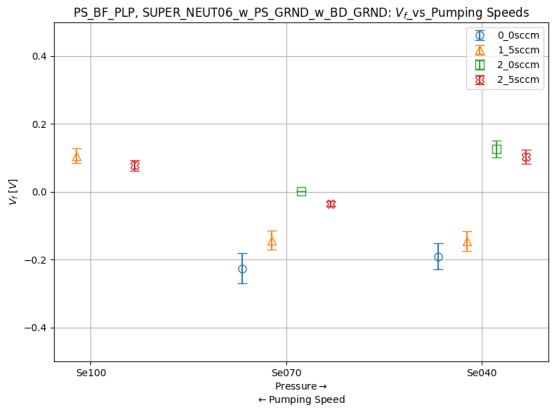

(a) PS grounded & BT grounded

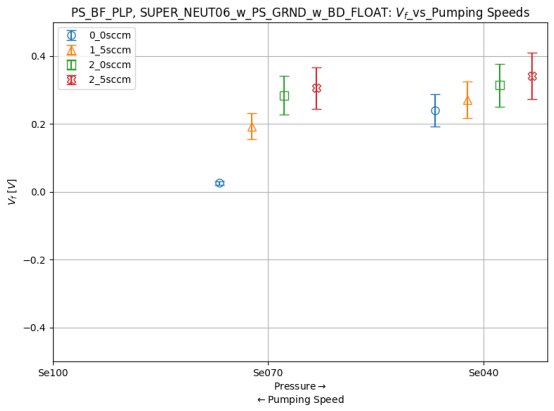

(b) PS grounded & BT floating

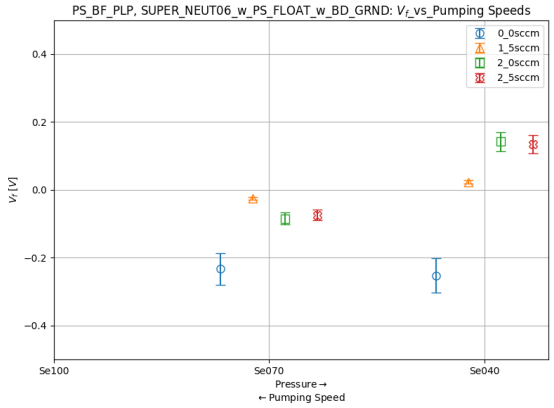

(c) PS floating & BT grounded

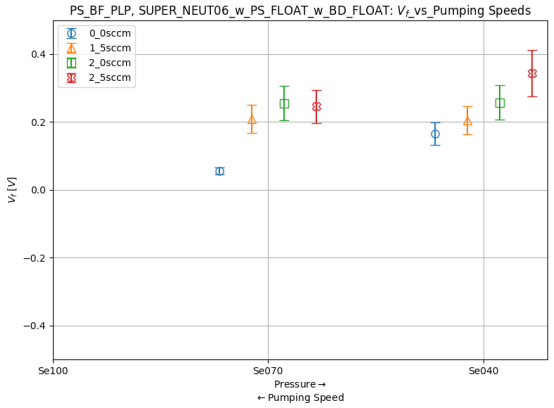

(d) PS floating & BT floating

Figure C.15: 2024-05 NASA 8 cm 100 W neutral flow injection floating potentials to the left-side of the plasma screen

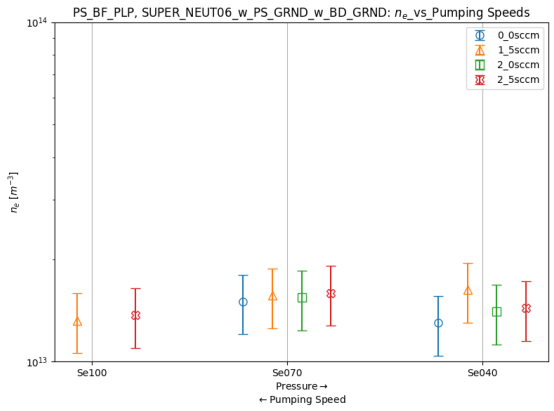

(a) PS grounded & BT grounded

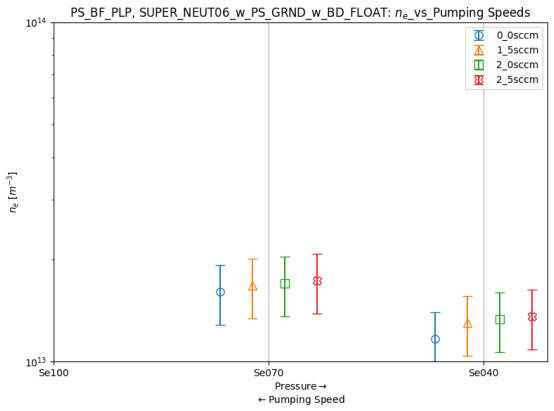

(b) PS grounded & BT floating

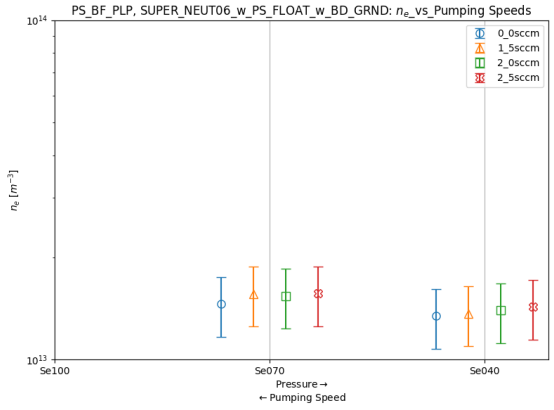

(c) PS floating & BT grounded

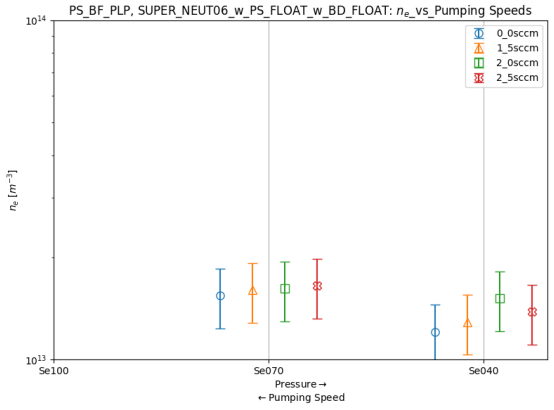

(d) PS floating & BT floating

Figure C.16: 2024-05 NASA 8 cm 100 W neutral flow injection electron density to the left-side of the plasma screen

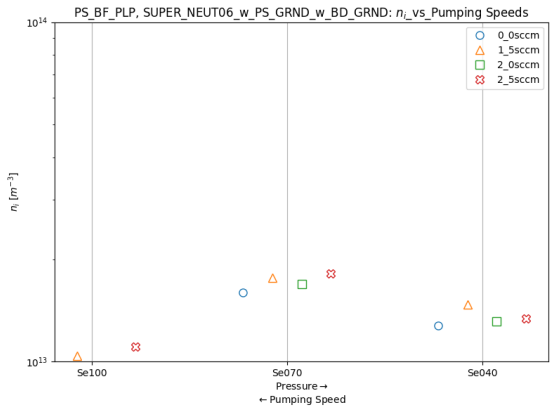

(a) PS grounded & BT grounded

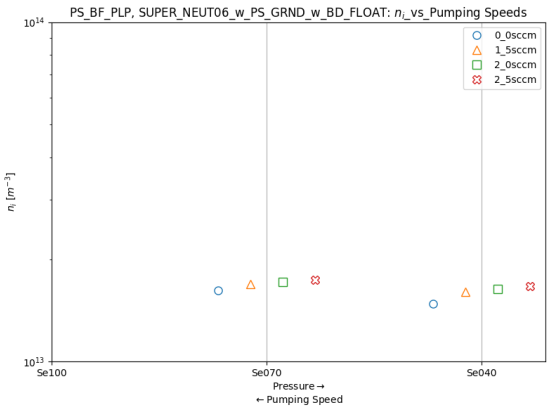

(b) PS grounded & BT floating

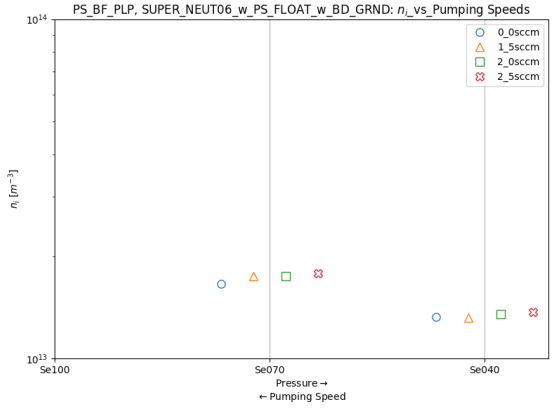

(c) PS floating & BT grounded

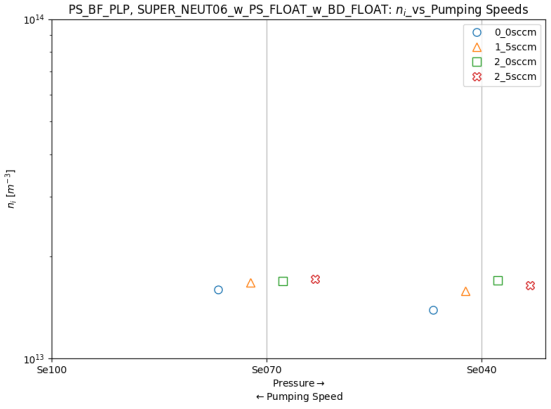

(d) PS floating & BT floating

Figure C.17: 2024-05 NASA 8 cm 100 W neutral flow injection ion density to the left-side of the plasma screen

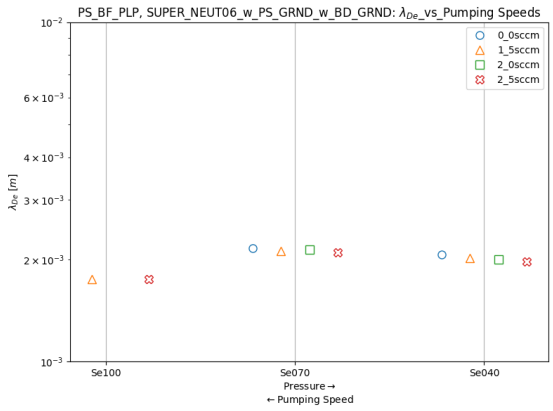

(a) PS grounded & BT grounded

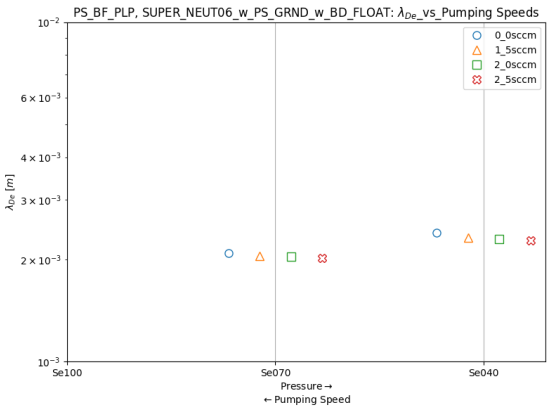

(b) PS grounded & BT floating

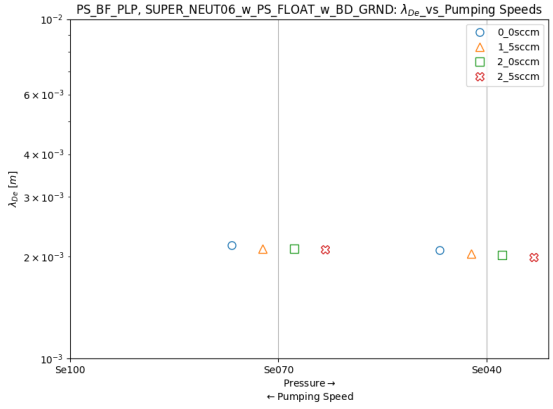

(c) PS floating & BT grounded

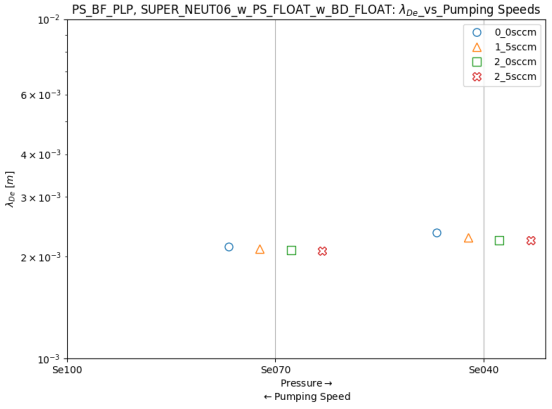

(d) PS floating & BT floating

Figure C.18: 2024-05 NASA 8 cm 100 W neutral flow injection Debye length to the left-side of the plasma screen

APPENDIX D

Plasma Spectroscopy

Table D.1: Plasma spectroscopy common line spectra of interest for argon [195]

λ (nm)	Chemical Symbol
696.5431	Ar I
706.7218	Ar I
738.3980	Ar I
750.3869	Ar I
751.4652	Ar I
763.5106	Ar I
772.3761	Ar I
772.4207	Ar I
794.8176	Ar I
800.6157	Ar I
801.4786	Ar I
810.3693	Ar I
811.5311	Ar I
826.4522	Ar I
840.8210	Ar I
842.4648	Ar I
458.98976	Ar II
472.68681	Ar II

Table D.2: Plasma spectroscopy common line spectra of interest for hydrogen, carbon & water species [196, 197]

λ (nm)	Chemical Symbol
434.0472	H_γ
656.28	H_α
400.9930	C I
437.13814	C I
447.8588	C I
473.4262	C I
385.22	C_2 I
473.71	C_2 I
516.52	C_2 I
541.59	C_2 II
404.98	C_3 I
431.42	CH I
506.79	C_4H_2 I
614.47	CHO I
351.4	CH_3O I
451.09	CO I
561.02	CO I
395.36	CO II
401.97	CO II
427.43	CO II
404.5	CO_2 I
410.4	CO_2 I
415.6	CO_2 I
426.0	CO_2 I
433.5	CO_2 I
434.4	CO_2 I
452.7	CO_2 I
476.8	CO_2 I
479.8	CO_2 I
489.3	CO_2 I
493.3	CO_2 I
351.7	O_2 I
384.1	O_2 I
308.90-402.18	OH I
809.7	H_2O I
519.4	H_2O II

APPENDIX E

Mass Spectroscopy

Table E.1: Hydrocarbon & cracking patterns RGA mass spectra 1-30 AMU [198, 199]

AMU	Chemical Symbol
1	H
2	H_2, D
3	$HD,^3H$
4	He
6	C
7	N
8	O
10	$Ne,^{10}B$
11	$Ne,^{11}B$
12	C
13	$C,^{13}C$
14	N, CH_2
15	CH_3
16	O, CH_4 (methane), NH_2
17	OH, NH_3 (ammonia)
18	H_2O
19	F
20	Ar^{2+}, Ne, HF
22	$^{22}Ne, CO_2$
24	C_2
25	C_2H
26	C_2H_2, CN, B_2H_6 (diborane)
27	C_2H_3, Al, HCN
28	$N_2, CO, C_2H_4, Si, C_2H_6$ (ethane)
29	CH_3CH_2
30	C_2H_6, NO, SiH_4 (silane)

Table E.2: Hydrocarbon & cracking patterns RGA mass spectra 31-132 AMU [198, 199]

AMU	Chemical Symbol
31	P, CH_2O, C_2H_5OH (ethanol),CH_3OH (methonal)
32	O_2, S
33	HS
34	H_2S,$^{34}S, O_2, PH_3$ (phosphine)
35	Cl
36	HCl,$^{36}Ar, C_3$
37	$^{37}Cl, C_3H$
38	$^{37}HCl, C_3H_2$
39	C_3H_3
40	Ar, C_3H_4
41	C_3H_5
42	C_3H_6
43	C_3H_7, CH_3CO, C_3H_6O (acetone)
44	CO_2, C_3H_8
45	CH_3CH_2O, C_3H_7OH (isopropyl alcohol)
46	CH_3CH_2OH
47	C_35Cl
48	$HC^{35}Cl, SO$
49	$C^{37}Cl$
50	$C^{37}Cl, CF_2, C_4H_2$
57	pumping oil
64	SO_2
69	CF_4, Fomblin oil
78	C_6H_6 (benzene)
81	BCl_3
84	Kr
85	CCl_2F_2 (Freon oil), SiF_4
132	Xe

BIBLIOGRAPHY

[1] Edgar Y Choueiri. A critical history of electric propulsion: The first 50 years (1906-1956). *Journal of propulsion and power*, 20(2):193–203, 2004.

[2] John Dankanich, Michael Swiatek, and John Yim. A step towards electric propulsion testing standards: Pressure measurements and effective pumping speeds. In *48th AIAA/ASME/SAE/ASEE Joint Propulsion Conference & Exhibit*, page 3737, 2012.

[3] John E Foster and Tyler J Topham. A review of the impact of ground test-related facility effects on gridded ion thruster operation and performance. *Physics of Plasmas*, 31(3), 2024.

[4] Mitchell LR Walker, Dan Lev, Maryam Saeedifard, Benjamin Jorns, John Foster, Alec D Gallimore, Alex Gorodetsky, Joshua L Rovey, Huck Beng Chew, Deborah Levin, et al. Overview of the joint advanced propulsion institute (janus). In *37th International Electric Propulsion Conference*, 2022.

[5] Dan M Goebel, Ira Katz, and Ioannis G Mikellides. *Fundamentals of electric propulsion*, volume 1. John Wiley & Sons, 2023.

[6] John R. Brophy. NASA's Deep Space 1 ion engine (plenary). *Review of Scientific Instruments*, 73(2):1071–1078, 02 2002.

[7] John R Brophy, Charles E Garner, and Steven C Mikes. Dawn ion propulsion system: Initial checkout after launch. *Journal of Propulsion and Power*, 25(6):1189–1202, 2009.

[8] H. Gold, R. Rulis, F. Maruna, and W. Hawersaat. Description and operation of spacecraft in sert i ion thrustor flight test. In *National Aeronautics and Space Administration*, number Report No. NASA-TM-X-1077. National Aeronautics and Space Administration, 1965.

[9] M Mandell and Ira Katz. Theory of hollow operation in spot and plume modes. In *30th Joint Propulsion Conference and Exhibit*, page 3134, 1994.

[10] Ioannis Mikellides, Lee Johnson, Ira Katz, and M Mandell. A high power ion thruster plume model. In *40th AIAA/ASME/SAE/ASEE Joint Propulsion Conference and Exhibit*, page 3816, 2004.

[11] Ioannis G Mikellides, Ira Katz, Robert A Kuharski, and Myron J Mandell. Elastic scattering of ions in electrostatic thruster plumes. *Journal of propulsion and power*, 21(1):111–118, 2005.

[12] Myron J Mandell. Next multi ion engine test: Plume modeling and test plans. In *29th Int. Electric Propulsion Conf.*, 2005.

[13] Myron J Mandell, Victoria A Davis, Eric J Pencil, Michael J Patterson, Heather K McEwen, John E Foster, and John Steve Snyder. Modeling the next multithruster array test with nascap-2k. *IEEE transactions on plasma science*, 36(5):2309–2318, 2008.

[14] Eric Pencil, John Foster, Michael Patterson, Esther Diaz, Jonathan Van Noord, and Heather McEwen. Ion beam characterization of the next multi-thruster array plume. In *42nd AIAA/ASME/SAE/ASEE Joint Propulsion Conference & Exhibit*, page 5182, 2006.

[15] John Foster, Michael Patterson, Eric Pencil, Heather McEwen, Esther Diaz, and Jon Van Noord. Plasma characteristics measured in the plume of a next multi-thruster array. In *42nd AIAA/ASME/SAE/ASEE Joint Propulsion Conference & Exhibit*, number NASA TM—2006-214402/AIAA 2006-5181, page 5181, 2006.

[16] Heather McEwen, John Foster, Jonathan Van Noord, Eric Pencil, Esther Diaz, and Michael Patterson. Characterization of plasma flux incident on a multi-thruster array. In *42nd AIAA/ASME/SAE/ASEE Joint Propulsion Conference & Exhibit*, number AIAA Paper No. AIAA 2006-5183, page 5183, 2006.

[17] Michael Patterson, John Foster, Heather McEwen, Daniel Herman, Eric Pencil, and Jonathan VanNoord. Next multi-thruster array test-engineering demonstration. In *42nd AIAA/ASME/SAE/ASEE Joint Propulsion Conference & Exhibit*, page 5180, 2006.

[18] Ethan T Dale and Benjamin A Jorns. Two-zone hall thruster breathing mode mechanism, part i: Theory. In *36th International Electric Propulsion Conference, University of Vienna, Austria*, volume 41, 2019.

[19] Ethan T Dale and Benjamin A Jorns. Two-zone hall thruster breathing mode mechanism, part ii: Experiment. In *36th International Electric Propulsion Conference, University of Vienna, Austria*, volume 41, 2019.

[20] S Nakanishi and EV Pawlik. Experimental investigation of a 1.5-m-diam kaufman thruster. *Journal of Spacecraft and Rockets*, 5(7):801–807, 1968.

[21] Michael J Patterson and James S Sovey. History of electric propulsion at nasa glenn research center: 1956 to present. *Journal of Aerospace Engineering*, 26(2):300–316, 2013.

[22] David R Jovel, Mitchell LR Walker, and Daniel Herman. Review of high-power electrostatic and electrothermal electric propulsion. *Journal of Propulsion and Power*, 38(6):1051–1081, 2022.

[23] James Sovey, Vincent Rawlin, and Michael Patterson. A synopsis of ion propulsion development projects in the united states-sert i to deep space 1. In *35th Joint Propulsion Conference and Exhibit*, page 2270, 1999.

[24] Michael J Patterson. personal communication, 2023.

[25] Rainer Killinger, Helmut Bassner, and Johann Mueller. Development of a high performance rf-ion thruster. In *35th Joint Propulsion Conference and Exhibit*, page 2445, 1999.

[26] Hitoshi Kuninaka, Kazutaka Nishiyama, Ikko Funaki, Tetsuya Yamada, Yukio Shimizu, and Jun'ichiro Kawaguchi. Powered flight of electron cyclotron resonance ion engines on hayabusa explorer. *Journal of Propulsion and Power*, 23(3):544–551, 2007.

[27] Dmytro Rafalskyi and Ane Aanesland. A neutralizer-free gridded ion thruster embedded into a 1u cubesat module. In *Proceedings of the 35th International Electric Propulsion Conference, Atlanta, GA, USA*, pages 8–12, 2017.

[28] G Sohl, Fosnight, VV, and SJ Goldner. Electron bombardment cesium ion engine system. *NASA CR–54711, April*, 1967.

[29] Paul D Reader, Dennis P White, and Gerald C Isaacson. Argon plasma bridge neutralizer operation with a 10-cm-beam-diameter ion etching source. *Journal of Vacuum Science and Technology*, 15(3):1093–1095, 1978.

[30] Vincent K Rawlin and Eugene V Pawlik. A mercury plasma-bridge neutralizer. *Journal of Spacecraft and Rockets*, 5(7):814–820, 1968.

[31] JW Ward and HJ King. Mercury hollow cathode plasma bridge neutralizers. *Journal of Spacecraft and Rockets*, 5(10):1161–1164, 1968.

[32] W Kerslake and S Domitz. Neutralization tests on the sert ii spacecraft. In *14th International Electric Propulsion Conference*, number Report No. NASATM-79271/AIAA79-2064, page 2064, 1979.

[33] C Othmer, KH Glassmeier, U Motschmann, J Schüle, and Ch Frick. Three-dimensional simulations of ion thruster beam neutralization. *Physics of Plasmas*, 7(12):5242–5251, 2000.

[34] Hideyuki Usui, Akihiko Hashimoto, and Yohei Miyake. Electron behavior in ion beam neutralization in electric propulsion: Full particle-in-cell simulation. In *Journal of Physics: Conference Series*, volume 454, page 012017. IOP Publishing, 2013.

[35] Ira B Bernstein, John M Greene, and Martin D Kruskal. Exact nonlinear plasma oscillations. *Physical Review*, 108(3):546, 1957.

[36] Ian Horner Hutchinson. Electron holes in phase space: What they are and why they matter. *Physics of Plasmas*, 24(5), 2017.

[37] AW Trivelpiece and RW Gould. Space charge waves in cylindrical plasma columns. *Journal of Applied Physics*, 30(11):1784–1793, 1959.

[38] Nakul Nuwal, Deborah A Levin, and Igor D Kaganovich. Excitation of surface waves in 3d ion beam neutralization. *Physics of Plasmas*, 30(4), 2023.

[39] Steven R Oleson, Laura M Burke, Lee S Mason, Elizabeth R Turnbull, Steven McCarty, Anthony J Colozza, James E Fittje, John T Yim, Michael Smith, Thomas W Packard, et al. Compass final report: Nuclear electric propulsion (nep)-chemical vehicle 1.2. Technical report, NASA, 2021.

[40] Michael Patterson and Timonthy Verhey. 5kw xenon ion thruster lifetest. In *21st International Electric Propulsion Conference*, page 2543, 1990.

[41] James S Sovey, Robert H Vetrone, Stanley P Grisnik, Roger M Myers, and James E Parkes. Test facilities for high-power electric propulsion. *Journal of Propulsion and Power*, 10(1):18–24, 1994.

[42] John W Dankanich, Mitchell Walker, Michael W Swiatek, and John T Yim. Recommended practice for pressure measurement and calculation of effective pumping speed in electric propulsion testing. *Journal of Propulsion and Power*, 33(3):668–680, 2017.

[43] Yinjian Zhao, Joseph Wang, and Hideyuki Usui. Simulations of ion thruster beam neutralization using a particle–particle model. *Journal of Propulsion and Power*, 34(5):1109–1115, 2018.

[44] Yuan Hu, Joseph Wang, and Quanhua Sun. Geometrically self-similar ion acceleration in collisionless plasma beam expansion. *Plasma Sources Science and Technology*, 29(12):125004, 2020.

[45] W R Kerslake, D C Byers, V K Rawlin, S G Jones, and F D Berkopec. Flight and ground performance of sert ii thruster, 1970.

[46] HS Ogawa, RK Cole, and John Michael Sellen. *Measurements of Equilibration Potential Between a Plasma" Thrust" Beam and a Dilute" Space" Plasma*. American Institute of Aeronautics and Astronautics, 1969.

[47] Joseph Wang, Ouliang Chang, and Yong Cao. Electron–ion coupling in mesothermal plasma beam emission: Full particle pic simulations. *IEEE transactions on plasma science*, 40(2):230–236, 2012.

[48] Iverson C Bell, Jesse K McTernan, Brian Gilchrist, and Sven G Bilen. Investigating miniature electrodynamic tethers and interaction with the low earth orbit plasma. In *AIAA Space 2013 Conference and Exposition*, page 5391, 2013.

[49] D Hall, R Kemp, and Haywood Shelton. Mercury discharge devices and technology. In *6th Electric Propulsion and Plasmadynamics Conference*, page 669, 1967.

[50] John E Foster, George J Williams, and Michael J Patterson. Characterization of an ion thruster neutralizer. *Journal of Propulsion and Power*, 23(4):828–835, 2007.

[51] Anita Sengupta, John Brophy, and Keith Goodfellow. Status of the extended life test of the deep space 1 flight spare ion engine after 30,000 hours of operation. In *39th AIAA/ASME/SAE/ASEE Joint Propulsion Conference and Exhibit*, page 4558, 2003.

[52] JGJ Williams, Tyler A Hickman, Thomas W Haag, John E Foster, and Michael J Patterson. Preliminary wear analysis following a 2000 h wear test of the hipep ion thruster. *IEPC Paper*, 260, 2005.

[53] Cesar E Huerta and Richard E Wirz. Ion-induced electron emission reduction via complex surface trapping. *AIP advances*, 9(12), 2019.

[54] Michael J Patterson and Kayhan Mohajeri. Neutralizer optimization. In *International Electric Propulsion Conference*, number Report No. NASA-TM-105578/IEPC 91-151/NAS 1.15: 105578, 1991.

[55] WR Kerslake and LR Ignaczak. Sertii1979-1981 tests: Plasma thrust and neutralizer measurements. *Journal of Spacecraft and Rockets*, 19(3):236–240, 1982.

[56] Y-C Feng and P WILBUR. The influence of stray magnetic fields on ion beam neutralization. In *16th International Electric Propulsion Conference*, page 1945, 1945.

[57] W Kerslake and L Ignaczak. Sert ii 1980 extended flight thruster experiments. In *15th International Electric Propulsion*, number AIAA-81-0665/NASA TM-81685, page 665, 1981.

[58] Ryan J Bell, Nicholas G Davey, Morten Martinsen, R Timothy Short, Chris G Gill, and Erik T Krogh. The effect of the earth's and stray magnetic fields on mobile mass spectrometer systems. *Journal of The American Society for Mass Spectrometry*, 26(2):201–211, 2014.

[59] J Wang, David Brinza, and M Young. Three-dimensional particle simulations of ion propulsion plasma environment for deep space 1. *Journal of Spacecraft and Rockets*, 38(3):433–440, 2001.

[60] George C Soulas. Design and performance of 40 cm ion optics. In *27th International Electric Propulsion Conference*, number NASA/TM-2001-211275, 2001.

[61] Vernon H Chaplin, James E Polk, Ira Katz, George Williams, George C Soulas, John Yim, and John R Anderson. 3d simulations of ion thruster accelerator grid erosion accounting for charge exchange ion space charge. In *2018 Joint Propulsion Conference*, number AIAA Paper No. AIAA 2018-4812, page 4812, 2018.

[62] James Polk, Vernon Chaplin, John Anderson, John Yim, George Soulas, George Williams, and Rohit Shastry. Modeling grid erosion in the next ion thruster using the cex2d and cex3d codes. *Journal of Electric Propulsion*, 2(1):14, 2023.

[63] Mark W Crofton and Iain D Boyd. Origins of accelerator grid current: analysis of t5 grid test results. *Journal of Propulsion and Power*, 17(1):203–211, 2001.

[64] J Wang, DE Brinza, DT Young, JE Nordholt, JE Polk, MD Henry, R Goldstein, JJ Hanley, DJ Lawrence, and M Shappirio. Deep space one investigations of ion propulsion plasma environment. *Journal of Spacecraft and Rockets*, 37(5):545–555, 2000.

[65] Edward A. Startsev, Igor D. Kaganovich, and Ronald C. Davidson. Effects of beam-plasma instabilities on neutralized propagation of intense ion beams in background plasma. *Nuclear Instruments and Methods in Physics Research Section A: Accelerators, Spectrometers, Detectors and Associated Equipment*, 733:80–85, 2014. 19th International Symposium on Heavy Ion Inertial Fusion.

[66] J. S. Sovey. Improved ion containment using a ring-cusp ion thruster. In *16th International Electric Propulsion Conference*, number Report No. NASA-TM-82990/E-1422, pages E–1422, 1982.

[67] JOHN BROPHY. Simulated ion thruster operation without beam extraction. In *21st International Electric Propulsion Conference*, page 2655, 1990.

[68] Rohit Shastry, Richard R Hofer, Bryan M Reid, and Alec D Gallimore. Method for analyzing exb probe spectra from hall thruster plumes. *Review of Scientific Instruments*, 80(6), 2009.

[69] Russell P Doerner, Dennis G Whyte, and Dan M Goebel. Sputtering yield measurements during low energy xenon plasma bombardment. *Journal of Applied Physics*, 93(9):5816–5823, 2003.

[70] Maris A Mantenieks, John E Foster, Pradosh K Ray, Shuttha V Shutthanandan, and Theva S Thevuthasan. Low energy xenon ion sputtering yield measurements. In *27th International Electric Propulsion Conference*, 2001.

[71] John D Williams, Michael M Gardner, Mark L Johnson, and Paul J Wilbur. Xenon sputter yield measurements for ion thruster materials. In *28th International Electric Propulsion Conference*, number NASA/CR-2003-212306, 2003.

[72] Kim de Groh, Bruce Banks, and Christina Karniotis. Nstar extended life test discharge chamber flake analyses. In *40th AIAA/ASME/SAE/ASEE Joint Propulsion Conference and Exhibit*, page 3612, 2004.

[73] Rohit Shastry and George C Soulas. Post-test examination of nasa's evolutionary xenon thruster long-duration test hardware: Discharge chamber. In *52nd AIAA/SAE/ASEE Joint Propulsion Conference*, page 4630, 2016.

[74] George C Soulas and Rohit Shastry. Post-test examination of nasa's evolutionary xenon thruster long-duration test hardware: Ion optics. In *52nd AIAA/SAE/ASEE Joint Propulsion Conference*, page 4632, 2016.

[75] George C Soulas. The impact of back-sputtered carbon on the accelerator grid wear rates of the next and nstar ion thrusters. In *International Electric Propulsion Conference*, number IEPC-2013-157, 2013.

[76] Mark W Crofton, John C Nocerino, William A Cox, Jason A Young, Kevin D Diamant, Edward J Beiting, Michael J Patterson, and George C Soulas. Next ion engine plume deposition rates: Qcm measurements. In *52nd Aerospace Sciences Meeting*, page 0140, 2014.

[77] James Pollard, Kevin Diamant, Mark Crofton, Michael Patterson, and George Soulas. Spatially-resolved beam current and charge-state distributions for the next ion engine. In *46th AIAA/ASME/SAE/ASEE Joint Propulsion Conference & Exhibit*, number No. AIAA 2010-6779, page 6779, 2010.

[78] J. Scott Miller, Steve H. Pullins, Dale J. Levandier, Yu-hui Chiu, and Rainer A. Dressler. Xenon charge exchange cross sections for electrostatic thruster models. *Journal of Applied Physics*, 91(3):984–991, 02 2002.

[79] Neil A Arthur and George J Williams. Near field probe measurements in the plume of a next ion thruster. In *International Electric Propulsion Conference*, number IEPC-2019-167/GRC-E-DAA-TN72319, 2019.

[80] P Wilbur. A model for nitrogen chemisorption in ion thrusters. In *14th International Electric Propulsion Conference*, number AIAA Paper No. AIAA 1979-2062, page 2062, 1979.

[81] V RAWLIN and M MANTENIEKS. Effect of facility background gases on internal erosion of the 30-cmhg ion thruster. In *13th International Electric Propulsion Conference*, number AIAA PAPER 78-665/NASA-TM-73803, page 665, 1978.

[82] RJ Cybulski, DM Shellhammer, RR Lovell, EJ Domino, JT Kotnik, J Cybulski, and RR Loveli. Results from sert i ion rocket flight test. In *Proceedings*, volume 1, pages 21/Report No. NASA TN D–2718. Air Force Office of Scientific Research, 1965.

[83] William R Kerslake and Louis R Ignaczak. Development and flight history of the sert ii spacecraft. *Journal of Spacecraft and Rockets*, 30(3):258–290, 1993.

[84] S. G. Jones, J. V. Staskus, and D. C. Byers. Preliminary results of sert ii spacecraft potential measurments using hot wire emissive probes. In *8th Electric Propulsion Conference*, number Report No. NASA-TM-X-52856, 1970.

[85] W. Kerslake and L. Ignaczak. In *AIAA*, number AIAA Paper No. AIAA 91-0665aR, 1991.

[86] JE Polk, RY Kakuda, JR Anderson, JR Brophy, VK Rawlin, J Sovey, and J Hamley. In-flight performance of the nstar ion propulsion system on the deep space one mission. In *2000 IEEE Aerospace Conference. Proceedings (Cat. No. 00TH8484)*, volume 4, pages 123–148. IEEE, 2000.

[87] Hitoshi Kuninaka and Pedro Molina-Morales. Spacecraft charging due to lack of neutralization on ion thrusters. *Acta Astronautica*, 55(1):27–38, 2004.

[88] T. Muranaka, M. Kato, K. Ueno, S. Hosoda, and K. Nishiyama. Estimation of charging for hayabusa2 by analysis of surface erosion in ion thruster operation. In *37th International Electric Propulsion Conference*, number IEPC-2022-275, 2022.

[89] Ayumu Nono, Takato Morishita, Satoshi Hosoda, Ryudo Tsukizaki, and Kazutaka Nishiyama. Effect of spacecraft surface conductivity on voltage of microwave neutralizer in gridded ion thrusters. *Acta Astronautica*, 212:130–138, 2023.

[90] Neil A Arthur. Ion thruster produced roll torque. In *AIAA Propulsion and Energy 2019 Forum*, page 4166, 2019.

[91] Jeremy John, Lew Roufberg, Geffrey K Ottman, and Elena Adams. Next-c lessons learned on the dart mission for future integration and test. In *2023 IEEE Aerospace Conference*, pages 1–7. IEEE, 2023.

[92] BR Weatherford, EV Barnat, and JE Foster. Two-dimensional laser collision-induced fluorescence measurements of plasma properties near an rf plasma cathode extraction aperture. *Plasma Sources Science and Technology*, 21(5):055030, 2012.

[93] LA Ribarov, JA Wehrmeyer, S Hu, and RW Pitz. Multiline hydroxyl tagging velocimetry measurements in reacting and nonreacting experimental flows. *Experiments in Fluids*, 37:65–74, 2004.

[94] AV Phelps and Z Lj Petrovic. Cold-cathode discharges and breakdown in argon: surface and gas phase production of secondary electrons. *Plasma Sources Science and Technology*, 8(3):R21, 1999.

[95] G. Sabiston and R.E. Wirz. Electric propulsion vacuum chamber design approaches for reducing sputtering effects. In *38th International Electric Propulsion Conference Toulouse, France, June 23-28,2024*, number IEPC-2024-187, 2024.

[96] Eric A Viges, Benjamin A Jorns, Alec D Gallimore, and JP Sheehan. University of michigan's upgraded large vacuum test facility. In *36th International Electric Propulsion Conference*, pages 1–18, 2019.

[97] University of michigan large vacuum test facility. https://pepl.engin.umich.edu/research/facilities/. Accessed: 2025-01-18.

[98] David R Jovel, Brandon A Sforzo, Kristopher L Manion, Nathan P Brown, Xingjian Wang, David J Wu, Mitchell LR Walker, and Vigor Yang. Research capabilities in propulsion and combustion science at the georgia institute of technology. In *AIAA Propulsion and Energy Forum*, 2017.

[99] Georgia tech vacuum test facility-2. https://hpepl.ae.gatech.edu/index.php/lab-capabilities/facilities. Accessed: 2025-01-18.

[100] Luis R Pinero, Michael J Patterson, and Vincent E Satterwhite. Power console development for nasa's electric propulsion outreach program. In *International Electric Propulsion Conference*, number NAS 1.15: 106428, 1993.

[101] Richard R Hofer, Peter Y Peterson, and Alec D Gallimore. Characterizing vacuum facility backpressure effects on the performance of a hall thruster. In *IEPC-01-045, 27th International Electric Propulsion Conference, Pasadena, CA*, 2001.

[102] Richard R Hofer, Sarah E Cusson, Robert B Lobbia, and Alec D Gallimore. The h9 magnetically shielded hall thruster. In *35th International Electric Propulsion Conference*, pages 2017–232. Electric Rocket Propulsion Soc., 2017.

[103] Leanne L Su, Parker J Roberts, Tate Gill, William Hurley, Thomas A Marks, Christopher L Sercel, Madison Allen, Collin B Whittaker, Matthew Byrne, Zachariah Brown, et al. Operation and performance of a magnetically shielded hall thruster at ultrahigh current densities on xenon and krypton. In *AIAA SCITECH 2023 Forum*, page 0842, 2023.

[104] H9. https://pepl.engin.umich.edu/project/9-kw-magnetically-shielded-hall-thruster/. Accessed: 2025-01-18.

[105] Nstar fmt. https://pepl.engin.umich.edu/project/nstar-fmt-ion-engine/. Accessed: 2025-01-18.

[106] Michael Patterson, Thomas Haag, Vincent Rawlin, and Michael Kussmaul. Nasa 30 cm ion thruster development status. In *30th Joint Propulsion Conference and Exhibit*, page 2849, 1994.

[107] George Jarvis Williams Jr. *The use of laser-induced fluorescence to characterize discharge cathode erosion in a 30 cm ring-cusp ion thruster*. University of Michigan, 2000.

[108] Daniel Andrew Herman. *The use of electrostatic probes to characterize the discharge plasma structure and identify discharge cathode erosion mechanisms in ring-cusp ion thrusters*. University of Michigan, 2005.

[109] J Polk, R Kakuda, J Anderson, J Brophy, V Rawlin, M Patterson, J Sovey, and J Hamley. Performance of the nstar ion propulsion system on the deep space one mission. In *39th Aerospace Sciences Meeting and Exhibit*, page 965, 2001.

[110] J Polk, J Anderson, J Brophy, V Rawlin, M Patterson, J Sovey, and J Hamley. An overview of the results from an 8200 hour wear test of the nstar ion thruster. In *35th Joint Propulsion Conference and Exhibit*, page 2446, 1999.

[111] Michael Patterson, Steven Oleson, Michael Patterson, and Steven Oleson. Low-power ion propulsion for small spacecraft. In *33rd Joint Propulsion Conference and Exhibit*, page 3060, 1997.

[112] Michael Patterson. Low-power ion thruster development status. In *34th AIAA/ASME/SAE/ASEE Joint Propulsion Conference and Exhibit*, page 3347, 1998.

[113] Nasa 8 cm. https://www.researchgate.net/figure/Prototype-8-cm-ion-thruster-with-plasma-screen-removed_fig1_24299689. Accessed: 2025-01-18.

[114] Michael J Patterson, Stanley P Grisnik, and George C Soulas. Scaling of ion thrusters to low power. In *International Electric Propulsion Conference*, number IEPC-97-098, 1998.

[115] Michael Patterson. Low-power ion thruster development status. In *34th AIAA/ASME/SAE/ASEE Joint Propulsion Conference and Exhibit*, page 3347, 1999.

[116] John E Foster and Michael J Patterson. Internal plasma properties and enhanced performance of 8-centimeter ion thruster discharge. *Journal of Propulsion and Power*, 17(2):428–432, 2001.

[117] Noah Hershkowitz, O Auciello, and DL Flamm. How langmuir probes work. *Plasma diagnostics*, 1:113–183, 1989.

[118] Francis F Chen. Langmuir probe diagnostics. In *Mini-Course on Plasma Diagnostics, IEEEICOPS meeting, Jeju, Korea*, pages 20–111. Citeseer, 2003.

[119] Robert L Merlino. Understanding langmuir probe current-voltage characteristics. *American Journal of Physics*, 75(12):1078–1085, 2007.

[120] Robert B Lobbia and Brian E Beal. Recommended practice for use of langmuir probes in electric propulsion testing. *Journal of Propulsion and Power*, 33(3):566–581, 2017.

[121] Daniel L Brown, Mitchell LR Walker, James Szabo, Wensheng Huang, and John E Foster. Recommended practice for use of faraday probes in electric propulsion testing. *Journal of Propulsion and Power*, 33(3):582–613, 2017.

[122] JP Sheehan and N Hershkowitz. Emissive probes. *Plasma Sources Science and Technology*, 20(6):063001, 2011.

[123] JP Sheehan, Yevgeny Raitses, Noah Hershkowitz, Igor Kaganovich, and Nathaniel J Fisch. A comparison of emissive probe techniques for electric potential measurements in a complex plasma. *Physics of Plasmas*, 18(7), 2011.

[124] JP Sheehan, Yevgeny Raitses, Noah Hershkowitz, and Michael McDonald. Recommended practice for use of emissive probes in electric propulsion testing. *Journal of Propulsion and Power*, 33(3):614–637, 2017.

[125] Stephanie Stephanie Jeanne Thomas. *Developing a space shuttle experiment for Hall and pulsed plasma thrusters*. PhD thesis, Massachusetts Institute of Technology, 2001.

[126] Austen Thomas, Kristina Lemmer, Janice Cabrera, Mitchell LR Walker, Tyler Topham, and John Foster. High-speed far-field energy measurements in a 9-kw hall effect thruster for model inference and calibration. In *38th International Electric Propulsion Conference*, 2024.

[127] Austen Thomas and Kristina Lemmer. Time-resolved ion energy measurements using a retarding potential analyzer for electric propulsion applications. *Review of Scientific Instruments*, 95(2), 2024.

[128] Matthew Baird, Ron McGee-Sinclair, Kristina Lemmer, and Wensheng Huang. Time-resolved ion energy measurements using a retarding potential analyzer. *Review of Scientific Instruments*, 92(7), 2021.

[129] Toyofumi Yamauchi and Joshua Rovey. Analysis of the ion collection model in the exb probe. *Journal of Electric Propulsion*, 3(1):10, 2024.

[130] Toyofumi Yamauchi and Joshua L Rovey. Uncertainty and data analysis of exb probe including field non-uniformity and transmittancy. In *AIAA SCITECH 2024 Forum*, page 0688, 2024.

[131] Keita Nishii and Deborah A Levin. Kinetic simulation of ion thruster plume neutralization in a vacuum chamber. *Plasma Sources Science and Technology*, 32(11):115009, 6 2023.

[132] BA Jorns and MP Byrne. Model for the dependence of cathode voltage in a hall thruster on facility pressure. *Plasma Sources Science and Technology*, 30(1):015012, 2021.

[133] Jason D Frieman, Jonathan A Walker, Mitchell LR Walker, Vadim Khayms, and David Q King. Electrical facility effects on hall thruster cathode coupling: Performance and plume properties. *Journal of Propulsion and Power*, 32(1):251–264, 2016.

[134] NING Zhongxi, CHU Yanfeng, LIU Xiaoyu, LI Fan, ZHU Ximing, and YU Daren. Effect of vacuum backpressure on discharge characteristics of hollow cathode. *Plasma Science and Technology*, 21(12):125402, 2019.

[135] Scott J Hall, Timothy G Gray, John T Yim, Maria Choi, Timothy R Sarver-Verhey, and Hani Kamhawi. The effect of facility background pressure on hollow cathode operation. *Journal of Applied Physics*, 130(11), 2021.

[136] Robert Thomas, Rittu S Raju, and James J Bontempo. Characterizing electrical arc behavior in ion engines. In *AIAA SCITECH 2025 Forum*, page 2041, 2025.

[137] Dan M Goebel, Kristina K Jameson, Ira Katz, and Ioannis G Mikellides. Potential fluctuations and energetic ion production in hollow cathode discharges. *Physics of Plasmas*, 14(10), 2007.

[138] Marlene I Patino and Richard E Wirz. Characterization of xenon ion and neutral interactions in a well-characterized experiment. *Physics of Plasmas*, 25(6), 2018.

[139] Michael Tartz, Darina Manova, Horst Neumann, Hans Leiter, and Joachim Esch. Sputter investigation of ion thrusters grid materials. In *41st AIAA/ASME/SAE/ASEE Joint Propulsion Conference & Exhibit*, page 4414, 2005.

[140] Bolton Ferda. Retarding potential analyzer theory and design. *Princeton University*, page 18, 2015.

[141] Dan M Goebel and Giulia Becatti. Compact scanning retarding potential analyzer. *Review of Scientific Instruments*, 92(1), 2021.

[142] Ruslan Kozakov, Maximilian Maigler, Jochen Schein, and Neil Wallace. Determination of self-neutralization phenomena of ion beams with langmuir probe measurements and pic-dsmc simulations. *Applied Sciences*, 14(8):3470, 2024.

[143] Charles Lipscomb, Iain D Boyd, Kaelan B Hansson, Joshua Eckels, and Alex Gorodetsky. Simulation of vacuum chamber pressure distribution with surrogate modeling and uncertainty quantification. In *AIAA SCITECH 2024 Forum*, page 2369, 2024.

[144] James K Olthoff and KE Greenberg. The gaseous electronics conference rf reference cell—an introduction. *Journal of research of the National Institute of Standards and Technology*, 100(4):327, 1995.

[145] Y. Hirohata, M. Okita, T. Hino, and T. Yamashina. Desorption behavior for h2o from isotropic graphite dipped in water. *Carbon*, 32(2):369–372, 1994.

[146] M Langhoff and BMU Scherzer. The hydrogen inventory in plasma exposed graphite surfaces. *Journal of nuclear materials*, 245(1):60–65, 1997.

[147] HF Dylla. A review of the wall problem and conditioning techniques for tokamaks. *Journal of Nuclear Materials*, 93:61–74, 1980.

[148] JE Simpkins, RA Strehlow, PK Mioduszewski, and T Uckan. Control of water absorption by purification of graphite. *Journal of Nuclear Materials*, 162:871–875, 1989.

[149] J Bohdansky, RA Causey, CD Croessmann, AE Pontau, and JB Whitley. Preconditioning of graphite and its influence on the gas desorption. *Journal of Nuclear Materials*, 162:861–864, 1989.

[150] DV Chakarov, Lars Österlund, and B Kasemo. Water adsorption on graphite (0001). *Vacuum*, 46(8-10):1109–1112, 1995.

[151] D Douai, D Kogut, T Wauters, S Brezinsek, GJM Hagelaar, SH Hong, PJ Lomas, A Lyssoivan, I Nunes, RA Pitts, et al. Wall conditioning for iter: Current experimental and modeling activities. *Journal of nuclear materials*, 463:150–156, 2015.

[152] J Li, M Shimada, Y Zhao, J Hu, X Gong, YW Yu, and GZ Zhuo. Wall conditioning towards the utilization in iter. *Journal of nuclear materials*, 415(1):S35–S41, 2011.

[153] TL Thomas and EL Battle. Effects of contamination on langmuir probe measurements in glow discharge plasmas. *Journal of Applied Physics*, 41(8):3428–3432, 1970.

[154] Lyon Bradley King. *Transport-property and mass spectral measurements in the plasma exhaust plume of a Hall-effect space propulsion system*. University of Michigan, 1998.

[155] Lyudmila Vshivkova, Konstantin Vshivkov, and Galina Dudnikova. 3d numerical modeling of the plasma beam expansion using the mhd-kinetic approach. In *Journal of Physics: Conference Series*, volume 1336, page 012022. IOP Publishing, Institute of Physics Publishing, 11 2019.

[156] ID Kaganovich, RC Davidson, MA Dorf, EA Startsev, AB Sefkow, EP Lee, and A Friedman. Physics of neutralization of intense high-energy ion beam pulses by electrons. *Physics of Plasmas*, 17(5), 2010.

[157] W Kerslake and S Domitz. *Neutralization Tests on the SERT II Spacecraft*, pages 450–468. American Institute of Aeronautics and Astronautics, 1981.

[158] J Polk, R Kakuda, J Anderson, J Brophy, V Rawlin, M Patterson, J Sovey, and J Hamley. Validation of the nstar ion propulsion system on the deep space one mission-overview and initial results. In *35th Joint Propulsion Conference and Exhibit*, page 2274, 1999.

[159] JE Polk, D Brinza, RY Kakuda, JR Brophy, I Katz, JR Anderson, VK Rawlin, MJ Patterson, J Sovey, and J Hamley. Demonstration of the nstar ion propulsion system on the deep space one mission. In *27th International Electric Propulsion Conference*, pages 01–075, 2001.

[160] R. J. Lomax. Transient space-charge flow. *Journal of Electronics and Control*, 9:127–140, 8 1960.

[161] Charles K. Birdsall and William B. Bridges. Space-charge instabilities in electron diodes and plasma converters. *Journal of Applied Physics*, 32:2611–2618, 1961.

[162] O. Buneman and G. Kooyers. Computer simulation of the electron mixing mechanism in ion propulsion. *AIAA Journal*, 1, 1963.

[163] D. A. Dunn and I. T. Ho. Computer experiments on ion-beam neutralization with initially cold electrons. *AIAA Journal*, 1, 1963.

[164] Revathi Jambunathan and Deborah A. Levin. Chaos: An octree-based pic-dsmc code for modeling of electron kinetic properties in a plasma plume using mpi-cuda parallelization. *Journal of Computational Physics*, 373, 2018.

[165] Nakul Nuwal, Revathi Jambunathan, and Deborah A. Levin. Kinetic modeling of spacecraft surfaces in a plume backflow region. *IEEE Transactions on Plasma Science*, 48, 2020.

[166] L Brieda and J Wang. Modeling of ion thruster beam neutralization using a fully kinetic es-pic code. *41 st AIAA/ASME/SAE/ASEE Joint Propulsion Conference and Exhibit*, 2005.

[167] Joseph Wang and Hideyuki Usui. Kinetic simulations of ion beam neutralization. In *31st International Electric Propulsion Conference*, 2009. Wang, J., and Usui, H. (2009). Kinetic Simulations of Ion Beam Neutralization.

[168] Yuan Hu and Joseph Wang. Electron properties in collisionless mesothermal plasma expansion: Fully kinetic simulations. *IEEE Transactions on Plasma Science*, 43, 2015.

[169] Yuan Hu and Joseph Wang. Fully kinetic simulations of collisionless, mesothermal plasma emission: Macroscopic plume structure and microscopic electron characteristics. *Physics of Plasmas*, 24, 2017.

[170] Lubos Brieda. Model for steady-state fully kinetic ion beam neutralization studies. *IEEE Transactions on Plasma Science*, 46, 2018.

[171] Min Li, Mario Merino, Eduardo Ahedo, and Haibin Tang. On electron boundary conditions in pic plasma thruster plume simulations. *Plasma Sources Science and Technology*, 28, 2019.

[172] Yinjian Zhao, Joseph Wang, and Hideyuki Usui. Simulations of ion thruster beam neutralization using a particle–particle model. *Journal of Propulsion and Power*, 34, 2018.

[173] W. Bernstein and J. M. Sellen. Oscillations in synthetic plasma beams. *Physics of Fluids*, 6, 1963.

[174] R. P. Wadhwa, O. Buneman, and D. F. Brauch. Two-dimensional computer experiments on ion- beam neutralization. *AIAA Journal*, 3(6):1076–1081, 1965.

[175] R P Wadhwa and D F Brauch. Analysis of electron-ion mixing in ion engines final report, 30 apr. 1964-30 jun. 1965. Technical report, National Aeronautics and Space Administration, 7 1965. (No. NASA-CR-54419).

[176] C. Lan and I. D. Kaganovich. Electrostatic solitary waves in ion beam neutralization. *Physics of Plasmas*, 26, 2019.

[177] Nakul Nuwal, Deborah A. Levin, and Igor D. Kaganovich. Excitation of surface waves in 3d ion beam neutralization. *Physics of Plasmas*, 30, 2023.

[178] C. Lan and I. D. Kaganovich. Neutralization of ion beam by electron injection: Accumulation of cold electrons. *Physics of Plasmas*, 27, 2020.

[179] Chaohui Lan, Qiming Chen, Jianli Liu, Liangchao Zhao, and E. Peng. Deterioration of ion beam neutralization caused by reflection of electrostatic solitary waves within pulsed ion beam. *Plasma Sources Science and Technology*, 31, 2022.

[180] Adrian Wheelock, David L. Cooke, and Nikolaos A. Gatsonis. Ion beam neutralization processes for electric micropropulsion applications. In *39th AIAA/ASME/SAE/ASEE Joint Propulsion Conference and Exhibit*, page 5148, 2003.

[181] T. Intrator, M. H. Cho, E. Y. Wang, N. Hershkowitz, D. Diebold, and J. Dekock. The virtual cathode as a transient double sheath. *Journal of Applied Physics*, 64:2927–2933, 1988.

[182] Adrian Wheelock, David L Cooke, and Nikolaos A Gatsonis. Investigation of ion beam neutralization processes with 2d and 3d pic simulations. *Computer Physics Communications*, 164(1-3):336–343, 2004.

[183] Adrian Wheelock, David L. Cooke, and Nikolaos A. Gatsonis. Computational analysis of current coupling of ion beam-neutralizer interactions. In *41st AIAA/ASME/SAE/ASEE Joint Propulsion Conference & Exhibit*, page 3692, 2005.

[184] Min Li, Mario Merino, Eduardo Ahedo, Junxue Ren, and Haibin Tang. Full-pic code validation and comparison against fluid models on plasma plume expansions. In *Proc. Int. Electric Propulsion Conf.* Georgia Institute of Technology, 2017.

[185] Daoru Han, Sergey Averkin, and Nikolaos A Gatsonis. 3d particle-in-cell simulations of electric propulsion ion beam neutralization. In *Proc. 35th Int. Electr. Propuls. Conf.*, pages 1–5, 2017.

[186] O. Chang and J. Wang. Kinetic simulations of ion beam neutralization. In *AIP Conference Proceedings*, volume 1333, pages 1073–1078. American Institute of Physics, 2011.

[187] Joseph Wang, Daoru Han, and Yuan Hu. Kinetic simulations of plasma plume potential in a vacuum chamber. *IEEE Transactions on Plasma Science*, 43(9):3047–3053, 2015.

[188] Yuan Hu, Joseph Wang, and Quanhua Sun. Geometrically self-similar ion acceleration in collisionless plasma beam expansion. *Plasma Sources Science and Technology*, 29, 2020.

[189] G. Sohl, F. A. Barcatta, and S. Zafran. Electron bombardment cesium ion engine system, 10 1965.

[190] V. K. Rawlin and E. V. Pawlik. A mercury plasma-bridge neutralizer. *Journal of Spacecraft and Rockets*, 5, 1968.

[191] J. W. Ward and H. J. King. Mercury hollow cathode plasma bridge neutralizers. *Journal of Spacecraft and Rockets*, 5, 1968.

[192] D. C. Byers and Aaron Snyder. Parametric investigation of mercury hollow-cathode neutralizers. *Journal of Spacecraft and Rockets*, 8:133–139, 1971.

[193] Paul D. Reader, Dennis P. White, and Gerald C. Isaacson. Argon plasma bridge neutralizer operation with a 10-cm- beam-diameter ion etching source. *J Vac Sci Technol*, 15, 1978.

[194] Revathi Jambunathan and Deborah A. Levin. Kinetic, 3-d, pic-dsmc simulations of ion thruster plumes and the backflow region. *IEEE Transactions on Plasma Science*, 48, 2020.

[195] Nist argon. https://physics.nist.gov/cgi-bin/ASD/lines1.pl?spectra=Ar&output_type=0&low_w=&upp_w=&unit=1&submit=Retrieve+Data&de=0&plot_out=0&I_scale_type=1&format=0&line_out=0&en_unit=0&output=0&bibrefs=1&page_size=15&show_obs_wl=1&show_calc_wl=1&unc_out=1&order_out=0&max_low_enrg=&show_av=2&max_upp_enrg=&tsb_value=0&min_str=&A_out=0&intens_out=on&max_str=&allowed_out=1&forbid_out=1&min_accur=&min_intens=&conf_out=on&term_out=on&enrg_out=on&J_out=on. Accessed: 2025-02-24.

[196] Nist carbon. https://physics.nist.gov/cgi-bin/ASD/lines1.pl?spectra=C&output_type=0&low_w=&upp_w=&unit=1&submit=Retrieve+Data&de=0&plot_out=0&I_scale_type=1&format=0&line_out=0&en_unit=0&output=0&bibrefs=1&page_size=15&show_obs_wl=1&show_calc_wl=1&unc_out=1&order_out=0&max_low_enrg=&show_av=2&max_upp_enrg=&tsb_value=0&min_str=&A_out=0&intens_out=on&max_str=&allowed_out=1&forbid_out=1&min_accur=&min_intens=&conf_out=on&term_out=on&enrg_out=on&J_out=on. Accessed: 2025-02-24.

[197] Reginald William Blake Pearse, Alfred Gordon Gaydon, Reginald William Blake Pearse, and Alfred Gordon Gaydon. *The identification of molecular spectra*, volume 297. Chapman and Hall London, 1976.

[198] Hiden cracking patterns. https://www.hidenanalytical.com/tech-data/cracking-patterns/. Accessed: 2025-02-23.

[199] Rga mass spectra amu. https://www.lesker.com/newweb/technical_info/vacuumtech/rga-spectra-amu-guide.cfm. Accessed: 2025-02-23.